PREDICTION OF SHEAR STRENGTH OF REINFORCED CONCRETE BEAMS BY FINITE ELEMENT METHOD

By

REDA MANAA

Ingenieur civil

Ecole Nationale polytechnique d'Alger

A Thesis submitted for the degree of

Master of Science

Department of Civil Engineering,

Glasgow university,

April, 1989.

BY THE NAME OF *'ALLAH'* THE COMPASSIONATE, THE MERCIFUL

CONTENTS

ACKNOWLEDGEMENTS

The work described in this thesis was carried out in the Department of Civil Engineering at the University of Glasgow.

The author would like to express his appreciation to Professor A. Coull and Dr D. R. Green for the facilities of the department.

The author is greatly indebted to Dr P. Bhatt for his valuable supervision, encouragement and advice during the course of this study.

My grateful thanks are also due to :

Dr. D.V. Phillips for his interest and for giving permission to use his program in this work.

* The Algerian government for giving me the opportunity for higher education.
* My friends M. Bendahgane, S.E. Djellab for their useful discussion and comments.
* My friends D.E. Abderrahmane, and A. Bouazza for their help and encouragement at the difficult moments.
* My friends Douadi Rahmani, J. Moussa, Z.E. Merouani, M. Benredouane, M. Souici, R. Saadi, Y.K. To, for their encouragement.
* My dear parents for their love and care that I can never forget.
* My wife for her boundless patience and moral support throughout this study.
* My daughters Amina and Esma Sarah and my son Abdessalam for keeping me cheerful throughout this study.
* My sisters and brothers for their encouragement and help.
* Finally, my thanks are to **'ALLAH'** for giving me patience and helping me to accomplish this study with success.

SUMMARY

This work is concerned with the prediction using nonlinear finite element program, of the ultimate strength of reinforced concrete beams failing in shear.

Nearly one hundred rectangular beams and a few T–beams were analysed. The beams analysed have been tested by various investigators covering the important variables such as :

–a) Shear– span to depth ratio a_v/d.

–b) Amount of shear reinforcement.

–c) Amount of tensile reinforcement.

–d) Effective depth and width of the beam.

–e) Type of loading.

The work can be divided into two main parts:

1) Parametric study involving the following parameters:

– Shear retention factor β.

– Concrete uniaxial compressive strength f_c.

– Concrete tensile strength f_t.

– Concrete crushing factor C_f.

2) Statistical study involving concrete crushing factor C_f as parameter.

The following results were obtained:

i) The shear retention factor and concrete tensile strength have little effect on the ultimate load

ii) Concrte uniaxial compressive strength and crushing factor both have a great effect on the ultimate load and mode of failure of reinforced concrete beams.

From the statistical study it was found that :

1) Generally, smaller the value of C_f, lower the predicted failure load.

2) Better result were obtained for beams with shear reinforcement and for beams with uniformly distributed loads.

3) Concrete crushing factor C_f effect decrease as concrete strength f_c' increases.

4) Best results were obtained for $C_f = 0.60$.

NOTATIONS

Major symbols used in the text are listed below. Others are defined when they first appear in the text.

A_s	Area of longitudinal reinforcement.
A_{st}	Total cross sectional area of stirrups.
a_v	Shear span.
b	Width of beam web.
b_f	Width of the flange in T–beam.
[B]	Strain matrix.
C	Compression force resisted by concrete in compression zone
c	Cohesion.
C_f	Concrete crushing factor.
C_1, C_2	Constants.
d	Effective depth of beam.
$[D_T]$	Tangential elasticity matrix for uncracked concrete.
$[D_T]^*$	Tangential elasticity matrix in the crack directions for cracked concrete.
det[J]	Determinant of the Jacobian matrix.
dv	Incremental volume.
E_c	Young's modulus for concrete.
E_s	Young's modulus for steel.
E_w	Hardening angle for steel.
f_c	Numerical value given to concrete uniaxial cylinder compressive strength in finite element studies.
f_c'	Experimental value of concrete uniaxial cylinder compressive strength.

f_{cb}	Maximum biaxial compressive strength for concrete.
f_{cu}	Uniaxial compressive strength of concrete cube.
f_t	Concrete tensile strength.
f_y	Yield strength of tensile reinforcement.
f_{yt}	Yield strength of shear reinforcement.
$\{F\}$	Applied forces on the continuum.
$\{F^e\}$	Applied forces on the element.
$\{F_p^e\}$	Element node point load vector.
G	Shear modulus for uncracked concrete.
G_0	Initial shear modulus for concrete.
G'	Reduced shear modulus for cracked concrete.
G_T	Tangent values of the shear modulus.
h or (h_t)	Total height of the beam.
h_f	Thickness of the flange in T–beams.
I_1, I_1'	First invariant of stress and strain, respectively.
J_2, J_2'	Second deviatoric invariant of stress and strain respectively.
$[J]$	Jacobian matrix.
K_0	Initial bulk modulus.
K_T	Tangent bulk modulus.
$[K]$	Stiffness matrix of the continuum.
$[K^e]$	Element stiffness matrix.
L	Total span of the beam.
M	Bending moment.
m	Ratio of concrete tensile to compressive strength.

$[N(\xi,\eta)]$	Shape functions matrix.
$\{p\}$	Body force per unit volume.
P_i^*	Norm of the total applied loads.
$\{q\}$	Applied suface pressure.
r	Shear reinforcement ratio given by : $A_{st}/b.s$.
s	Spacing of stirrups.
S_e	Loaded suface area of element.
T	Tensile force resisted by reinforcement.
t	Thickness of the element.
Tol	Specified convergence tolerance.
u, v	Components of displacement vector $\{\delta\}$.
u_i, v_i	Components of nodal displacement vector $\{\delta_i\}$.
V	Total shear force.
V_a	Aggregate interlock force.
V_{ax},V_{ay}	Components of aggregate force in x and y directions respectively.
V_c	Total shear force carried by concrete.
V_{cy}	Shear force carried by uncracked concrete.
V_d	Dowel force.
V_e	Element volume.
V_s	Part of shear force carried by shear reinforcement.
V_t	Shear force at the supports.
V_u	Shear strength of the beam.
W_i	Weighting factor for Gaussian integration.
x, y	Cartesian coordinate of a point.
X_{mean}	Mean value

α_1, α_2	Material constants.
β	Shear retention factor.
$\beta_1, \beta_2, \beta_3$	Material constants for defining the variation of β.
$\{\delta\}$	Displacement vector
$\{\delta^e\}$	Element nodal displacement vector.
$\{\delta_i\}$	Nodal displacement vector.
$\Delta\{\delta\}$	Incremental displacement vector.
$\{\epsilon\}$	Strain vector.
ϵ_{cr} (ϵ_n^*)	Concrete cracking strain.
$\epsilon_x, \epsilon_y, \gamma_{xy}$	Strain vector components in cartesian coordinates.
$\{\epsilon'\}$	Deviatoric strain vector.
$\epsilon_x', \epsilon_y', \gamma_{xy}'$	Deviatoric strain vector components in cartesian coordinates.
$\{\epsilon''\}$	Hydrostatic strain vector.
$\epsilon_x'', \epsilon_y'', \gamma_{xy}''$	Hydrostatic strain vector components in cartesian coordinates.
$\epsilon_{oct}, \gamma_{oct}$	Octahedral normal and shear strains.
ϵ_m	Mean strain.
ϵ_v	Volumetric strain.
$\Delta\epsilon_i$	Steel incremental strain.
$\Delta\{\epsilon\}$	Incremental strain $\Delta\{\epsilon\}$.
Φ	Angle of internal friction.
φ	Inclination of reinforcement to x axis.
ξ, η	Intrinsic coordinates of any point within the element.
ξ_i, η_j	Coordinate of the ith integration point.

ν	Poisson's ratio.
π	Total potential energy of the continuum.
π_e	Element potential energy.
$\{\psi\}$	Unbalanced nodal forces.
$\Delta \Psi_i^*$	Norm of the residuals.
ρ_s	Longitudinal reinforcement ratio.
σ, τ	Normal and shear stress.
$\underline{\sigma}$	Standard deviation
$\{\sigma\}$	Stress vector.
$\{\sigma_0\}$	Initial stress vector.
σ_m	Mean stress.
σ_t^*	Normal stress parallel to the crack.
$\sigma_x, \sigma_y, \tau_{xy}$	Stress vector components in cartesian coordinates.
$\{\sigma'\}$	Deviatoric stress vector.
$\sigma_x', \sigma_y', \tau_{xy}'$	Deviatoric stress vector components in cartesian coordinates
$\{\sigma''\}$	Hydrostatic stress vector.
$\sigma_x'', \sigma_y'', \tau_{xy}''$	Hydrostatic stress vector components in cartesian coordinates.
σ_{oct}, τ_{oct}	Octahedral normal and shear stresses.
$\{\sigma_{ex}\}$	Difference between true stress and computed stress.
$\Delta\{\sigma\}$	Incremental stress.
θ	Angle of crack.
τ^*, γ^*	Shear stress and strain along the crack

CHAPTER 1

INTRODUCTION

Since the early days of use of reinforced concrete, engineers have attempted to develop conceptual models of structures as a first step in the design process. While structural analysis has undergone immense progress with computer programs available to analyse almost any type of structure, lack of conceptual models for certain aspects of design is still a major problem. A prime example of this is the semi–empirical rules used for the design against shear failure of reinforced concrete beams. Currently, the design methods lack structural insight into the physical behaviour under the action of shear forces.

At the begining of this century, E. MORSCH and W. RITTER, developed design formulae for the shear design of reinforced concrete beams assuming a truss model with 45° compression diagonals.

After more than half a century of extensive experimental and theoretical work on the shear strength of reinforced concrete members there is still strong disagreement over the cause of the so–called shear failure and especially over the associated mechanism. As long as there is strong disagreement on what the mechanism of failure is, we cannot claim to know what *'shear failure'* is.

Many attempts at solving the problem by means of empirical formulae have brought about no satisfactory solution as the results always apply only to the type of beams used in these particular series of tests from which these formulae have been derived. The main difficulty is that the factors influencing the behaviour and strength of concrete beams failing in shear are numerous and complex.

They include :

a) proportions and shape of the beam,

b) structural restraints and the interaction of the beam with other components in the system,

c) amount and arrangement of longitudinal and shear reinforcement.

d) the load distribution and loading history,

c) properties of the concrete and steel,

e) concrete placement and curing and the environmental history.

Most of the investigators strongly encourage further research work not only to explore other areas of the problem, but also to establish basically a rational theory for the effects of shear and diagonal tension on the behaviour of reinforced concrete beams. This is because an enquiring designer will not only want to know how to apply a safe design procedure, but would also wish to understand the reason why a particular structural member is likely to fail in a particular mode.

Indeed, the last two decades, in particular, have seen a greater emphasis on fundamental studies in preference to empirical studies. In fact, it is only by investigating and understanding the internal mechanism of the so–called shear failure that we may expect to find the answer to the 'Riddle of shear failure'.

As mentioned previously, the amount of work accumulated over the years since the time of the pioneers is enourmous. There have been hundreds of papers published relating to the problem of reinforced concrete under shear and bending. Controversy is great on many aspects because the number of independant variables involved is unusually large, and dealing exhaustively with all these variables would be a monumental task. A comprehensive review is almost

impossible, because not only is the literature extensive, but also the individual contributions are resistant to integration into an orderly and comprehensive body of knowledge.

There are several reasons for the great interest in the shear strength analysis:

i) lack of knowledge of actual behaviour,

ii) fear of a typically sudden and *'brittle'* shear failure of members without shear reinforcement,

iii) the large number of structural members in practice that are subject to shear forces.

Using nonlinear finite element analysis, there has already been many attempts to predict the shear strength of reinforced concrete beams. The problem is that in these attempts comparisons were made with a small number of experimental tests which do not cover all the factors influencing the behaviour of reinforced concrete beams. Therefore, the set of input material parameters giving satisfactory agreement with experimental results differed from one attempt to the other depending on the set of experimental results chosen.

The objective of this investigation is to use a nonlinear finite element program and to tune the parameters so as to obtain the best fit to a large number of experimental results which cover all the factors affecting the shear strength of reinforced concrete beams.

This exercise should be able to recommend the values of the material parameters to predict safe ultimate load. In addition the study will be able to throw light on the mechanisms of shear failure based on 'stress and strain criteria' only.

CHAPTER 2

BASIC FACTS ABOUT SHEAR FAILURE OF REINFORCED CONCRETE BEAMS

2.1 INTRODUCTION

Developing a rational theory for shear strength prediction in the absence of a clear understanding of physical behaviour has always been a difficult task. For this reason fundamental behaviour, principal mechanisms of shear resistance and modes of failure have been examined herein.

2.2 NATURE OF INCLINED CRACKING

When a beam is loaded to a certain stage, inclined cracks in the web may develop between the support and the point load within the shear span. These cracks may develop either before a flexural crack occurs in the vicinity (web–shear–crack), or as an extension of a previously developed flexural crack (flexural–shear–crack). The flexural crack causing the inclined crack is referred to as the *'initiating flexural crack'*. In addition to the primary cracks, secondary cracks often result from splitiing forces developed by the deformed bars when slip between concrete and steel reinforcement occurs, or from dowel action in the longitudinal bars transferring shear across the crack Fig.(2.1).

When the inclined crack forms, it generally starts at or close to an existing flexural crack. The manner in which inclined cracks develop and grow and the type of failure that subsequently develops is strongly affected by the relative magnitudes of the shearing stress, τ, and the normal stress σ, which are

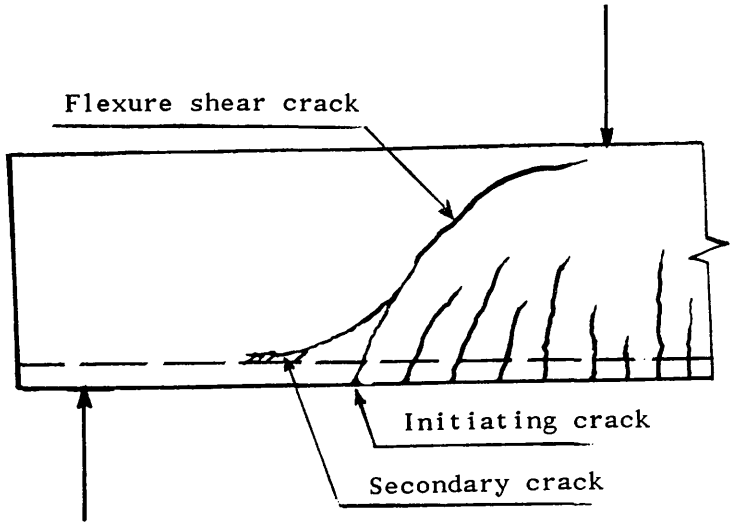

a) Flexure shear crack

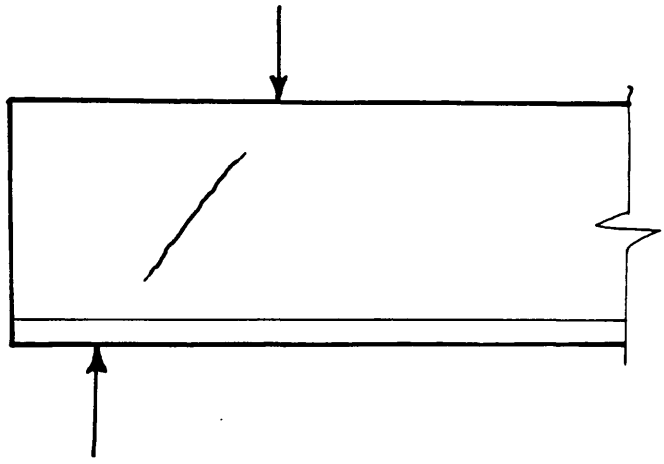

b) Web shear crack

FIGURE (2.1) : INCLINED CRACKS IN REINFORCED CONCRETE BEAMS

dependent on several variables, including the geometry of the beam, the type of loading, the amount and arrangement of reinforcement, the type of steel, and the interaction between steel and concrete.

2.3 MECHANISMS OF SHEAR FAILURE

If microcracks that already exist even before any load is applied are ignored, concrete is initially uncracked. As the beam is loaded, strains in the concrete reach the limiting tensile strain and flexural cracks form on the tension face of the beam at intervals along the span depending on the bending moment and the steel ratio. Redistribution of stress takes place due to the modified action of the member, and the rate of deflection of the beam increases with a corresponding increase in steel and concrete stress.

After the flexural cracks have extended upwards a short distance above the longitudinal reinforcement, they start to become inclined primarly due to the action of the shear stresses. The progressive changes in stresses in steel and concrete as the inclined cracks extend upward is due to further redistribution of stresses.

Figure (2.2) shows the internal force system after the formation of an inclined crack. The shear force is resisted by the compression zone, aggregate interlock action and to some extent by dowel action of the main steel. As the shear force is increased, the inclined crack opens up giving rise to tensions in the surrounding concrete and an increase in the dowel force. This in turn, produces splitting cracks in the concrete along the line of the reinforcement with an associated loss of bond. Further redistribution of stresses starts at the onset of these splitting cracks.

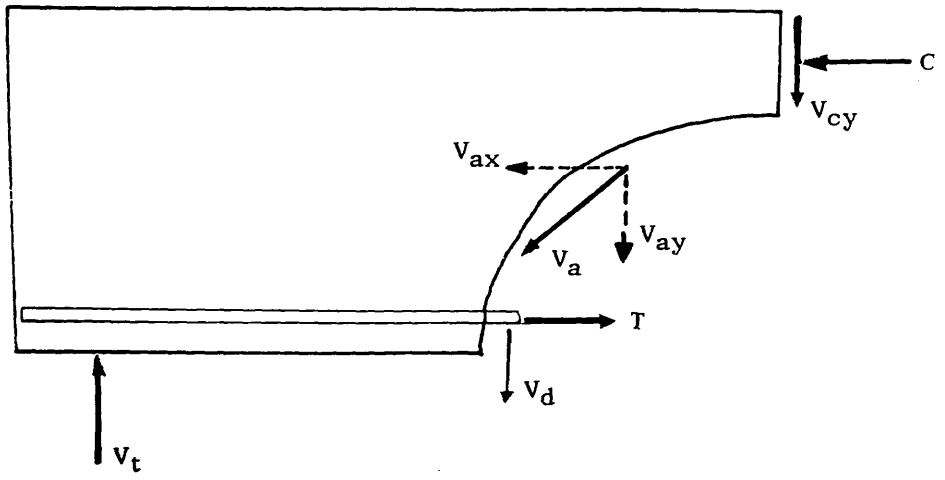

FIGURE (2.2) : FORCES ACTING AT INCLINED CRACK
(Beam without shear reinforcement)

The inclined crack propagates rapidly into the compression zone but with a flatter trajectory and in most cases its change in direction is abrupt. This third stage of redistribution of stresses continues until a complete split of the concrete occurs along the steel (shear–tension failure) Fig.(2.3a), or until the compression zone desintegrates (shear–compression failure) Fig.(2.3b).

In any treatment of the behaviour and strength of reinforced concrete beams failing in shear it is important to distinguish between the loads which cause inclined cracking and those which cause the shear failure itself. Because inclined cracking is an essential prerequisite to shear failure and it is important to be able to define the inclined cracking load before it is known whether shear failure can occur. In some ranges of variables (small values of the shear–span to depth ratio a_v/d, with no shear reinforcement) the shear failure load is equal to the inclined cracking load, whereas for a different set of variables (higher values of a_v/d) it may exceed the cracking load[1].

Providing suitable web reinforcement in beams can greatly increase the shear capacity and usually can assure flexural failure under given loading conditions. Indeed, one of the principal objectives in providing web reinforcement is to eliminate shear as a mode of failure.

This approach to the design of web reinforcement does not eliminate the problem but only changes its form, as the question will then be focused on how much web reinforcement will be required to prevent shear failure. A rational answer to this question awaits the general theoretical solution of the problem. In the meantime, web reinforcement is usually designed to carry that portion of the shear forces in excess of that which can be sustained by the concrete alone. This can be achieved by using models based on concepts such as the arch, frame, and truss analogies ..etc.

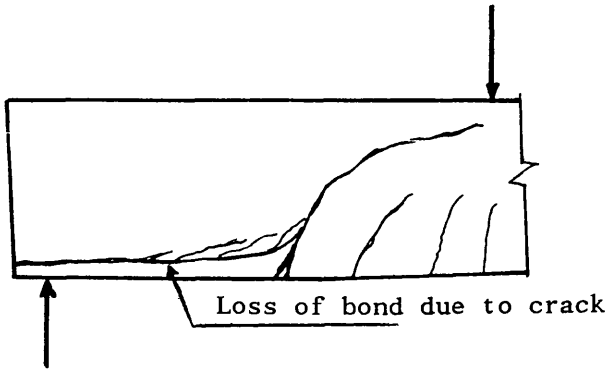

a) Shear–tension failure

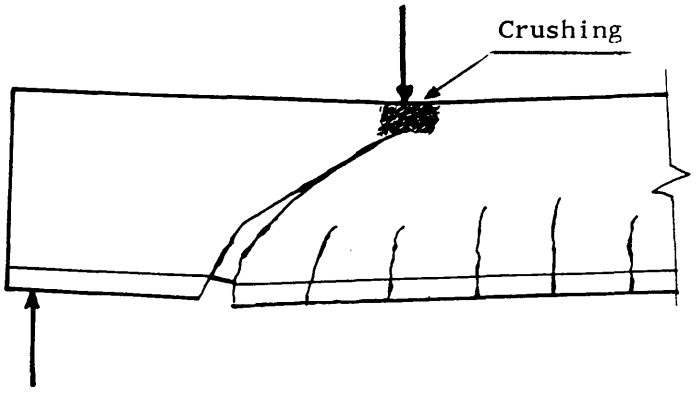

b) Shear–compression failure

FIGURE (2.3) : TYPICAL SHEAR FAILURES

However, tests on reinforced concrete beams under a single point load have indicated that while shear failure of beams with transversel reinforcement occurs within a region of the shear span closer to the applied load, it occurs closer to the support in beams with the same geometry and longitudinal reinforcement but without shear reinforcement[2] Fig.(2.4).

Since the shear force remains constant within the shear span, this translation of the position of shear failure implies that, although the presence of shear forces is essential for the occurence of shear failure, the causes of this may only partially be attributed to the shear forces[3].

2.4 MODES OF DIAGONAL FAILURE

Shear failure is usually investigated by testing reinforced concrete beams under two–point loads Fig.(2.5). This arrangement has the advantage of combining two different test conditions : pure bending between the two loads and constant shear force in the two end sections.

2.4.1 Flexural failure:

The behaviour of a slender beam subject to a gradually increasing load is well known. The first cracks will appear long before the allowable load is reached. These cracks are narrow and often unimportant. Under further loading, cracks increase both in width and length thereby decreasing the area of the compressive zone. The internal mechanism of such a beam nearing flexural failure has transformed the reinforced concrete beam into a comb–like structure : the compressive zone of the beam is the backbone of the comb, while in the tensile zone the *'concrete teeth'*, separated from each other by flexural cracks, represent the teeth of the comb[4] Fig.(2.6).

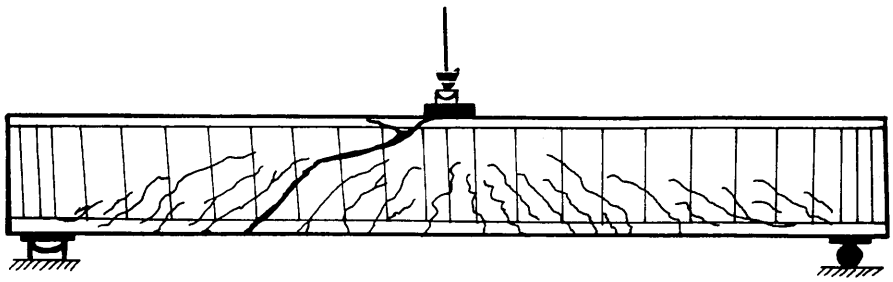

a) Beam with shear reinforcement

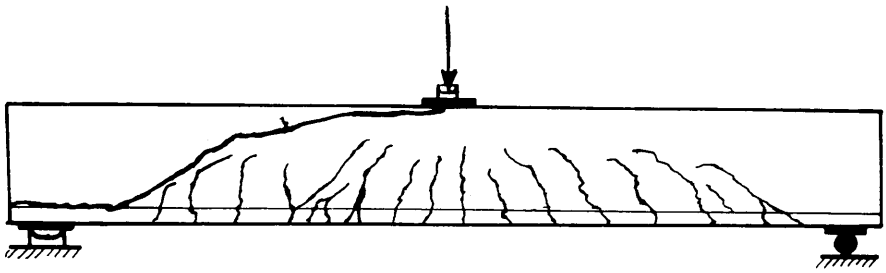

b) Beam without shear reinforcement

FIGURE (2.4) : EFFECT OF SHEAR REINFORCEMENT UPON SHEAR FAILURE

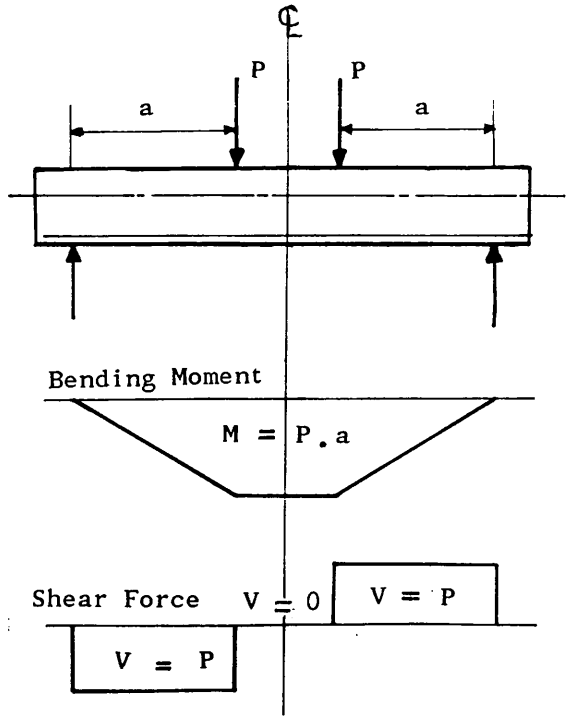

FIGURE (2.5) : TYPICAL LOADING ARRANGEMENT OF BEAMS FOR INVESTIGATION OF SHEAR FAILURE

When the bending process is continued the failure of the beam happens either by crushing of the concrete compression zone, or by yielding of the tensile reinforcement Fig.(2.7). Thus, a slight increase in loads is immediately followed by a large increase of displacements which causes the lengthening and widening of cracks. Consequently, the compression zone height decreases and the compressive stresses increase rapidly to reach the compressive strength of concrete and thereby causing the flexural failure of the beam by destruction of its compressive zone.

2.4.2 Shear failure:

Failures are induced by cracks in the shear span Fig.(2.3). They occur generally only if there is shear force present, hence they were called *'shear failures'*. By assuming that the shear force or shear stress was responsible, it was thought for many years that *'shear failure'* could be treated similarly to flexural failure, i.e. shear failure takes place when the shear stress reaches the shear strength of concrete. However, in the most common type of loading, i.e. uniformly distributed loading, no shear crack appear near the supports although it is there that the shear force is maximum[4]. This is because local stress concentration due to concentrated reaction was ignored.

From the large number of experimental tests carried out for almost a century it was established that, for a constant cross section and reinforcement, their corresponding mode of failure is dependent upon the shear span to depth ratio a_v / d $(=M/V.d)$. On the basis of this dependance Kotsovos[3] stated that the beam behaviour may be divided into four types Fig.(2.8):

Type 1: characterized by flexural failure which allows the beam to develop its full flexural capacity.

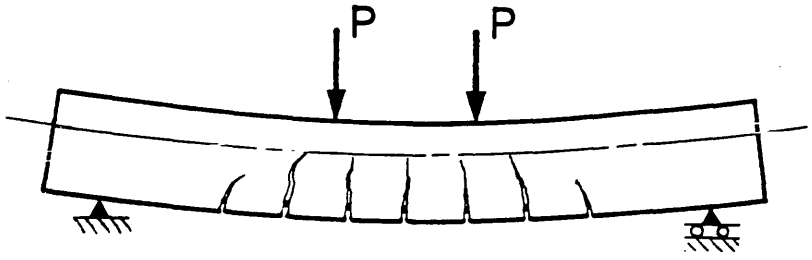

FIGURE (2.6) : DEFORMATION OF A REINFORCED CONCRETE BEAM NEARING FLEXURAL FAILURE

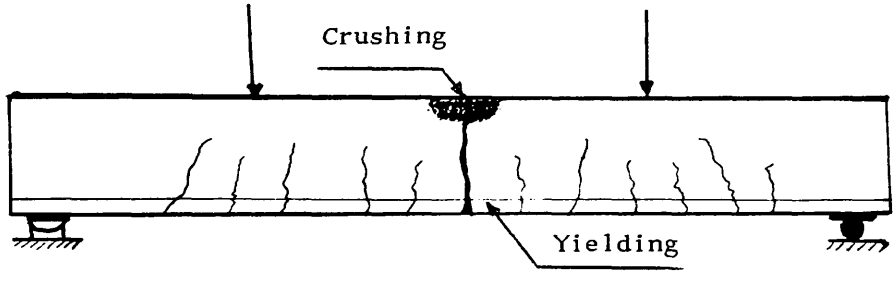

FIGURE (2.7) : FLEXURAL FAILURE

Type 2: characterized by a mode of failure caused by an inclined crack which initiates near the tip of the flexural crack closest to the support and propagates toward the load point. It may also propagate toward the support along the reinforcement, but anchorage failure can be avoided by correctly anchoring the steel. However, the flexural capacity decreases with a_v/d to reach a critical value.

Type 3: characterized by a mode of failure caused by an inclined crack which forms independently of the flexural cracks. The flexural capacity increases from the critical value in *type 2* to a higher value, at which it becomes equal to the full flexural capacity.

Type 4: characterized by failure caused by an inclined crack joining the support to the load point.

2.5 BASIC MECHANISMS OF SHEAR TRANSFER

Shear is transmitted from one plane to another in various ways in reinforced concrete members. The behaviour, including the failure modes, depends on the method of shear transmission.

The main types of shear transfer are as follows :

2.5.1 Shear transfer by shear stress in concrete:

The simplest method of shear transfer is by shearing stresses. This occurs in uncracked members or in the uncracked portions of structural members. The interaction of shear stresses with tensile and compressive stresses produces principal stresses which may cause inclined cracking or crushing failure of concrete[5].

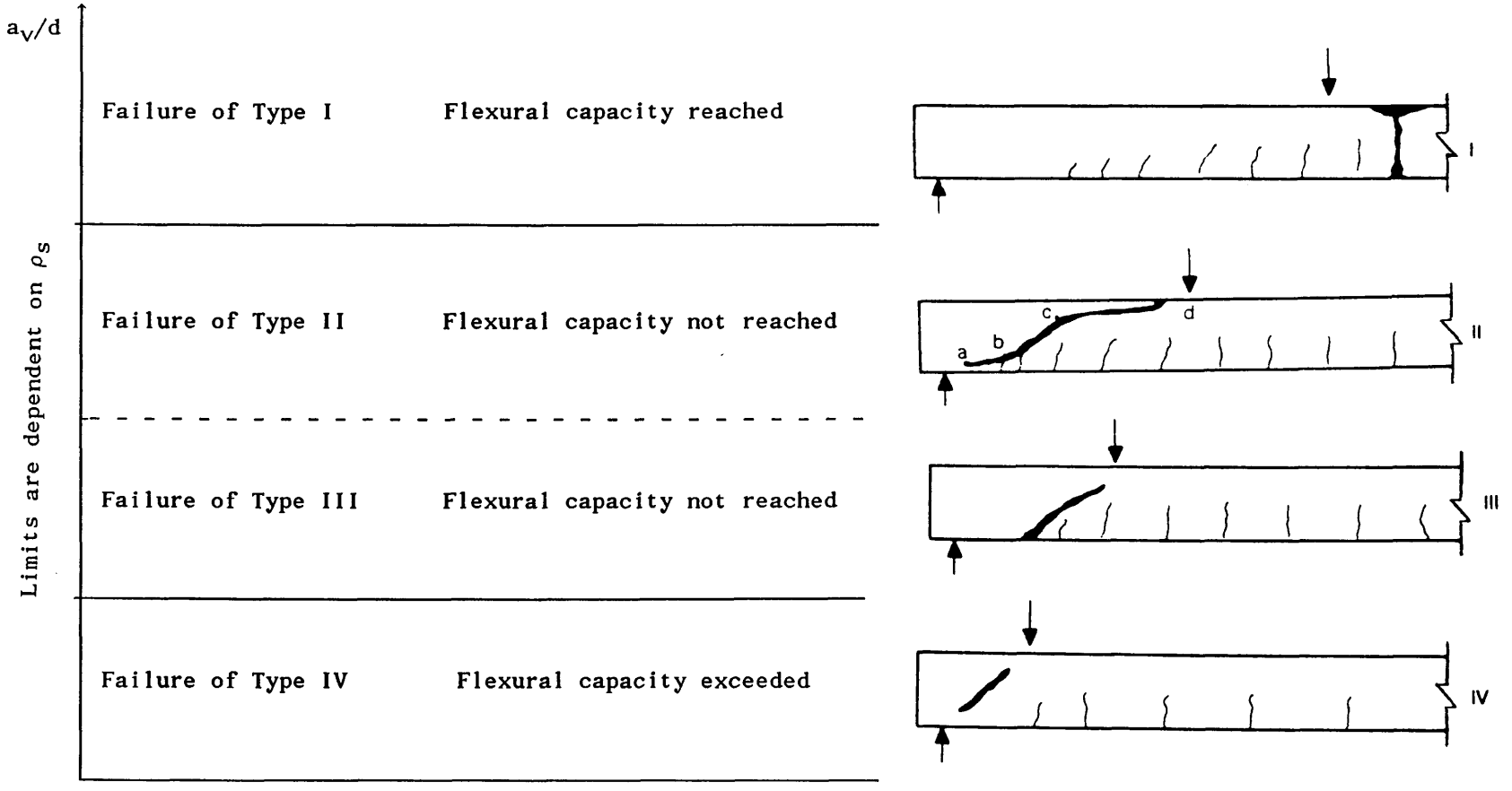

FIGURE (2.8) : TYPES OF BEHAVIOUR EXHIBITED BY BEAMS SUBJECTED TO TWO-POINT LOADING

2.5.2 Aggregate interlock:

There are several instances in which shear must be transferred across a definite plane or surface where slip may occur. The mechanism has been called aggregate interlock action. If the plane under consideration is an existing crack or interface, failure usually involves slippage or relative movement along the crack or plane. If the plane is located in monolithic concrete, a number of diagonal cracks occur across the interface. Therefore, inclined stirrups or bent–up bars are required to prevent shear failure Fig.(2.10).

2.5.3 Dowel action:

If reinforcing bars cross a crack, shearing displacements along the crack will be resisted, in part, by a dowel force in the bar. The dowel force gives rise to tension in the surrounding concrete and these in combination with the wedging action of the bar produce splitting cracks along the reinforcement. This in turn decreases the stiffness of the concrete around the bar and thereby the dowel force. Following splitting, the dowel force will be a function of the stiffness of the concrete directly under the bars and the distance from the point where the doweling shear is applied to the first stirrups supporting the dowel.

In the analysis of his results Chana[16] showed that by including stirrups along the dowel cracking region , shear failures are accompanied by yielding of the main reinforcement. Conversely, for beams without shear reinforcement, or in those with large stirrup spacing, dowel force causes splitting of the concrete along the steel and leads to a premature failure of the beam.

2.5.4 Arch action:

In deep beams and slabs part of the load is transmitted to the support by arch action. This is not a shear mechanism in the sense that it does not transmit a tangential force to a nearby parallel plane. However, arch action does permit the transfer of a vertical concentrated force to a reaction in a deep member Fig.(2.9).

For arch action to develop, a horizontal reaction component is required at the base of the arch. In beams, this is usually provided by the tie of the longitudinal bars. Frequently deep beams will fail due to a failure of the anchorage of the bars. In beams, arch action occurs not only outside the outermost cracks but also between diagonal tension cracks. Part of the arch compression is resisted by dowel forces and therefore splitting cracks may develop along the bars. It was found that stirrups close to the base of diagonal cracks can provide support to the arches[7] Fig.(2.10).

2.5.5 Shear reinforcement:

It has been customary to view the action of web reinforcement in beams as part of a truss. However, it is also helpful to examine the action of shear reinforcement from the view point of how it aids the several kinds of shear transfers action. In addition to any shear carried by the stirrup itself, when an inclined crack crosses shear reinforcement, the steel may contribute significantly to the capacity of the member by increasing or maintaining the shear transferred by aggregate interlock, dowel and arch actions. Thus, shear reinforcement restricts the widening of inclined cracks in beams and thus slows down the decrease of aggregate interlock action quite effectively[5]. The effect of web reinforcement in beams is discussed later.

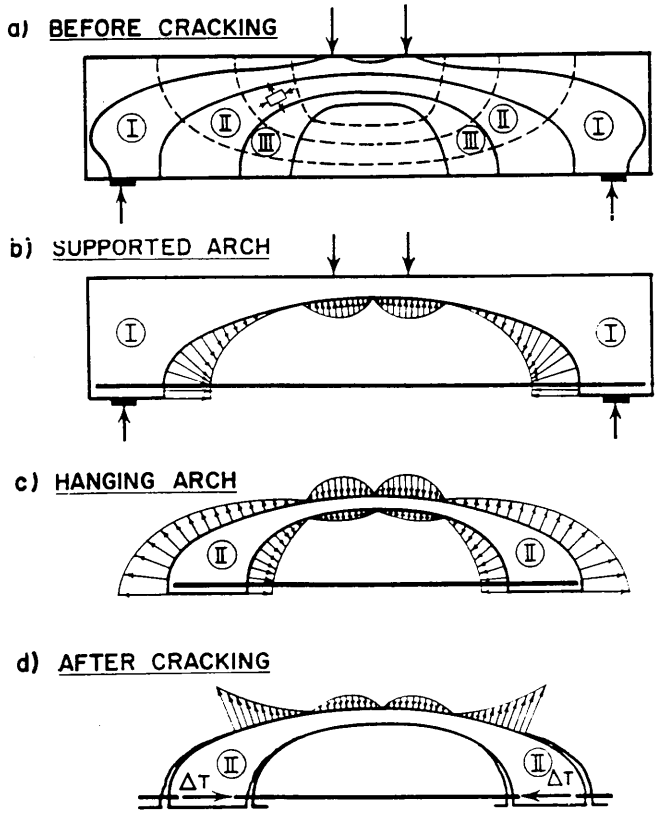

FIGURE 2.9 : Arch analogy for reinforced concrete beam (without transverse reinforcement)

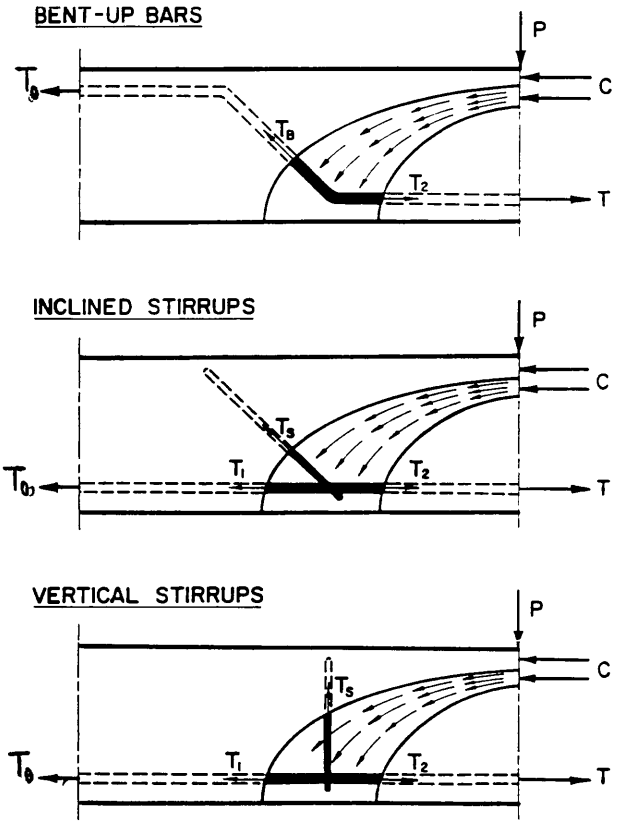

FIGURE 2.10 : Arch supports provided by three conventional types of web reinforcement

2.6 FORCES IN BEAMS WITH DIAGONAL TENSION CRACKS

Traditionally, the transfer of shear across a section in a cracked beam has been explained using a *'truss analogy'* in which the beam is represented by a truss with parallel chords and a web composed of diagonal concrete compression struts and vertical or inclined stirrups acting in tension. It has formed the principal basis for the interpretation of forces in beams and for the design of reinforced concrete beams for shear. On the other hand, recent studies have shown that several significant components of the shear force shown in Fig.(2.11) are not included in the basic truss analogy. These will be examined in the following paragraphs :

2.6.1 Beams without web reinforcement:

A number of experimental investigations have been carried out on beams without stirrups to assess the relative magnitude of the forces shown in Fig.(2.2). These tests[12] showed that only 40% of the total shear on a section can be carried by the compression zone if the stress conditions at the tip of the crack are to be compatible with an accepted failure criterion for concrete subjected to combined shear and normal force. Experimental work carried out by Fenwick and Paulay[6] among others shows a variation of shear resisted by compression zone of between 20% and 40% of the total shear on beams. This range depended mainly on the shape and nature of the cracks in the beams.

A number of investigations have been carried out on dowel action indicated that the dowel shear force is betwwen 15% and 25% of the total shear force.

Tests carried out on aggregate interlock indicate that between 33% and 50% of the total force on a beam may be carried by aggregate interlock.

The figures given in the preceding were measured on rectangular beams without web reinforcement at loads near their failure load. Different distributions of shear force apply for lesser loads on the beams. Thus, before cracking, a parabolic distribution of shear stress across a beam cross section can be expected and after cracking, as the shear displacement across the cracks increase, dowel and aggregate interlock action become increasingly significant.

2.6.2 Beams with web reinforcement:

Web reinforcement has three primary effects on the strength of a beam Fig.(2.11) :

1– It carries part of the shear, V_s.

2– It restricts the growth of the diagonal tension crack width and thereby helps to maintain the aggregate interlock force, V_{ay}.

3– It supports the longitudinal bars and increases their dowel capacity V_d.

In addition to these three actions, stirrups may transfer a small force across the crack by dowel action and they tend to enhance the strength of the compression zone by confining the concrete.

If a stirrup happens to be near the bottom of a major diagonal crack it is very effective in maintaining the dowel force and restraining the splitting failure, provided that the stirrups are of sufficient size, are well anchored and are spaced close enough together such that each potential diagonal crack reaches the tension steel near a stirrup[7].

Figure(2.12) shows the way the different shear force components shown in Figure(2.11) vary. Prior to flexural cracking all the shear is carried by the uncracked concrete. Between flexural and inclined cracking, the external shear is

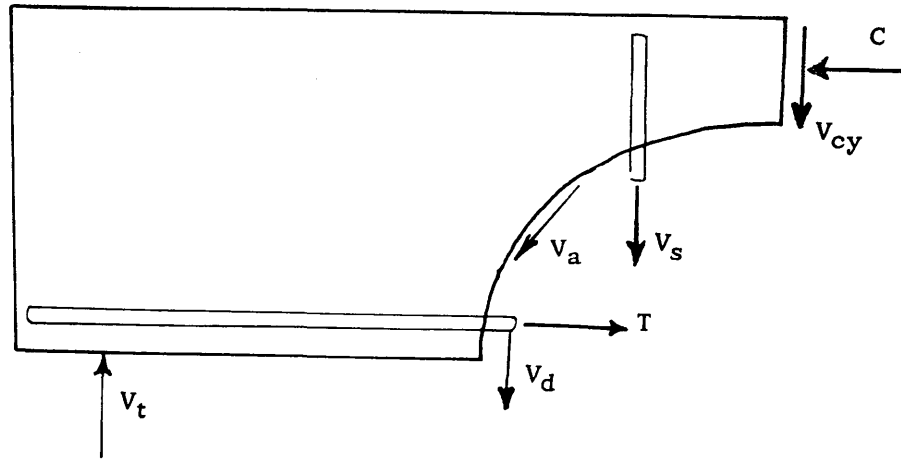

FIGURE (2.11) : FORCES ACTING AT INCLINED CRACK FOR BEAMS WITH WEB REINFORCEMENT

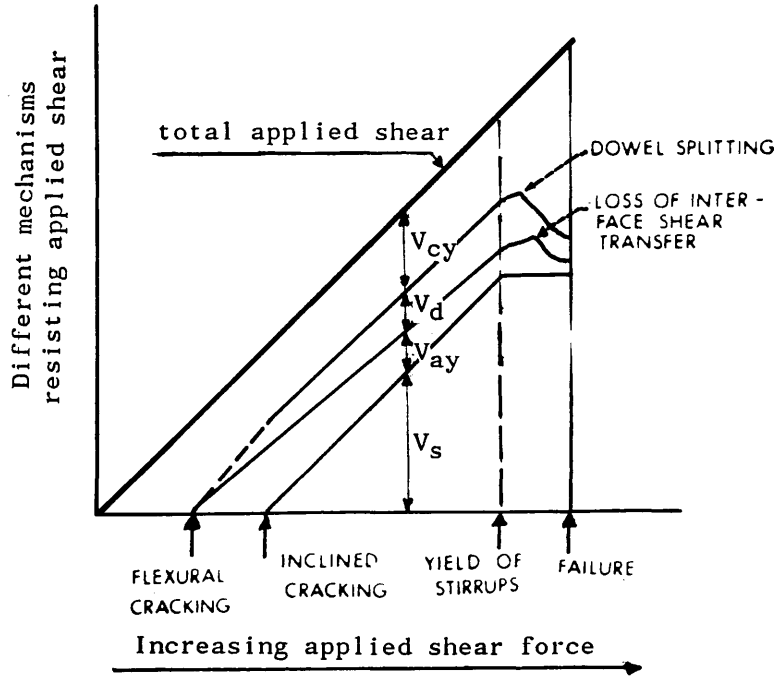

FIGURE (2.12) : DISTRIBUTION OF INTERNAL SHEARS IN BEAMS WITH WEB REINFORCEMENT

resisted by the concrete V_{cy}, the aggregate interlock V_{ay} and by dowel action V_d. Following the formation of inclined cracks a portion of shear is carried by the web reinforcement V_s. Once the web steel yields, the shear carried by the web reinforcement can no longer increase, and any additional shear must be carried by V_{cy}, V_d and V_{ay}. As the inclined crack widens, the aggregate interlock V_{ay} decreases forcing V_d and V_{cy} to increase at an accelerated rate until either splitting (dowel) failure occurs, or the compression zone fails due to combined shear and compression.

Each of the ways in which force is carried across beams, apart from the force carried by stirrups has a load deformation curve which initially rises rapidly, followed by a falling portion. In the case of the force carried in the compression zone, the falling portion of the curve follows that of the concrete under combined shear and compression stress system. Dowel failure has a very steep falling portion, except where the dowel is restrained from splitting the surrounding concrete by stirrups enclosing the longitudinal bars. The failure of the aggregate interlock can be abrupt, particularly if a crack is inclined over most its length and the predominant movement across the crack tends to open the crack rather than shear it. Because of this, it is very difficult to say which mechanism of shear breaks down to cause the failure of beams with stirrups.

2.7 FACTORS AFFECTING THE SHEAR STRENGTH OF BEAMS

Before discussing the analytical models, it is helpful to briefly present the important parameters affecting the shear strength of reinforced concrete beams.

Most of the building codes express the shear strength of beams in terms of an equation of the form :

$$V_u = V_c + V_s \quad (2.1)$$

in which :

$$V_c = V_{cy} + V_d + V_{ay} \quad (2.2)$$

Where : V_u = The shear strength of the beam.

V_c = Part of the beam shear strength carried by concrete

V_s = Part of the beam shear strength carried by shear reinforcement.

Other terms are defined in Figure (2.11)

2.7.1 Reinforcement details:

2.7.1.a Percentage of longitudinal reinforcement:

Tests[8,9,10] and analysis[9] have shown that the shear strength of reinforced concrete beams without web reinforcement increases significantly with the longitudinal reinforcement ratio ρ_s, where ρ_s is given by :

$$\rho_s = \frac{A_s}{b.d}$$

where A_s : area of longitudinal reinforcement.

b : width of the beam.

d : effective depth of the beam.

The effect of steel percentage may be explained in two ways :

1– Greater the value of ρ_s, the greater is the dowel shear V_d.

2– As ρ_s is increased, the flexural cracks do not extend higher into the beam and are narrower, increasing both the shear capacity of the the compression zone and the aggregate interlock.

Some of the empirical equations which take account of this parameter are :

a. RAJAGOPALAN and FERGUSON[10]:

$$V_c = (0.066 + 8.3\rho_s)(f_c)^{\frac{1}{2}} < 0.166(f_c)^{\frac{1}{2}} \quad (N/mm^2) \quad (2.3)$$

Where : f_c = uniaxial cylinder compressive strength of concrete.

b. ZSUTTY[11]:

$$V_c = 2.14(f_c\ \rho_s\ d/a_v)^{1/3} \quad (N/mm^2) \quad (2.4)$$

2.7.1.b Yield strength of longitudinal reinforcement:

Tests by Mathey and Watstein[14] have shown that shear strength is not as dependant on yield point of longitudinal steel as it is on the longitudinal reinforcement ratio ρ_s. These tests were carried out on beams without any shear reinforcement and with shear–span to depth ratios varying from 1.5 to 3.8 . At failure, splitting cracks along the reinforcement were observed, showing the effect of dowel action.

Unlike pure flexural failure where the ultimate load is governed by the product of (longitudinal reinforcement ratio, ρ_s) and (steel yield strength, fy). In shear failure, the effect of dowel action was found to be very important. In fact, it was found that the most important factor in the longitudinal reinforcement is not its yielding strength as one would excpect it to be, but its total area, because of its contribution to dowel shear force.

2.7.1.c Cutoff and bent–up reinforcement:

Major inclined cracks frequently develop near the ends of reinforcing bars cut off in tension zone. Adjacent to a cutoff point the stresses and deformations are decreasing in the cutoff bars and increasing in the remaining bars. This combined with the eccentric pull in the cutoff bars, leads to a state of high shearing and diagonal tensile stresses in the vicinity of the cutoff.

Baron[13] has shown that the changes in moment arm in the region lead to increased shear in the cutoff zone.

These tests[13] with others[15] show that :

1– Cutting off bars in tension zone will lower the shear strength of a beam.

2– Closely spaced stirrups in the cutoff zone will prevent premature failure.

3– Bending bars up instead of cutting them off will largely nullify these ill effects, probably because the bend discontinuity is less severe. On the hand a major inclined crack frequently occurs at the bend point.

2.7.1.d Web reinforcement:

It was shown in a comprehensive survey of test data regarding the influence of web reinforcement, that small amounts of web reinforcement have a significantly larger effect on the the shear strength than predicted by the modified truss analogy.

A few tests on beams with bent up bars as shear reinforcement have been reported by Leonhardt and Walter[17]. These tended to have a lower shear strength and much wider cracks than similar beams with stirrups.

2.7.2.Concrete strength:

Equations (2.3) and (2.4) indicate that the shear strength of beams without shear reinforcement can be considered as being proportional to $(f_c)^{1/n}$, n being taken as 2 or 3.

Most of the test data on shear is on concrete with cylinder strength $f_c < 40$ N/mm^2. Recently there has been considerable interest in the shear resistance of high strength concrete[18]. However, it should be observed that failure of beams without shear reinforcement becomes even more sudden and more explosive as its strength increases.

2.7.3 Dimensions of beams:

2.7.3.a The shear span to depth ratio (M/V.d or a_v/d):

It is now well established, that the shear–span to depth ratio is one of the most important, if not the most important factor influencing the shear strength of reinforced concrete beams and as it gets smaller, the structural action can be assumed to be one of a strut and tie, giving an enhanced shear strength[19]. Therefore many investigators take it as a major parameter in their studies.

2.7.3.b Effect of size:

It was reported from several tests that the relative shear strength of reinforced concrete beams without shear reinforcement decreases as the size of the beams increases. Furthermore it was found that the shear stress at failure decreased with increasing beam depth [17,20,21]. Most of this work was carried out before recent ideas on the mechanisms of shear force transfer had been fully developed. Hence, little attention was paid to scaling concrete cover and reinforcement layout (affecting dowel strengths) and maximum aggregate size (affecting interlock).

Taylor[21] argued that the increased shear strength of shallow beams was due to lack of scaling of the aggregate size. Since crack widths in shallow beams are smaller, they would have enhanced interlock strengths leading to greater shear capacity. He showed in the tests he carried out with the size of aggregate scaled that, there is a smaller scale effect in comparison to previous investigators, accepting the fact that, even when the aggregate is scaled, beams tend to lose strength as their size increases.

However, it appears reasonable to expect that, while V_c has a scale effect V_s has little if any, and therefore there is smaller effect of size on beams with web reinforcement.

2.7.3.c b/d ratio of rectangular beams:

The effect of b/d ratio in rectangular beams has been studied by **Diaz De Cossio** [22], **Leonhardt** and **Walter**[17] and **Kani**[20].

Diaz De Cossio found that the shear strength of beams without web reinforcement increases with b/d ratio. **Leonhardt** and **Walter** who tested slab strips also found slightly higher nominal ultimate shear stresses than in normal beams. **Kani** did not find any significant change in strength when the beam width was increased from 150mm to 600mm.

2.7.3.d Flange width:

Regan[9] and others , have reported an increase in resistance of beams with web reinforcement as the flange width increases.

2.7.3.e Type of loading:

In most beams tests the loads and reactions are applied on the top and bottom of the beam respectively. Such beams are said to be *'directly loaded'*. For directly loaded beams with a_v/d ratios less than 2.5, this leads to a significant vertical compressive stress component between the load and reaction and as a result the shear strength is increased.

Frequently in practice, beams are loaded or supported by intersecting beams so that the load transfer is by shear rather than by bearing on the top and bottom surface. These are referred to as *'indirectly'* loaded beams and a number of investigators have reported tests of such beams[23,24] Fig.(2.13).

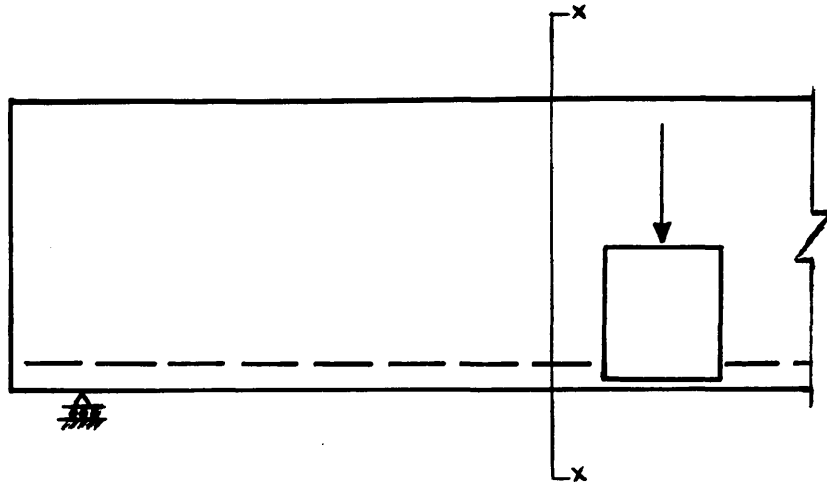

Beam loaded by an intersecting beam

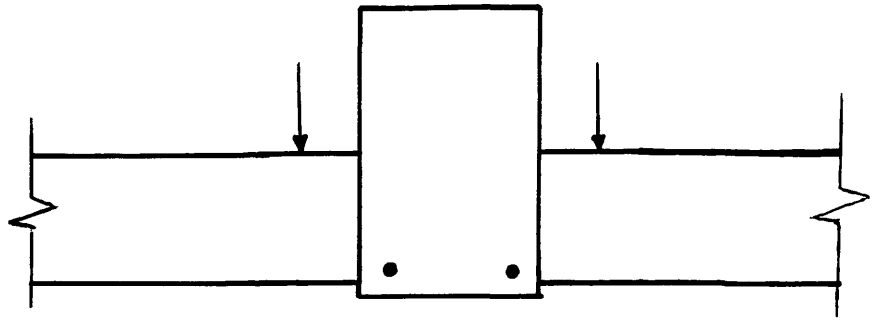

Cross section X–X

FIGURE (2.13) Example of indirectly loaded beams

For beams having a_v/d ratios greater than 2.5 to 3.0 there was no reduction in shear strength in such beams due to indirect loading provided that there was sufficient reinforcement in the intersection region to transfer the load from the supported member to the supporting member.

For a_v/d less than 2.5, however, indirectly loaded beams are weaker than directly loaded beams as arch action cannot develop mainly because while in directly loaded beams the load tends to create compressive paths, in the indirectly loaded beams it tends to create tensile stresses which act as pull out forces causing tensile cracks to develop in the zone above that where load is applied. Such beams tend to fail in diagonal tension at the inclined cracking load.

2.8 METHODS AND MODELS OF ANALYSIS OF SHEAR STRENGTH OF BEAMS

In the search for a general understanding of the shear failure mechanisms and for simple realistic models which would provide a basis for determining the failure loads of reinforced concrete beams, many attempts have been made, and a number of models have been proposed.

In this section a brief review is given of some of these conceptual models for beams with and without stirrups.

Certainly a review of this kind cannot do justice to the vast amount of research work carried out in this field. Nevertheless, this study should give the reader a general appreciation of the types of models proposed over the years.

2.8.1 Beams without web reinforcement:

Various theoretical approaches have been suggested for the behaviour of beams without web reinforcement under the action of shear forces. These are briefly reviewed in this section.

2.8.1.a Analytical shear compression theories:

These theories consider the load carrying capacity of concrete in its compression zone due to shear, e.g. Bresler[25], Ojha[26]. The forces acting on the free body above the shear crack are shown in Fig.(2.14). In this approach any force transfer across the inclined crack by dowel action or aggregate interlock action is ignored. The external load is supported by an inclined thrust in the concrete above the crack and the horizontal component of the thrust at the support is resisted by the tension steel acting as a tie Fig.(2.14).

These theories are now only of historical interest. They represent the first serious attempts to analyse the shear capacity of beams without stirrups. However, it should be noted that these theories are unrealistic, in that they ignore any shear force transfer across the diagonal crack. Acharya and Kemp[12] showed by means of series of careful experiments that this assumption leads to unacceptably high stress in the concrete at the tip of the diagonal crack.

2.8.1.b Concept of the concrete cantilever:

The causes of the diagonal mode of failure are generally considered to be associated with the response of the concrete to the force transmitted to it from steel through bond in the region of shear span below the neutral axis[27,28]. In fact, it has been observed that an improvement of bond between steel and concrete, which should result in an increase in the force transmitted to the concrete, leads to a significant reduction of the load sufficient to cause diagonal failure[27].

It has been suggested that, under the action of the bond forces, concrete between consecutive flexural cracks reacts as a cantilever fixed to the compression zone of the beam[27] Fig.(2.15).

Kotsovos, stated that in spite of a number of detailed investigations of the stress conditions of a concrete cantilever[6], the above assumption neither explains why the diagonal crack leading to failure invariably initiates near the tip of the flexural crack closest to the support, nor is it compatible with the formation of a diagonal crack, which is indicative of failure of the support (compressive zone) of the cantilever rather than the cantilever itself.

2.8.1.c Concept of the compressive path:[3]

Although the presence of shear forces is essential for the occurence of diagonal failure, the cause of it may only be partially attributed to shear forces. In fact, it has been suggested that the causes of such a failure are very closely related to the shape of the path along which the compressive force is transmitted to the supports and not with the stress conditions in the region of the beam below the neutral axis, as widely believed.

On the basis of the concept of the compressive force path, it has also been found that collapse of beams never occurs after the compressive strength of concrete is exceeded, and that even in the compressive zone where concrete fails under combined compressive and tensile stresses, failure occurs by splitting of the compressive zone connecting the point where the load is applied to the the supports rather than by *'crushing'* of the loading point region as it is generally thought Fig.(2.16).

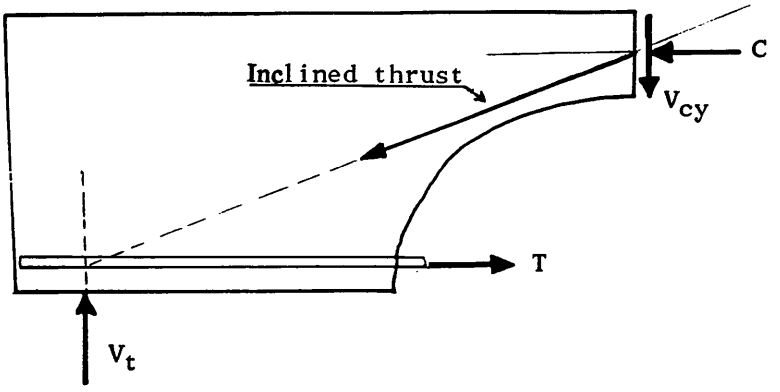

FIGURE 2.14 : Forces acting on free body above shear (ignored are : dowel and aggregate interlock)

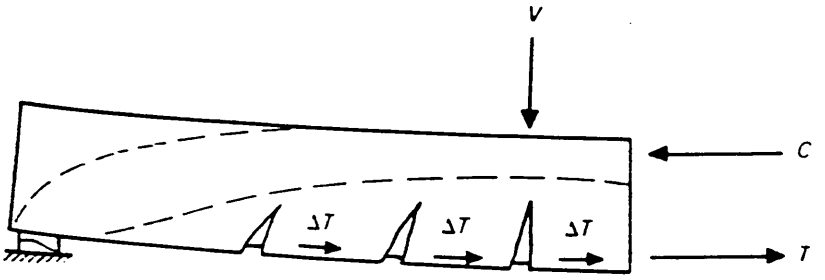

FIGURE 2.15 : Concrete cantilevers

Finally, it appeared from experiment that, unlike the concept of shear capacity of critical sections (which forms the basis of current shear design procedures), the concept of compressive force path provides a rational explanation of the shear failure of beams, and therefore it may form a suitable basis for review of these procedures[3].

2.8.2 Beams with web reinforcement:

2.8.2.a Truss analogy:

At the begining of this century **Ritter** and **Morsch** introduced the truss analogy for the design of web reinforcement in beams. The internal structure of a beam containing shear cracks is assumed to act as a pin jointed truss in which the concrete compression zone and the tensile steel are the main chords, while the vertical shear reinforcement and strips of web concrete inclined at 45° to the tension steel form the lattice Fig.(2.17).

This method of design was widely used in codes of practice. In its most common form the crack angle is assumed to be 45°. This model is extremely over simplified, ignoring the shearing forces V_{cy}, V_{ay}, and V_d.

Regardless of its shortcomings, however, it is an excellent conceptual tool in the study of beams with web reinforcement. It shows correctly the effect of variation in the stirrup angle on the stresses in each member of the truss.

In the last 25 years, various interesting attempts have been made to modify the basic truss model. These attempts were mainly along the following lines :

i) Decrease of angle of concrete struts in the web.

ii) Sloping of compression chord to take account of direct arch action Fig(2.18).

iii) Consideration of bending stiffness of compression members.

iv) Introduction of compatibility conditions.

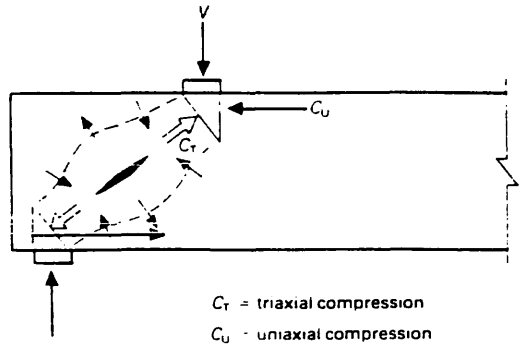

FIGURE 2.16 : Stress conditions within shear span

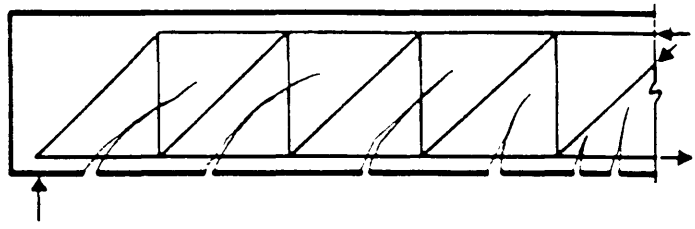

FIGURE 2.17 : Classical Truss Analogy

For example **Leonhardt**[17] proposed a modified truss model which now forms the basis for the shear provisions in CEB code. This was based on extensive series of tests carried out at Stuttgart University.

2.8.2.b Arch analogy:

Arch analogy like truss and frame analogies, representing behaviour of reinforced concrete beams subjected to flexure and shear, were recognized in the earliest investigations. Observations of crack patterns in different beams suggested such analogies, the aims of which were to reduce the complexity and indeterminancy of the actual cracked beams.

For example, in a beam cracked as shown in Fig.(2.14) an element between adjacent cracks can be isolated and considered as a *'tied arch freebody'* Fig(2.9).

Here, neglecting dowel action in longitudinal reinforcement, the transverse shear is carried by stress components along the arbitrary arch boundaries in the uncracked parts of the beam.

The arch ribs are capable of supporting transverse loads only as long as they act essentially in compression, not in bending. Without transverse reinforcement only short deep beams can develop tied–arch action. As the length of the span increases, bending develops in the rib and failure occurs. With transverse reinforcement Fig.(2.10) it is possible to develop arch action in longer spans, and substantial shear loads can be transmitted essentially by compression forces in the arch ribs.

Partly because the geometry of the arch rib elements is not precisely defined, and partly because stress analysis of a system of statically indeterminate arches is relatively complicated, this analogy has been used largely as a model to describe beam behaviour, rather than as a precise analytical tool.

2.8.2.c Frame analogy:

This model was proposed as an analogy consisting of curvilinear concrete elements, which more nearly approximate the geometry of the concrete segments in a cracked beam, and linear steel elements, which represent longitudinal and transverse reinforcement Fig.(2.19).

The nodal points are considered rigid joints, and the stiffness of the frame elements is varied along their length to approximate stiffness of the beam segments. Analysis of such a frame is greatly complicated by the irregular geometry of its elements and by the difficulty of defining the appropriate stiffness of each element.

It is clear that none of the above analogies provides a sufficiently accurate and, at the same time, sufficiently simple solution. Therefore, when the finite element method was first developed, it gave a very good alternative as a general analytical tool for studying the behaviour of reinforced concrete beams, this method will be presented in detail in chapter four.

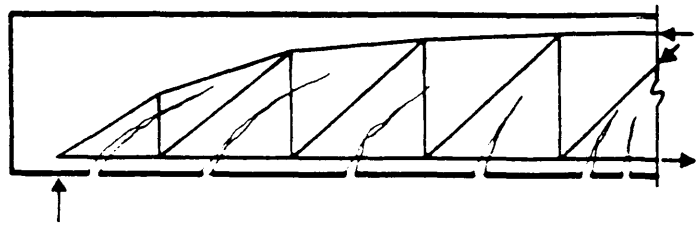

FIGURE 2.18 : Modified Truss Analogy

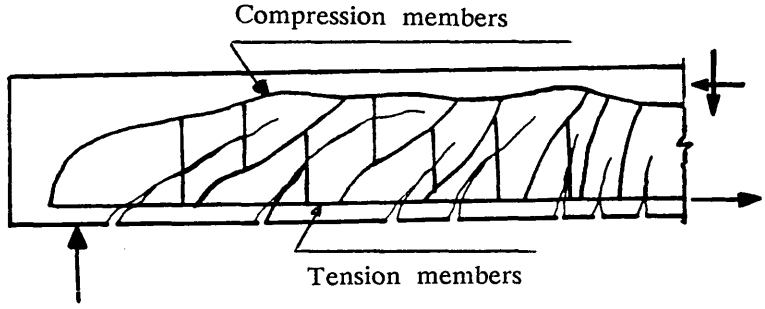

FIGURE 2.19 : Frame Analogy

CHAPTER 3

MATERIAL BEHAVIOUR AND NUMERICAL MODELLING

3.1 INTRODUCTION

A reliable prediction of behaviour of reinforced concrete structures requires a fundamental knowledge of the physical properties, and the behaviour of concrete under variour stress combinations. Developing of laws governing the deformation behaviour of the structure accurately, requires a good material law based on experimental data. Recently, a great deal of test data has become available with respect to the deformation and strength properties of concrete under various stress states.

It would be preferrable to combine the information obtained experimentally with some basic theory in order to produce a set of mathematical formulae for use in analyses. With the present state of development of powerful computer programs based on the finite element method, inadequate modeling of reinforced concrete material still remains a major factor in limiting the capability of accurate structural analysis. This is because reinforced concrete has a very complex behaviour involving phenomena such as inelasticity, cracking, and interactive effects between concrete and steel. Mainly for this reason, the problem of defining a suitable law for it still persists, although much progress has been made in the development of material models for uncracked and cracked concrete for all stages of loading, and as a result of it, several numerical models have been developed[33].

3.2 MECHANICAL BEHAVIOUR OF CONCRETE

3.2.1 General:

Despite the widespread use of concrete as a structural material, our knowledge about its exact physical properties and behaviour under various stress combination is rather deficient. This is not surprising to any one who is aware of the heterogeneous structure of concrete. In fact, concrete contains a large number of microcracks at the interfaces between coarse aggregate and mortar, and this even before any load has been applied. This is the primary reason for the low tensile strength of concrete materials. During loading, the propagation of these microcracks contributes enormously to the nonlinear behaviour of concrete at low stress level and causes dilatancy when nearing failure.

3.2.2 Uniaxial state of stress:

The behaviour of concrete under uniaxial compression loading can be explained with the aid of the uniaxial stress–strain curve in Figure (3.1). When concrete is subjected to small compressive loads, it behaves in a quasi–elastic manner. Under increasing loads, deviation from linearity takes place. The material has got only limited ductility and under high compressive stresses, the material fails by crushing Fig.(3.2).

For mathematical representation of experimental stress–strain curves of plain concrete, many formulae have been proposed by different investigators[34,35,36]. These range from the use of standard mathematical curves, to more complex formulae based on curve fitting to experimental data. However, equation (5.1) originally proposed by Liu et al[46], representing uniaxial stress–strain curve for concrete is commonlly used for numerical analysis :

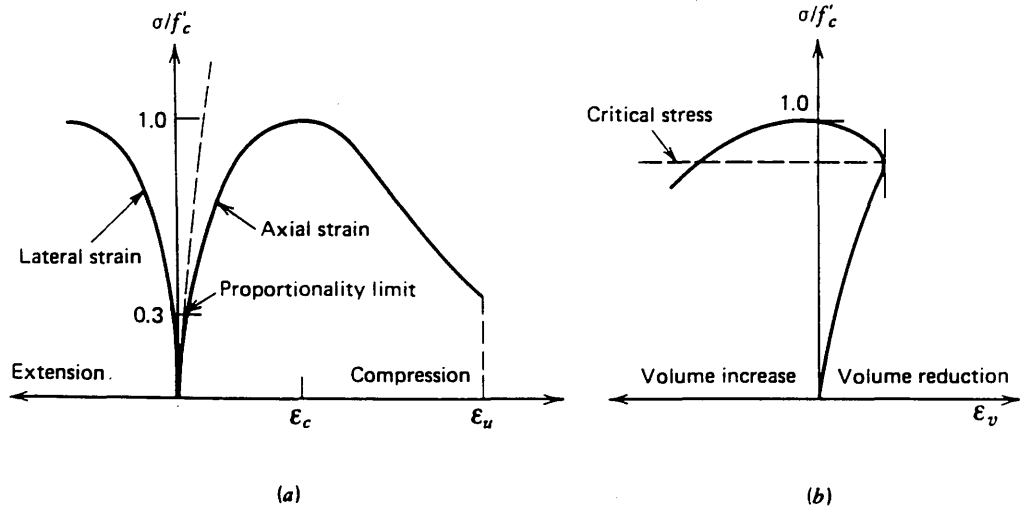

FIGURE (3.1) : Typical stress–strain curves for concrete in uniaxial compression test. (a) Axial and lateral strains. (b) volumetric strain ($\epsilon_v = \epsilon_1 + \epsilon_2 + \epsilon_3$).

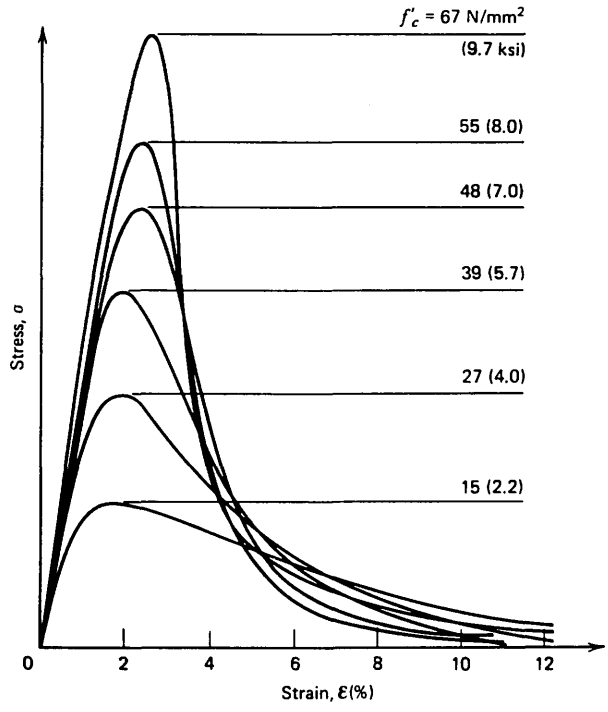

FIGURE (3.2) : Uniaxial compressive stress–strain curves for concrete with different strengths (Wischers, 1978)

$$\sigma = E_c . \epsilon \left[1 + \left(\frac{E_c . \epsilon_p}{\sigma_p} - 2\right)\left(\frac{\epsilon}{\epsilon_p}\right) + \left(\frac{\epsilon}{\epsilon_p}\right)^2 \right]^{-1} \qquad (3.1)$$

Where : σ = is the level of stress reached in the material and corresponding to a state of strain equal to ϵ,

σ_p = is equal to f_{cu}' for uniaxial compression,

f_{cu}' = is the ultimate compressive stress of concrete cube,

ϵ_p = is the strain corresponding to σ_p and may be taken equal to 0.0025 .

Under uniaxial tensile loading, the general mechanical behaviour of concrete, shows many similarities to the behaviour observed in uniaxial compression. Typical stress–strain curves for concrete in uniaxial tension are shown in Figure (3.3)[37]. The curves are nearly linear up to relatively high stress level. More details on the tensile strength of concrete can be found in references[33,34,35,39].

3.2.3 Biaxial state of stress:

Many important classes of structures can be approximated as being in a state of plane stress, such as beams, panels and thin shells. In modeling these structures, tests results for concrete under biaxial states of stress are very useful. Therefore, in recent years, a large amount of research has been done on the mechanical properties of concrete under biaxial loading. In early works, the interest was focused essentially on the strength of concrete. Considerable experimental data are now available regarding strength and deformational characteristics of concrete subjected to biaxial states of stress. With the aid of Figure (3.4a)[44], it is possible to summarize the main observed characteristics of concrete behaviour as follows :

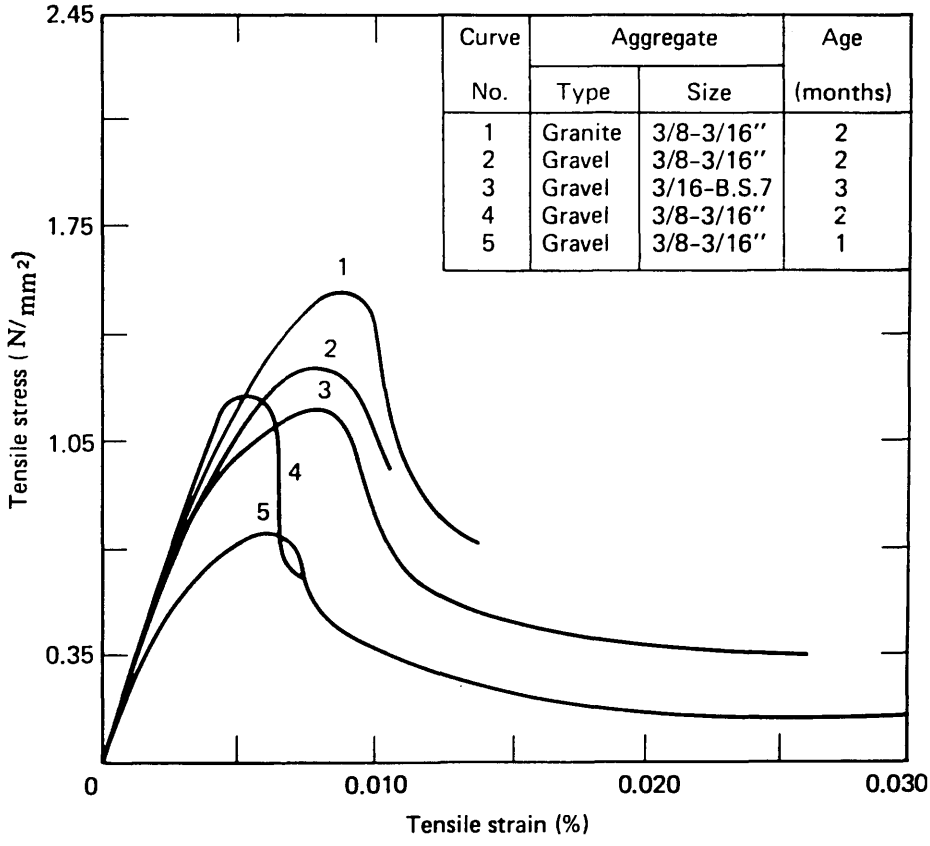

FIGURE (3.3) : Typical tensile stress–strain curves for concrete (Hughes and Chapman, 1966).

1. The ultimate strength of concrete under biaxial compression is greater than that under uniaxial compression. The main reason for this increase is due to the confinement of microcracks.

2. The ultimate strength increase under biaxial compression is dependent on the ratio of principal stresses, and appears to be maximum (up to about 25% higher than the uniaxial value) at a stress ratio of about 0.5, diminishing somewhat (to about 16%) as the ratio is increased to 1.0.

3. The compressive stress at failure in the case of combined compression and tension decreases as the tensile stress increases.

4. The biaxial tensile strength of concrete is approximately equal to its uniaxial strength, and stress–strain curves are similar in shape in both uniaxial and biaxial tension.

5. In biaxial compression–tension, the magnitude at failure of both the principal compressive strain and the principal tensile strain decreases as the tensile stress increases. Figure (3.4b) shows concrete strain under different state of stress.

Further details on the biaxial states of stress can be found in references([33,41]).

3.2.4 Hydrostatic and deviatoric stress vector:

It is convenient in material modeling to decompose the stress vector into two parts, one called the hydrostatic stress vector and the other the deviatoric stress vector i.e. :

$$\{\sigma\} = \{\sigma'\} + \{\sigma''\} \tag{3.2}$$

where the stress vector is given by :

$$\{\sigma\} = \{\sigma_x \ \sigma_y \ \tau_{xy}\}^T \tag{3.3}$$

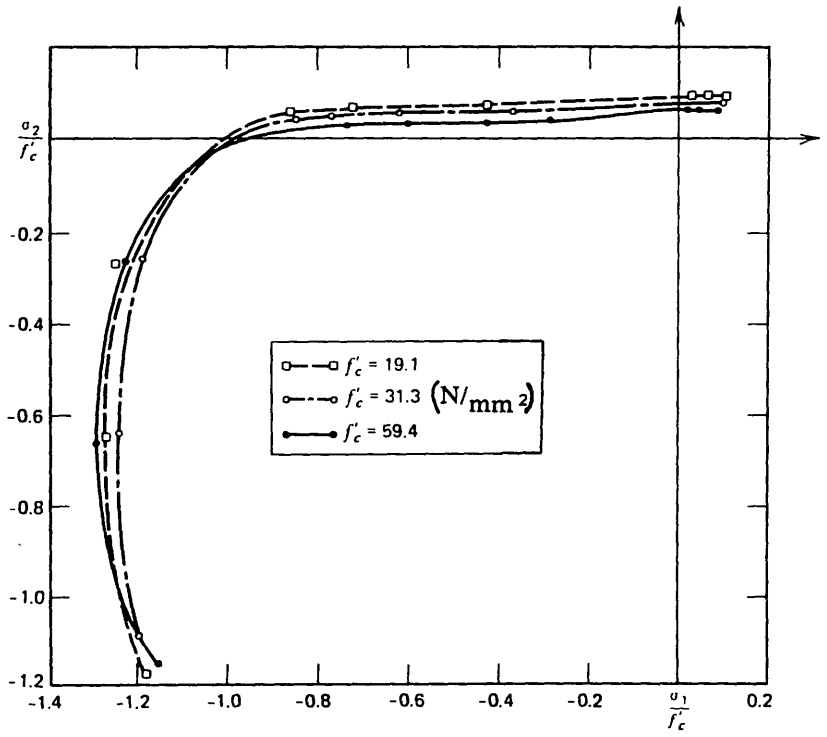

FIGURE (3.4a) : Biaxial strength envelope of concrete (Kupfer et al., 1969).

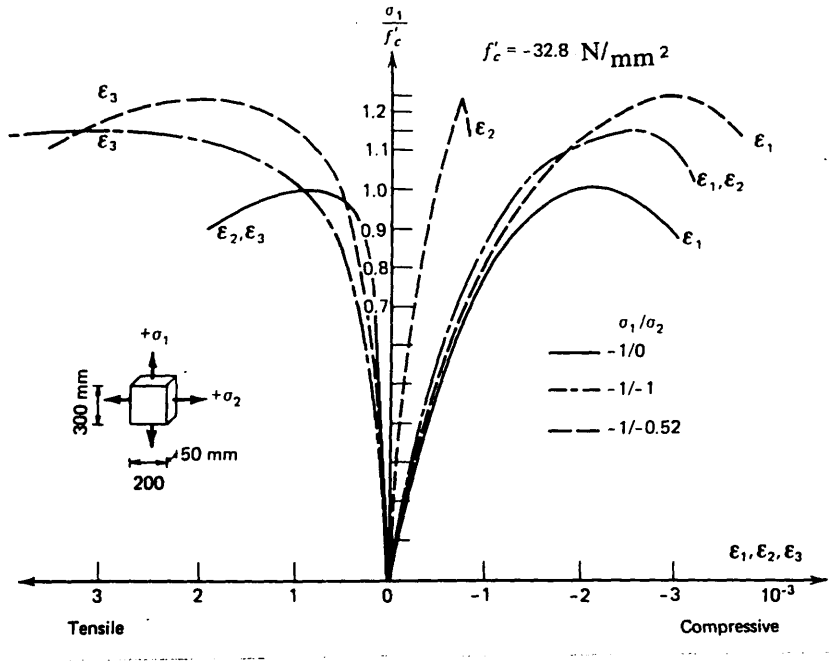

FIGURE (3.4b) : Stress–strain relationships of concrete under biaxial compression (Kupfer, 1969).

and the deviatoric stress vector is given by :

$$\{\sigma'\} = \begin{Bmatrix} \sigma_x' \\ \sigma_y' \\ \tau_{xy}' \end{Bmatrix} = \begin{Bmatrix} \sigma_x - \sigma_m \\ \sigma_y - \sigma_m \\ \tau_{xy} \end{Bmatrix} \tag{3.4}$$

and the hydrostatic stress vector is given by :

$$\{\sigma''\} = \begin{Bmatrix} \sigma_x'' \\ \sigma_y'' \\ \tau_{xy}'' \end{Bmatrix} = \begin{Bmatrix} \sigma_m \\ \sigma_m \\ 0 \end{Bmatrix} \tag{3.5}$$

The mean stress σ_m is given by :

$$\sigma_m = \frac{\sigma_x + \sigma_y}{3} \tag{3.6}$$

The octahedral normal and shear stresses, σ_{oct} and τ_{oct}, respectively, are related to stress invariants I_1 and J_2 as follows :

$$\sigma_{oct} = 1/3\ I_1 = \sigma_m \tag{3.7}$$

and :

$$\tau_{oct} = \sqrt{2}/3\ J_2 \tag{3.8}$$

where the first invariant of stress I_1 is given by :

$$I_1 = \sigma_x + \sigma_y \tag{3.9}$$

and the second deviatoric invariant J_2 is given by :

$$J_2 = 1/3[\sigma_x^2 - \sigma_x\sigma_y + \sigma_y^2] + \tau_{xy}^2 \tag{3.10}$$

3.2.5 Hydrostatic and deviatoric strain vector:

As in the case of stress vector, the strain vector can be decomposed into a hydrostatic part associated with the volume change and a deviatoric part associated with the change in shape (distortion) that is :

$$\{\epsilon\} = \{\epsilon'\} + \{\epsilon''\} \tag{3.11}$$

where the strain vector is given by :

$$\{\epsilon\} = \{\epsilon_x \ \epsilon_y \ \gamma_{xy}/2\}^T \tag{3.12}$$

the deviatoric strain vector is given by :

$$\{\epsilon'\} = \begin{Bmatrix} \epsilon_x' \\ \epsilon_y' \\ \dfrac{\gamma_{xy}'}{2} \end{Bmatrix} = \begin{Bmatrix} \epsilon_x - \epsilon_m \\ \epsilon_y - \epsilon_m \\ \dfrac{\gamma_{xy}}{2} \end{Bmatrix} \tag{3.13}$$

The hydrostatic strain vector is given by :

$$\{\epsilon''\} = \begin{Bmatrix} \epsilon_x'' \\ \epsilon_y'' \\ \gamma_{xy}''/2 \end{Bmatrix} = \begin{Bmatrix} \epsilon_m \\ \epsilon_m \\ 0 \end{Bmatrix} \tag{3.14}$$

ϵ_m is the mean strain given by :

$$\epsilon_m = \frac{\epsilon_x + \epsilon_y}{3} \tag{3.15}$$

It can be shown that for small strains, volumetric strain ϵ_v is given by :

$$\epsilon_v = \epsilon_x + \epsilon_y \qquad (3.16)$$

Thus, the dilatance or simply the volume change is given by :

$$\epsilon_v = 3\ \epsilon_m \qquad (3.17)$$

Similarly to the stress case, the octahedral normal and shear strains, ϵ_{oct} and γ_{oct}, respectively, are related to I_1' and J_2' as follows :

$$\epsilon_{oct} = 1/3\ I_1' = \epsilon_v \qquad (3.18)$$

and :

$$\gamma_{oct} = 2\sqrt{2}/3\ J_2' \qquad (3.19)$$

where I_1' is the first invariant of strain given by :

$$I_1' = \epsilon_x + \epsilon_y \qquad (3.20)$$

and J_2' is the second deviatoric invariant given by :

$$J_2' = 1/3[\ \epsilon_x^2 - \epsilon_x\epsilon_y + \epsilon_y^2\ ] + \tfrac{1}{4}\ \gamma_{xy}^2 \qquad (3.21)$$

Figure (3.5)[44] shows a replotting of the volumetric strains ϵ_{oct} against the first invariant I_1. Then a unique relationship between hydrostatic strain and hydrostatic stress, was suggested. The points at which these curves bend over at the onset of volume expansion is obviously governed by some other criterion, but this seems not to be very significant as it occurs very close to ultimate conditions. Meanwhile, the slight scatter of results may reflect a real dependence on deviatoric stresses. This is not surprising in a frictional material such as concrete. though, this dependence does not appear to be significant.

After examining several types of concrete, it was found that, the averaged curves of ϵ_{oct} against I_1 Fig.(3.6), are fairly linear. Moreover, they were found to become more linear and that the slopes get steeper for higher values of concrete strengths. These slopes represent the *'tangent'* bulk modulus K_T (which is constant for linear elastic material) i.e.:

$$K_T = \frac{d(\sigma_{oct})}{d(\epsilon_{oct})} \tag{3.22}$$

A plot of τ_{oct} against γ_{oct} Fig.(3.7), suggests a fairly unique relationship between the two quantities for the greater part of the loading range. The only diiference between the curves starts near points close to the critical load level.

The slopes of the curve representing τ_{oct} versus γ_{oct}, is in fact tangent values of the shear modulus G_T i.e. :

$$G_T = \frac{d\tau_{oct}}{d\gamma_{oct}} \tag{3.23}$$

which is clearly constant in linear elastic applications.

Thus, evidence suggests that deviatoric strains depend only on deviatoric stresses and hydrostatic strains (volume change ϵ_{oct}) depend only on hydrostatic stress σ_{oct}, and that hydrostatic strains are independent of deviatoric stresses. However, for concrete, and after analysing some test data [47],there was indications that concrete subjected to a constant hydrostatic stress (constant σ_{oct}) and an increasing deviatoric stress ($\tau_{oct} > 0$), not only undergoes compressive octahedral normal strain, γ_{oct} Fig.(3.8)[47], but undergoes consolidation in the form of compressive octahedral normal strain ϵ_{oct}.

Further details about stress and strain invariants can be found in references[33,41].

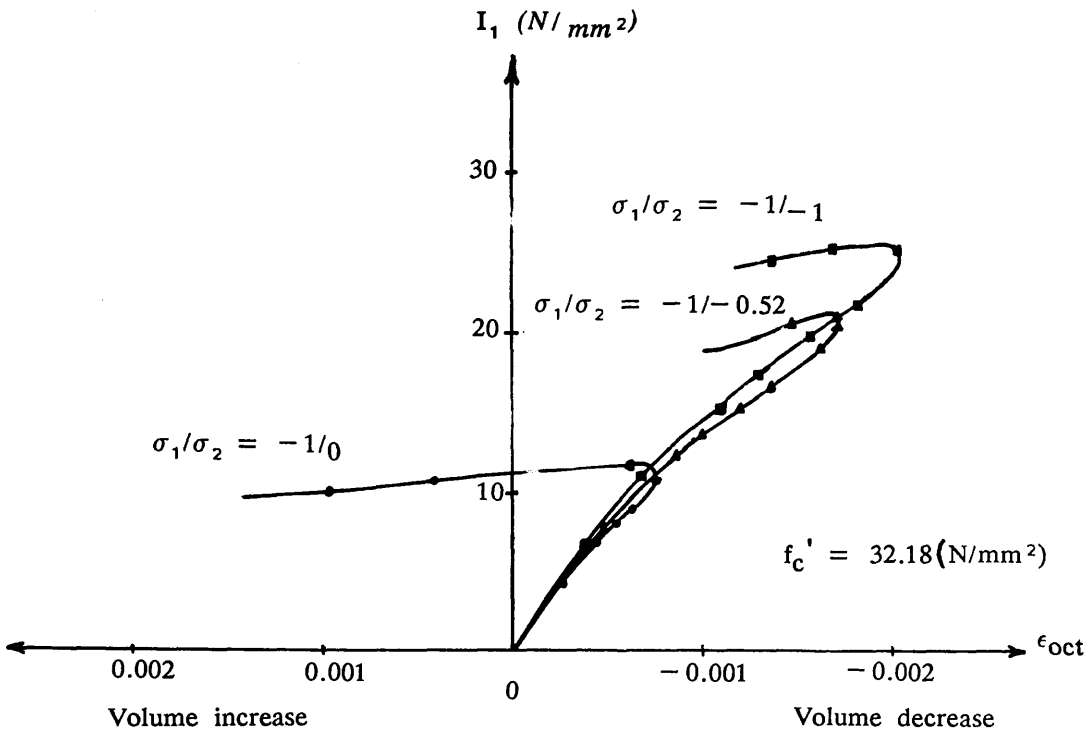

FIGURE (3.5) : Volumetric strain versus 1st invariant curves (Kupfer et al)

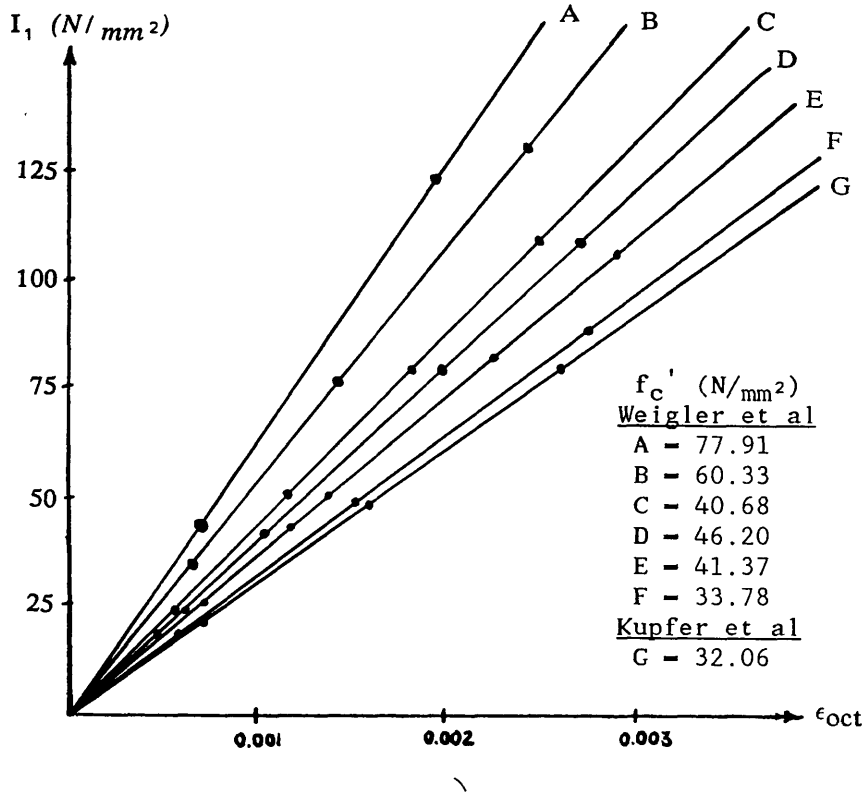

FIGURE (3.6) : A verage I_1 versus ϵ_0 curves.

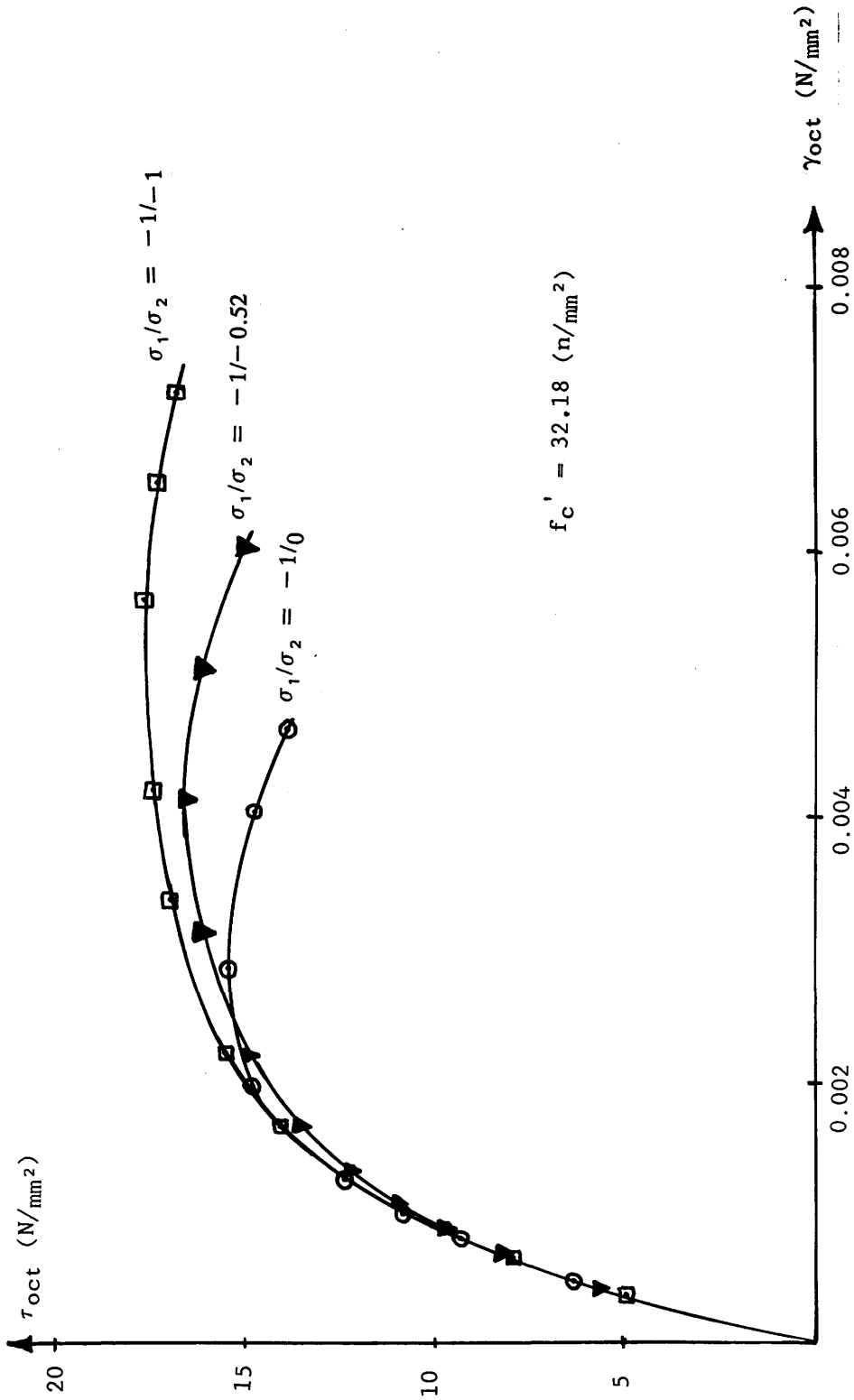

FIGURE (3.7) : τ_{oct} versus γ_{oct} (Kupfer et al).

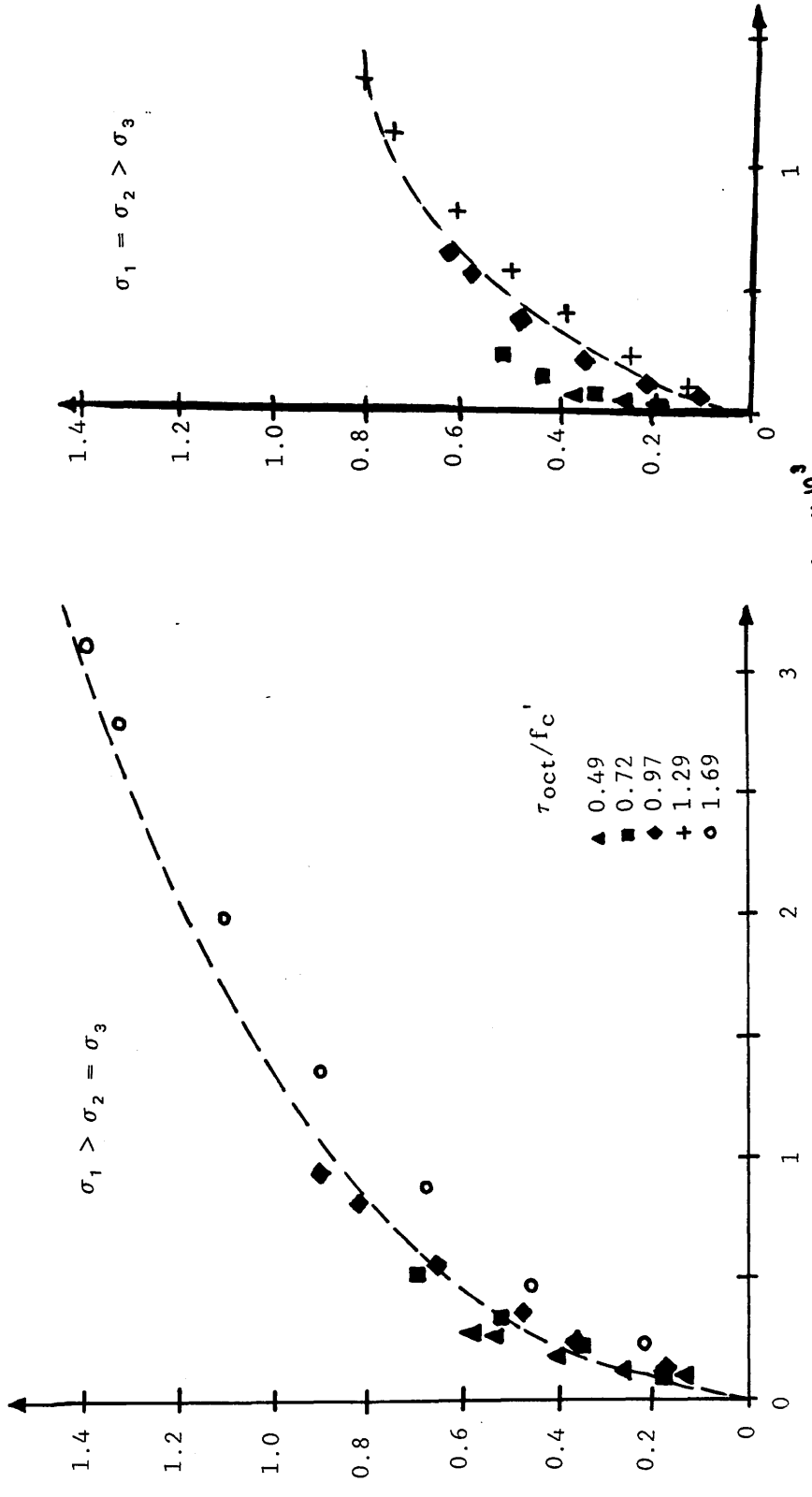

FIGURE (3.8) : Variation of ϵ_{oct} with τ_{oct} for concrete under deviatoric stress portion test test

3.2.6 Failure theories:

In general, failures of concrete can be divided into two types : tensile and compressive types. These are generally characterized by brittleness and ductility, respectively.

Many failure criteria for concrete can be found in the literature. The most commonly used failure criterion are defined in stress space by a number of material constants varying from one to five independent control parameters.

Early proposals have used simple failure models of one– and two–parameter types which are suitable for manual calculations. With the advent of computer technology and as more test data have become available, these simpler models have been refined and generalized by adding additional parameters.

a) The brittle fracture of concrete under tensile and small compressive stresses is best described by the maximum tensile stress criterion of Rankine (1876). This criterion assumes that cracking occurs when the maximum tensile stress in any direction exceeds a limiting value equal to the tensile strength f_t.

b) Another theory used to predict cracking failure is the maximum tensile strain theory, it is assumed that cracking occurs when a maximum tensile strain reaches a limiting value. These two theories are very similar, and are identical for $\nu = 0$. Figure (3.9) compares the two criteria against a typical two dimensional failure envelope for concrete in the tensile domains, and while the stress criterion overestimates the fracture stress, the strain criterion underestimates it.

c) In the intermediate compressive stress range, the failure criteria of concrete are sensitive to hydrostatic states of stress. The simple one–parameter models described above are not adequate for describing failure in the fracture–ductile

state under this intermediate level of compressive stresses, and therefore pressure–dependent failure models must be used. The simplest and most commonly used models of this type are the Mohr–Coulomb and Drucker–Prager failure criteria. In the Mohr–Coulomb criterion, failure is assumed to occur when the shear stress, τ, at a point in a concrete material reaches a value that depends linearly upon the normal stress, σ, this is expressed as :

$$| \tau | = c - \sigma \tan\Phi \qquad (3.24)$$

where c and Φ material constants that represent the cohesion and angle of internal friction, respectively Fig.(3.10).

d) To obtain a better approximation when tensile stresses occur, it is sometimes necessary to combine the Mohr–Coulomb criterion with the maximum tensile stress criterion. This has been suggested by Cowan (1953)[48] among others. It should be noted that this combined criterion is a three–parameter criterion.

e) Many stuctures can be modeled quite adequately as two–dimensional structures subjected to a state of plane stress. Biaxial maximum stress (or failure) envelopes serve a useful purpose for this case.

As widely accepted representation is that developed by (Kupfer, Hilsdorf and Rush; 1969)[44]. As illustrated in Figure (3.11), the failure surface is expressed individually for the regions of biaxial tension, tension–compression and biaxial compression :

Biaxial Tension:

Since there is no increase in the ultimate strength due to biaxial tensile state of stress the simple circular condition was sufficient i.e. :

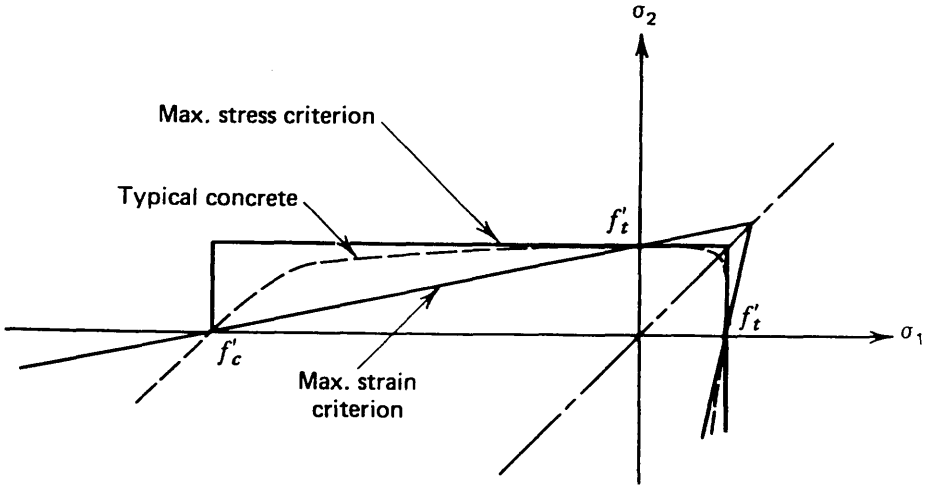

FIGURE (3.9) : Comparison of biaxial failure criteria in tensile zones

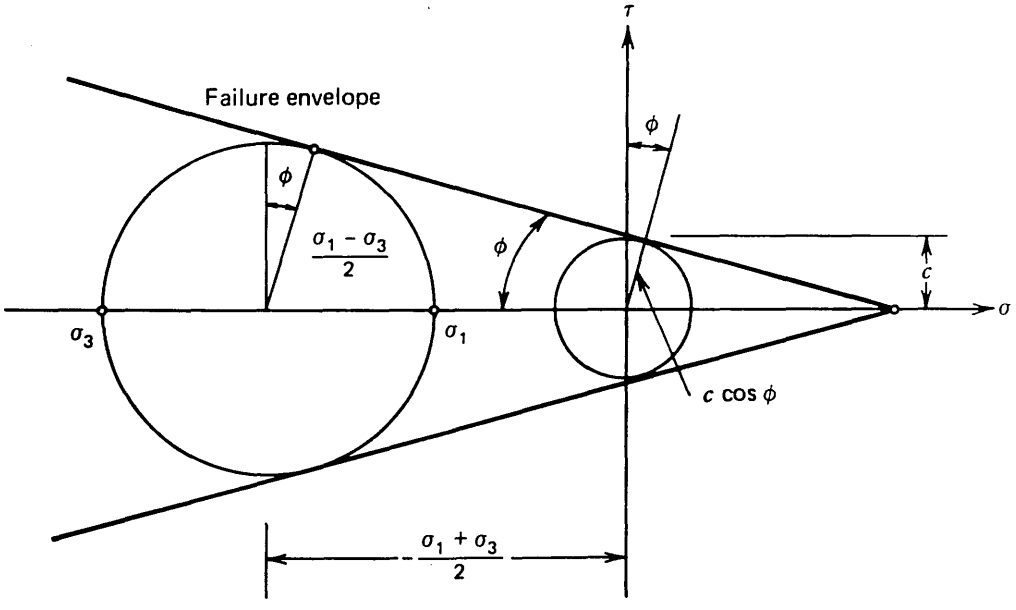

FIGURE (3.10) : Relationships between principal stresses for Mohr–Coulomb criterion

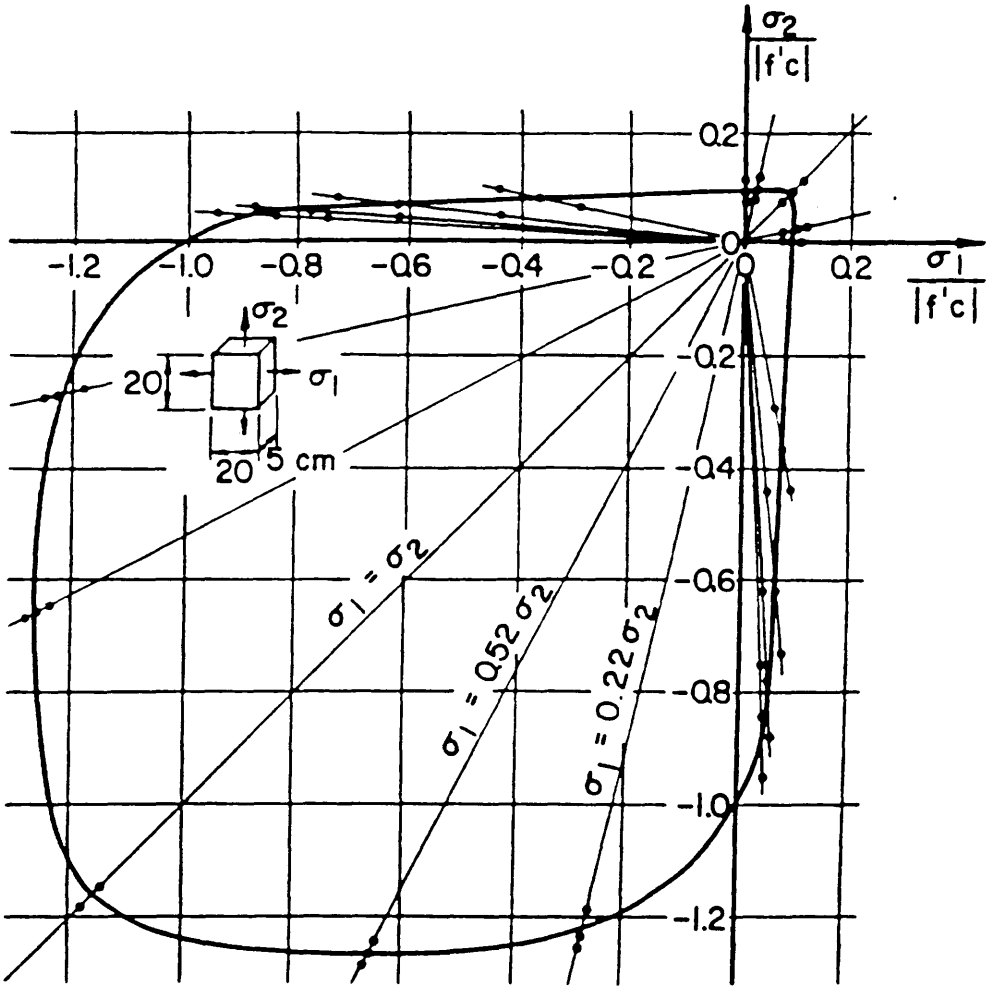

FIGURE (3.11) : Yield surface for biaxial stress in plain concrete (Kupfer, Hilsdorf, and Rush).

$$\left[\frac{\sigma_1}{f_t}\right]^2 + \left[\frac{\sigma_2}{f_t}\right]^2 - 1.0 = 0.0 \qquad (3.25)$$

Very often simple principle tension criterion is used.

Tension–Compression:

$$\frac{\tau_{oct}}{f_c'} + \sqrt{2}\,\frac{1-m}{1+m}\,\frac{\sigma_{oct}}{f_c'} - \frac{2\sqrt{2}}{3}\,\frac{m}{1+m} = 0.0 \qquad (3.26)$$

with m the ratio of concrete tensile to compressive strength.

Biaxial Compression:

$$\frac{\tau_{oct}}{f_c'} + 0.1714\,\frac{\sigma_{oct}}{f_c'} - 0.4143 = 0.0 \qquad (3.27)$$

3.3 MECHANICAL BEHAVIOUR OF STEEL

As steel is normally in the form of slender bars, which are consequently loaded mainly in direct compression or tension, it is generally not necessary to introduce the complexity of a multiaxial constitutive relationship for it. Hence, its behaviour can be adequately approximated by the uniaxial stress–strain curves.

A typical uniaxial stress–strain diagram for steel is shown in Figure (3.12). Initially, the relationship is linear and elastic. After reaching the '*proportional limit*' P, and for further small range of stress increase, this relationship remains elastic but no longer linear. The '*yield point*' is then reached and this marks the start of plastic deformation. The difference between P and Y is slight for most materials and is usually neglected in practical applications. Beyond the yield point, plastic flow occurs with strain increasing at a much greater rate than before. Generally, further deformation are caused by an increase in stress and

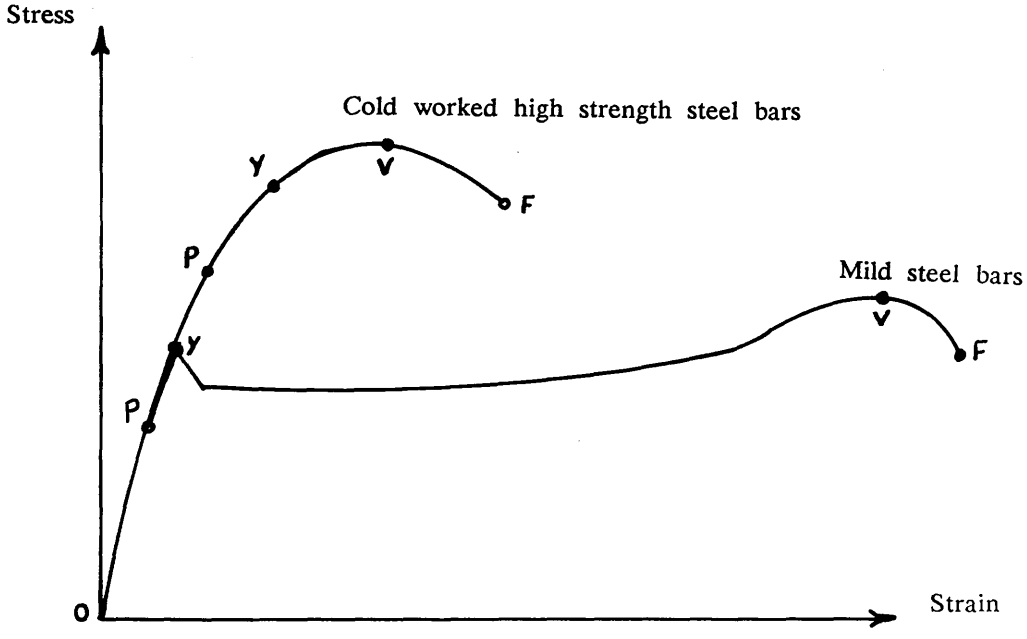

FIGURE (3.12) : Typical steel used in reinforcement.

this condition is termed strain or work hardening. Eventually, a maximum stress is reached at point V, after which a descending tail rapidly reaches fracture at F.

For practical purposes, steel exists in various forms. Basically, these are :

1. Plain round hot–rolled bars of either, mild steel, medium–strength steel, or high strength steel. Yield stresses vary from about 250 N/mm^2, to 360 N/mm^2, whilst the corresponding ultimate strength vary from 460 N/mm^2, to 600 N/mm^2.

2. Cold worked bars, or high tensile steel bars. Such reinforcement exhibits considerably higher yield stresses.

The Young's modulus of steel E_s is around 2.0×10^5 N/mm^2. Figure (3.12) shows typical stress–strain curves for mild steel and high tensile strength cold worked steel.

3.4 INTERACTION PROPERTIES

3.4.1 Shear retention factor:

As explained earlier (section 2.5.1), prior to any crack formation, shear transfer is provided by solid concrete. The interaction of shear, tensile and compressive normal stresses produces principal stresses which may cause inclined cracking. After cracking shear forces are transferred across the crack by aggregate interlock. However, due to cracking, shear modulus G is reduced to a smaller value. This is expressed by :

$$G' = \beta.G \qquad (3.28)$$

where G : initial shear modulus

G': reduced shear modulus of cracked concrete.

β : shear retention factor.

It is appreciated that, as the crack widens less aggregate interlocking is produced and as a result the value of the shear retention factor β is reduced to a smaller value.

The shear retention factor was introduced by Phillips[32] and (Schnobrich et al)[49]. It was defined as an assumed numerical factor < 1.0 .

There are two main methods using the shear retention factor :

a) The constant shear retention factor method, where β is chosen rather arbitrarily and kept constant[49].

b) The variable shear retention factor method, where β is assumed to vary as a function of the strain normal to the crack[50,52], or as a function of the average crack width[51]. Some of these models are given by :

1) $$\beta = 0.4.G/(\epsilon/\epsilon_{cr}) \qquad (3.29)$$

2) $$\beta = 1.0 \qquad \text{For} \quad \epsilon_{cr} < \epsilon \qquad (3.30a)$$

$$\beta = \frac{(\beta_1-\beta_2)}{(\beta_3-1)}\left(\beta_3 - \frac{\epsilon}{\epsilon_{cr}}\right)+\beta_2 \qquad \text{For } \beta_3.\epsilon_{cr} > \epsilon \geqslant \epsilon_{cr} \qquad (3.30b)$$

$$\beta = \beta_2 \qquad \text{For } \epsilon \geqslant \beta_3.\epsilon_{cr} \qquad (3.30c)$$

where ϵ and ϵ_{cr} are the current and cracking strain, respectively, and β_1, β_2, and β_3 are material constants[52]. when β_1 is set to 0.0 then we have the constant shear retention factor method.

Figure (3.13) shows curves representing different models for shear retention factor.

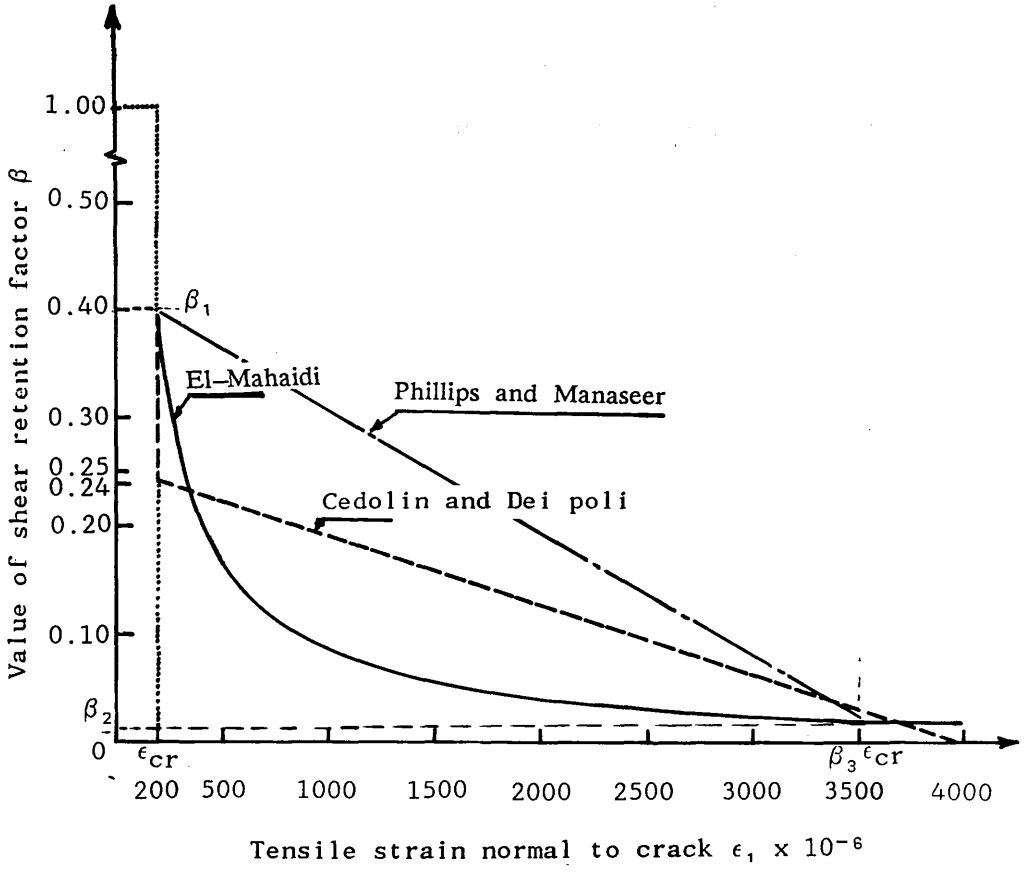

FIGURE (3.13) : Different relationships giving values of shear retention factor β

3.4.2 Tension stiffening

When cracks occur in reinforced concrete all the tensile force across these cracks is carried out by the tensile reinforcement Fig.(3.14a). However in the part of concrete between cracks the force is shared between steel and concrete Fig.(3.14b). This ability of concrete to share the tensile force between cracks is termed tension stiffening. This method of taking into account tension stiffening was introduced by Phillips[32] and Schnobrich[84] in early seventies. Ever since, it has been used by many investigators to show that it can have a significant effect on load deflection behaviour of structures. Several approaches have been used for approximating tension stiffening, e.g : a descending branch beyond the cracking point, and the use of coarse convergence tolerance[52].

Currently, the descending branch approach is most commonly used Fig (3.14c). The following are expressions of one of the model used[52] :

$$\sigma = \frac{\alpha_2 f_t \ (\alpha_1 - \epsilon/\epsilon_{cr})}{(\alpha_1 - 1)} \qquad \text{For } \alpha_1 . \epsilon_{cr} > \epsilon \geq \epsilon_{cr} \qquad (3.31a)$$

$$\sigma = 0.0 \qquad \text{For } \epsilon \geq \alpha_1 . \epsilon_{cr} \qquad (3.31b)$$

where : f_t = the tensile strength of concrete

ϵ_{cr} = the concrete cracking strain

σ, ϵ = stress and strain normal to the crack directions

α_1, α_2 = material constants.

3.4.3 Bond–slip and dowel action:

Bond stress is the name given to the shearing stress on the steel–concrete interface and parallel to the bar axis. By means of this bond, forces are transferred from the steel bar to the surrounding concrete and vice versa. This

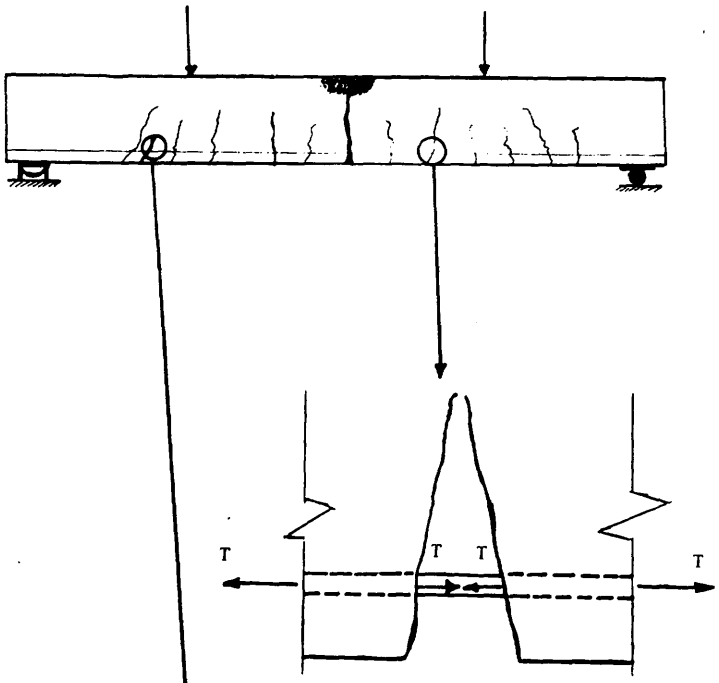

FIGURE (3.14a) : Tensile force across the crack carried out by reinforcement

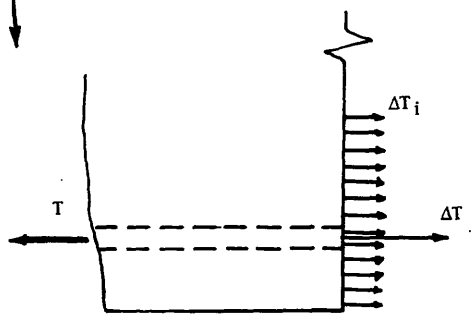

FIGURE (3.14b) : Tensile force in the part of concrete between cracks shared between steel concrete $\Sigma \Delta T_i + \Delta T = T$

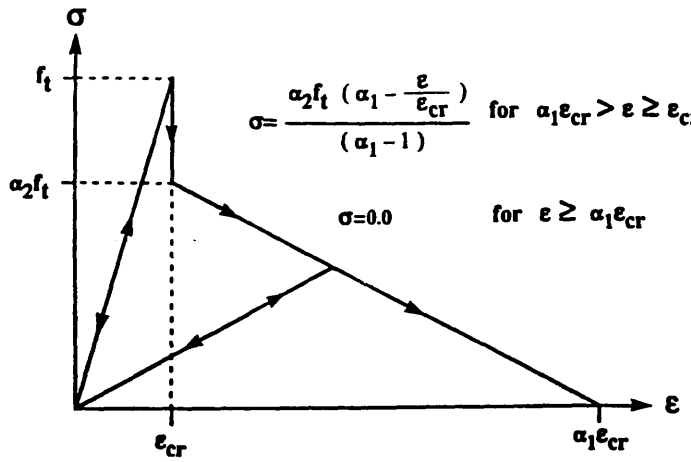

FIGURE (3.14c) : Tension stiffening model

bond between concrete and steel results from chemical adhesion, friction and mechanical interaction between concrete and steel.

For plain reinforced bars, chemical adhesion and friction are the major contributory factors to the bond strength, while mechanical interaction plays a minor role.

Considerable slip has been observed between the steel bar and the concrete, suggesting the loss of adhesion at relatively low stresses[42]. Bond failure is a common phenomenon in beam shear tests, where beams are reinforced with plain bars. This type of failure is characterized by the separation of the bar from the concrete.

Deformed bars were introduced to alter this behaviour patttern, and the projecting deformations, ribs or lugs, add to the bond resistance by bearing on the concrete and thereby minimizing slip considerably.

Furthermore, other factors may well affect the ultimate bond strengths[43] such as : type of loading, concrete cover, bar spacing, etc...

Normally full bond is assumed. However, bond–slip elements have been used in some studies to allow for bond–slip phenomenon[85].

Moreover, reinforcing bars also act as dowels as shown in Figure (3.15), generally, this happens when major shear deformations occur after tension cracking has occured. As a result, the bar will take concentrated shear force.

Many factors can affect the dowel action such as : bar diameters, geometry of the tested beam, length of the reinforcement and its arrangement, concrete cover, degree of restraint of the bar provided by shear links.

3.5 CONCRETE NUMERICAL MODEL

3.5.1 Introduction:

The remaining part of this chapter is concerned with the detailed formulation of the constitutive relationships of concrete and steel used in this study.

The laws for each material are developed separately, the process of combining these should then duplicate the composite response of reinforced concrete. Moreover, individual behaviour of each material is then available, and bars can be discretely placed. For these reasons, this approach is preferred to the alternative policy where homogeneous equivalent mass of reinforced concrete is used. The behaviour of concrete is treated in two distinct phases :

1. The linear–brittle response under tensile stresses, including compression–tension zones,
2. and the apparent ductile response and crushing under compressive stresses.

The first is undoubtebly the most important feature of nonlinearity in concrete, and is therefore emphasized above all.

Cracking is handled by adjusting stresses and material properties in the cracked zones, hence, natural crack directions are obtained, and redistribution of stresses are taken into account.

The model for approximating the compressive response of concrete, is based on the relationships between the deviatoric and volumetric components of stress and strain.

In finite element analysis three different approaches have been most commonly used for the representation of the cracks. These are (1) smeared cracking modeling, (2) discrete cracking modeling, and (3) fracture mechanics modeling. The particular cracking model to be selected from the three alternatives depends on the purpose of the analysis. However, for most strucural engineering applications, the smeared cracking modeling is generally used.

(i) Smeared– cracking Model

The cracked concrete is assumed to remain a continuum i.e the cracks are smeared out in a continuous fashion. A crack is not discrete but is represented by an infinite number of parallel fissures across the concrete element, as shown in Figure (3.16). Once concrete is cracked, the material is assumed to change from isotropic to an orthotropic with one of the material axes being oriented along the direction of the crack.

The smeared cracking model was used in this work.

(ii) Discrete– cracking Model

In discrete cracking models, the nodes of the adjacent elements are assumed to be separated when a crack occurs, as shown in Figure (3.17). The most obvious difficulty in this approach is that the occurence, location and orientation of cracks are not known in advance. Thus, geometrical restrictions imposed by the preselected finite element mesh can hardly be avoided. The model also requires, the ability to redefine the element nodes, making this technique extremely complex and time consuming.

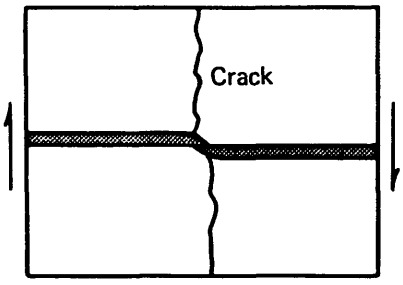

FIGURE (3.15) : Interactive effect between concrete and reinforcement: Dowel effect

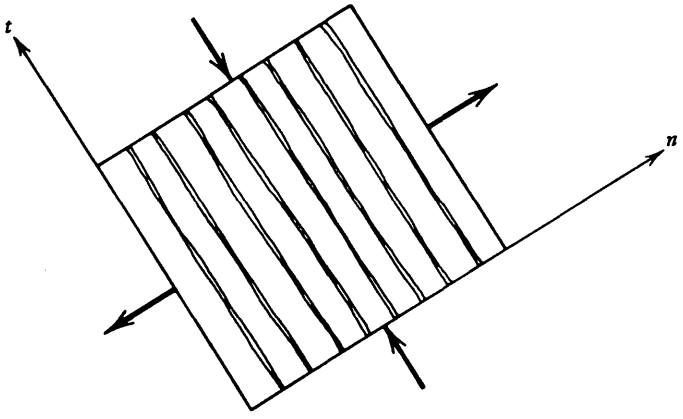

FIGURE (3.16) : Idealized representation of a single crack in the smeared cracking modeling approach

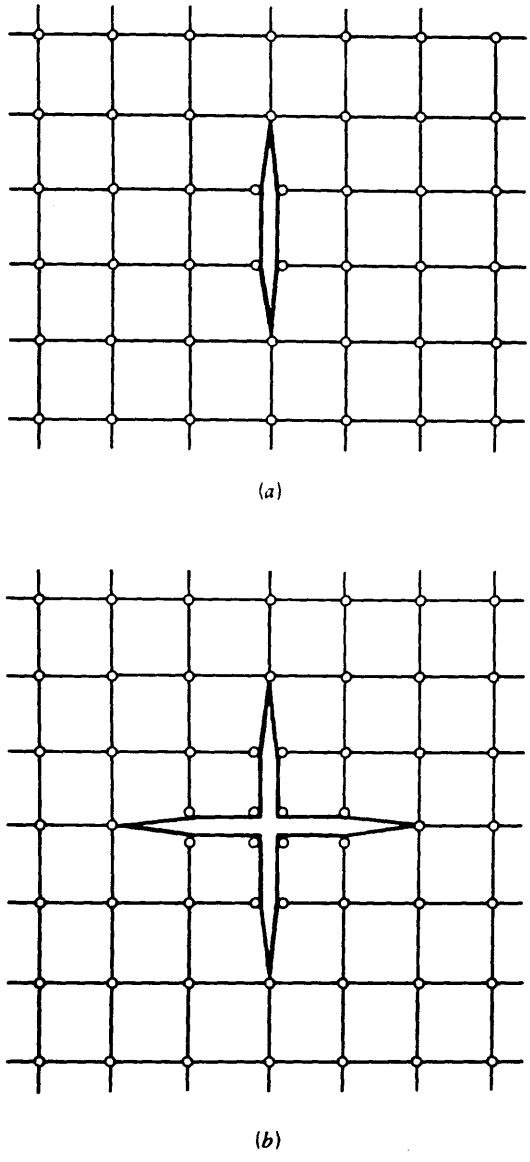

FIGURE (3.17) : Cracking representation in discrete cracking modeling approach. a) One-directional cracking. b) Two-directional cracking.

(iii) Fracture– mechanics Model

The success of fracture– mechanics theory in solving various types of cracking problems in metals, ceramics, and rocks has lead to its use in finite element analysis of reinforced concrete structures. However, in its current state of development, the use of this model in reinforced concrete is still questionable and much remains to be done[41].

3.5.2 Crack simulation:

a. Opening of cracks:

The basic hypothesis of the fracture model is that, when a principal stress exceeds the limiting tensile stress, the material cracks in a plane normal to the offending principal stress. The angle of the crack is then fixed once and for all. Thus, for cracking :

$$\sigma_i \geqslant f_t \qquad i = 1, 2 \qquad (3.33)$$

It is assumed that up to the point of cracking, concrete behaves linearly in tension Fig.(3.14). This is advatageous, as unloading will retrace the same linear path if cracking has not occured.

Initially, concrete is assumed to be homogeneous and isotropic. However, after undergoing fracture, the material assumes orthotropic properties. When a crack first occurs, it is assumed that direct tensile stresses cannot be supported in the direction normal to the crack Fig.(3.18). In this work, the tension stiffening is not taken into account, therefore the tensile stress drops to a negligeable value once the crack has occured Fig.(3.19). Moreover, the modulus of elasticity is instantaneously reduced to a comparatively small value. It is assumed that

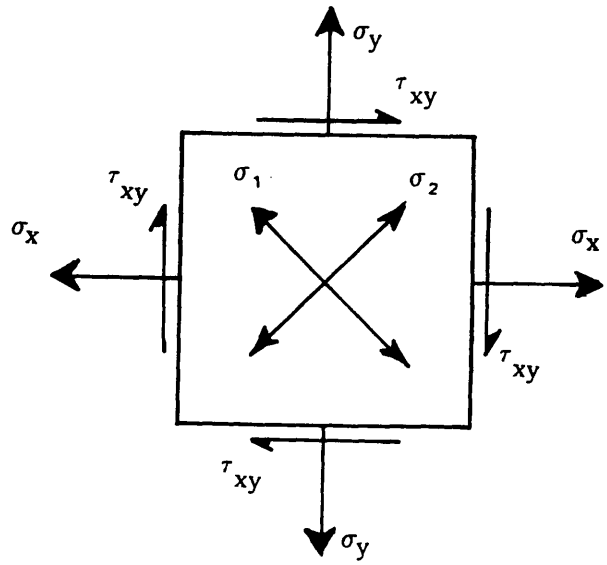

Stress before cracking

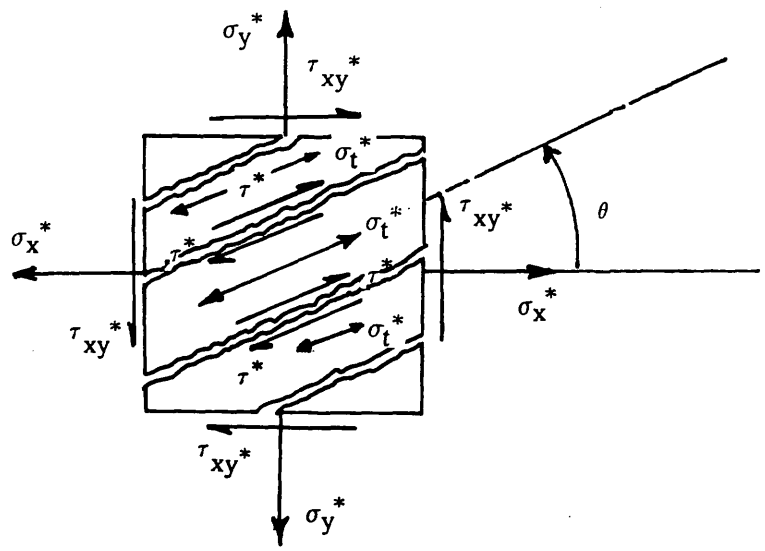

stress after cracking

FIGURE (3.18) : Cracking model

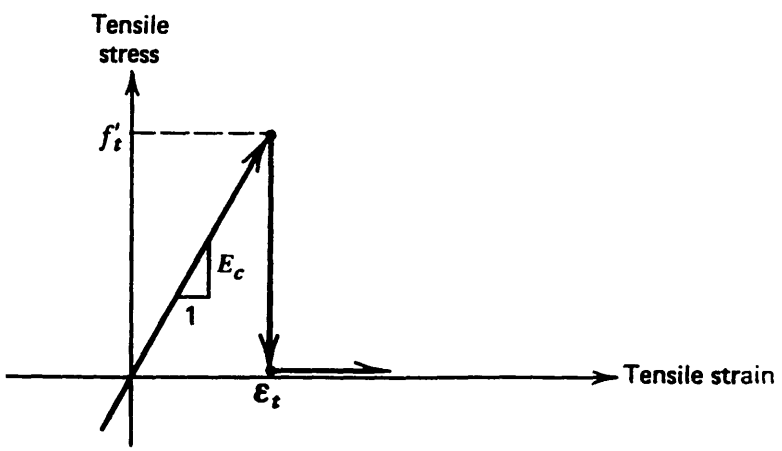

FIGURE (3.19) : Assumed tensile elastic–fracture relationship.

material parallel to the crack is still capable of carrying stress given by new constitutive relationships consistent with the uniaxial or biaxial conditions prevailing in the plane parallel to the crack. On further loading, it is possible that new cracks will occur. For simplicity, it is assumed that the cracks occurs orthogonal to each other. Thus, for further cracking :

$$\sigma_t^* \geqslant f_t \tag{3.34}$$

where : σ_t^* is the stress parallel to the crack.

b. <u>Shear on open cracks:</u>

In general, the surfaces of a crack are rough and irregular. Although a crack may be open in normal direction, it is possible that opposite faces will interlock when subject to differential movement. Aggregate interlocking is undoubtedly a complex phenomenon depending on many factors, and unfortunately very inadequate information exists concerning its behaviour. The frictional forces due to this aggregate interlock and the subsequent volume changes are then transmitted accross the crack. These frictional forces are dependent mainly on the properties of the aggregate and mortar. With increasing differential movement, these frictional forces reduce considerably as the crack suface is altered (becoming smoother), and if the crack keeps widening, it would completly separate and as a result there would be no interlock action at all.

One of the most important effect of the interlock action is that shear along the crack will not be zero. In fact, it is taken into account by a simple artifice called '*shear retention factor* β', whereby the shear strain along the crack is assumed to represent the differential movement, and the shear stress is thereafter evaluated as a linear function of this strain.

i.e : $$\tau^* = \beta\, G\, \gamma^* \tag{3.35}$$

where : G = is the shear modulus of the original uncracked material,

τ^*, γ^* = are shear stress and strain along the crack.

and β = is a preselected constant such that : $0 \leqslant \beta \leqslant 1$.

In this approximation, it is implicitly assumed that the relationships between normal stresses and strains perpendicular and parallel to the crack are uncoupled from any shear behaviour along the crack. When shear stress exists, then neither principal strains nor stresses will coincide in direction with the crack, nor probably with each other.

c. Closing of cracks:

On further loading, it is possible that a crack will close. However, the condition for this to occur is dependent on complex factors. In practice, it is probable that differential movement between faces of the crack causing deterioration of surfaces, will result in preventing the crack from closing perfectly.

However, through lack of any definite data, it is assumed that cracks do close perfectly, and thus the following procedure was adopted. If the normal strain across the crack is compressive, this will close, hence :

$$\epsilon_n^* < 0 \tag{3.36}$$

and then compressive stress can again be transmitted across the crack. Thus, there is now a plane of weakness along the crack and shear resistance will depend on a number of factors. This problem is similar to that of interlocking, therefore, same analogous solution was adopted :

$$\tau^* = \alpha \, G \, \gamma^* \tag{3.37}$$

where : α = is a preselected constant such that : $0 \leqslant \alpha \leqslant 1$.

In this work ($\alpha = 1$) was adopted, implying a perfect *'healing'* of the crack.

Clearly, if a crack re–opens the same procedure as before will apply except that now this condition is recognised by tensile strain across the crack, i.e. for re–opening cracks :

$$\epsilon_n^* \geqslant 0 \tag{3.38}$$

3.5.3 Constitutive relations:

At any stage of loading the incremental stress is related to the incremental strain by the following expression :

$$\Delta\{\sigma\} = [D_T]\, \Delta\{\epsilon\} \tag{3.39}$$

where $[D_T]$ is the tangential elasticity matrix.
For uncracked concrete, and in the case of plane stress, the tangential elasticity matrix is given by :

$$[D]_T = \frac{E}{(1-\nu^2)} \begin{bmatrix} 1 & \nu & 0 \\ \nu & 1 & 0 \\ 0 & 0 & \frac{(1-\nu)}{2} \end{bmatrix} \tag{3.40}$$

where : E = Young's modulus for concrete

and ν = Poisson's ratio.

The onset of cracking will introduce orthotropic conditions, and new incremental constitutive relationships will apply for material parallel to the cracks. Total normal stress across the crack is reduced to zero, and a new elasticity matrix in crack directions takes place and is given by :

$$[D]_T^* = \begin{bmatrix} 0 & 0 & 0 \\ 0 & E & 0 \\ 0 & 0 & \beta G \end{bmatrix} \qquad (3.41)$$

3.5.4 Tangent elasticity matrix $[D_T]^*$:

At this stage, it is perhaps necessary to examine what is implied by the tangent elasticity matrix $[D_T]^*$ in the context of cracking without any compressive nonlinearity. After cracking, the constitutive laws are still linear elastic, which means that if there is unloading the curve will pass through the origin, i.e. no residual strains will exist. The only change is that an orthotropic material is now defined. Thus, $[D_T]^*$ is not a tangent matrix in the orthodox sense, but is an instantaneous elaticity matrix reflecting a sudden change from one elastic state to another.

Overall, this implies that crack propagation is, in effect, solved by a series of transitions from one instanteneous elastic stiffness to another, each of which radiate from the origin of a load–displacement diagram.

When using $[D_T]^*$ for new stiffness calculations, it is essential, for numerical reasons, to avoid zero values on the diagonals. Thus, if a crack has occured, the value of the corresponding diagonal term is set to a comparatively small value.

As $[D_T]^*$ is constructed in a coordinate system coinciding with the angle of crack, it is necessary to transform it back to the global coordinate system for stiffness calculations.

3.5.5 Compressive model:

a. Basic assumptions:

It was apparent from experimental evidence in section 3.2 that hydrostatic stress markedly influences the behaviour of concrete. Therefore, a model based on deviatoric and hydrostatic stress and strain has been used. It was demonstrated previously that approximately unique relationships existed between volumetric strain and hydrostatic stress, and between deviatoric stress and strain, until close to failure. Therefore, it is assumed that the deformational response can be represented by unique relationships which continues until failure. The deformational response is then simulated in an incremental manner by assuming the tangent bulk modulus to be a function of I_1 :

i.e. $$K_T = f_1(I_1) \qquad (3.43)$$

and the tangent shear modulus to be a function of J_2 :

i.e. $$G_T = f_2(J_2) \qquad (3.44)$$

For sake of simplicity, the material is assumed to be isotropic throughout loading.

The invariant relationships are obtained directly from the curves of I_1 versus ϵ_{oct} Fig.(3.6), and τ_{oct} versus γ_{oct} Fig.(3.7). From a number of experimental data Phillips[32] ploted $\sqrt{J_2}/f_c'$ versus G_T/G_0 where the tangent bulk modulus K_T was assumed constant Fig.(3.20). From that experimental data it was found that, for plots of G_T versus $\sqrt{J_2}$ the only differences for the whole range of loading, start to be apparent fairly close to ultimate stress.

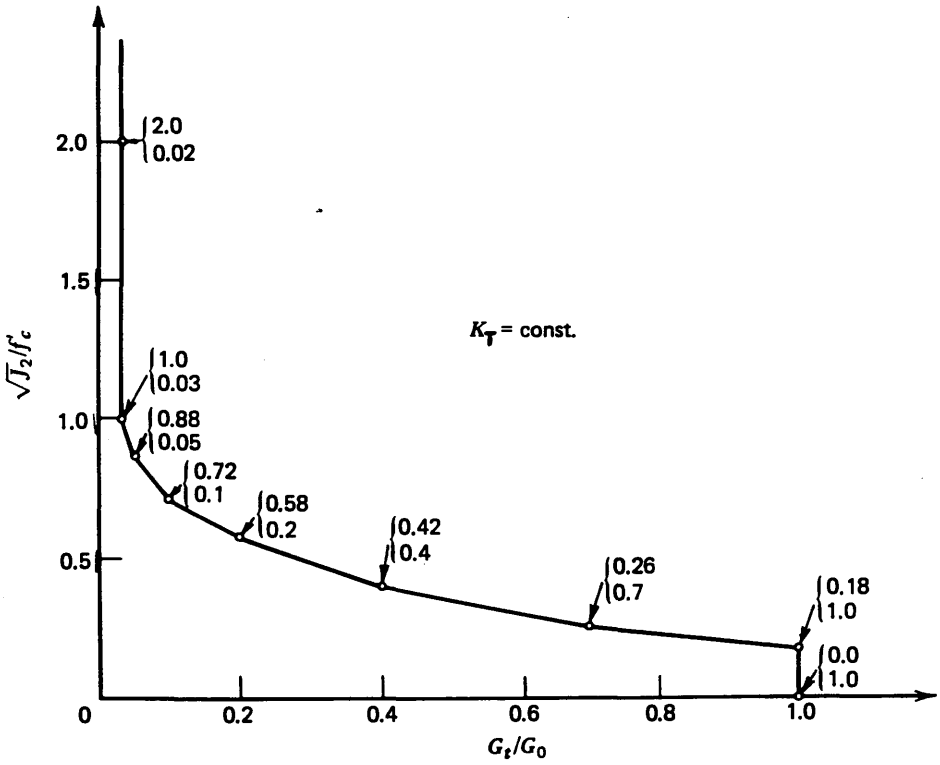

FIGURE (3.20) Variation of the tangent shear modulus, G_t, as a function of J_2 (Phillips and Zienkiewicz, 1976).

b. Procedure:

Curves relating G_T to $J_2^{\frac{1}{2}}$, and K_T to I_1 are introduced as linear piecewise curves, specified in tabulated form such that a value of I_1 (or $J_2^{\frac{1}{2}}$) is entered with a corresponding value of K_T (or G_T).

At the beginning of a load increment, values of K_T and G_T are evaluated from a knowledge of I_1 and $J_2^{\frac{1}{2}}$ prevailing at this time. Values of E_T and ν_t are then obtained by using standard expressions :

$$E_T = \frac{9\ K_T\ G_T}{3\ K_T + G_T} \tag{3.45}$$

$$\nu_t = \frac{3\ K_T - 2\ G_T}{6\ K_T + 2\ G_T} \tag{3.46}$$

From which the current tangential elasticity matrix $[D_T]$ is evaluated.
An estimate of incremental stress $\Delta\{\sigma\}$ is then found. Total stress $\{\sigma\}$ follows by accumulating $\Delta\{\sigma\}$ on the previous level of stress $\{\sigma\}_0$,

i.e. $$\{\sigma\} = \{\sigma\}_0 + \Delta\{\sigma\} \tag{3.47}$$

This procedure alone will lead to divergence of the calculated stresses and strains from the specified constitutive law. This divergence is even worse for larger increments. Therefore, a corrective process is introduced to eleminate this effect. With the update values of $\{\sigma\}$, intermediate values of G_T and K_T are evaluated. Final values of G_T and K_T are then calculated by a weighted mean of the original values and these newly calculated ones are:

i.e. $$G_{i+1} = G_i + c'\ (G_0 - G_i) \tag{3.48}$$

$$K_{i+1} = K_i + c'\ (K_0 - K_i) \tag{3.49}$$

where K_0, G_0 are the values at the start of the increment, K_i, G_i are the intermediate values calculated using the first assesment of $\{\sigma\}$, and G_{i+1}, K_{i+1} are the final values. $\Delta\{\sigma\}$ is then recalculated by means of G_{i+1}, and K_{i+1} and new values of total stress are obtained.

This present investigation was carried out with (c' = 0.6) after finding that this factor had no effect on the final result Fig.(3.21).

c. Compression failure:

From the previous section, it was clear that the deformation laws do not apply close to ultimate load relatively to a particular state of stress. Therefore, a criterion identifying this point was used, and causes the termination of this particular nonlinear response.

Thus, octahedral shear stress and normal stress are evaluated using Mohr–Coulomb theory for a particular state of stress $\{\sigma\}$, and ultimate stress conditions are assumed if :

$$\tau_{oct} \geqslant n\,\sigma_{oct} + c \qquad (3.50)$$

where n, and c are octahedral coefficients which can be evaluated from plot of τ_{oct} against σ_{oct} [45] Fig.(3.22).

In this work, it was considered that occurence of crushing reflected ultimate conditions of the actual structure, which would be in a considerable state of desintegration. Therefore a numerical factor (concrete crushing factor,C_f) was used to define behaviour after crushing of concrete. Thus, after peak stress is reached, K_T, and G_T are simultaneously reduced to relatively small values and the stress can be either kept constant or reduced allowing some strain softening in concrete, depending on the value of C_f. The effect of this factor (C_f) will be analysed in chapter 6.

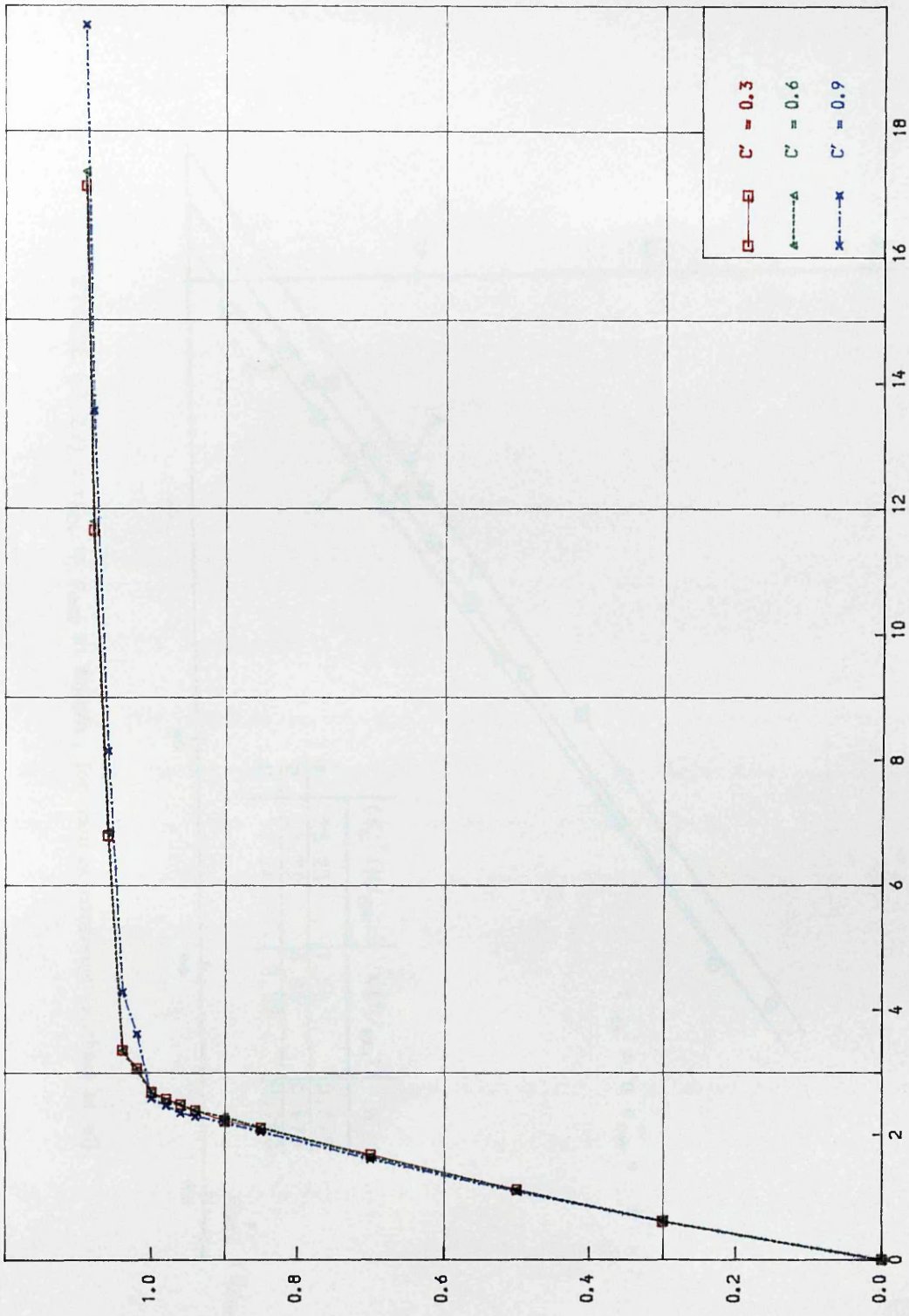

BEAM MID-SPAN DEFLEXION CURVE VARYING WITH C'

FIGURE (3.21) EFFECT OF C' ON FAILURE LOAD AND MODE OF FAILURE OF R.C. BEAMS

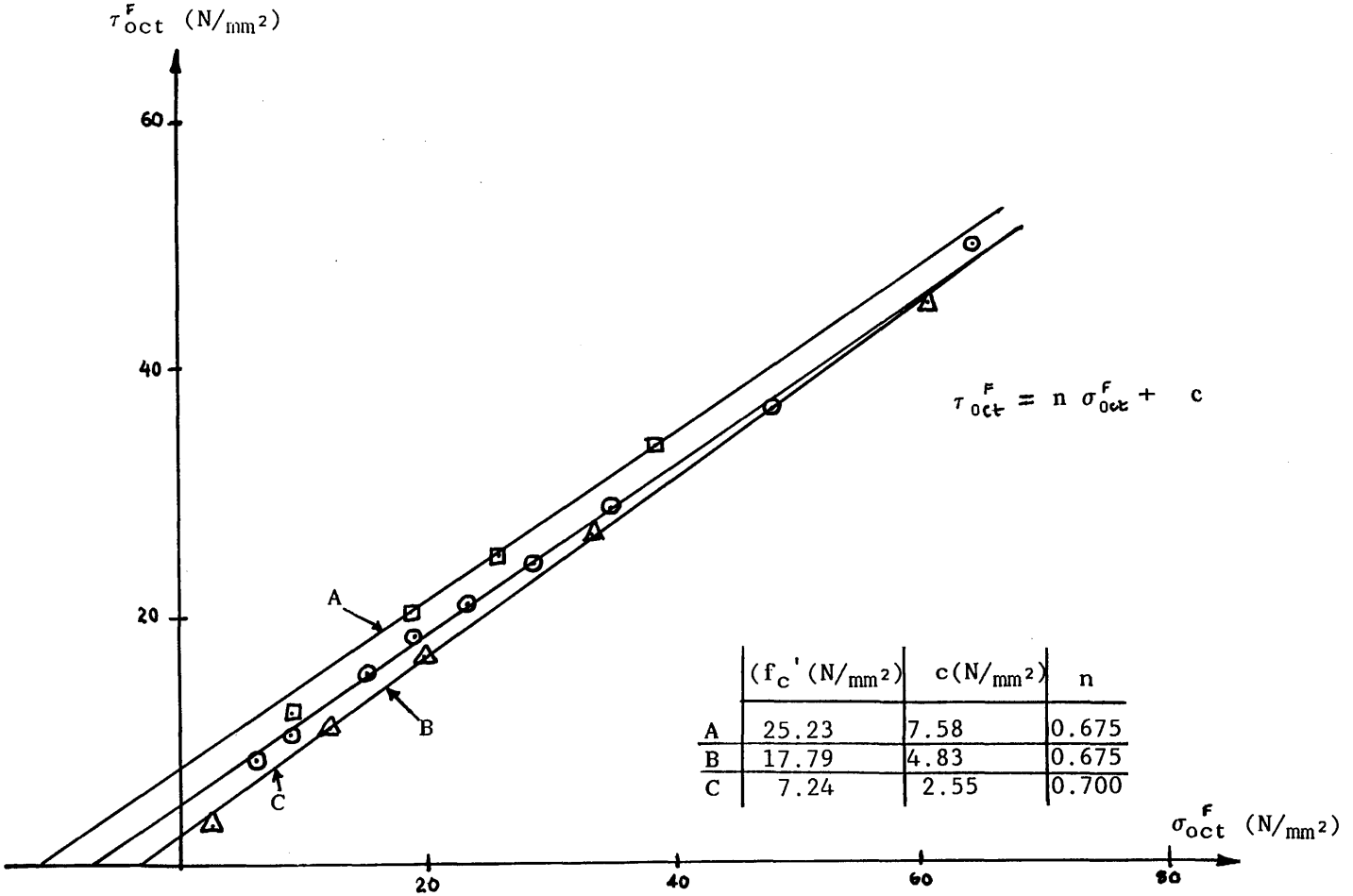

	$(f_c'$ (N/mm²)	c(N/mm²)	n
A	25.23	7.58	0.675
B	17.79	4.83	0.675
C	7.24	2.55	0.700

FIGURE (3.22) : τ_{oct} vs σ_{oct} at failure , for various concretes (Richart et al).

3.6 Numerical modelling of reinforcement:

There three possible representations for steel in finite element modeling Fig.(3.23) :

3.6.1 Smeared approach:

The steel is assumed to be distributed over the concrete element, with a particular orientation φ, but capable of resisting forces only along the bar direction. A composite concrete reinforcement constitutive relation is used in this case, assuming full bond. A stiffness matrix is built for the distributed steel separately then added to the stiffness matrix due to concrete to form the global stiffness matrix of an element.

3.6.2 Discrete representation:

The reinforcement herein, are represented using one dimensional elements. This representation has been most widely used. Axial force members, or bar links, may be used and assumed to be pin connected with two degrees of freedom at nodal points. One–dimensional reinforcement elements are easily superimposed on a two–dimensional finite element mesh.

3.6.3 Embedded representation:

This can be used in connection with higher order isoparametric concrete elements. The reinforcement bar is considered to be an axial member built into the isoparametric element such that its displacements are consistent with those of the main element. This type of representation is used in this study.

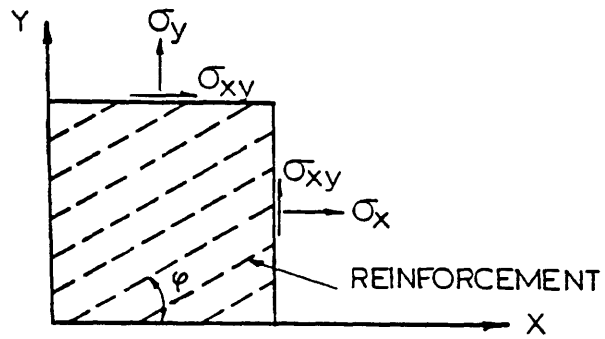

a) Smeared Approach

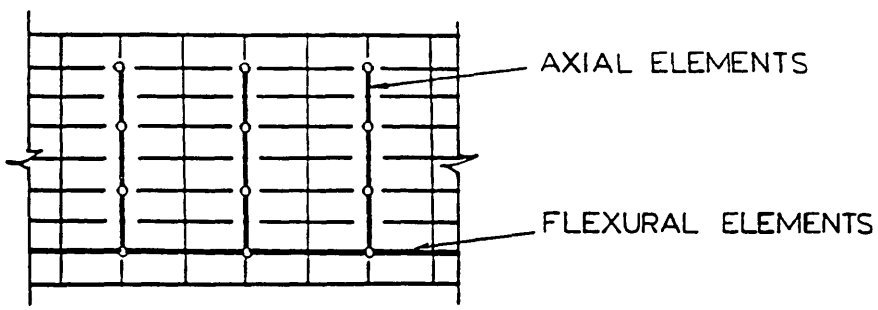

b) discrete representation

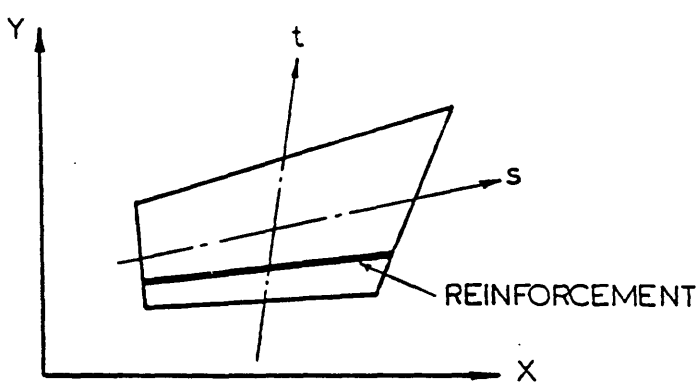

c) Embedded bars

FIGURE (3.23) : Alternative representation of steel

In order to approximate the real behaviour of reinforcing steel, the actual stress– strain curve is replaced by a bilinear curve with the strain hardening effect, as shown in Figure (3.24). Elastic–perfectly plastic behaviour is given by the hardening angle $E_w = 0$.

The main flow of operations in steel behaviour is summarized as follows :

1. Enter with initial stress σ_i, initial strain ϵ_i, current yield stress σ_i^y and increment strain $\Delta\epsilon_i$

2. Calculate total strain

$$\epsilon_{i+1} = \epsilon_i + \Delta\epsilon_i \tag{3.51}$$

3. Calculate first approximation to total stress

$$\sigma_{i+1} = \sigma_i + E_0 \, \Delta\epsilon_i \tag{3.52}$$

where E_0 is the linear elastic modulus.

4. If the magnitude of this stress is less than the current yield stress :

$$|\sigma_{i+1}| \leqslant |\sigma_i^y| \tag{3.53}$$

then plastic flow does not occur and the value of stress is correct. This step automatically accounts for elastic unloading. Step 5 to 7 are omited.

5. If $|\sigma_{i+1}| > |\sigma_i^y|$ then the stress is corrected by :

$$|\sigma_{i+1}^c| = |\sigma_i^y| + \frac{E_w}{E_0} \left\{ |\sigma_{i+1}| - |\sigma_i^y| \right\} \tag{3.54}$$

where : E_w = is the hardening angle

and σ_{i+1}^c = is the corrected value of stress.

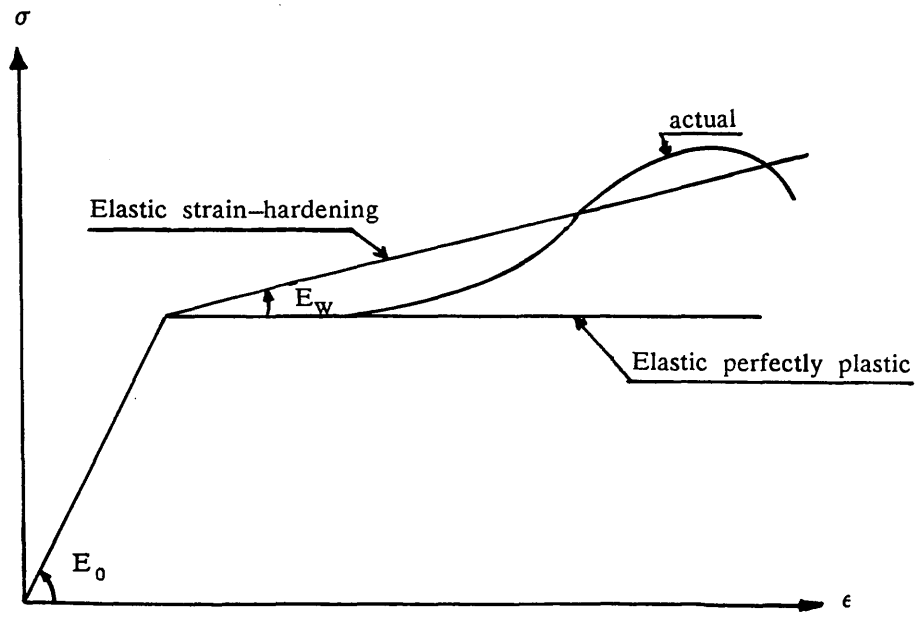

FIGURE (3.24) : Assumed steel laws.

6. The current yield stress is updated by :

$$\sigma_{i+1}^{y} = |\sigma_{i+1}^{c}| \tag{3.55}$$

and the modulus of any new stiffness calculations is set to E_w

7. If $\Delta\epsilon_i < 0$, i.e. compressive incremental strain, then stress must be compressive i.e. :

$$\sigma_{i+1}^{y} = -|\sigma_{i+1}^{c}| \tag{3.56}$$

8. Updated values σ_{i+1}, ϵ_{i+1}, and σ_{i+1}^{y} are stored in readiness for next cycle.

CHAPTER 4

THE FINITE ELEMENT METHOD

4.1 INTRODUCTION

Since the name *'finite element'* was originally coined in a paper by Clough in 1960, in which the technique was presented for plane stress analysis, there has been such a rapid progress that the method is now firmly established as probably the most powerful tool for studying the behaviour of reinforced concrete. Cracking, tension stiffening, non–linear multi–axial material properties, complex steel–concrete interface behaviour, and other effects previously ignored or treated in a very approximate way, can now be considered rationaly by the finite element method. Through such studies, in which the important parameters may be varied conveniently and systematically, new insights are gained and might provide a firmer basis for the codes and specifications on which ordinary design is based.

Along with the improvements in analytical techniques, the need for experimental research continues, both to provide a firm basis for empirical equations still likely to be used for many aspects of ordinary design, and to provide needed information for a more refined finite element analysis. It is also necessary to obtain information experimentally on materials properties and interface behaviour, both of these representing fundamental input for finite element analysis. Furthermore, it is necessary to have test results against which the finite element analysis results may be compared. As a result, tests can be fewer in number and more fundamental, and then, test results will be more generally useful, and the need for large scale testing of members over the full range of variables will be greatly reduced.

4.2 FINITE ELEMENT FORMULATION

The finite element method has been described extensively in the literature, and a comprehensive discussion of the theory and application of the method to two and three–dimensional systems involving plane stress, plane strain, plate bending, shells and solids is given in the text by Zienkiewicz[30], which covers all these developments and includes an extensive bibliography of the publications reflecting these activities. No attempt will be made here to review the vast literature in these fields. Instead, a brief review of the method will be presented in the following sections.

The finite element method started as an extension of the stiffness (or displacement) method, in which a skeletal structure is assumed to be made up of an assemblage of one–dimensional elements (axial, bending and torsional actions).

In the stiffness method for skeletal structures the elements of an actual structure are connected together at discrete joints, and equations of equilibrium involving external loads and member end forces expressed in terms of displacements are established at all joints. These equations are solved for joint displacements. The relationship between the end forces and end displacements of each member is represented by the stiffness matrix which can be derived directly through the solution of differential equations, use of various energy theorems, or the principle of virtual work. However, unlike skeletal structures, in the finite element method, there are no well–defined joints where equilibrium of forces can be established and therefore, the continuum must be discretized into a number of elements of arbitrary shapes and also artificial joints or nodes must be created.

In this way the continuum is approximated by a system with finite degree of freedom, so that a numerical solution can be achieved.

In recent years the most intensive work has taken place in solving nonlinear problems. The general procedure for solving such problems is to approximate the nonlinear behaviour by series of linear solutions[30]. So, the linear solution procedure is a basic and important part of any nonlinear solution method.

4.3 ELEMENT SELECTION

The starting point of the analysis is to decide on the type of element to be used, and then to subdivide the continuum into a suitable number of elements with associated nodes.

The selection of the element will be related to the type of problem to be solved, and with each type different levels of accuracy can be obtained. This is mainly dependent on the number of nodal points and corresponding degrees of freedom which are associated with the element type Fig.(4.1). Nodal points are usually placed on the boundaries of the elements, although internal nodes can also be included in certain elements in order to increase efficiency. Usually the higher the order of element (the more nodal degrees of freedom), the more accurate the solution. Elements edges can be straight or curved, this usually depends on the number of nodes defining the element edges Fig.(4.2).

In the present investigation, isoparametric elements – an 8–noded isoparametric element for the representation of concrete, and a 3–noded isoparametric element for the steel representation – were used.

(a) Truss and cable elements

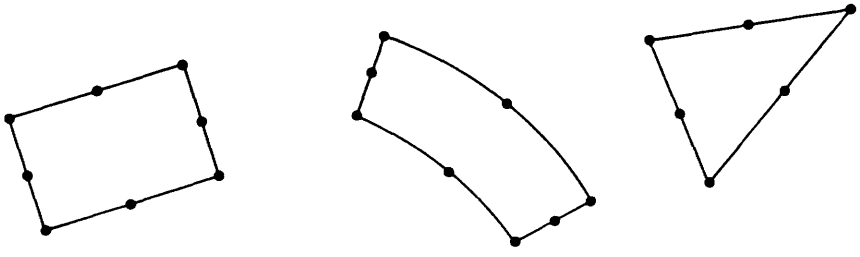

(b) Two-dimensional elements

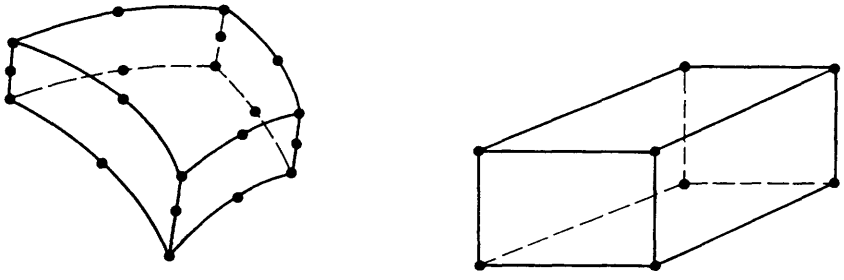

(c) Three-dimensional elements

FIGURE (4.1) : Some typical continuum elements.

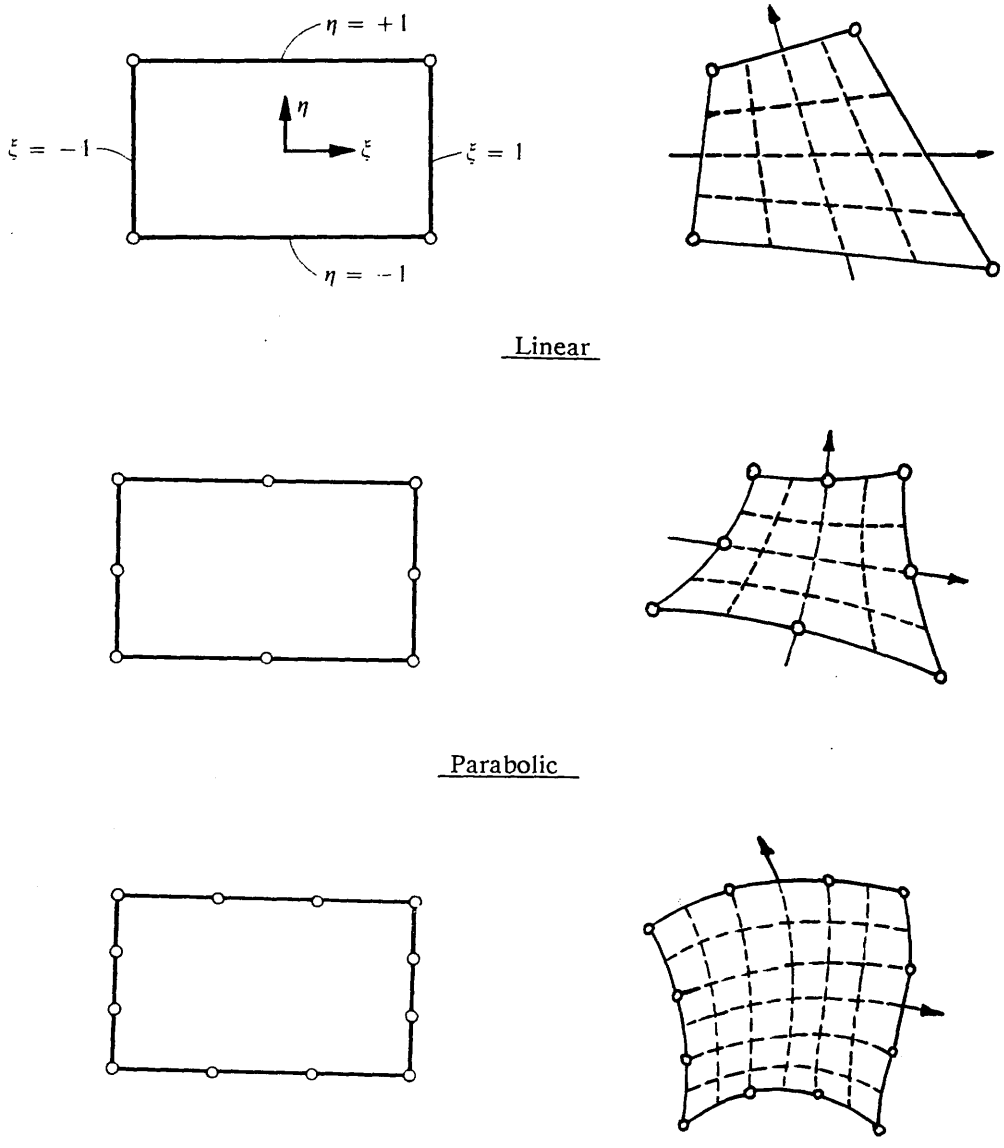

FIGURE (4.2) : Two dimensional mapping of some elements (Serendipity family).

4.4 ISOPARAMETRIC ELEMENTS

4.4.1 Introduction:

In the present investigation, isoparametric elements have been used. These elements are based on strain (displacement) assumptions. The name *'isoparametric'* came as the same interpolation function used for defining the displacement variation within the element is also used to define the element geometry.

The basic procedure is to express the element coordinates and element displacements by functions expressed in terms of the natural coordinates of the element. A natural coordinate system is a local system defined by the element geometry and not by the element orientation in the global system. Moreover, these systems are usually arranged such that the natural coordinate has unit magnitude at primary external boundaries. Figure (4.3) shows this type of element and its natural coordinate systems.

What follow are some of the reasons for using isoparametric elements :

1– The isoparametric elements are far more accurate than simple elements.
2– The simultaneous description of element geometry and displacement variation by the shape functions leads to efficient computing effort.
3– Curved elements can model the cuved boundaries of a structure.

4.4.2 Shape functions:

A shape function defines the variation of the field variable and its derivatives through an element in terms of its values at the nodes. Therefore, shape functions are closely related to the number of nodes and consequently, to the type of element.

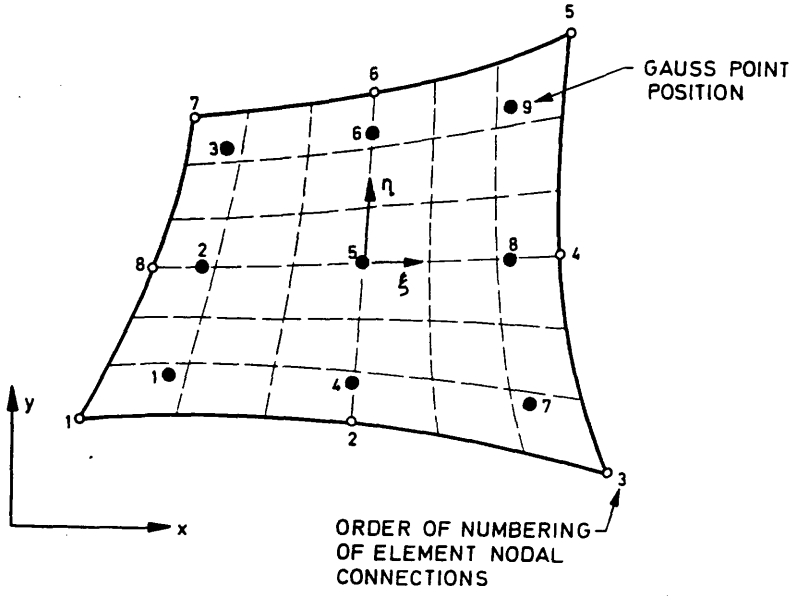

FIGURE (4.3) : Typical 8–noded isoparametric element.

Polynomials are often selected as shape functions because they are relatively easy to manipulate mathematically, particularly with regard to integration and differentiation. However, the degree of polynomial chosen will clearly depend on the number of nodes and the degrees of freedom associated with the element.

The shape function for the eight–noded strain element, are given in equation(4.1) and equation(4.2) in the curvilinear coordinate ξ and η :

For corner nodes:

$$N_i = \tfrac{1}{4}(1+\xi\xi_i)(1+\eta\eta_i)(\xi\xi_i+\eta\eta_i-1) \qquad i=1,3,5,7 \qquad (4.1)$$

For midside nodes:

$$N_i = \tfrac{1}{2}\xi_i^2(1+\xi\xi_i)(1-\eta^2)+\tfrac{1}{2}\eta_i(1+\eta\eta_i)(1-\xi^2) \qquad i=2,4,6,8 \qquad (4.2)$$

where ξ and η are the intrinsic coordinates of any point within the element. By definition, ξ and η have values in the interval $[-1,+1]$.

These shape functions are part of the so–called serendipity family[30], and they are shown pictorially in Figure (4.4). The displacement at any point inside the element, namely u and v, can be expressed in terms of these shape functions as follows :

$$u = \sum_{i=1}^{8} N_i(\xi,\eta)\, u_i \qquad (4.3)$$

$$v = \sum_{i=1}^{8} N_i(\xi,\eta)\, v_i \qquad (4.4)$$

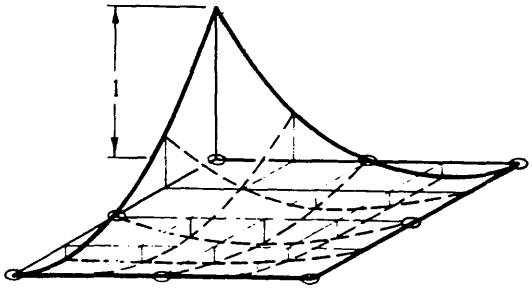

corner

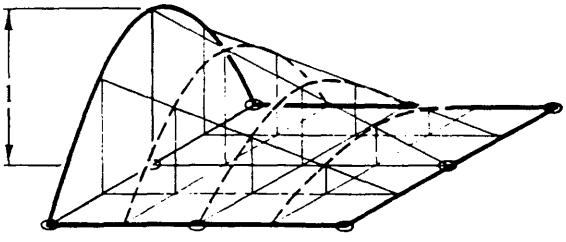

Midside

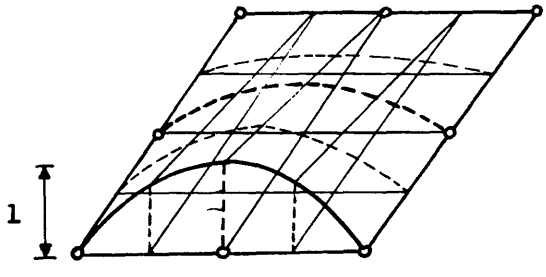

Midside

FIGURE (4.4) : Shape function for 8–noded isoparametric element.

It should be noted that the displacements u and v are parallel to the x and y, not to the ξ and η axes. Similarly, the position of a point within the element in global coordinates is given by :

$$x = \sum_{i=1}^{8} N_i(\xi,\eta)\ x_i \tag{4.5}$$

$$y = \sum_{i=1}^{8} N_i(\xi,\eta)\ y_i \tag{4.6}$$

Since each element has two degrees of freedom at each node, namely the displacement u_i, v_i, then it has a total of 16 degrees of freedom, and the element nodal displacement vector $\{\delta^e\}$ can be written as :

$$\{\delta^e\} = \{\{\delta_1\}, \{\delta_2\}, \ldots, \{\delta_8\}\} \tag{4.7}$$

$\{\delta_i\}$ = The displacement components at a node.

$= \{u_i, v_i\}$

Having thus established the nodal displacements, the displacements at any point inside the element are expressed in terms of these through the shape functions $[N(\xi,\eta)]$ such as :

$$\{\delta\} = \{u, v\}$$

$$= [N(\xi,\eta)]^T \{\delta^e\} = \sum_{i=1}^{8} N_i(\xi,\eta)\ \{\delta_i\} \tag{4.8}$$

where

$$[N(\xi,\eta)]^T = \begin{bmatrix} N_1 & 0 & N_2 & 0 & \ldots & N_8 & 0 \\ 0 & N_1 & 0 & N_2 & \ldots & 0 & N_8 \end{bmatrix} \tag{4.9}$$

= shape functions matrix.

4.4.3 Stress and strain evaluation:

The strains within the element are expressed in terms of the derivatives of the displacements :

i.e. $$\{\epsilon\} = \{\ \epsilon_{xx} \quad \epsilon_{yy} \quad \gamma_{xy}\ \}^T \tag{4.10}$$

$$= \left\{ \frac{\partial u}{\partial x} \quad \frac{\partial v}{\partial y} \quad \left(\frac{\partial u}{\partial y} + \frac{\partial v}{\partial x} \right) \right\}^T \tag{4.11}$$

Substituting equations (4.3) and (4.4) into equation (4.11) leads to :

$$\{\epsilon\} = [B]\ \{\delta^e\} \tag{4.12}$$

where : $\{\delta^e\}^T = \{\ u_1\ , v_1\ , u_2\ , v_2\ , \ \ldots\ u_i\ , v_i\ , \ \ldots\ u_8\ , v_8\ \}$

and $$[B] = [B_1(\xi,\eta) \quad B_2(\xi,\eta) \quad \ldots\ B_i(\xi,\eta) \ \ldots\ B_8(\xi,\eta)\ ]$$

= strain matrix.

in which:

$$[B_i(\xi,\eta)\ ] = \begin{bmatrix} \dfrac{\partial N_i}{\partial x} & 0 \\ 0 & \dfrac{\partial N_i}{\partial y} \\ \dfrac{\partial N_i}{\partial y} & \dfrac{\partial N_i}{\partial x} \end{bmatrix} \tag{4.13}$$

Since the shape functions N_i are defined in terms of the curvilinear coordinates ξ and η, a coordinate transformation from local to global is required in equation (4.13).

The usual chain rules relating x, y, to ξ, and η derivatives is expressed as :

$$\begin{Bmatrix} \dfrac{\partial[N]}{\partial\xi} \\ \dfrac{\partial[N]}{\partial\eta} \end{Bmatrix} = \begin{bmatrix} \dfrac{\partial x}{\partial\xi} & \dfrac{\partial y}{\partial\xi} \\ \dfrac{\partial x}{\partial\eta} & \dfrac{\partial y}{\partial\eta} \end{bmatrix} \begin{Bmatrix} \dfrac{\partial[N]}{\partial x} \\ \dfrac{\partial[N]}{\partial y} \end{Bmatrix} = [J] \begin{Bmatrix} \dfrac{\partial[N]}{\partial x} \\ \dfrac{\partial[N]}{\partial y} \end{Bmatrix} \tag{4.14}$$

in which [J] is only a 2 x 2 matrix known as the Jacobian matrix. This matrix can be inverted quite simply and cheaply. Thus, by inverting the Jacobian operator [J], we obtain the required global derivatives :

$$\begin{Bmatrix} \dfrac{\partial[N]}{\partial x} \\ \dfrac{\partial[N]}{\partial y} \end{Bmatrix} = [J]^{-1} \begin{Bmatrix} \dfrac{\partial[N]}{\partial\xi} \\ \dfrac{\partial[N]}{\partial\eta} \end{Bmatrix} \tag{4.15}$$

Differentiating equation (4.5) and (4.6) in accordance with equation (4.15) gives :

$$[J] = \begin{bmatrix} \dfrac{\partial N_1}{\partial\xi}, \ldots, \dfrac{\partial N_i}{\partial\xi}, \ldots, \dfrac{\partial N_8}{\partial\xi} \\ \dfrac{\partial N_1}{\partial\eta}, \ldots, \dfrac{\partial N_i}{\partial\eta}, \ldots, \dfrac{\partial N_8}{\partial\eta} \end{bmatrix} \begin{bmatrix} x_1 & y_1 \\ . & . \\ . & . \\ x_i & y_i \\ . & . \\ . & . \\ x_8 & y_8 \end{bmatrix} \tag{4.16}$$

For For linear analysis of uncracked concrete, and in the absence of initial stresses and strains, the stress–strain relationship may be written in the form :

$$\{\sigma\} = [D]\{\epsilon\} \tag{4.17}$$

where : $\{\sigma\} = \{ \sigma_{xx} \quad \sigma_{yy} \quad \tau_{xy} \}^T$

The total potential energy of element e (π_e) can be expressed as :

$$\pi_e = \tfrac{1}{2} \int_{V_e} \{\sigma\}^T \{\epsilon\}\, dv - \int_{V_e} \{\delta^e\}^T [N]^T \{p\}\, dv$$

$$- \int_{S_e} \{\delta^e\}^T [N]^T \{q\}\, ds + \{F_p^e\}\{\delta^e\}^T \qquad (4.18)$$

where : $\{\sigma\}$, $\{\epsilon\}$ = stress and strain vectors, respectively.

$\{p\}$ = body force per unit volume,

$\{q\}$ = applied surface pressure,

$\{\delta\}$ = displacement vector,

$\{F_p^e\}$ = element node point load vector.

Integration is taken over the volume, V_e, and the loaded surface area S_e of the element.

However, from equation (4.17), we have :

$$\{\sigma\}^T = \{\epsilon\}^T [D]^T = \{\epsilon\}^T [D] \qquad (4.19)$$

as $[D]$ is a symmetrical matrix.

Similarly, from equation (4.12) we get :

$$\{\epsilon\}^T = \{\delta^e\}^T [B]^T \qquad (4.20)$$

replacing equation (4.20) into equation (4.19) gives :

$$\{\sigma\}^T = \{\delta^e\}^T [B]^T [D] \qquad (4.21)$$

and by using equation (4.12) and equation (4.21) in equation (4.18) we get the following equation :

$$\pi_e = \tfrac{1}{2} \int_{V_e} \{\delta^e\}^T [B]^T [D][B]\{\delta^e\}\, dv - \int_{V_e} \{\delta^e\}^T [N]^T\{p\}\, dv$$

$$- \int_{S_e} \{\delta^e\}^T [N]^T\{q\}\, ds + \{F_p^e\}\{\delta^e\}^T \qquad (4.22)$$

The first term on the right hand side of equation (4.22) is the internal strain energy, and the second, third and fourth terms are the work contributios of the body forces, distributed surface loads and point loads, respectively.

Performance of the minimisation for element e with respect to the nodal displacement $\{\delta^e\}$ for the element results in :

$$\frac{d\pi_e}{d\{\delta^e\}} = \int_{V_e} [B]^T[D][B]\, \{\delta^e\}\, dv - \int_{V_e} [N]^T\{p\}\, dv - \int_{S_e} [N]^T\{q\}\, ds + \{F_p^e\} \qquad (4.23)$$

$$= [K^e]\, \{\delta^e\} - \{F^e\} \qquad (4.24)$$

where : $$\{F^e\} = \int_{V_e} [N]^T\{p\}dv + \int_{S_e} [N]^T\{q\}ds + \{F_p^e\} \qquad (4.25)$$

and are the nodal forces for the element, and since the displacement is independent of the volume then we have :

$$[K^e] = \int_{V_e} [B]^T\, [D]\, [B]\, dv \qquad (4.26)$$

and is termed the stiffness matrix.

As the total potential energy of the continuum is the sum of energy contributions of individual elements, then we have :

$$\pi = \Sigma \pi_e \tag{4.27}$$

where π_e is the potential energy of element e.

The summation of the terms in equation (4.24) over all the elements, when equated to zero, result in a system of equations for the complete continuum i.e. :

$$\{F\} = [K] \cdot \{\delta\} \tag{4.28}$$

where : $\{F\}$ = the applied forces for the continuum,

$[K]$ = is the stiffness matrix of the continuum.

The final stage is the solution of equation (4.28) to obtain the unknown displacements as :

$$\{\delta\} = [K]^{-1} \{F\} \tag{4.29}$$

The solution of the system of equations for the complete continuum can be accomplished in several ways, the direct Gaussian elemination method is adopted here. Once displacement have been evaluated, strains and stresses are simply found by substitution into equations (4.12) and (4.17), respectively.

4.5 Numerical integration

For complex functions which cannot be integrated explicitly, numerical integration can be carried out. The general form of the integral using Gauss–Legendre quadrature will be :

$$\int_{-1}^{+1} f(\xi)\, d\xi = \sum_{i=1}^{M} W_i\, f(\xi_i) \tag{4.30}$$

where ξ_i : coordinate of the ith integration point.

W_i : Weighting factor

M : is the total number of integration points.

To extend equation (4.30) to two dimensions so as to meet fully the requirement of equation (4.26), it is required to integrate first with respect to one variable and then with respect to the other. Thus :

$$\int_{-1}^{+1}\int_{-1}^{+1} f(\xi,\eta)\, d\xi\, d\eta = \int_{-1}^{+1}\left[\int_{-1}^{+1} f(\xi,\eta)\, d\xi\right] d\eta$$

$$= \int_{-1}^{+1}\left[\sum_{i=1}^{M} W_i\, f(\xi_i,\eta)\right] d\eta$$

$$= \int_{-1}^{+1}\left[\sum_{i=1}^{M} W_i\, g_i(\eta)\right] d\eta$$

$$= \sum_{i=1}^{M}\sum_{j=1}^{M} W_i\, W_j\, g(\eta_j)$$

$$= \sum_{i=1}^{M}\sum_{j=1}^{M} W_i\, W_j\, g(\eta_j)$$

$$= \sum_{i=1}^{M}\sum_{j=1}^{M} W_i\, W_j\, f(\xi_i,\eta_j) \qquad (4.31)$$

where : M : is the total number of integration points.

W_i, W_j : are the ith and jth weighting factors.

ξ_i, η_j : are the coordinate of the ith integration point.

Then, this integration can be applied to equation (4.26) after transformation

$$\text{i.e} \qquad [K] = t \int_{-1}^{+1}\int_{-1}^{+1} [B]^T [D] [B] \det[J] \, d\xi \, d\eta \qquad (4.32)$$

The reason for the transformation is that for two–dimensional problems the incremental volume dv is given by :

$$dv = t \, dx \, dy \qquad (4.33)$$

where : t = the thickness of the element.

The relation between the cartesian and the curvilinear coordinates is given by:

$$dx \, dy = \det[J] \, d\xi \, d\eta \qquad (4.34)$$

in which $\det[J]$ is the determinant of the Jacobian matrix.

The values of W_i and ξ_i for various values of the total number of intergration points are given in table (4.1).

4.6 BAR ELEMENT REPRESENTATION

The concept of embedding isoparametric elements with reinforcing bars was first suggested for plane stress, plane strain and axisymmetric analysis in the early seventies.[32] Bars parallel to local coordinates ξ, and η can be used. In this program, bar elements are identified with a particular isoparametric 8–noded element, and any combination of six bars can be placed along the sides of the 8–noded element, or parallel to them passing by the opposite midside nodes, i.e. the bars lie along lines of constant ξ or η of the main isoparametric element as shown in Figure (4.5). In general, the bar elements will be defined by a single natural coordinate and thus, the formulation for any one of these six possible positions of the bars is identical.

TABLE (4.1) : Abscissae and weight coefficients of the Gaussian quadrature formula

$$\int_{-1}^{+1} f(x)\, dx = \sum W_i\, f(\xi_i)$$

m	i	W_i	$f(\xi_i)$
1	1	2	0
2	1	1	$-\frac{1}{\sqrt{3}}$
	2	1	$+\frac{1}{\sqrt{3}}$
3	1	$\frac{5}{9}$	$-\sqrt{0.6}$
	2	$\frac{8}{9}$	0
	3	$\frac{5}{9}$	$\sqrt{0.6}$
4	1	$\frac{1}{2} - \frac{\sqrt{30}}{36}$	$-\sqrt{\frac{3+\sqrt{4.8}}{7}}$
	2	$\frac{1}{2} - \frac{\sqrt{30}}{36}$	$+\sqrt{\frac{3+\sqrt{4.8}}{7}}$
	3	$\frac{1}{2} + \frac{\sqrt{30}}{36}$	$-\sqrt{\frac{3-\sqrt{4.8}}{7}}$
	4	$\frac{1}{2} + \frac{\sqrt{30}}{36}$	$+\sqrt{\frac{3-\sqrt{4.8}}{7}}$

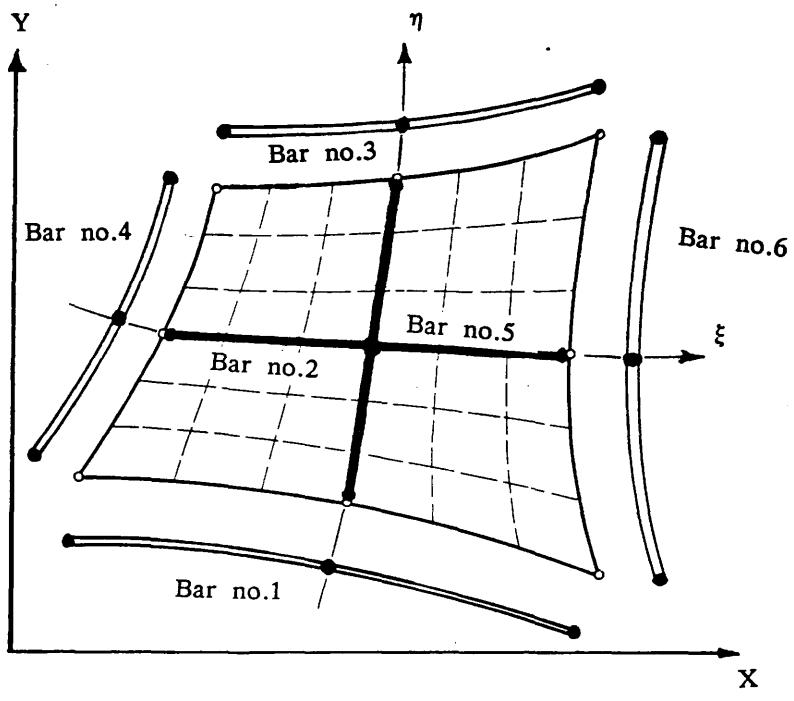

FIGURE (4.5) : Bar elements positions on the 8–noded isoparametric element.

4.7 CERTAIN ASPECTS OF THE F.E.M

As mentionned previously, in the finite element method, the continuum is discretized into a number of elements called the finite element mesh. The finite element method is greatly influenced by the size and relative dimensions ratios of the element composing the mesh (called the element aspect ratio).

4.7.1 The element size:

In general the finer the mesh better the accuracy, but at the same time higher the computational effort required. Generally, the number of elements to be used is decided by the type of structure to be analysed, but usually more elements are required in regions where displacement gradients are steepest, i.e. where there are rapid changes in stress and strain as shown in Figure (4.6). In addition, the size of element is governed by the position of reinforcement as explained before.

4.7.2 The element aspect ratio:

The aspect ratio for two–dimensional elements is defined as the ratio of the largest dimension of the element to the smallest dimension. The optimum aspect ratio at any location within the mesh depends largely upon the difference in rate of change of displacements in different directions. For instance if the displacements vary at about the same rate in each direction, the closer the aspect ratio to unity better the quality of the solution.

In a study on the aspect ratio[31] for the 8–noded isoparametric element, it was concluded that changing the aspect ratio had a minor effect, especially when using 3 x 3 Gauss rules.

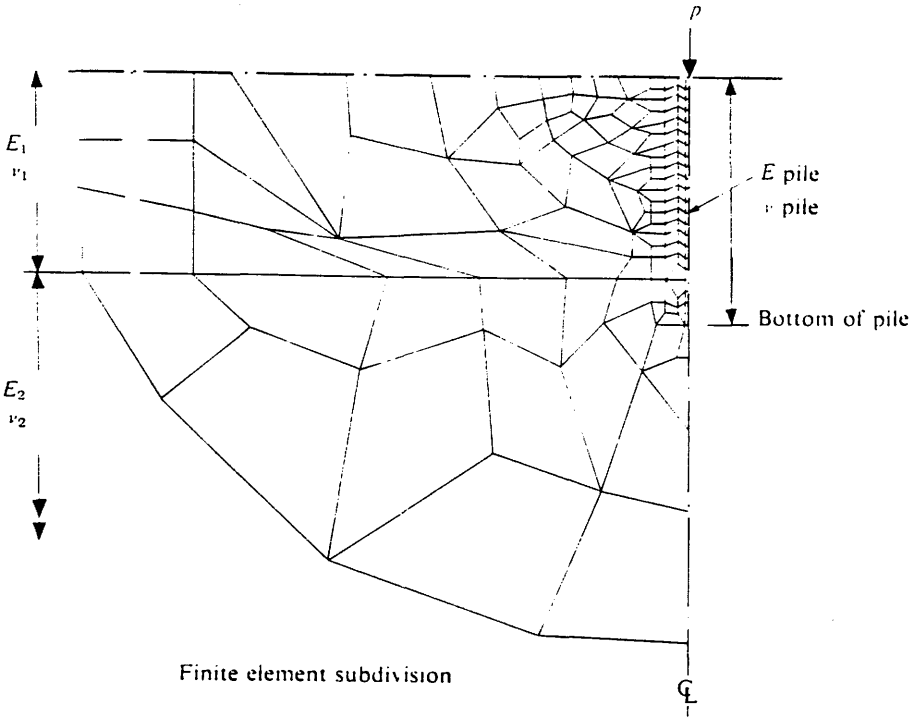

(*a*) A pile in stratified soil.

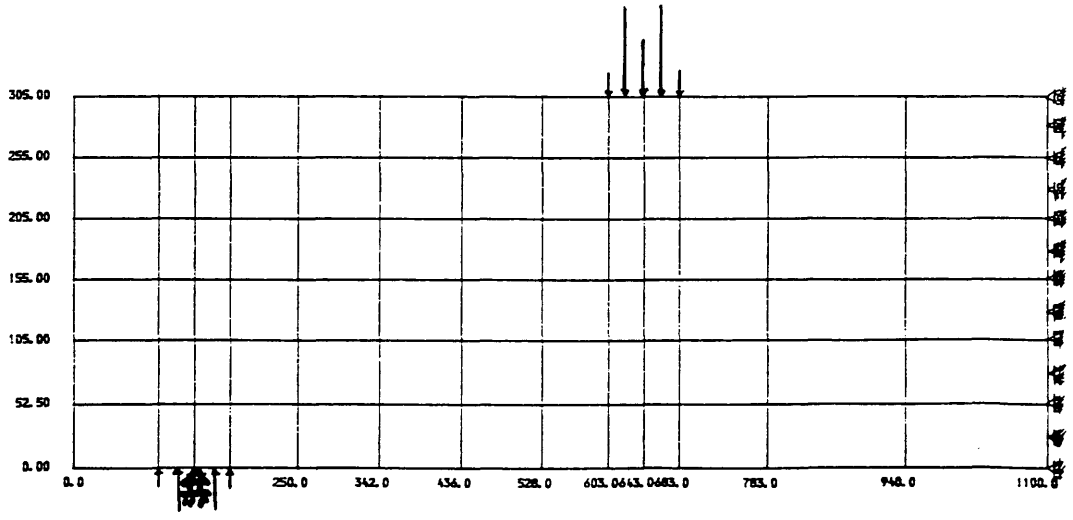

b) beam under Two–point load (Shear test).

FIGURE (4.6) : Examples of Finite Element Mesh.

In practical reinforced concrete analysis, it is unusual to select elements which have an aspect ratio of unity because the steel configuration will apply other constraints. However, large values which imply long narrow elements, should be avoided because of numerical problems.

CHAPTER 5

NONLINEAR METHODS OF ANALYSIS

5.1 INTRODUCTION

Structures may exhibit nonlinear behaviour due to material, or geometric nonlinearities. Whilst stress–strain relationships are a major source of material nonlinearity, geometric nonlinearities are due mainly to large deflections making the equilibrium equations based on the original geometry no longer valid.

A nonlinear structural problem must obey the basic laws of continuum mechanics, i.e. : equilibrium, compatibility and the constitutive relationship of the material. As in finite element method, continuity and compatibility are automatically satisfied at any stage, it becomes only necessary to enforce the nonlinear relationships to be satisfied whilst at the same time preserving the equilibrium of the structure.

5.2 Numerical techniques for nonlinear analysis:

For the solution of nonlinear problems by the finite element method, there are three basic techniques generally used :

1– **Incremental.** (Step– wise procedure)

2– **Iterative.** (Newton– Raphson method)

3– **Incremental–iterative** (mixed procedure).

All these techniques solve the basic linear elastic equations given by equation (4.1) :

i.e. $$[K]\{\delta\} - \{F\} = 0 \tag{5.1}$$

in which the assumed linear elastic constitutive law given by equation (5.2):

i.e. : $$[\sigma] = [D](\{\epsilon\}) + \{\sigma_0\} \tag{5.2}$$

where : $[D]$ = the constant, linear elastic matrix,

and $\{\sigma_0\}$ = the initial stress vector.

under nonlinear conditions is replaced by a different law of the form :

$$f\left[\left\{\sigma\right\}, \left\{\epsilon\right\}\right] = 0 \tag{5.3}$$

which represents the relationship between stress and strain.

The element stiffness matrix is a function of the material properties and can be written as :

$$[K] = [k(\sigma, \epsilon)] \tag{5.4}$$

The external nodal forces $\{F\}$ are related to the nodal displacements $\{\delta\}$ through the stiffnesses of the element and can be expressed by :

$$\{F\} = [k(\sigma, \epsilon)]\{\delta\} \tag{5.5}$$

which on inversion becomes :

$$\{\delta\} = [k(\sigma, \epsilon)]^{-1}\{F\} \tag{5.6}$$

This derivation illustrates the basic nonlinear relationship between $\{\delta\}$ and $\{F\}$, due to influence of the material law on $[K]$.

However, equation (5.6) is solved by a succession of linear approximations, and different methods of applying these linear approximations will lead, in general, to different load–displacement paths influencing the final solution.

5.2.1 Incremental method[30]:

The principle used in this method is to subdivide the total applied load into smaller load increments, which do not need to be equal. At each load increment, it is assumed that equation (5.1) is linear i.e. $[K]$ has a fixed value, and by using material data already available from the previous increment, nodal displacements can then be obtained for each increment and these are added to previously accumulated displacements. The process is repeated until total load is reached.

From what preceeded, it is very clear that this procedure is increment size dependent, and smaller the increments better the accuracy, but at the same time more computational effort required.

The main disadvantage of the incremental method is that it does not account for force redistribution during the application of the increment owing to the fact that there is no iteration process to restore equilibrium.

5.2.2 Iterative method[30]:

In this method, the full load is applied and stresses are evaluated at that load according to the material law. This gives equivalent forces which may not be equal to the external applied forces Fig.(5.1). Since the equilibrium is not satisfied, then the *'out of balance'* portion of the total loading is calculated as the difference between applied load and internal nodal forces. These unbalanced nodal forces $\{\psi\}$ are then used to compute additional increment of displacements,

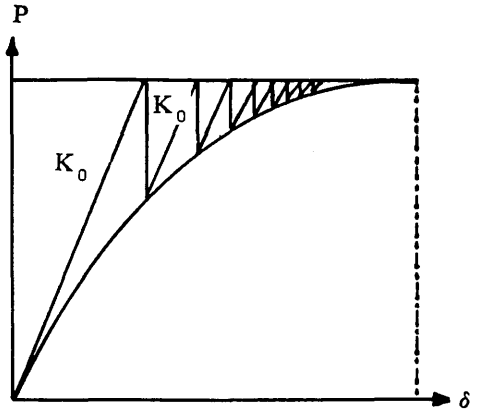

a) Constant stiffness procedure

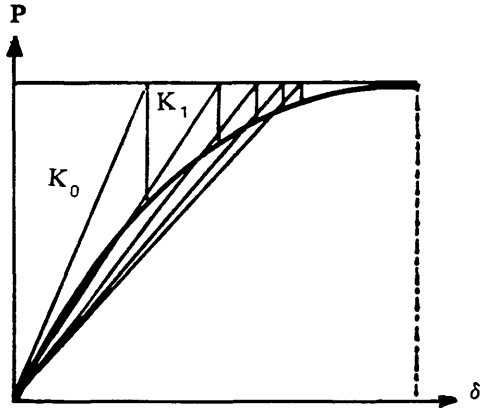

b) Variable stiffness procedure
Secant modlus approach

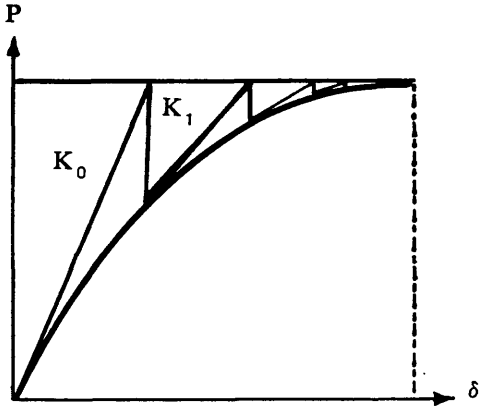

c) Variable stiffness procedure
Tangent modulus approach

FIGURE (5.1) : Iterative process

hence, new stresses which give new set of equivalent nodal forces. This process is repeated until equilibrium is approximated to a certain degree of accuracy. When this aim is reached, the total displacement is calculated by summing the displacements from each iteration.

However, this solution is very dependent on the method used for the computation of the stiffness matrix $[K]$ and the unbalanced nodal forces $\{\psi\}$.

5.2.3 Mixed method:

This method is obtained by combining the incremental and iterative processes. Thus, the load is applied in increments and the solution at that load is obtained iteratively until equilibrium is obtained. Figure(5.2) shows the mixed procedure.

5.3 COMPARISON OF BASIC METHODS

When using the incremental procedure, a relatively complete description of the load–deflection behaviour is provided, which represents the main advantage of this procedure. On the other hand, the main disadvantage is the difficulty to know in advance how many increments of load are necessary to have a good approximation to the exact solution.

In general the incremental method is more time consuming than the iterative one. The iterative procedure presents the advantage of being easier to be incorporated in a linear elastic program. However, its main disadvantage is that, there is no assurance that it will converge to the exact solution. Furthermore, displacements, stresses and strains are determined for only one increment which represents a considerable limitation.

BASIC PROCEDURE FOR NONLINEAR SOLUTION

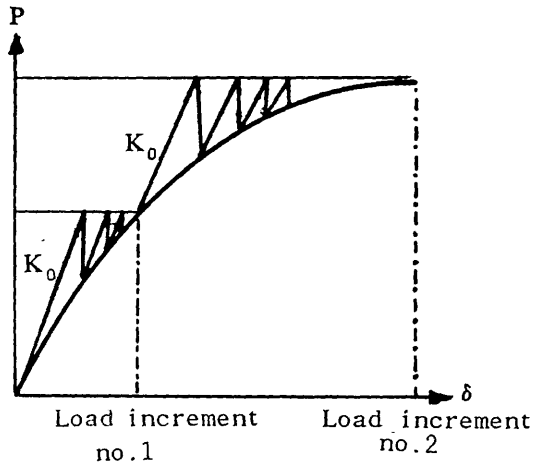

a) Constant stiffness procedure

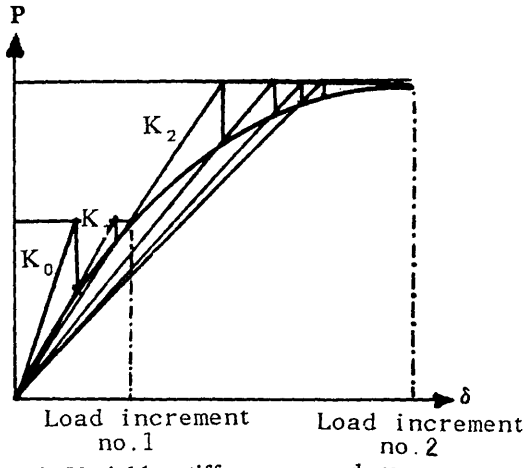

b) Variable stiffness procedure
Secant modlus approach

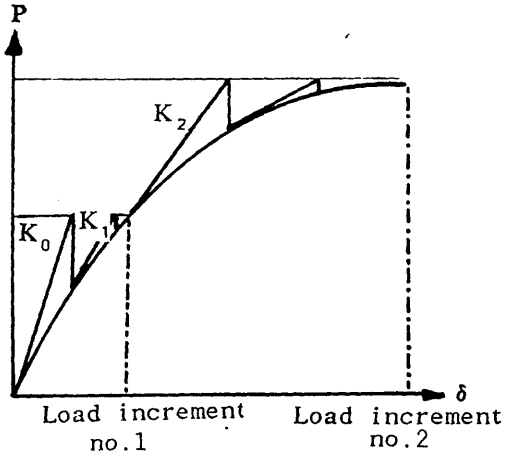

c) Variable stiffness procedure
Tangent modulus approach

FIGURE (5.2) : Mixed procedure

Finally, the mixed procedure which has been adopted in this work combines the advantage of both the incremental and iterative procedures, and at the same time minimizes their disadvantages. Therefore, it can give a full description of the load–deflection behaviour at every load level to the desired accuracy. However, it presents the disadvantage of being very expensive as more computing time is required.

5.4 COMPUTATION OF UNBALANCED NODAL FORCES

In the present investigation, the process called the initial stress method was adopted. Thus, at any loading stage, a first estimate of the incremental displacement $\Delta\{\delta\}$ is made using equation (5.6). Subsequently, the corresponding strain is calculated using equation (5.7) :

$$\Delta\{\epsilon\} = [B]\,\Delta\{\delta\} \tag{5.7}$$

elastic stresses are then calculated and compared with the true stress increment corresponding to the given law (equation (5.3)), and the difference between these stresses $\{\sigma_{ex}\}$ is used to calculate the equivalent unbalanced nodal forces $\{\psi\}$:

i.e.
$$\{\psi\} = \int_V [B]^T \{\sigma_{ex}\}\, dv \tag{5.8}$$

These forces are removed by applying them to the structure which causes a correction to $\{\delta\}$. This is repeated until $\{\psi\}$ is sufficiently small to be neglected.

5.5 METHODS FOR COMPUTING STIFFNESSES[30,31]

Generally throughout a solution process, the stiffness matrix can be either constant or variable. In the constant stiffness method, the initial linear stiffness matrix : $[K_0] = [k(\sigma_0, \epsilon_0)]$ is used at every stage in the analysis.

In the constant stiffness method, the main advantage is economic, as calculating the stiffness and fully solving the equations is a time consuming and therefore a costly operation. However, it usually requires a large number of iterations to obtain the desired accuracy, especially when cracking and yielding of reinforcement has occured, and this represents a main disadvantage.
In the variable stiffness method, a linear solution is performed but the $[D]$ matrix is adjusted during the iteration process. This can be achieved either by using a secant modulus approach, or a tangential modulus approach.

If the stiffnesses are updated every iteration then the method is a form of the well known '*Newton–Raphson*' method. In general the variable stiffness method requires considerably less number of iterations than the constant stiffness method, although a full solution is more expensive than a resolution with a constant stiffness.

However, a cheaper way of using the variable stiffness approach is obtained by updating the stiffness only during certain iterations. This approach is better known as the '*modified Newton–Raphson*' method, and has been adopted in this investigation as the stiffness matrix is re–calculated at the first iteration of each increment.

5.6 CONVERGENCE CRITERIA

Introducing a reliable criterion which will check for the gradual elimination of the residual forces and terminate the iterative process when convergence to the desired accuracy has been achieved, is a matter of prime importance. The user specifies the degree of accuracy of equilibrium that is acceptable. Convergence criteria can be based on various quantities; either directly on the unbalanced forces, or indirectly on the displacement increment or on changes in stress values. In this investigation, only the first option has been used.

Since it is difficult and expensive to check for the decay of residual forces for every degree of freedom, an overall evaluation is preferable. This, is achieved by using so–called force norms.

This criterion assumes that convergence is achieved if :

$$\frac{\Delta \Psi_i^*}{P_i^*} \leqslant Tol \qquad (5.9)$$

Where : $\Delta \Psi_i^*$ = the norm of the residuals.

$$= \surd \{\psi\}_i^T \{\psi\}_i \qquad (5.10)$$

P_i^* = the norm of the total applied loads

$$= \surd \{P\}_i^T \{P\}_i \qquad (5.11)$$

and : Tol = specified convergence tolerance.

5.6.1 General discussion on convergence criteria:

The control of the number of iterations in an increment is the main function of the convergence criteria. This is generally achieved by choosing convergence tolerances and the type of norm. In most cases the user will also specify the maximum number of iterations allowed, irrespective of the state of convergence, though the number of iterations will influence the predicted shape of the load–deflection curve, and the ultimate load, e.g. too few iterations might yield an overstiff response. Hence, it is of a paramount importance that the user understands the factors influencing the convergence behaviour, and the redistribution of forces. However, very little information on these aspects exist in the published literature. Fine tolerances are theoretically desirable but are very expensive to obtain, as they quiet often need a lot of iterations to be obtained. With these fine tolerances, convergence can be particularly difficult to be achieved especially when discontinuous material law (such as : tension cracking) form part of the nonlinear behaviour. Moreover, high discontinuities in the material laws can cause large residuals, and these need to be redistributed. However this redistribution will cause more discontinuities and consequently, residuals can be higher than the rate of distributing them. Another case is when residuals are almost completely redistributed and another discontinuity occurs which increases the residuals again, and therefore will require more iterations. These effects cause a large number of iterations to be needed before a stable crack situation is reached.

Finally, it can be added that the rate of convergence depends particularly on the method used in the solution, and it is well known for example that constant stiffness will lead to slow convergence and this needs many iterations, which is without any doubt a very costy operation.

A flow chart of the nonlinear procedure used is shown in Figure (5.3).

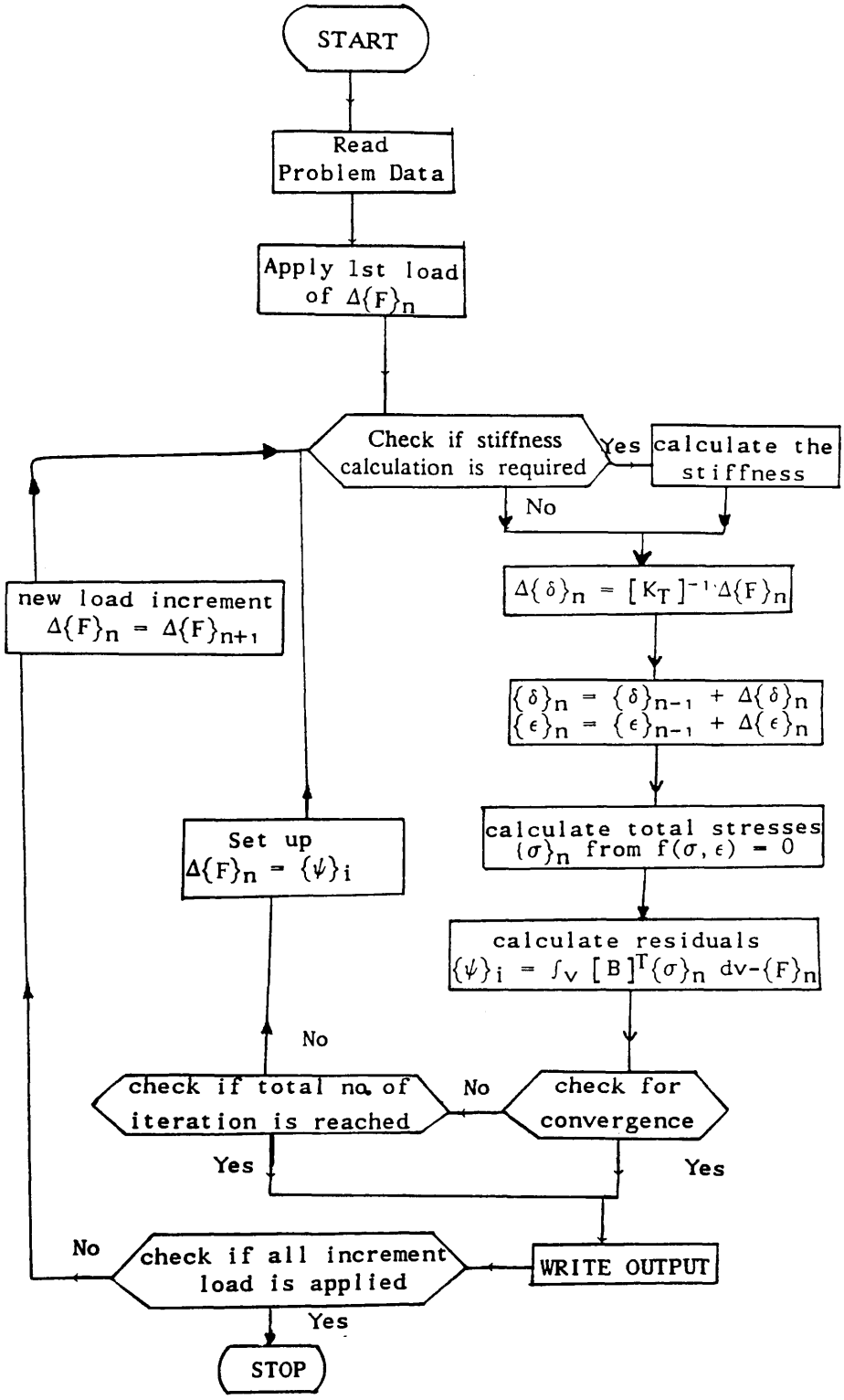

FIGURE (5.3) : Flow chart for nonlinear procedure used in this analysis

CHAPTER 6

NUMERICAL ANALYSIS

6.1 INTRODUCTION

The aim of this chapter is to present and discuss the numerical results obtained using the nonlinear options of FECON, a finite element program for structural concrete developed by Phillips[32]. The finite element method and the mathematical modeling of materials used in this program have already been presented in previous chapters. More details can be found in reference (32).
The numerical results are presented in three stages :

First, a detailed convergence study is carried out where the effect of mesh size and the norm of convergence tolerance on the results are studied.

Then, a parametric study is presented. In this part of the analysis the effects of the following parameters are investigated :

a) Shear retention factor β.

b) Concrete compressive strength f_c'.

c) Concrete tensile strength f_t.

d) Concrete crushing factor C_f.

This part of the analysis can be divided into two parts; the first part of it is concerned with the effect of β, f_c', while in the second part the effect of β, f_t, and C_f are investigated.

Finally, a statistical study involving the concrete crushing factor C_f as parameter was carried out.

6.2 CONVERGENCE STUDY

In order to have confidence in the accuracy of the results obtained from the finite element analysis, a convergence study was carried out. The main objective of this part of the work is to reduce the computing cost while maintaining good accuracy. The sensitivity of the solution to the mesh size and to the convergence tolerance were studied for the case of simply supported reinforced concrete beams under point loads. Because of symmetry, only half of the beam was considered in this nonlinear analysis.

6.2.1 Mesh size:

As different mesh sizes may be required for different values of the shear span to depth ratio a_v/d, a study for two values of a_v/d (1.0, 2.5) was carried out, and for each of these values five different mesh sizes were compared using the same boundary conditions and loads.

Figures (6.1) to (6.5) show the 10–, 18–, 24–, 36–, and 48–elements meshes used for ($a_v/d = 1.0$), while Figures (6.6) to (6.10) show the 12–, 30–, 39–, 60–, and 78–elements meshes used for ($a_v/d = 2.5$).

It can be seen from these figures that meshes with higher number of elements are obtained from the mesh with the lower number of elements by further division in the horizontal or/and vertical direction.

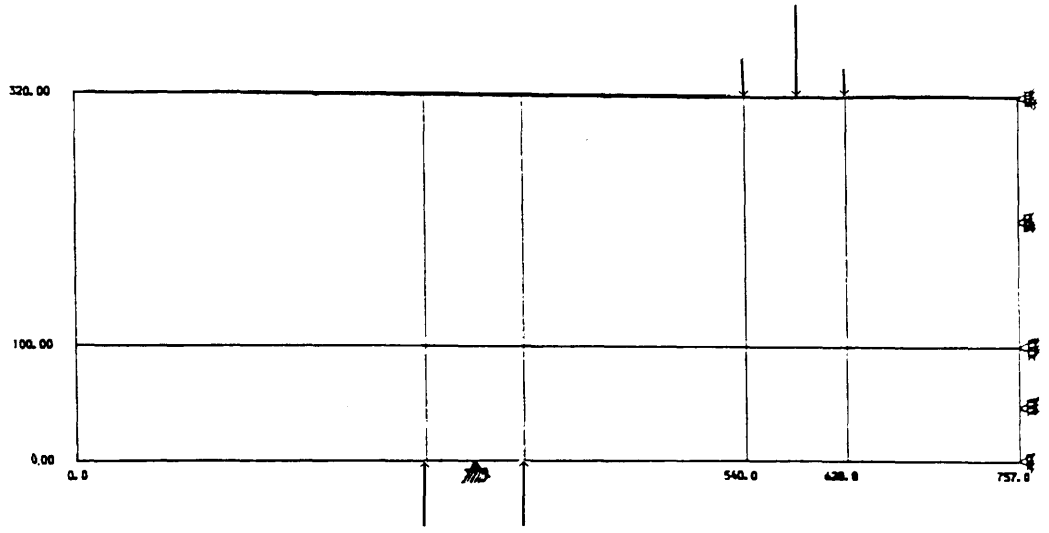

FIGURE (6.1) : 10 elements mesh for $a_v/d = 1.0$

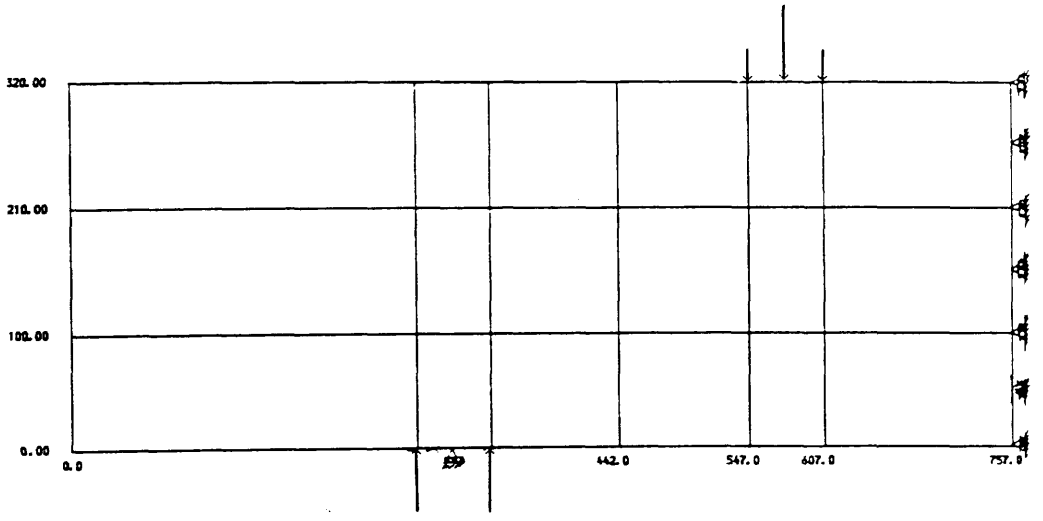

FIGURE (6.2) : 18 elements mesh for $a_v/d = 1.0$

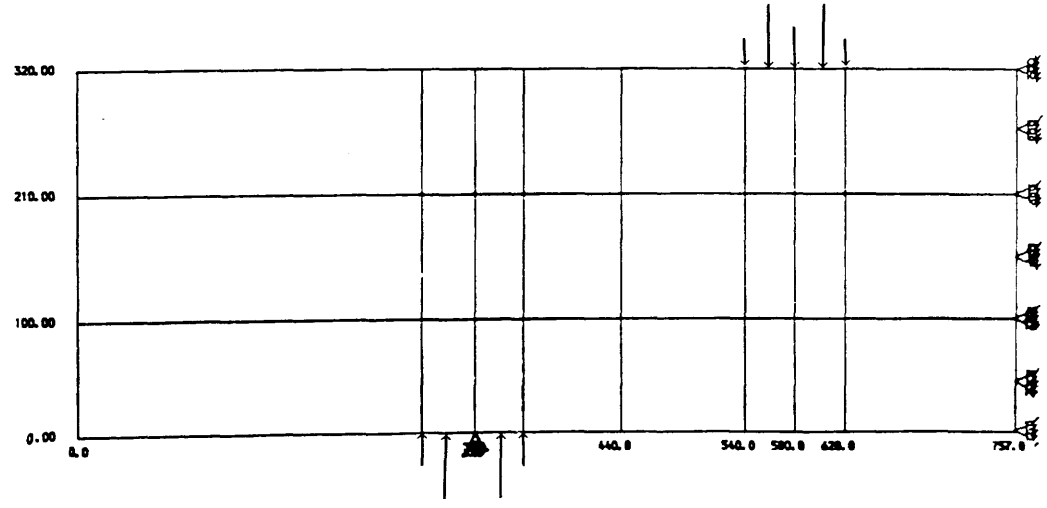

FIGURE (6.3) : 24 elements mesh for $a_v/d = 1.0$

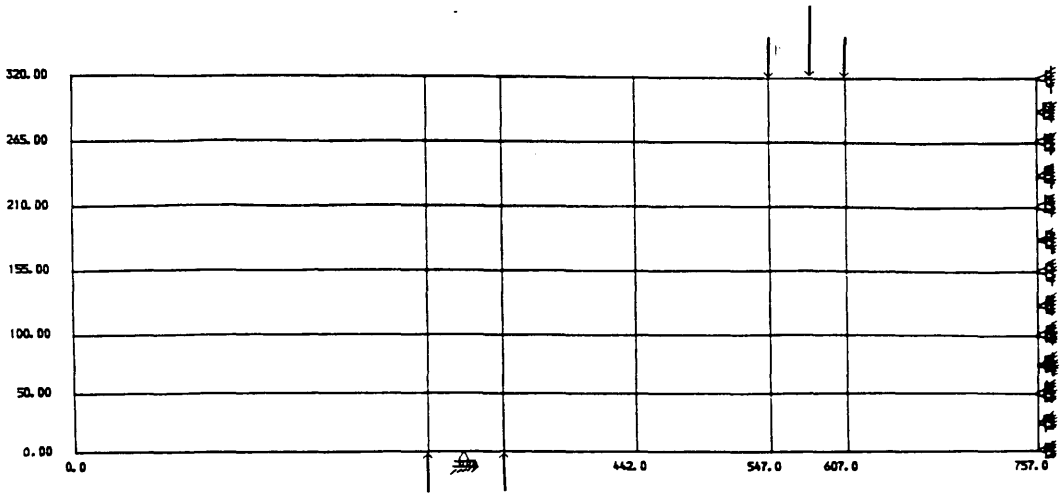

FIGURE (6.4) : 36 elements mesh for $a_v/d = 1.0$

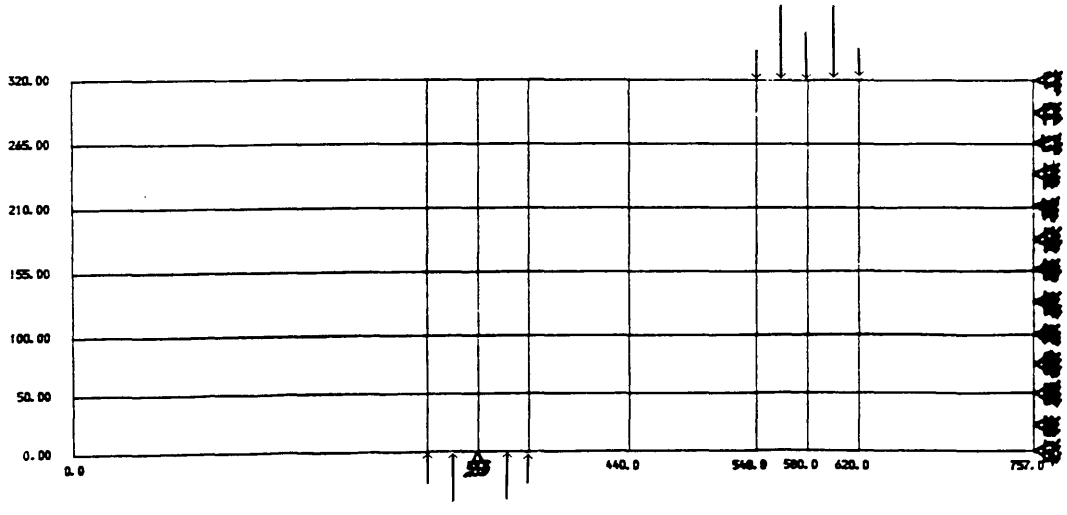

FIGURE (6.5) : 48 elements mesh for $a_v/d = 1.0$

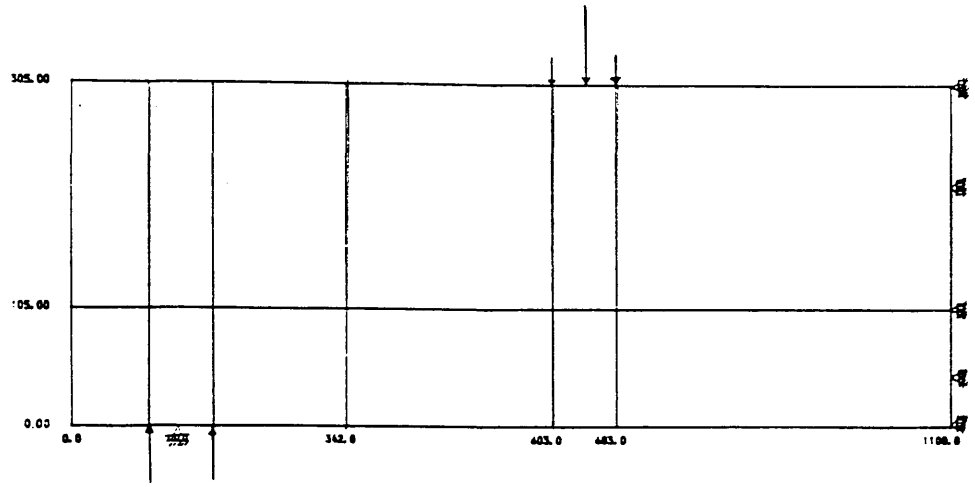

FIGURE (6.6) : 12 elements mesh for $a_v/d = 2.5$

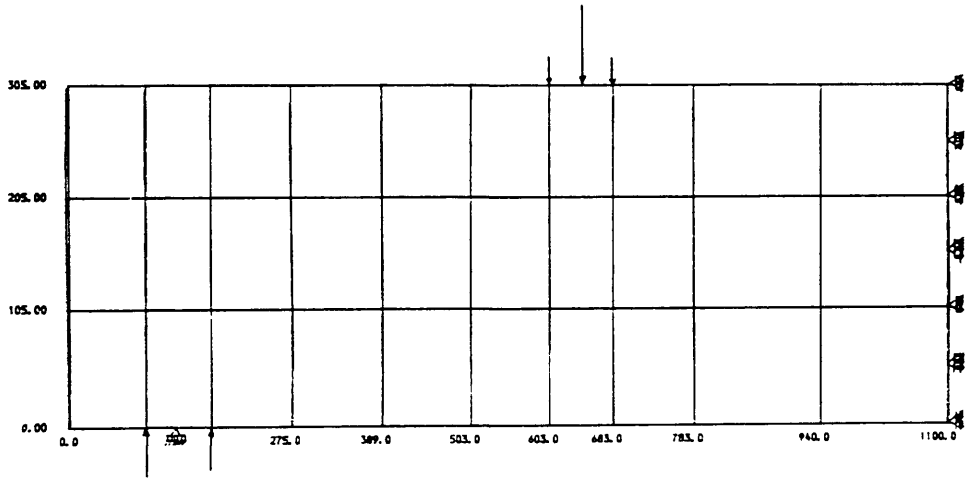

FIGURE (6.7) : 30 elements mesh for $a_v/d = 2.5$

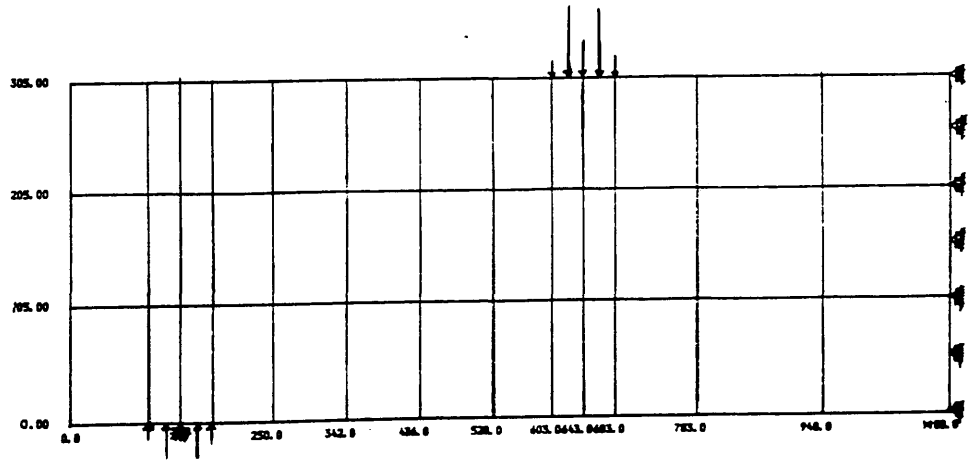

FIGURE (6.8) : 39 elements mesh for $a_v/d = 2.5$

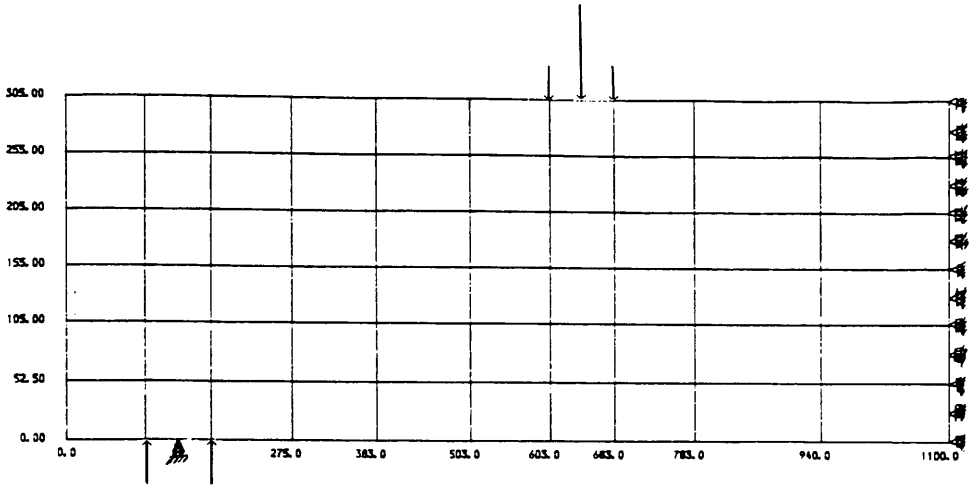

FIGURE (6.9) : 60 elements mesh for $a_v/d = 2.5$

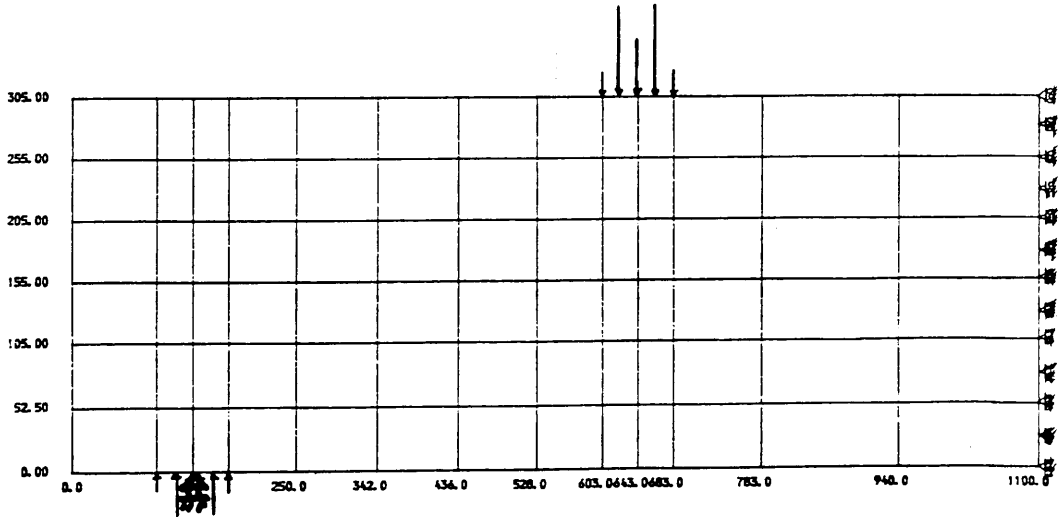

FIGURE (6.10) : 78 elements mesh for $a_v/d = 2.5$

Details of the analysed beams:

Details of the analysed beams are given in Figure (6.11) and Table (6.1). The other material variables required as input in the program are calculate using some well known formulae given in section **6.3.3** .

Figure (6.12) shows the load versus displacement curve at the mid–span of beam with (a_v/d = 1.0) for different sizes of mesh. From this curve it can be seen that the overall behaviour of the beam is not affected by the mesh refinement. The obtained failure loads for each mesh are shown in Table (6.2).

Table (6.2):

Computed load / Experimental failure load for various meshes for beams with shear span to depth ratio a_v/d = 1.0

Number of elements	Computed load / Exper. Failure load
10	1.14
18	1.12
24	1.07
36	1.06
48	1.05

Tolerance (Tol) = 5% .

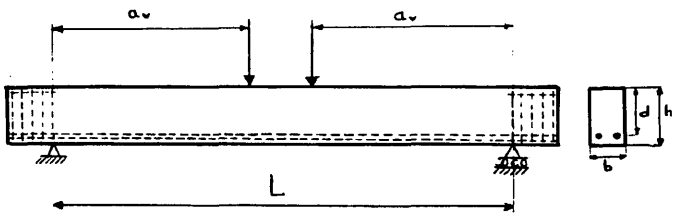

a) Test for $a_v/d = 1.0$

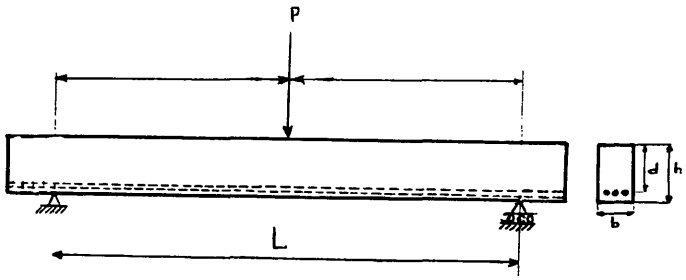

b) Test for $a_v/d = 2.50$

Figure (6.11):

TABLE (6.1):

a_v/d	a_v (mm)	L (mm)	h (mm)	d (mm)	b (mm)	ρ	f_y (N/mm²)	r	f_{yt} (N/mm²)	f_c' (N/mm²)	Experimental ultimate load (KN)
1.00	270	3600	320	270	190	0.0207	474	0	———	27.69	776.952
2.50	745	1490	337	298	152	0.0336	465	0	———	83.86	356.491

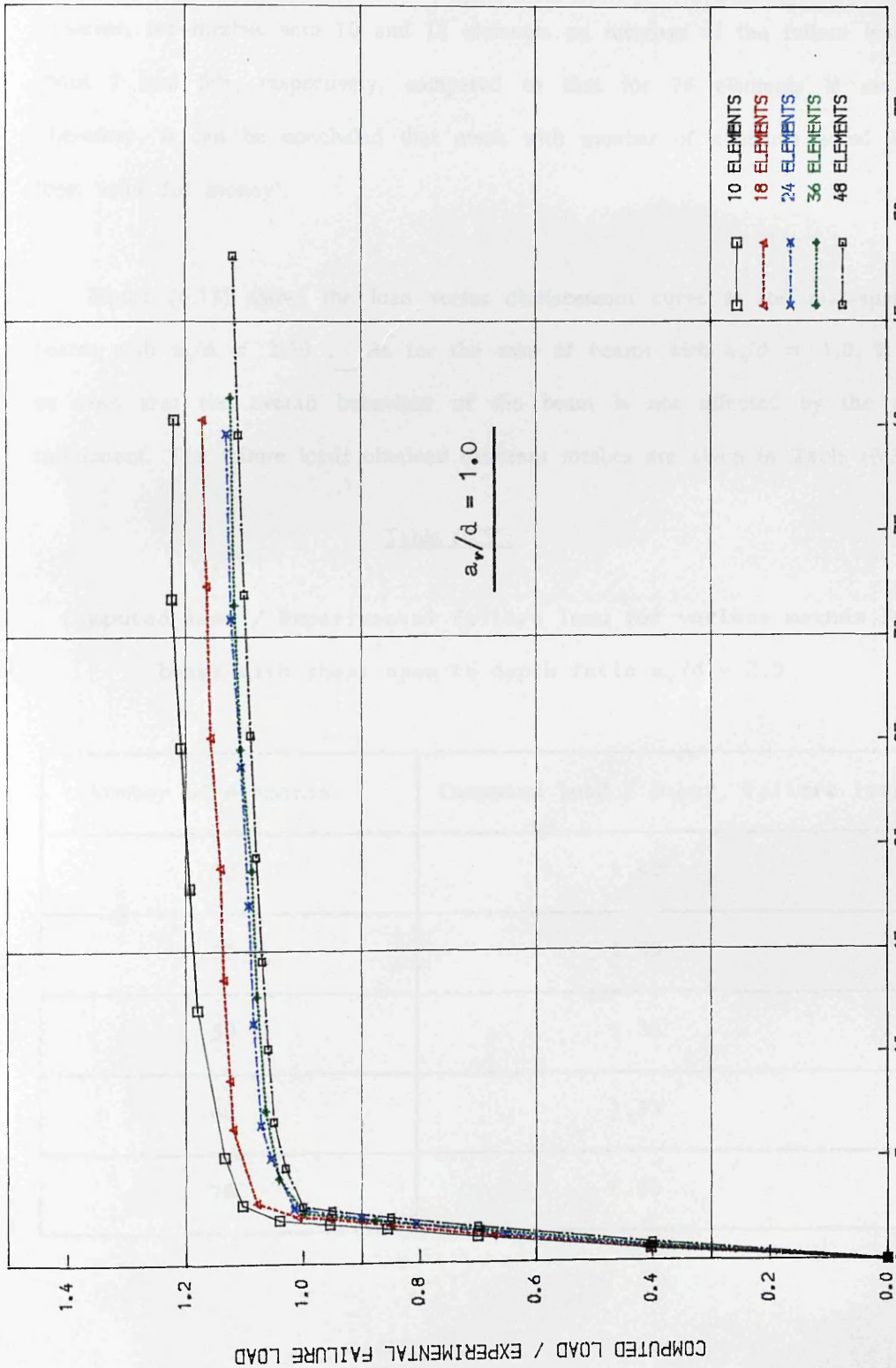

LOAD Vs DISPLACEMENT AT MID SPAN OF BEAM

FIGURE (6.12) EFFECT OF THE MESH SIZE ON THE NONLINEAR SOLUTION (a_v/d = 1.0)

From these results it can be seen that while the number of elements has doubled (from 24 to 48), the variation of the failure load is about 3%. However, for meshes with 10 and 18 elements an increase of the failure load of about 7 and 5%, respectively, compared to that for 24 elements is noticed. Therefore, it can be concluded that mesh with number of elements equal 24 is 'best value for money'.

Figure (6.13) shows the load versus displacement curve at the mid–span of beams with $a_v/d = 2.50$. As for the case of beams with $a_v/d = 1.0$, it can be seen that the overall behaviour of the beam is not affected by the mesh refinement. The failure loads obtained different meshes are given in Table (6.3) :

Table (6.3):

Computed load / Experimental failure load for various meshes for beams with shear span to depth ratio $a_v/d = 2.5$

Number of elements	Computed load / Exper. Failure load
12	1.42
30	1.35
39	1.34
60	1.33
78	1.32

LOAD Vs DISPLACEMENT AT MID SPAN OF BEAM

FIGURE (6.13) EFFECT OF THE MESH SIZE ON THE NONLINEAR SOLUTION (a_v/d = 2.5)

These results show that while the number of elements has more than doubled (from 30 to 78), the variation of the failure was only about 3%. However, for mesh with 12 elements 9% increase of the failure load compared to that with 30 elements was noticed. Therefore, it can be concluded that the 30 elements mesh gives satisfactory results.

6.2.2 Variation of the convergence tolerance (Tol):

As the norm of convergence tolerance (Tol) given by the ratio of the norm of residuals to the norm of the total applied loads, can have important effect on the nonlinear solution, four different values of Tol : 10%, 5%, 2%, and 1% have been investigated. The corresponding values of the maximum number of iterations used for each value of Tol are : 15, 15, 30, and 40, respectively.

These tests were carried out for two different values of a_v/d : 1.0 and 2.5, in which meshes with 48 and 60 elements, respectively, were used. The results obtained are summarized in Table (6.4) :

Table (6.4)

Ratio of the computed / experimental failure load for various values of the norm of convergence tolerance Tol

No. of elements	a_v/d	Tol = 10%	5%	2%	1%
48	1.0	1.10	1.05	1.03	1.02
60	2.5	1.40	1.33	1.32	1.32

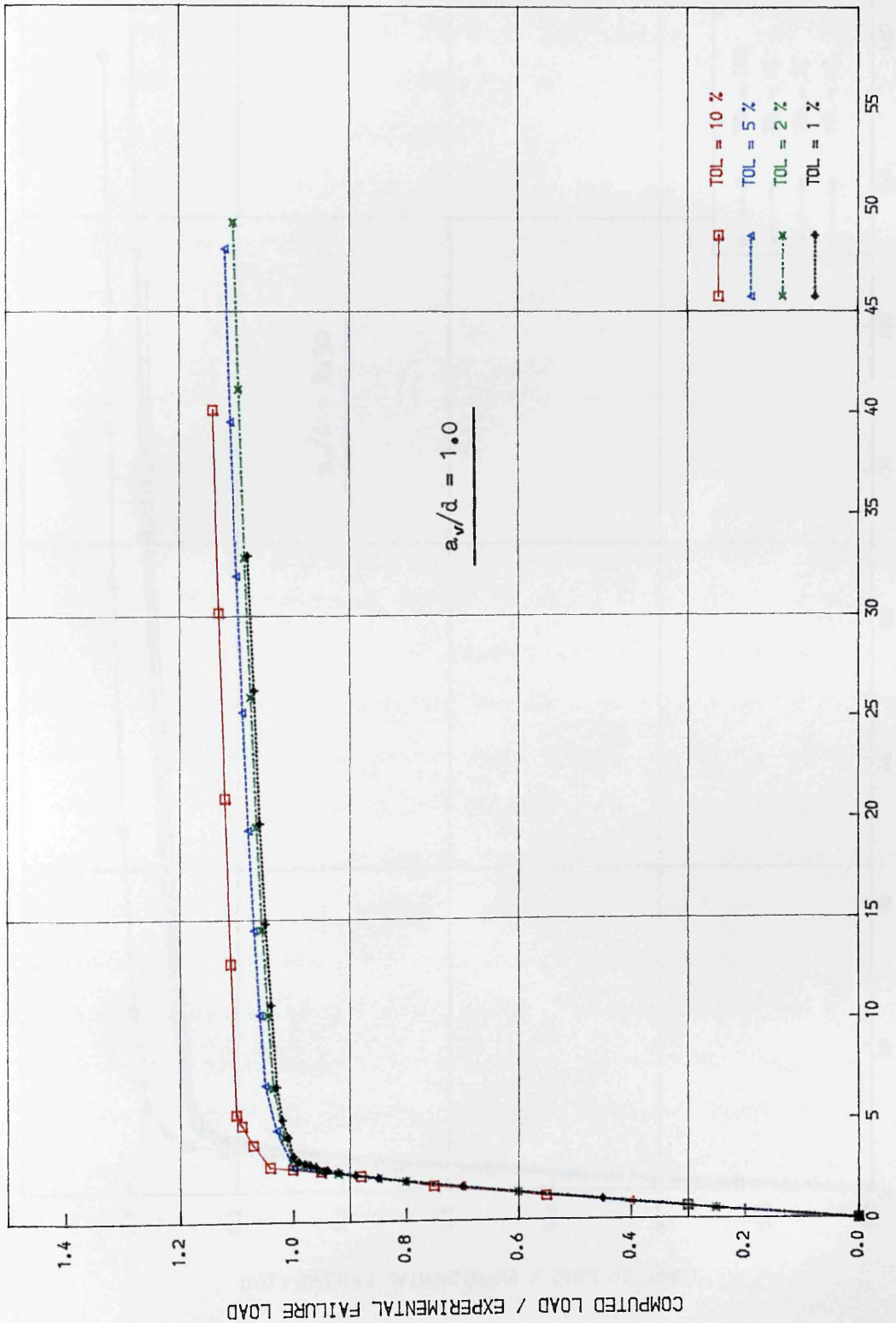

LOAD Vs DISPLACEMENT AT MID SPAN OF BEAM

FIGURE (6.14) CONVERGENCE TOLERANCE NORM EFFECT ON NONLINEAR SOLUTION (a_v/d=1.0)

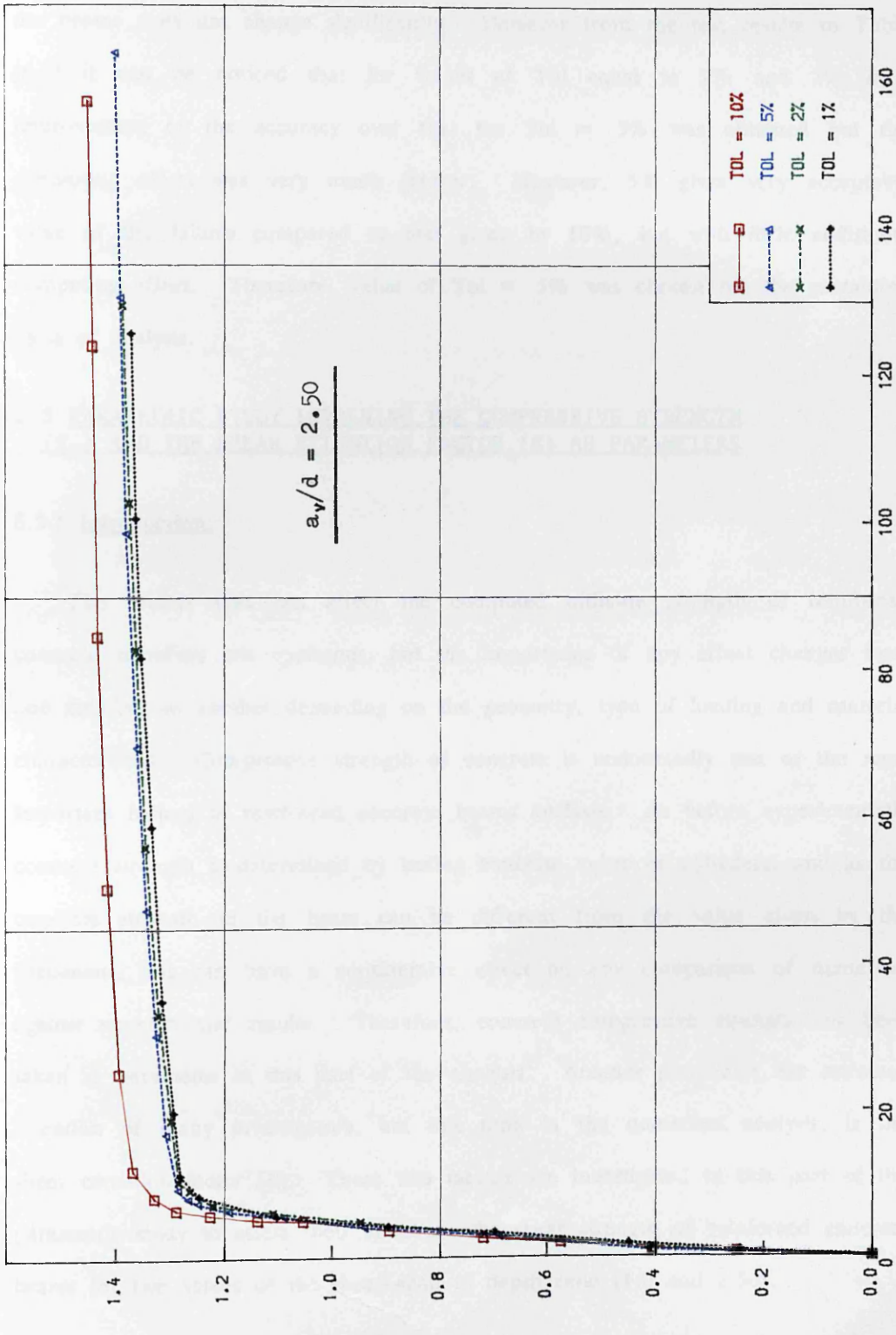

LOAD Vs DISPLACEMENT AT MID SPAN OF BEAM

FIGURE (6.15) CONVERGENCE TOLERANCE NORM EFFECT ON NONLINEAR SOLUTION (a_v/d=2.5)

From Figures (6.14) and (6.15), it can be seen that the general behaviour of the beams does not change significantly. However from the test results in Table (6.4) it can be noticed that for values of Tol equal to 1% and 2% little improvement of the accuracy over that for Tol = 5% was obtained but the computing effort was very much greater. However, 5% gives very acceptable value of the failure compared to that given by 10%, but with little additional computing effort. Therefore, value of Tol = 5% was chosen for the remaining parts of analysis.

6.3 PARAMETRIC STUDY INVOLVING THE COMPRESSIVE STRENGTH (f_c) AND THE SHEAR RETENTION FACTOR (β) AS PARAMETERS

6.3.1 Introduction:

The factors that can affect the computed ultimate strength of reinforced concrete members are numerous, but the importance of any effect changes from one member to another depending on the geometry, type of loading and material characteristics. Compressive strength of concrete is undoubtedly one of the most important factors in reinforced concrete beams analysis. As before experimentally concrete strength is determined by testing concrete cubes or cylinders, and as the concrete strength in the beam can be different from the value given by the specimens, this can have a considerable effect on any comparison of numerical against experimental results. Therefore, concrete compressive strength has been taken as parameter in this part of the analysis. Another parameter has attracted attention of many investigators, but this time in the numerical analysis, is the shear retention factor (β). These two factors are investigated in this part of the parametric study to assess their effect on the shear strength of reinforced concrete beams for two values of the shear–span to depth ratio (1.0 and 2.50).

6.3.2 General procedure:

As mentioned earlier, this part of the paramertric study is carried out for two values of the shear–span to depth ratio. The reason for this is that as shown in Figure (2.8), the mode of failure for different values of a_v/d tends to be different so that the effect of each of these two parameters could have an important change from one value to the other.

The general procedure adopted is first of all to take from the large number of existing experimental data, two tests where the values of a_v/d are 1.0 and 2.5, respectively. Then, these two are analysed numerically. Finally, a comparison of the numerical and experimental results is made for each value of the parameter.

From what preceeded, it appears inevitable that some assumptions have to be made whenever one, or some of the necessary input data are missing in the original experimental data. Since the only material property quoted is concrete compressive strength, other properties where computed as explained below :

6.3.3 Derived material properties:

It should be noted that the same beams used for the convergence study are used in this part of the parametric study. Therefore, details can be found in Table (6.1) and Figure (6.11). Some material variables required as input in the program are calculated using some well known formulae as follows :

1– The uniaxial compessive strength of a cylinder f_c' is obtained from the uniaxial compressive strength of a cube by :

$$f_c' = 0.78\ f_{cu} \qquad (N/mm^2) \qquad (6.1)$$

2– The tensile strength of concrete f_t is calculated from the uniaxial compressive strength of concrete cube f_{cu} by :

$$f_t = \frac{f_{cu}}{20} + 0.7 \qquad (N/mm^2) \qquad (6.2)$$

3– The maximum biaxial compressive strength for concrete is given by :

$$f_{cb} = 1.16\ f_{cu} \qquad (N/mm^2) \qquad (6.3)$$

4– Poisson's ratio :

$$\nu = 0.15 \qquad (N/mm^2) \qquad (6.4)$$

5– The maximum tensile strain is calculated by :

$$\epsilon_{cr} = \frac{f_t}{E_c} \qquad (6.5)$$

6– Steel elastic modulus whenever missing in the experimental data is given a constant value of 2.1×10^5 (N/mm^2).

7– Finally, the work hardening effect of steel is ignored throughout this study.

It can be seen from what preceeded that, by varying the value f_c', values of ϵ_{cr}, f_t and f_{cb} are all affected.

6.3.4 General comments about load vs displacement and steel strain curves:

a) Load–Displacement curves:

These curves give the Numerical/experimental failure load ratio versus the deflexion of the bottom at mid–span of the beam.

b) Load–Strain of tensile reinforcement:

These curves give the Numerical/experimental failure load ratio versus the strain of the tensile reinforcement at the Gauss point closest to the mid–span of the beam.

6.3.5 Presentation of results:

The aim of this part of the study is to assess the effect of each parameter. This was accomplished by varying one while keeping all others constant.

It should be noted that the same beams used for the convergence study are used in this part of the parametric study. Therefore for details see Table (6.1) and Figure (6.11).

a) $a_v/d = 1.0$:

For this value of shear–span to depth ratio, the theoretical value of concrete uniaxial strength f_c was studied for three values 100%, 90%, and 80% of the experimental values f_c'. The shear retention factor β was studied for four values 0.3, 0.5, 0.8, and 1.0 . The results are summarized in Table (6.5).

b) $a_v/d = 2.5$:

For this value of shear–span to depth ratio, the theoretical value of concrete uniaxial compressive strength f_c was studied for three values 100%, 80%, and 70% of the experimental values f_c'. The shear retention factor β was studied for four values 0.3, 0.5, 0.8, and 1.0 . The obtained results are summarized in Table (6.6).

TABLE (6.5):

Effect of concrete compressive strength f_c', and shear retention factor β on the computed /experimental failure load of reinforced for reinforced concrete beams with $a_v/d = 1.0$

f_c	β = 0.30	0.50	0.80	1.00
100 % f_c'	1.03	1.05	1.06	1.07
90 % f_c'	0.97	0.98	1.00	1.01
80 % f_c'	0.85	0.87	0.88	0.89

TABLE (6.6):

Effect of concrete compressive strength f_c', and shear retention factor β on the computed /experimental failure load of reinforced concrete beams with $a_v/d = 2.5$

f_c	β = 0.30	0.50	0.80	1.00
100 % f_c'	1.28	1.32	1.32	1.33
80 % f_c'	1.07	1.09	1.09	1.12
70 % f_c'	0.96	0.97	0.98	1.01

6.3.6 Discussion of results:

a) $a_v/d = 1.0$:

i) Effect of f_c':

From Table (6.5), it appears clearly that the concrete uniaxial compressive strength f_c has a great influence on the computed the failure load of the beam . In fact, as the the value of f_c is decreased by 10% (from 100% to 90%) of f_c', the failure load decreases by around 6%. This effect is even more important as the value of f_c is decreased to 80% of f_c' where it can be seen that for 20% decrease in f_c a corresponding 18.5% decrease of the failure load is obtained.

Moreover, the value of f_c can influence greatly the behaviour of the beam and its mode of failure. This can be seen in Figure (6.17) which shows clearly that the mode of failure of the beam has changed from the pure shear failure when f_c is reduced to 80% of f_c' to a more ductile type of failure, allowing the reinforcement to yield before the total collapse of the beam when 90 or 100% of f_c' is used.

ii) Effect of β:

From Table (6.5) it can be noticed that only 4% increase of the failure load was obtained for a variation β from 0.3 to 1.0 (more than three times). In fact it can be seen from the general trend in Figures (6.18) and (6.19) that β has a negligible effect on the behaviour of the beam and its mode of failure.

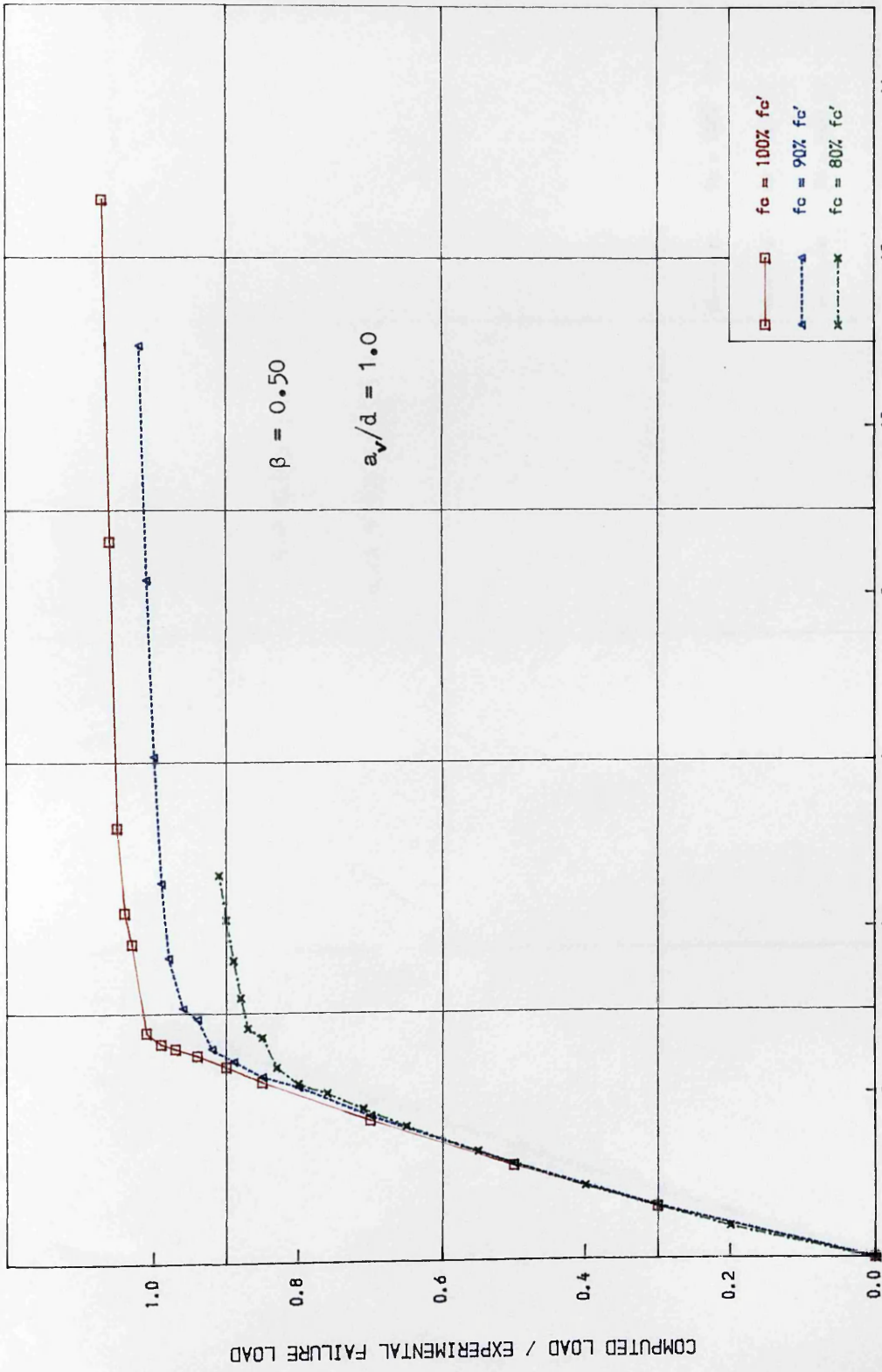

BEAM MID-SPAN DEFLEXION CURVE VARYING WITH fc

FIGURE (6.16) EFFECT OF fc ON FAILURE LOAD AND MODE OF FAILURE OF R.C. BEAMS

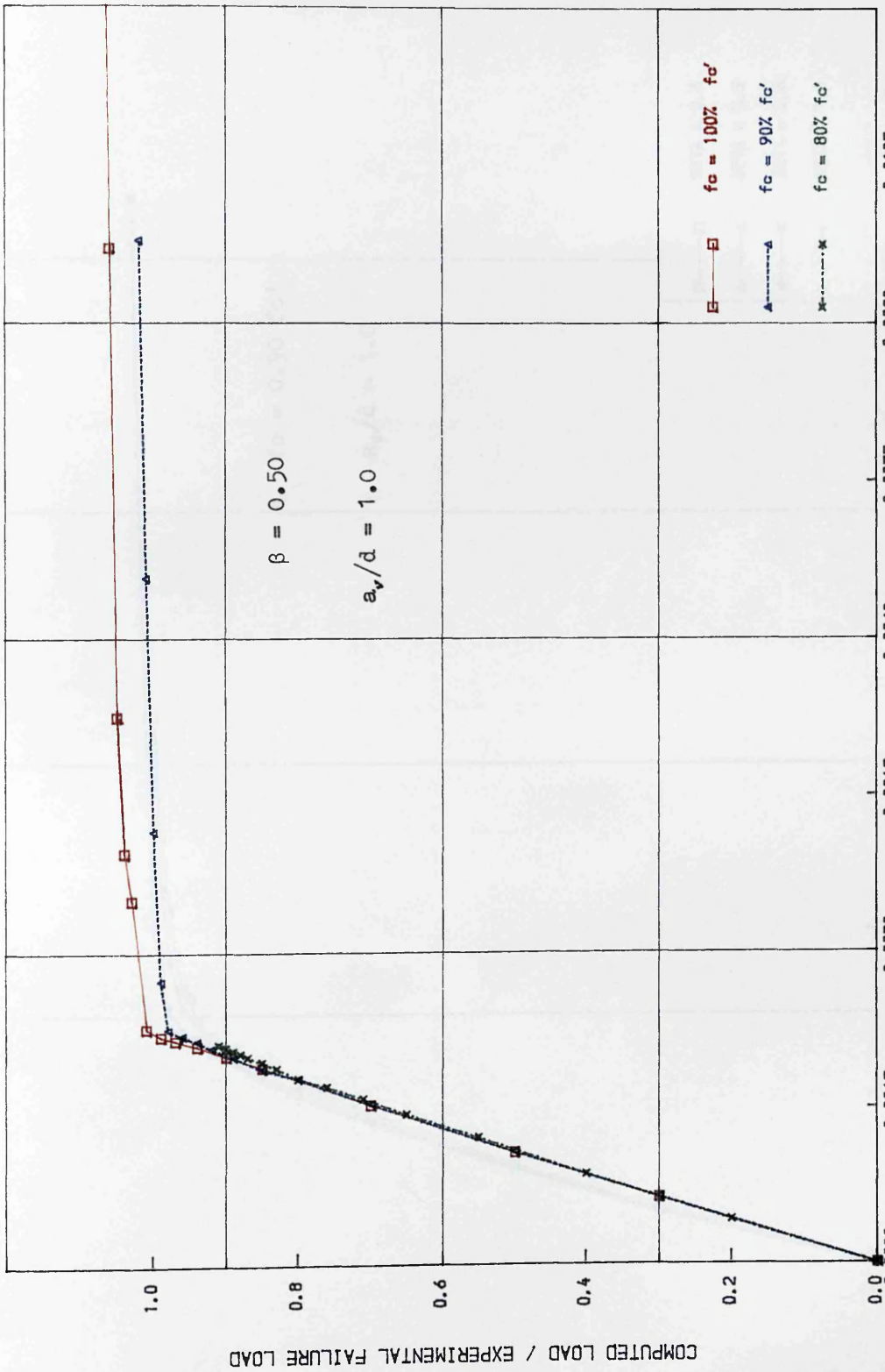

TENSILE REINFORCEMENT STRAIN AT MID SPAN FOR DIFFERENT VALUES OF fc

FIGURE (6.17) EFFECT OF fc ON FAILURE LOAD AND MODE OF FAILURE OF R.C. BEAMS

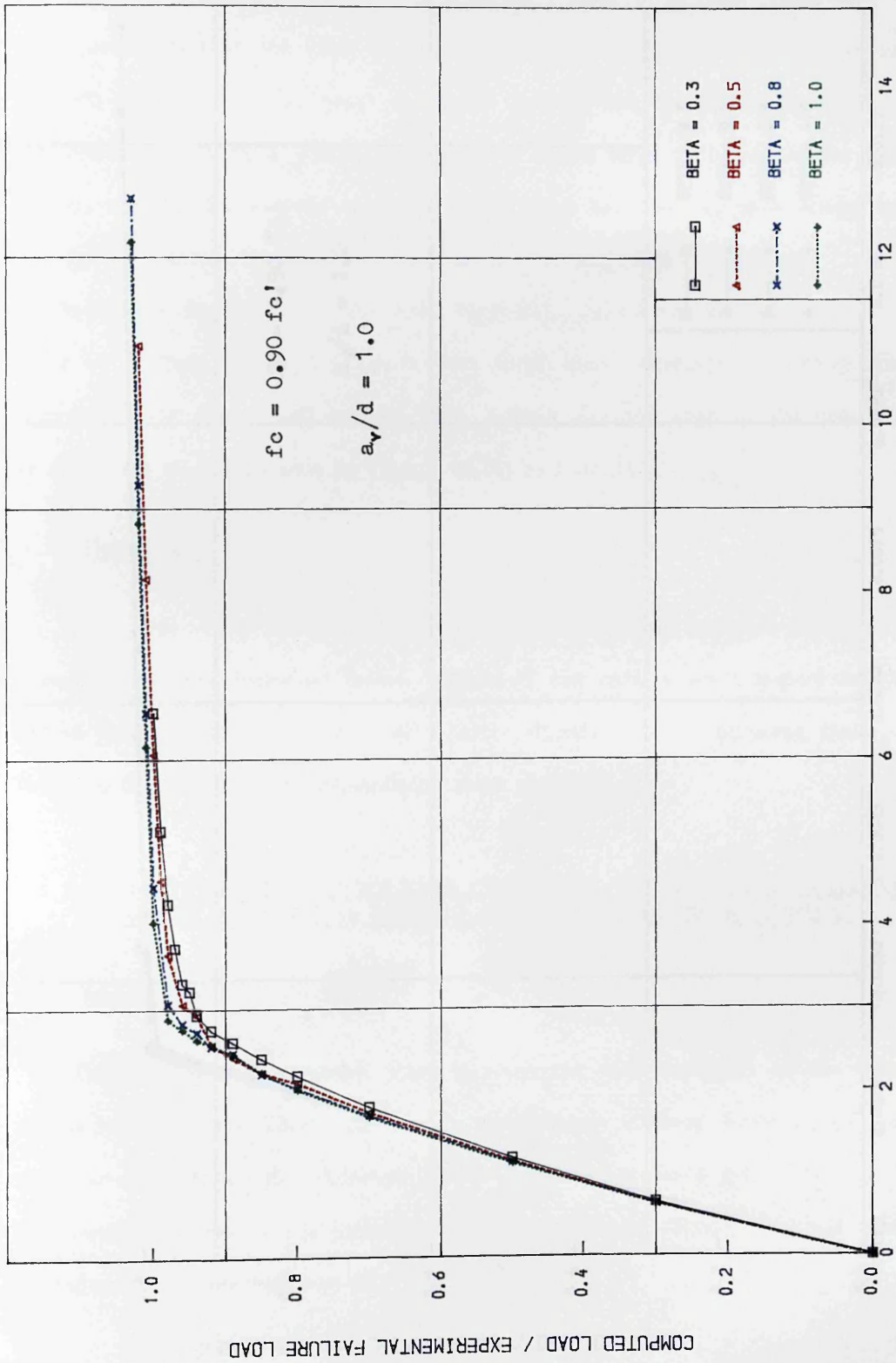

BEAM MID-SPAN DEFLEXION CURVE VARYING WITH BETA

FIGURE (6.18) EFFECT OF BETA ON FAILURE LOAD AND MODE OF FAILURE OF R.C BEAMS

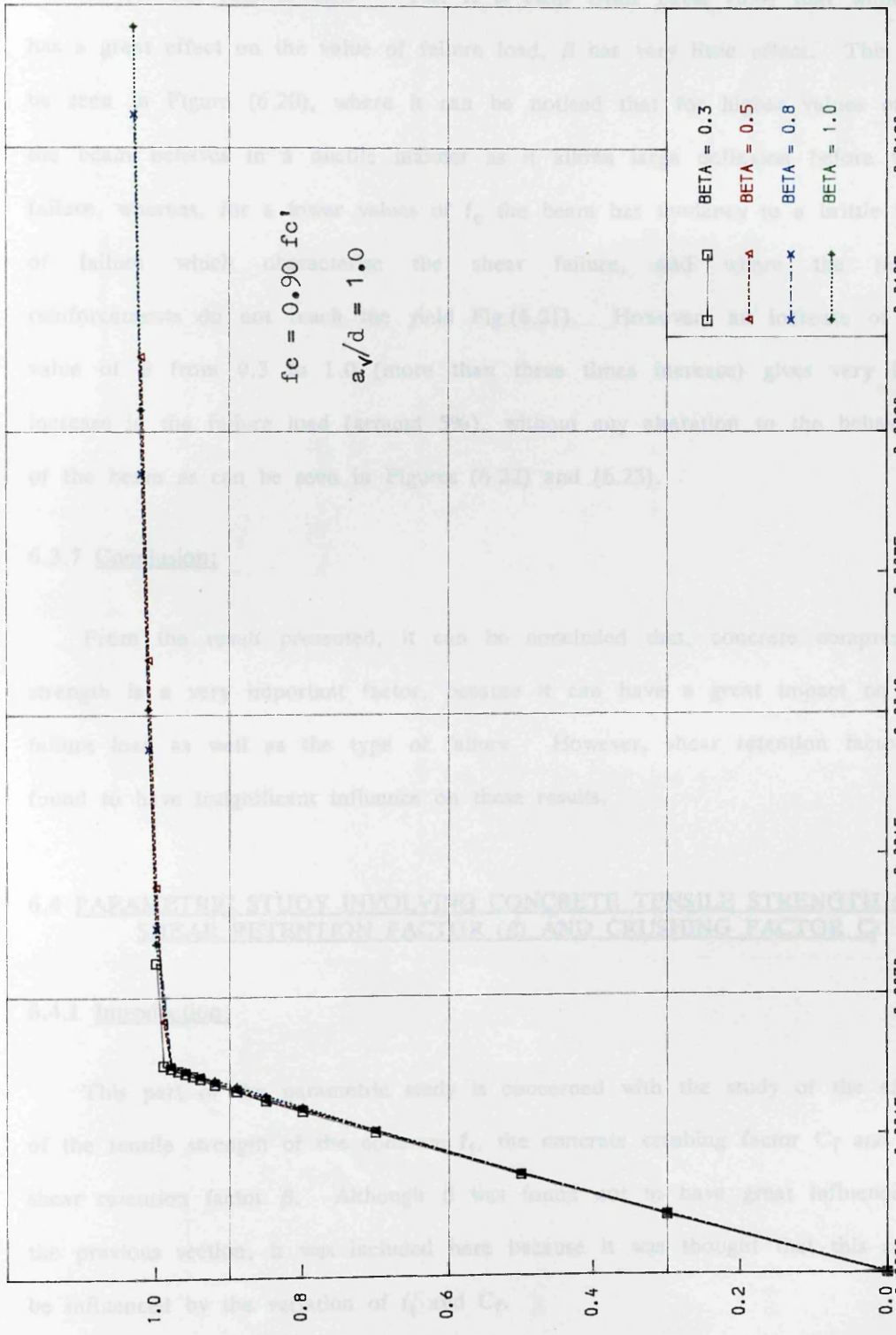

TENSILE REINFORCEMENT STRAIN AT MID SPAN FOR DIFFERENT VALUES OF BETA

FIGURE (6.19) EFFECT OF BETA ON FAILURE LOAD AND MODE OF FAILURE OF R.C. BEAMS

b) $a_v/d = 2.5$:

As for the case of $a_v/d = 1.0$, it is clear from Table (6.6) that while f_c has a great effect on the value of failure load, β has very little effect. This can be seen in Figure (6.20), where it can be noticed that for higher values of f_c the beam behaves in a ductile manner as it allows large deflexion before total failure, whereas, for a lower values of f_c the beam has tendency to a brittle type of failure which characterise the shear failure, and where the tensile reinforcements do not reach the yield Fig.(6.21). However, an increase of the value of β from 0.3 to 1.0 (more than three times increase) gives very little increase in the failure load (around 5%), without any alteration to the behaviour of the beam as can be seen in Figures (6.22) and (6.23).

6.3.7 Conclusion:

From the result presented, it can be concluded that, concrete compressive strength is a very important factor, because it can have a great impact on the failure load as well as the type of failure. However, shear retention factor is found to have insignificant influence on these results.

6.4 PARAMETRIC STUDY INVOLVING CONCRETE TENSILE STRENGTH (f_t) SHEAR RETENTION FACTOR (β) AND CRUSHING FACTOR C_f

6.4.1 Introduction:

This part of the parametric study is concerned with the study of the effect of the tensile strength of the concrete f_t, the concrete crushing factor C_f and the shear retention factor β. Although β was found not to have great influence in the previous section, it was included here because it was thought that this could be influenced by the variation of f_t and C_f.

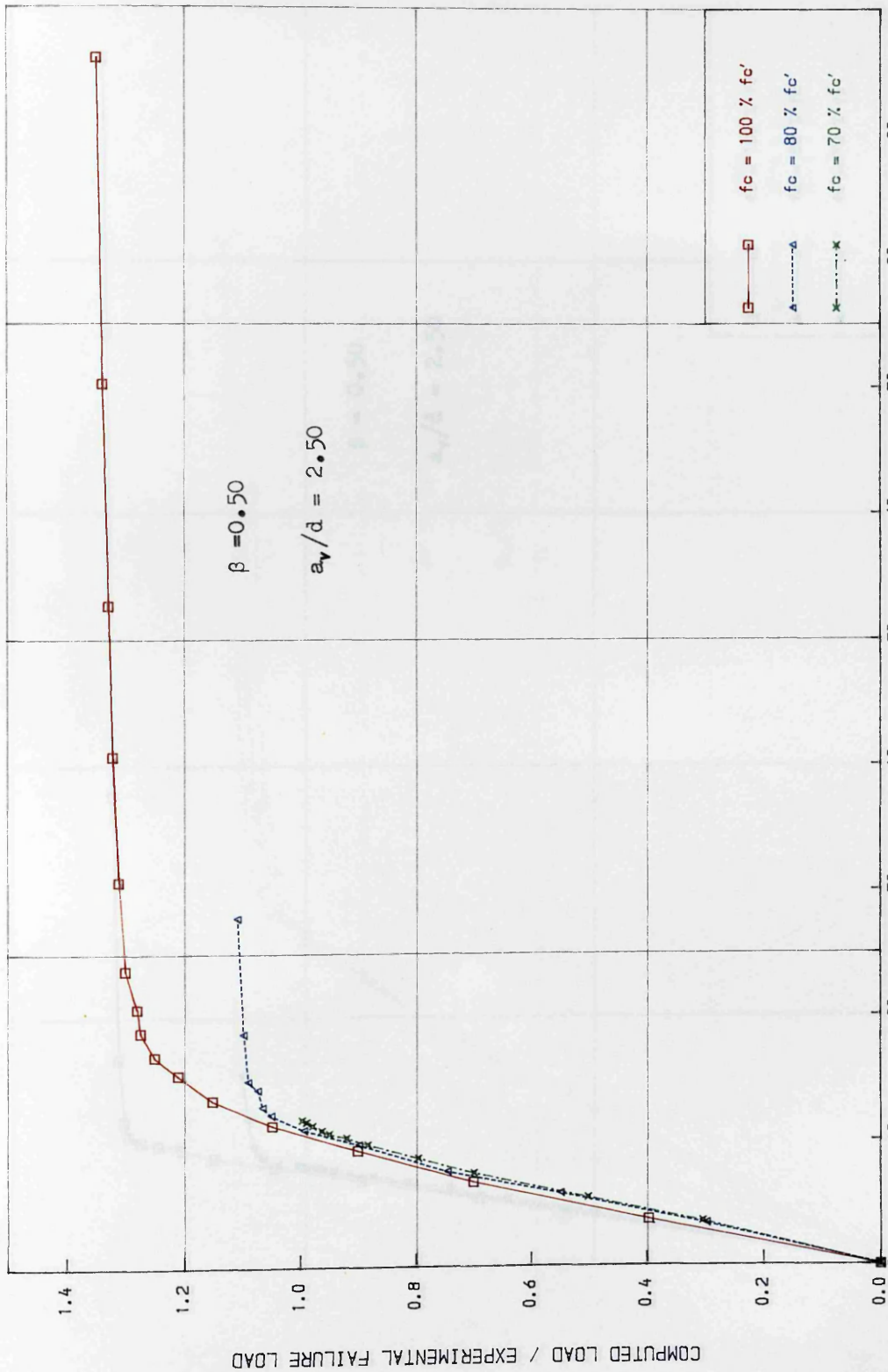

BEAM MID-SPAN DEFLEXION CURVE VARYING WITH fc

FIGURE (6.20) EFFECT OF fc ON FAILURE LOAD AND MODE OF FAILURE OF R.C BEAMS

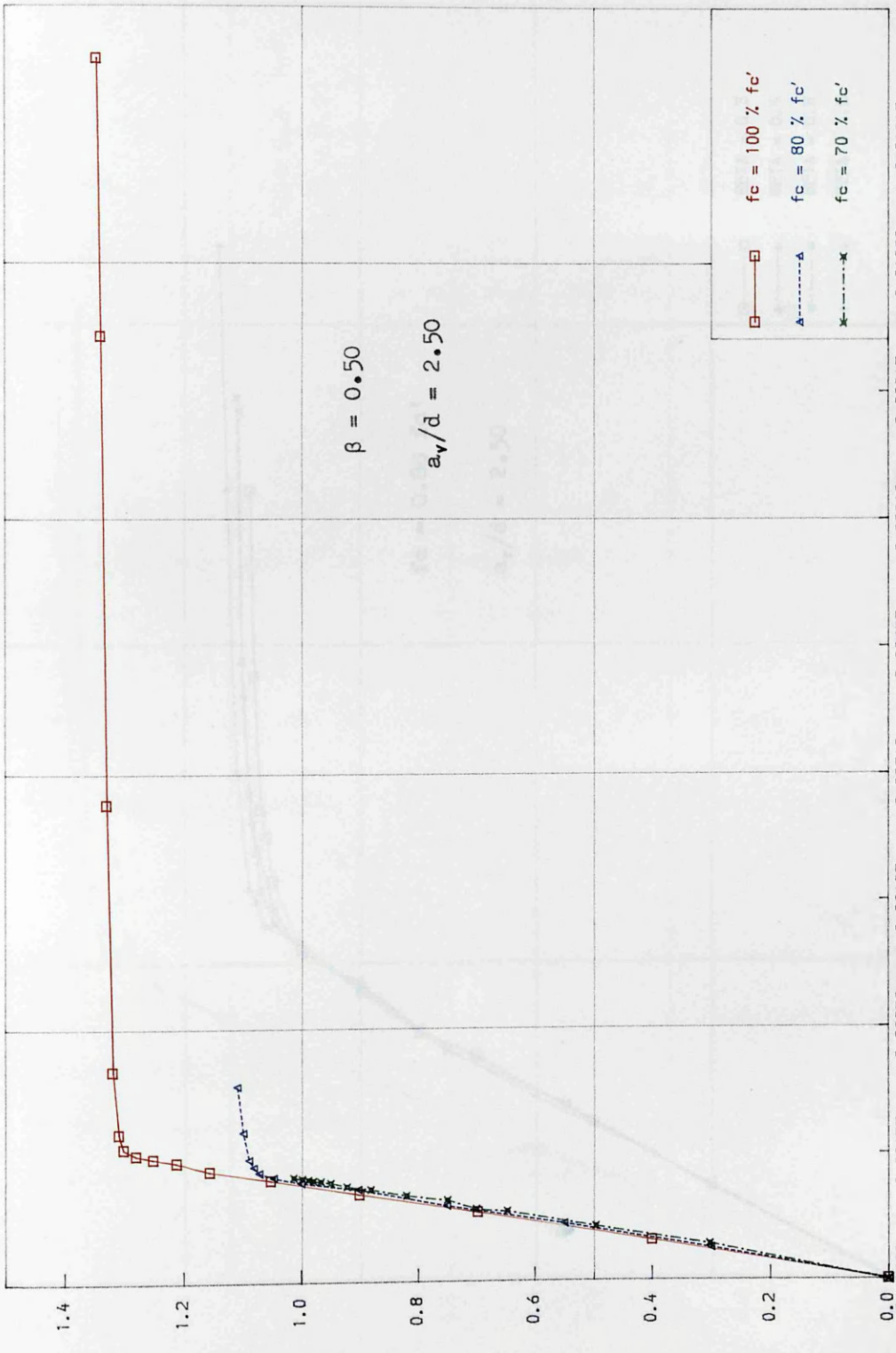

TENSILE REINFORCEMENT STRAIN AT MID SPAN FOR DIFFERENT VALUES OF fc

FIGURE (6.21) EFFECT OF fc ON FAILURE LOAD AND MODE OF FAILURE OF R.C. BEAMS

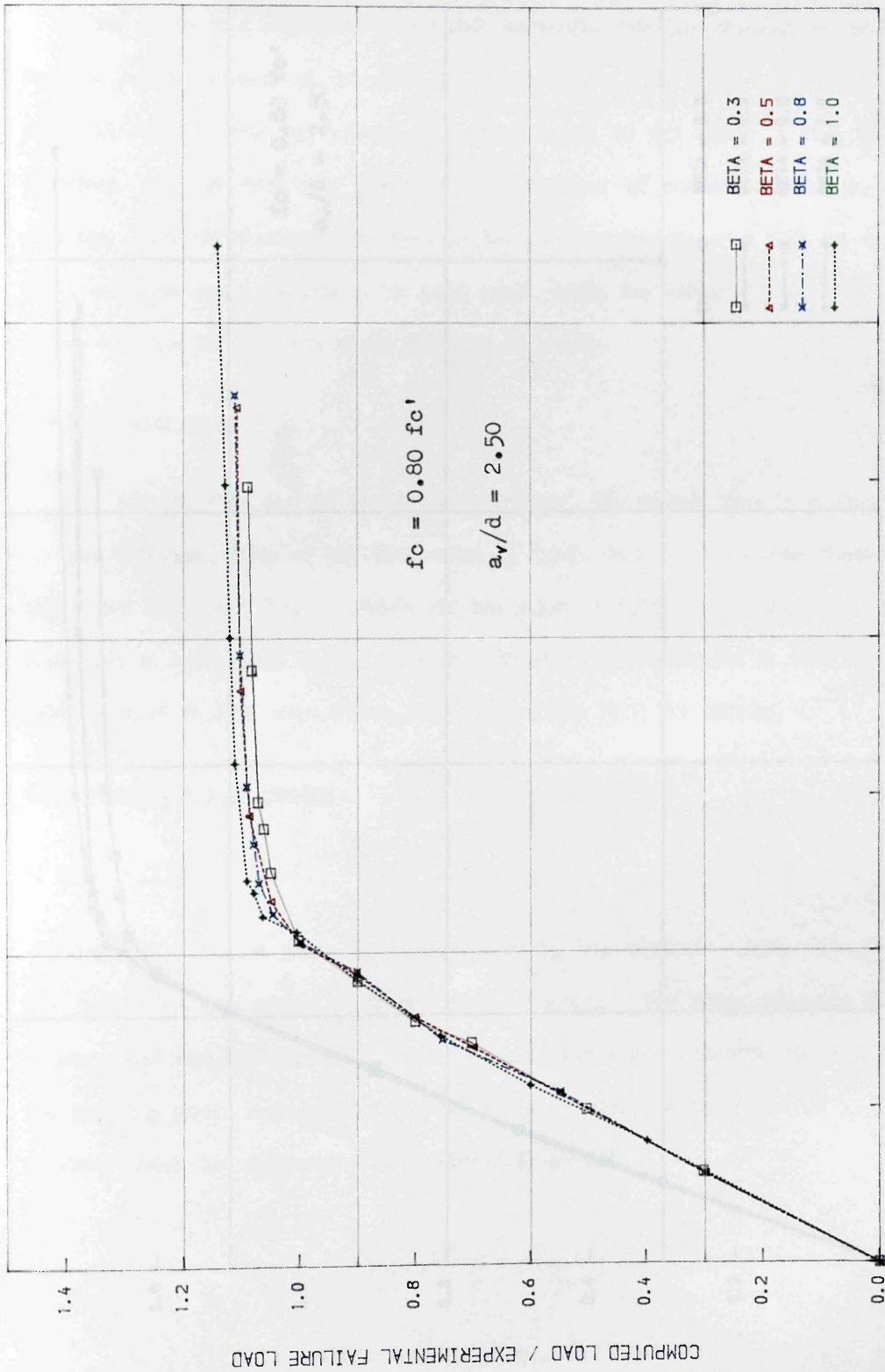

BEAM MID-SPAN DEFLEXION CURVE VARYING WITH BETA

FIGURE (6.22) EFFECT OF BETA ON FAILURE LOAD AND MODE OF FAILURE OF R.C BEAMS

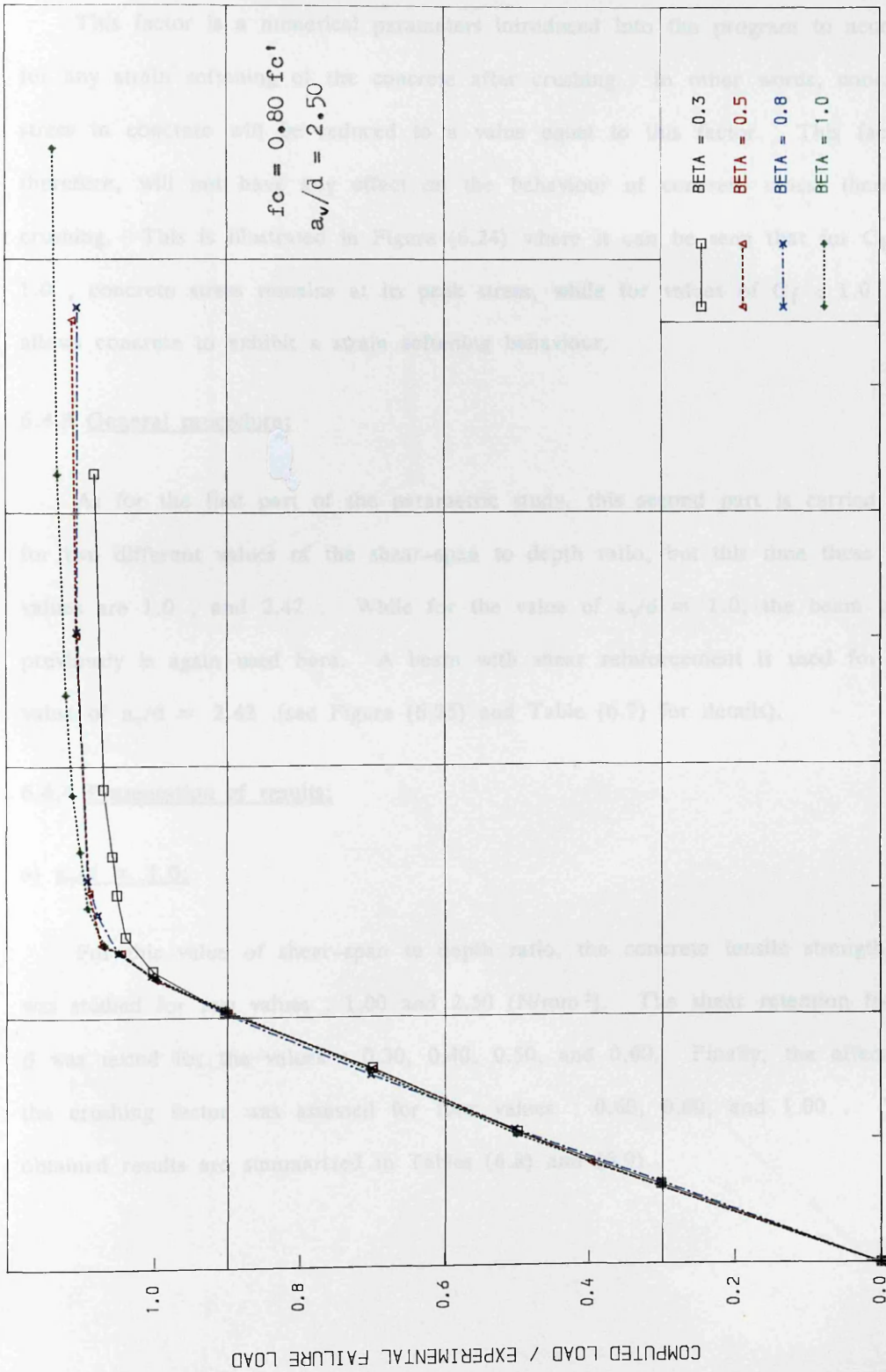

FIGURE (6.23) EFFECT OF BETA ON FAILURE LOAD AND MODE OF FAILURE OF R.C. BEAMS TENSILE REINFORCEMENT STRAIN AT MID SPAN FOR DIFFERENT VALUES OF BETA

6.4.2 Concrete crushing factor C_f:

This factor is a numerical parameters introduced into the program to account for any strain softening of the concrete after crushing. In other words, concrete stress in concrete will be reduced to a value equal to this factor. This factor, therefore, will not have any effect on the behaviour of concrete unless there is crushing. This is illustrated in Figure (6.24) where it can be seen that for $C_f = 1.0$, concrete stress remains at its peak stress, while for values of $C_f < 1.0$, it allows concrete to exhibit a strain softening behaviour.

6.4.3 General procedure:

As for the first part of the parametric study, this second part is carried out for two different values of the shear–span to depth ratio, but this time these two values are 1.0 , and 2.42 . While for the value of $a_v/d = 1.0$, the beam used previously is again used here. A beam with shear reinforcement is used for the value of $a_v/d = 2.42$.(see Figure (6.25) and Table (6.7) for details).

6.4.4 Presentation of results:

a) $a_v/d = 1.0$:

For this value of shear–span to depth ratio, the concrete tensile strength f_t, was studied for two values : 1.00 and 2.50 (N/mm^2). The shear retention factor β was tested for the values : 0.30, 0.40, 0.50, and 0.60. Finally, the effect of the crushing factor was assessed for four values : 0.60, 0.80, and 1.00 . The obtained results are summarized in Tables (6.8) and (6.9).

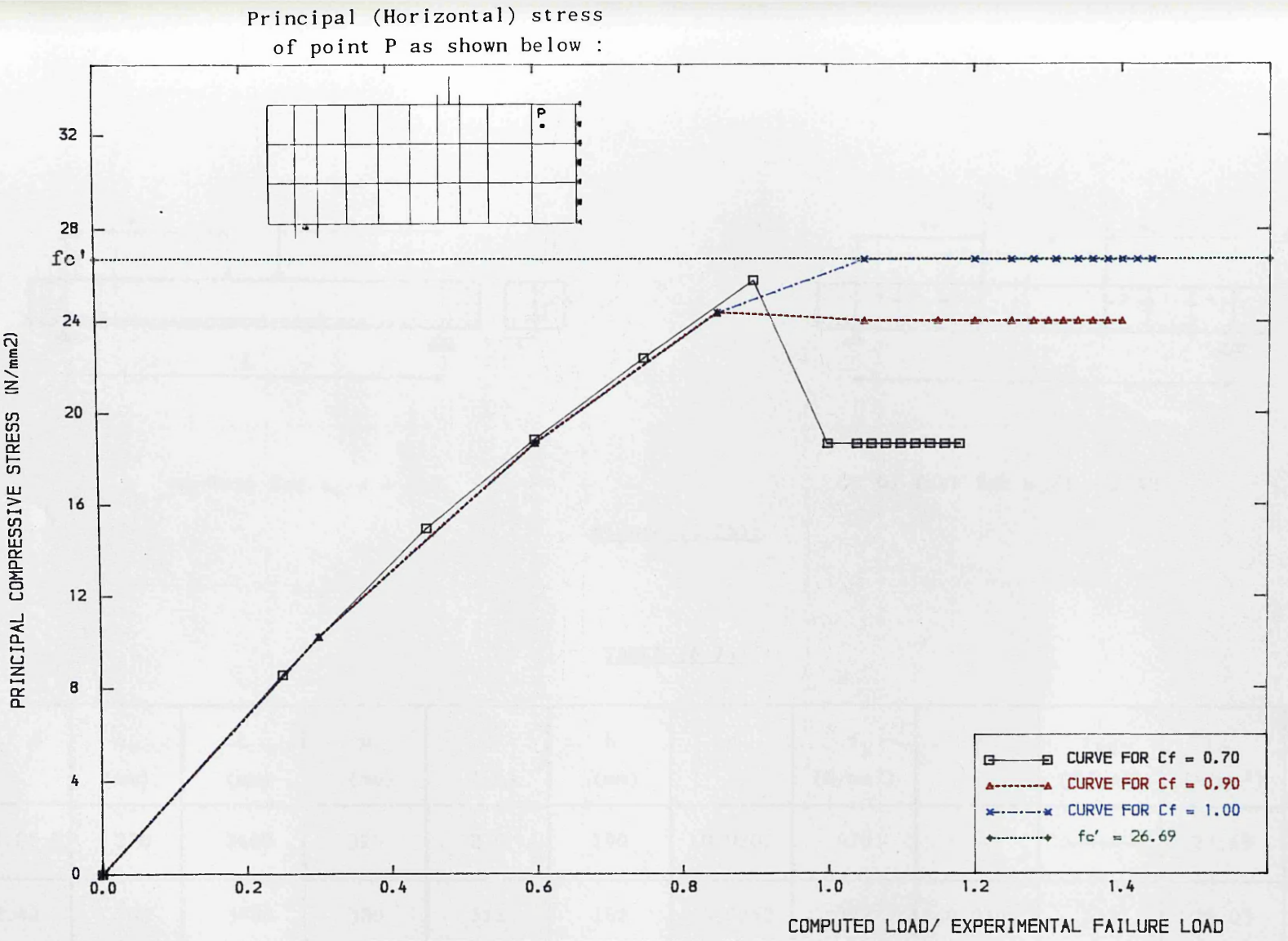

STRESS vs COMPUTED LOAD/ EXPERIMENTAL FAILURE LOAD CURVE

FIGURE (6.24) EFFECT OF THE CRUSHING FACTOR ON CONCRETE BEHAVIOUR

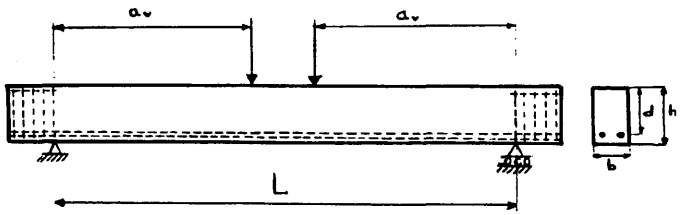

a) Test for $a_v/d = 1.0$

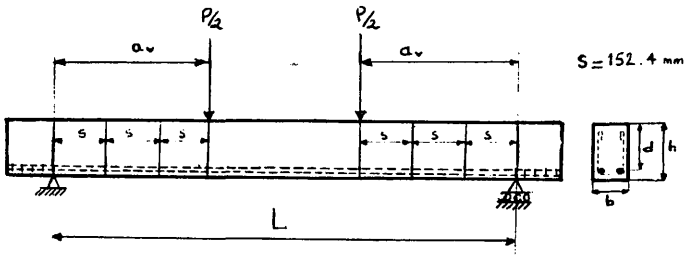

b) Test for $a_v/d = 2.42$

Figure (6.25):

TABLE (6.7):

a_v/d	a_v (mm)	L (mm)	h (mm)	d (mm)	b (mm)	ρ	f_y (N/mm²)	r	f_{yt} (N/mm²)	f_c' (N/mm²)	Experimental ultimate load (KN)
1.00	270	3600	320	270	190	0.0207	474	0	———	27.69	776.952
2.42	762	3050	380	315	152	0.0342	322	0.0342	332	28.05	308.219

TABLE (6.8):

Effect of concrete tensile strength f_t, shear retention factor β and crushing factor C_f on the computed / experimental failure load of reinforced concrete beams with $a_v/d = 1.0$, $f_t = 2.5$

C_f	β = 0.30	0.40	0.50	0.60
0.60	0.91	0.93	0.92	0.93
0.80	1.00	1.01	1.01	1.01
1.00	1.05	1.06	1.06	1.07

TABLE (6.9):

Effect of concrete tensile strength f_t, shear retention factor β and crushing factor C_f on the computed / experimental failure load of reinforced concrete beams with $a_v/d = 1.0$, $f_t = 1.0$

C_f	β = 0.30	0.40	0.50	0.60
0.60	0.89	0.91	0.91	0.92
0.80	0.99	1.00	1.00	1.00
1.00	1.05	1.05	1.05	1.06

b) $a_v/d = 2.42$:

As for $a_v/d = 1.0$, f_t was studied for two values : 1.00 and 2.50 (N/mm^2), and β was tested for the values : 0.30, 0.40, 0.50, and 0.60. However, the effect of C_f was assessed for : 0.60, 0.70, 0.80 and 1.00. The obtained results are summarized in Tables (6.10) and (6.11).

TABLE (6.10):

Effect of concrete tensile strength f_t, shear retention factor β and crushing factor C_f on the computed / experimental failure load of reinforced concrete beams with $a_v/d = 2.42$, $f_t = 2.50$

C_f	β = 0.30	0.40	0.50	0.60
0.60	0.99	0.99	1.01	1.02
0.70	1.05	1.06	1.07	1.08
0.80	1.11	1.12	1.12	1.14
1.00	1.17	1.18	1.19	1.21

TABLE(6.11):

Effect of concrete tensile strength f_t, shear retention factor β and crushing factor C_f on the computed / experimental failure load of reinforced concrete beams with $a_v/d = 2.42$, $f_t = 1.00$

C_f	β = 0.30	0.40	0.50	0.60
0.60	0.98	0.99	1.01	1.02
0.70	1.05	1.06	1.07	1.08
0.80	1.09	1.10	1.11	1.12
1.00	1.19	1.18	1.19	1.20

6.4.5 Discussion of the results:

a) Effect of the tensile strength of concrete f_t:

1- $a_v/d = 1.0$:

From the results, Tables (6.8) and (6.9), it is clear that this factor has a negligible effect (less than 1% in most cases). Moreover, load–displacement curves Fig.(6.26) and load–strain of tensile reinforcement at mid span Fig.(6.27), show that the curves for different values of f_t are similar at least until failure has occured.

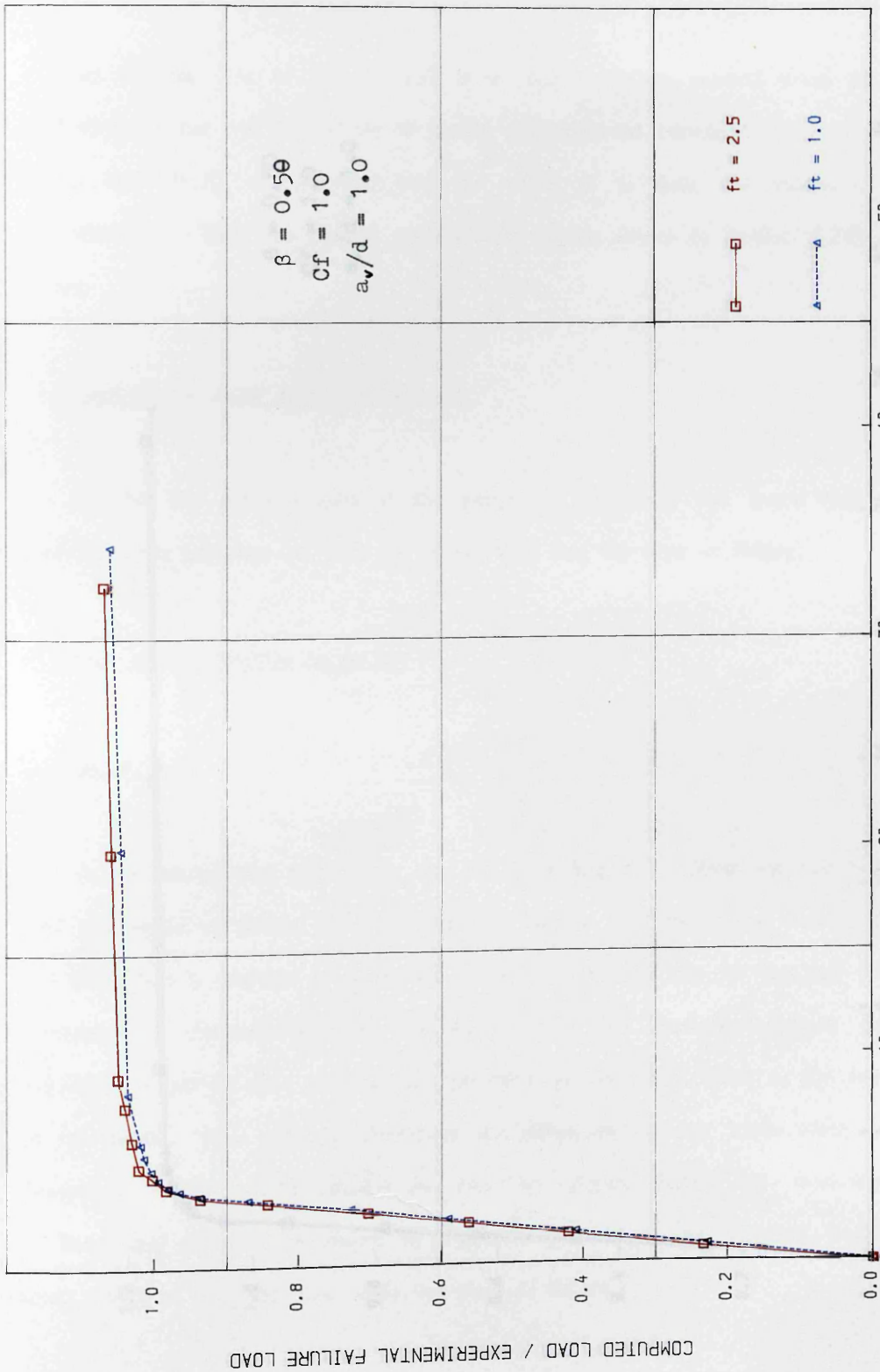

BEAM MID-SPAN DEFLEXION CURVE VARYING WITH ft

FIGURE (6.26) EFFECT OF ft ON FAILURE LOAD AND MODE OF FAILURE OF R.C BEAMS

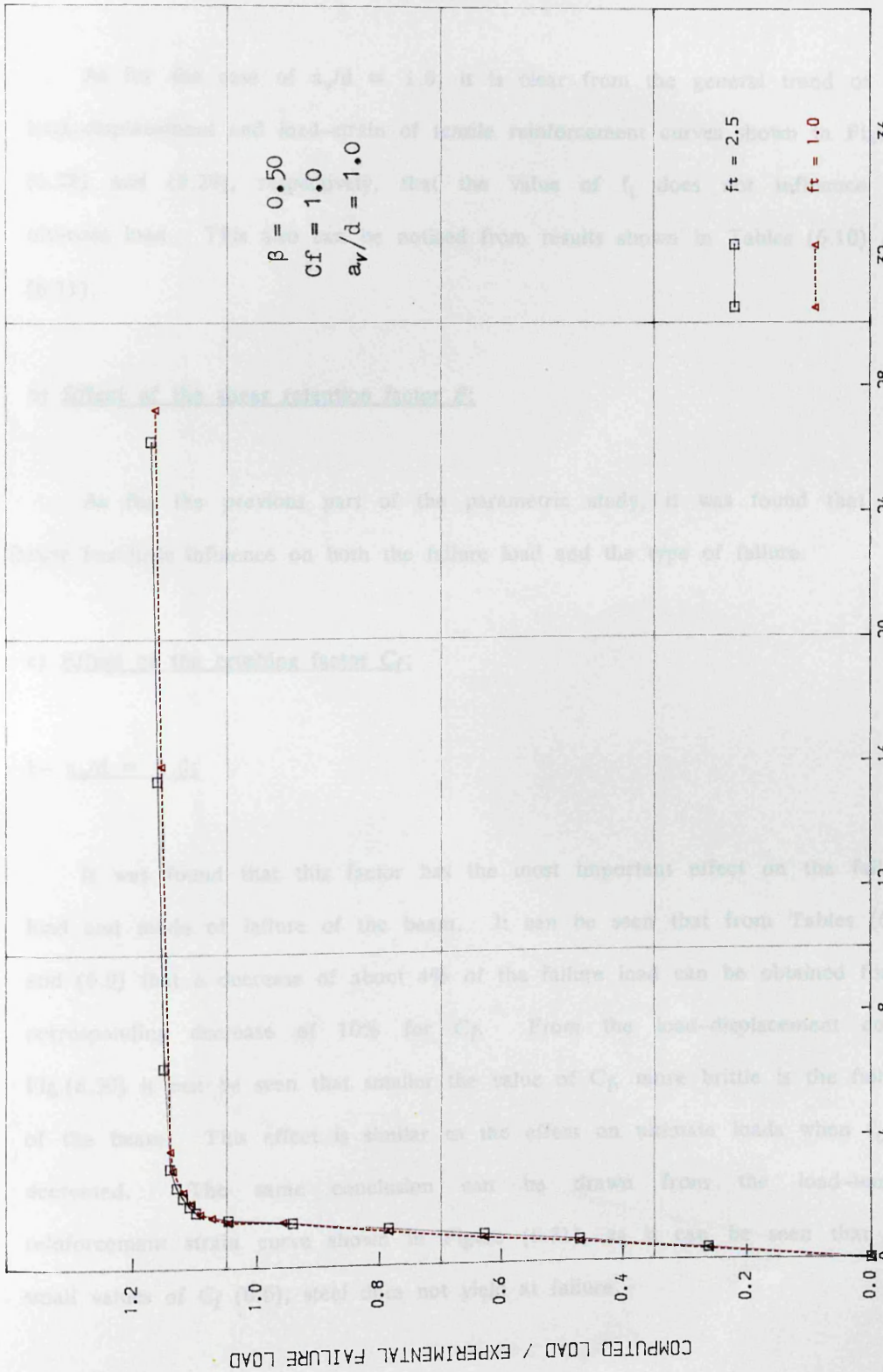

FIGURE (6.27) EFFECT OF ft ON FAILURE LOAD AND MODE OF FAILURE OF R.C. BEAMS
MAIN STEEL STRAIN AT MID-SPAN VARYING WITH ft

2– $a_v/d = 2.42$:

As for the case of $a_v/d = 1.0$, it is clear from the general trend of the load–displacement and load–strain of tensile reinforcement curves shown in Figures (6.28) and (6.29), respectively, that the value of f_t does not influence the ultimate load. This also can be noticed from results shown in Tables (6.10) and (6.11).

b) **Effect of the shear retention factor β:**

As for the previous part of the parametric study, it was found that this factor has little influence on both the failure load and the type of failure.

c) **Effect of the crushing factor C_f:**

1– $a_v/d = 1.0$:

It was found that this factor has the most important effect on the failure load and mode of failure of the beam. It can be seen that from Tables (6.8) and (6.9) that a decrease of about 4% of the failure load can be obtained for a corresponding decrease of 10% for C_f. From the load–displacement curve Fig.(6.30) it can be seen that smaller the value of C_f, more brittle is the failure of the beam. This effect is similar to the effect on ultimate loads when f_c is decreased. The same conclusion can be drawn from the load–tensile reinforcement strain curve shown in Figure (6.31), as it can be seen that for small values of C_f (0.6), steel does not yield at failure.

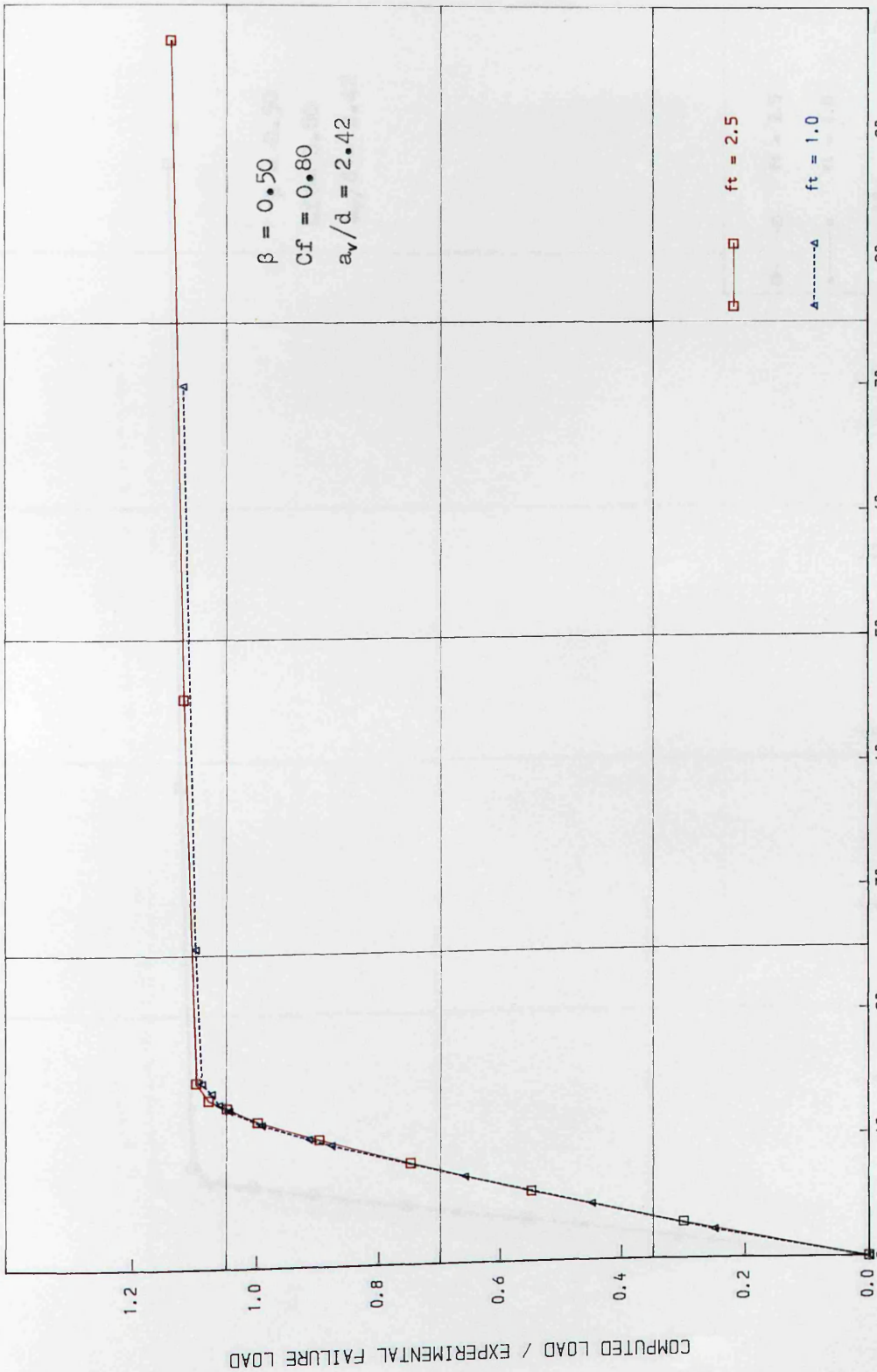

BEAM MID-SPAN DEFLEXION CURVE VARYING WITH ft

FIGURE (6.28) EFFECT OF ft ON FAILURE LOAD AND MODE OF FAILURE OF R.C BEAMS

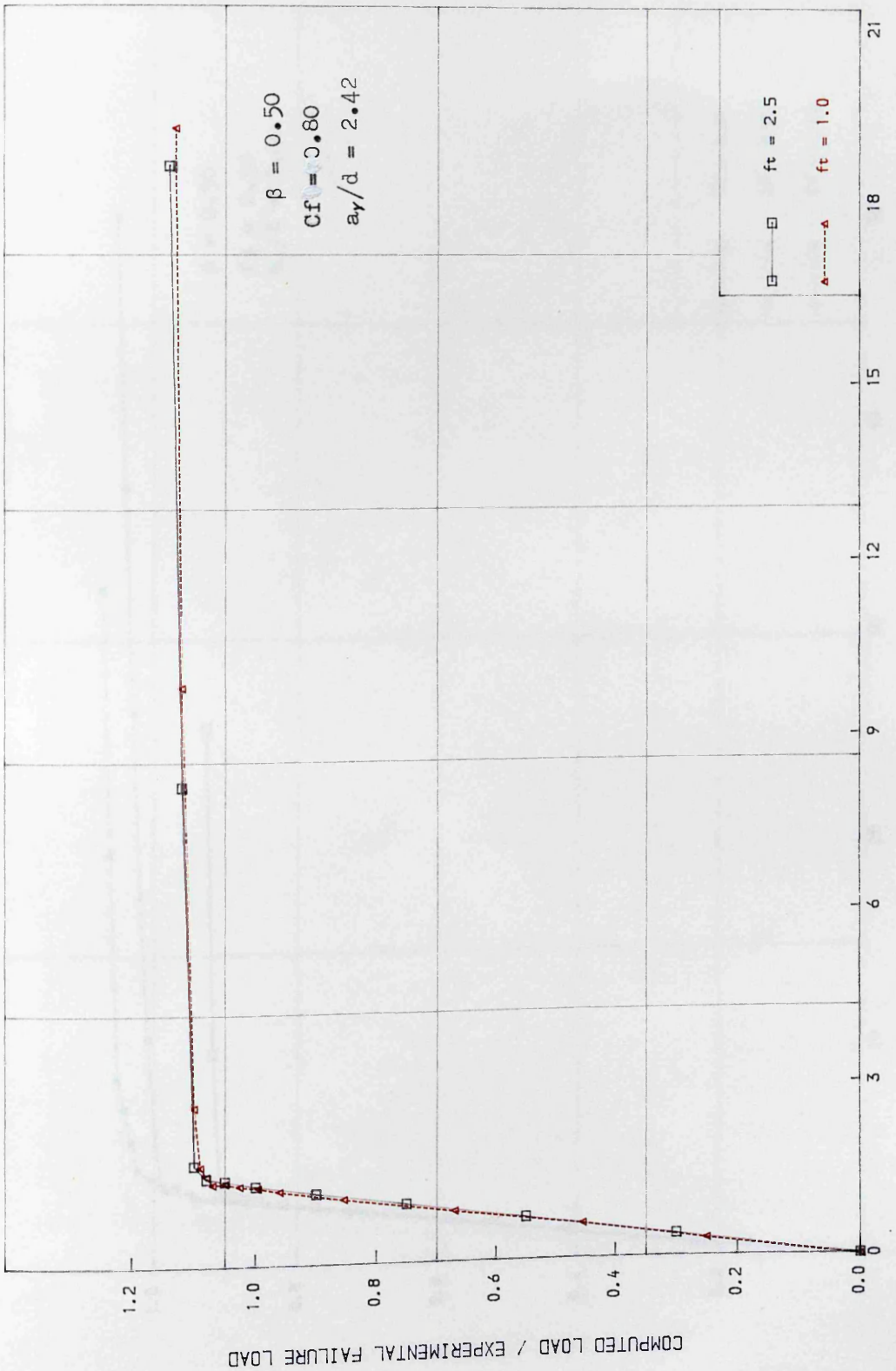

FIGURE (6.29) EFFECT OF ft ON FAILURE LOAD AND MODE OF FAILURE OF R.C. BEAMS MAIN STEEL STRAIN AT MID-SPAN VARYING WITH ft

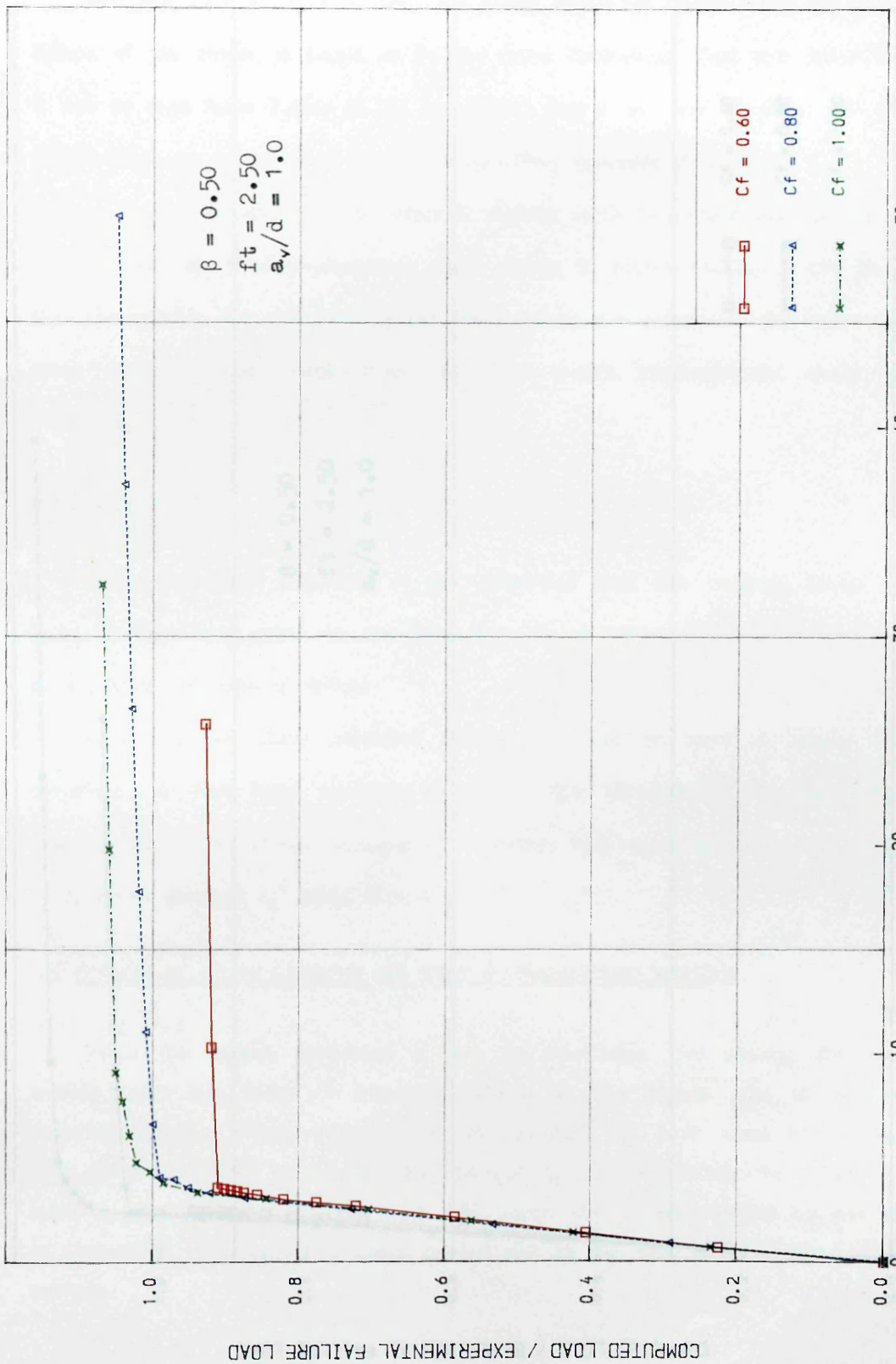

BEAM MID-SPAN DEFLEXION CURVE VARYING WITH Cf

FIGURE (6.30) EFFECT OF Cf ON FAILURE LOAD AND MODE OF FAILURE OF R.C BEAMS

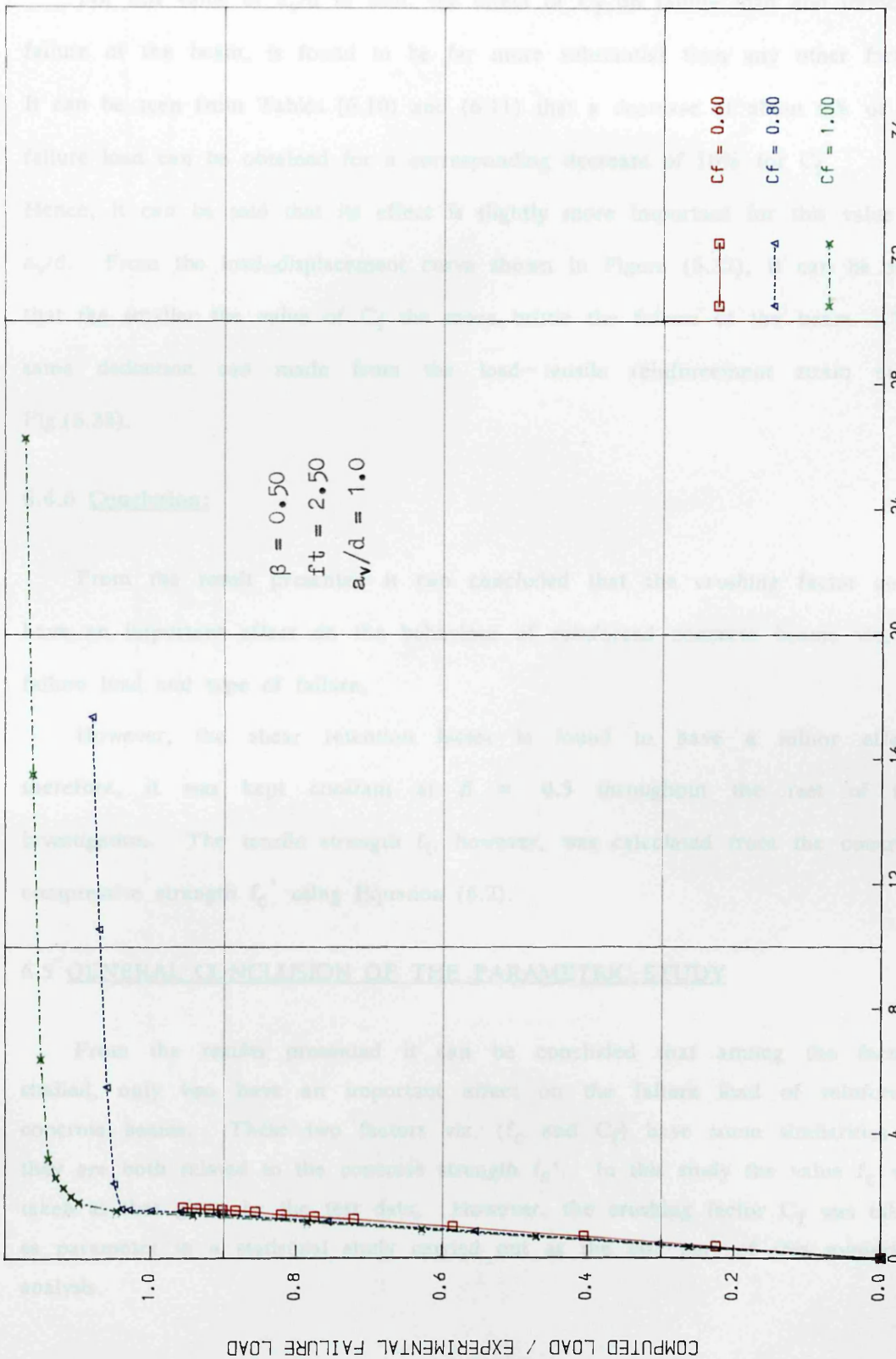

MAIN STEEL STRAIN AT MID-SPAN VARYING WITH Cf

FIGURE (6.31) EFFECT OF Cf ON FAILURE LOAD AND MODE OF FAILURE OF R.C. BEAMS

2– $a_v/d = 2.42$:

For this value of a_v/d as well, the effect of C_f on failure load and mode of failure of the beam, is found to be far more substantial than any other factor. It can be seen from Tables (6.10) and (6.11) that a decrease of about 6% of the failure load can be obtained for a corresponding decrease of 10% for C_f. Hence, it can be said that its effect is slightly more important for this value of a_v/d. From the load–displacement curve shown in Figure (6.32), it can be seen that the smaller the value of C_f the more brittle the failure of the beam. The same deduction can made from the load– tensile reinforcement strain curve Fig.(6.33).

6.4.6 Conclusion:

From the result presented it can concluded that the crushing factor could have an important effect on the behaviour of reinforced concrete beams viz. its failure load and type of failure.

However, the shear retention factor is found to have a minor effect, therefore, it was kept constant at $\beta = 0.5$ throughout the rest of this investigation. The tensile strength f_t, however, was calculated from the concrete compressive strength f_c' using Equation (6.2).

6.5 GENERAL CONCLUSION OF THE PARAMETRIC STUDY

From the results presented it can be concluded that among the factors studied, only two have an important effect on the failure load of reinforced concrete beams. These two factors viz. (f_c and C_f) have some similarities as they are both related to the concrete strength f_c'. In this study the value f_c was taken as that given by the test data. However, the crushing factor C_f was taken as parameter in a statistical study carried out as the last part of this numerical analysis.

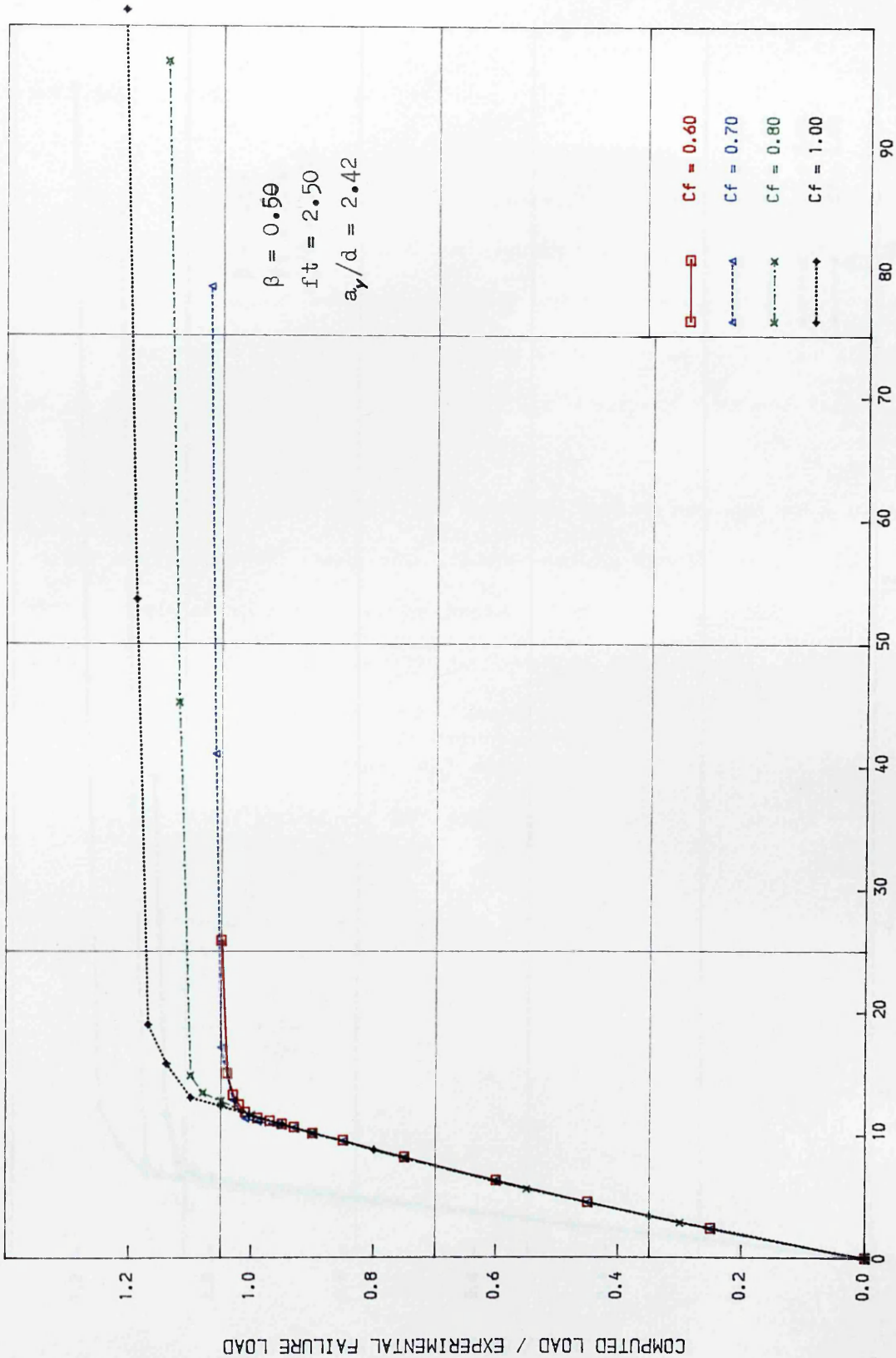

BEAM MID-SPAN DEFLEXION CURVE VARYING WITH Cf

FIGURE (6.32) EFFECT OF Cf ON FAILURE LOAD AND MODE OF FAILURE OF R.C BEAMS

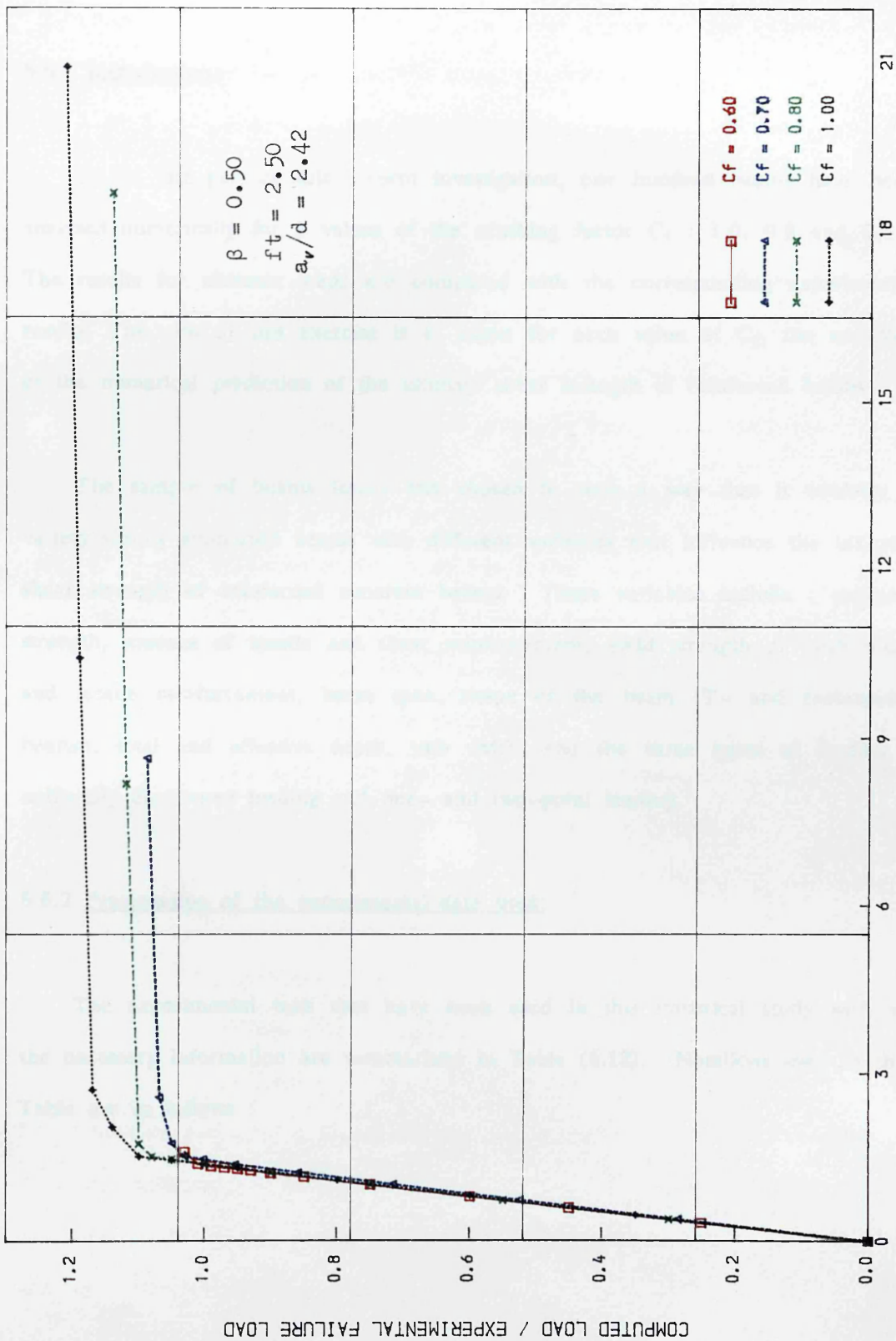

MAIN STEEL STRAIN AT MID-SPAN VARYING WITH Cf

FIGURE (6.33) EFFECT OF Cf ON FAILURE LOAD AND MODE OF FAILURE OF R.C. BEAMS

6.6 STATISTICAL STUDY

6.6.1 Introduction:

In the last part of this present investigation, one hundred beams have been analysed numerically for 3 values of the crushing factor C_f : 1.0, 0.8 and 0.6 . The results for ultimate loads are compared with the corresponding experimental results. The aim of this exercise is to assess for each value of C_f, the accuracy of the numerical prediction of the ultimate shear strength of reinforced beams.

The sample of beams tested was chosen in such a way that it contains a variety simply supported beams with different variables that influence the ultimate shear strength of reinforced concrete beams. These variables include : concrete strength, amount of tensile and shear reinforcement, yield strength of both shear and tensile reinforcement, beam span, shape of the beam (T– and rectangular beams), total and effective depth, web width, and the three types of loading : uniformly distributed loading and one– and two–point loading.

6.6.2 Presentation of the experimental data used:

The experimental tests that have been used in this statistical study with all the necessary information are summarized in Table (6.12). Notations used in this Table are as follows :

1– Ref. no. : The number of the reference from reference list from which the experimental data was obtained

2– Code : In this column is the name given by the author of the reference to the experimental test.

3– 1.Pt.L : Abbreviation used to denote the type of loading, here one point load applied at mid–span of the beam.

4– 2.Pt.L : Two point load applied at equal distance from the mid span either side of it.

5– U.D.L : Uniformly distributed load.

6– ρ : Ratio of tensile reinforcement and given by : $A_s/b.d$ (A_s : total area of tensile reinforcement).

7– b : Width of the web.

8– b_f : Width of the flange in T–beams.

9– d : Effective depth of the beam.

10– f_y : Yield strength of tensile reinforcement.

11– f_{yt} : Yield strength of shear reinforcement.

12– h or h_t : Total height of the beam.

13– h_f : Thickness of the flange in T–beams.

14– r : Ratio of shear reinforcement and given by : $A_{st}/b.s$ (A_{st}: stirrups total area and s spacing of stirrups).

15– s : Spacing of stirrups.

16– (*) : Asterisk used in this Table next to the test number to show that the beam in this test is a T–beams. (example : 21*).

17– Whenever two yield strengths of steel are given, it means that two types of steel with different yield strengths are used.

It should be noted that except the nine T–beams indicated by (*), the rest of the analysis is concerned with rectangular beams.

TABLE (6.12):

Test no.	Ref. no.	code	Loading Type	ρ	f_y (N/mm^2)	r	f_{yt} (N/mm^2)	b (mm)	f_c' (N/mm^2)	a_v/d	h_t (mm)	d (mm)	Total experim. Failure load (N)
01	68	A1–(1 to4)	1.Pt.L	0.0310	322	0.0038	332	203	24.22	2.35	457	390	450,970
02	68	B1–(1 to5)	2.Pt.L	0.0310	322	0.0037	332	203	24.15	1.95	457	390	533,784
03	68	B2–(1 to3)	2.Pt.L	0.0310	322	0.0073	332	203	24.92	1.95	457	390	640,978
04	68	C1–(1 to4)	2.Pt.L	0.0207	322	0.0034	332	203	26.36	1.56	457	390	562,266
05	68	C2–(1 to4)	2.Pt.L	0.0207	322	0.0069	332	203	25.04	1.56	457	390	603,555
06	68	C3–(1 to3)	2.PT.L	0.0207	322	0.0034	332	203	13.98	1.56	457	390	409,440
07	68	C4 – 1	2.Pt.L	0.0310	322	0.0034	332	203	24.56	1.56	457	390	620,718
08	68	C6–(2 to4)	2.PT.L	0.0310	322	0.0046	332	203	45.99	1.56	457	390	861,241
09	68	D1–(1 to3)	2.Pt.L	0.0163	336	0.0061	332	203	25.72	1.17	457	390	611,683
10	68	D2–(1 to4)	2.Pt.L	0.0163	336	0.0061	332	203	24.87	1.17	457	390	637,934

... CONTINUED TABLE (6.12):

Test no.	Ref. no.	code	Loading Type	ρ	f_y (N/mm²)	r	f_{yt} (N/mm²)	b (mm)	f_c' (N/mm²)	a_v/d	h_t (mm)	d (mm)	Total experim. Failure load (N)
11	68	D3 – 1	2.Pt.L	0.0244	336	0.0092	332	203	28.30	1.17	457	390	792,568
12	68	D4 – 1	2.Pt.L	0.0163	336	0.0122	332	203	23.18	1.17	457	390	626,561
13	68	D1–(6 to8)	2.Pt.L	0.0342	322	0.0046	332	152	27.90	1.94	380	315	361,081
14	68	E1 – 2	2.Pt.L	0.0342	322	0.0073	332	152	30.27	2.02	380	315	445,100
15	68	D2–(6 to8)	2.Pt.L	0.0342	322	0.0061	332	152	28.11	2.42	380	315	330,538
16	68	D4–(1 to3)	2.Pt.L	0.0342	322	0.0049	332	152	25.12	2.42	380	315	328,305
17	68	D5–(1 to3)	2.Pt.L	0.0342	322	0.0037	332	152	28.05	2.42	380	315	308,219
18	68	A0–(1 to3)	1.Pt.L	0.0098	372	0.0	———	203	23.81	2.35	380	390	211,425
19	68	B0–(1 to3)	2.Pt.L	0.0098	372	0.0	———	203	23.75	1.95	457	390	229,654
20	68	C0–(1 to3)	2.Pt.L	0.0098	372	0.0	———	203	24.00	1.56	457	390	347,124

... CONTINUED TABLE (6.12):

Test no.	Ref. no.	code	Loading Type	ρ	f_y (N/mm²)	r	f_{yt} (N/mm²)	b (mm)	f_c' (N/mm²)	a_v/d	h_t (mm)	d (mm)	Total experim. Failure load (N)
21	68	D0–(1 to3)	2.Pt.L	0.0098	372	0.0	——	203	26.10	1.17	457	390	471,449
22*	82	B10	U.D.L	0.0402	479	0.0	——	b = 100 b_f= 300	29.02	2.50	h =240 h_f =40	200	190,000
23*	82	D10	U.D.L	0.0402	479	0.0	——	b = 100 b_f= 400	27.77	2.50	h =240 h_f =40	200	179,600
24*	82	D10	U.D.L	0.0402	479	0.0	——	b = 100 b_f= 500	26.60	2.50	h =240 h_f =40	200	178,400
25*	82	E10	U.D.L	0.0402	479	0.0	——	b = 100 b_f= 300	25.90	2.50	h =240 h_f =60	200	203,400
26*	82	F10	U.D.L	0.0402	479	0.0	——	b = 100 b_f= 400	21.06	2.50	h =240 h_f =60	200	191,200
27*	82	G10	U.D.L	0.0402	479	0.0	——	b = 100 b_f= 500	28.16	2.50	h =240 h_f =60	200	213,200
28*	82	H10	U.D.L	0.0402	479	0.0	——	b = 100 b_f= 300	27.30	2.50	h =240 h_f =80	200	256,200
29*	82	J10	U.D.L	0.0402	479	0.0	——	b = 100 b_f= 400	32.37	2.50	h =240 h_f =80	200	277,600
30*	82	K10	U.D.L	0.0402	479	0.0	——	b = 100 b_f= 500	27.22	2.50	h =240 h_f =80	200	234,800

... CONTINUED TABLE (6.12):

Test no.	Ref. no.	code	Loading Type	ρ	f_y (N/mm²)	r	f_{yt} (N/mm²)	b (mm)	f_c' (N/mm²)	a_v/d	h_t (mm)	d (mm)	Total experim. Failure load (N)
31	14	I– (1–2)	2.Pt.L	0.0305	268	0.0	——	203	24.23	1.51	457	403	625,165
32	14	II– (3–4)	2.Pt.L	0.0188	467	0.0	——	203	24.19	1.51	457	403	576,115
33	14	III– (5–6)	2.Pt.L	0.0185	491	0.0	——	203	25.71	1.51	457	403	580,574
34	14	IV – (7–8)	2.Pt.L	0.0186	492 425	0.0	——	203	24.57	1.51	457	403	596,292
35	14	V – (9–10)	2.Pt.L	0.0116	683 722	0.0	——	203	25.09	1.51	457	403	493,621
36	14	VI–(11–12)	2.Pt.L	0.0117	721 735	0.0	——	203	25.57	1.51	457	403	493,621
37	14	V –(13–14)	2.Pt.L	0.0075	713	0.0	——	203	24.61	1.51	457	403	447,470
38	14	VI–(15–16)	2.Pt.L	0.0075	699	0.0	——	203	24.23	1.51	457	403	368,990
39	18	AO–3–3b	1.Pt.L	0.0336	465	0.0	——	152	20.78	3.60	337	298	129,650
40	18	AO–3–3c	1.Pt.L	0.0232	680 721	0.0	——	152	27.16	3.60	337	298	134,056

... CONTINUED TABLE (6.12):

Test no.	Ref. no.	code	Loading Type	ρ	f_y (N/mm^2)	r	f_{yt} (N/mm^2)	b (mm)	f_c' (N/mm^2)	a_v/d	h_t (mm)	d (mm)	Total experim. Failure load (N)
41	67	4A3	1.Pt.L	0.0206	332	0.0	———	203	24.40	2.35	457	390	224,545
42	67	5A3	1.Pt.L	0.0309	332	0.0	———	203	23.80	2.35	457	390	348,182
43	67	11A2	1.Pt.L	0.0341	332	0.0	———	152	24.07	2.91	381	314	150,000
44	67	18A,B,C&D2	1.Pt.L	0.0268	343	0.0	———	152	21.42	2.90	381	316	137,273
45	67	13A2	1.Pt.L	0.0080	378	0.0	———	152	20.36	2.87	381	319	099,091
46	18	AO–3–2	1.Pt.L	0.0336	465	0.0	———	152	20.61	2.50	337	298	155,925
47	18	AO–7–2	1.Pt.L	0.0336	465	0.0	———	152	45.21	2.50	337	298	236,403
48	18	AO–11–2	1.Pt.L	0.0336	465	0.0	———	152	79.37	2.50	337	298	223,200
49	18	AO–15–2a	1.Pt.L	0.0336	465	0.0	———	152	83.86	2.50	337	298	356,491
50	18	AO–15–2b	1.Pt.L	0.0336	465	0.0	———	152	69.48	2.50	337	298	412,448

... CONTINUED TABLE (6.12):

Test no.	Ref. no.	code	Loading Type	ρ	f_y (N/mm^2)	r	f_{yt} (N/mm^2)	b (mm)	f_c' (N/mm^2)	a_v/d	h_t (mm)	d (mm)	Total experim. Failure load (N)
51	18	AO–3–1	1.Pt.L	0.0336	465	0.0	———	152	23.10	1.50	337	298	232,631
52	18	AO–7–1	1.Pt.L	0.0036	465	0.0	———	152	41.87	1.50	337	298	624,331
53	18	AO–11–1	1.Pt.L	0.0336	465	0.0	———	152	65.82	1.50	337	298	867,021
54	18	AO–15–1a	1.Pt.L	0.0336	465	0.0	———	152	79.55	1.50	337	298	552,655
55	18	AO–15–1b	1.Pt.L	0.0336	465	0.0	———	152	81.35	1.50	337	298	992,139
56	18	AO–7–3a	1.Pt.L	0.0336	465	0.0	———	152	37.71	3.60	337	298	164,728
57	18	AO–7–3b	1.Pt.L	0.0336	465	0.0	———	152	41.67	3.60	337	298	165,985
58	18	AO–11–3a	1.Pt.L	0.0336	465	0.0	———	152	75.01	3.60	337	298	179,817
59	18	AO–11–3b	1.Pt.L	0.0336	465	0.0	———	152	74.72	3.60	337	298	179,189
60	18	AO–15–3a	1.Pt.L	0.0336	465	0.0	———	152	81.43	3.60	337	298	187,362

... CONTINUED TABLE (6.12):

Test no.	Ref. no.	code	Loading Type	ρ	f_y (N/mm^2)	r	f_{yt} (N/mm^2)	b (mm)	f_c' (N/mm^2)	a_v/d	h_t (mm)	d (mm)	Total experim. Failure load (N)
61	18	AO–15–3b	1.Pt.L	0.0336	465	0.0	——	152	93.79	3.60	337	298	200,565
62	18	AO–15–3c	1.Pt.L	0.0336	465	0.0	——	152	91.94	3.60	337	298	156,164
63	14	IIIa–17&18	2.Pt.L	0.0254	504	0.0	——	203	27.23	3.78	457	403	169,223
64	14	Va–(19–20)	2.Pt.L	0.0093	689	0.0	——	203	24.57	3.78	457	403	129,537
65	14	VIb–(21–22–23)	2.Pt.L	0.0084	706	0.0	——	203	27.52	3.78	457	403	139,570
66	14	VIa– 24&25	2.Pt.L	0.0047	695	0.0	——	203	26.09	3.78	457	403	104,677
67	17	01	2.Pt.L	0.0207	474	0.0	——	190	27.69	1.00	320	270	776,952
68	17	02	2.Pt.L	0.0207	474	0.0	——	190	27.69	1.50	320	270	519,930
69	17	03	2.Pt.L	0.0207	474	0.0	——	190	27.69	2.00	320	270	294,300
70	17	04	2.Pt.L	0.0207	474	0.0	——	190	27.69	2.50	320	270	166,280

... CONTINUED TABLE (6.12):

Test no.	Ref. no.	code	Loading Type	ρ	f_y (N/mm^2)	r	f_{yt} (N/mm^2)	b (mm)	f_c' (N/mm^2)	a_v/d	h_t (mm)	d (mm)	Total experim. Failure load (N)
71	67	15(A&B)2	1.Pt.L	0.0134	336	0.0	———	152	20.46	2.89	381	316	098,150
72	67	18E2	1.Pt.L	0.0268	336	0.0	———	152	19.84	2.89	381	316	164,094
73	67	4A(1&2) & 4B1	U.D.L	0.0206	321	0.0	———	203	28.34	1.17	457	390	422,870
74	67	5A(1&2) & 5B1	U.D.L	0.0309	397	0.0	———	153	18.11	1.17	304	272	401,318
75	67	11A1	U.D.L	0.0341	321	0.0	———	152	27.03	1.46	381	314	535,980
76	67	C	1.Pt.L	0.0156	394	0.0	———	203	16.80	3.16	533	482	169,450
77	67	6U	U.D.L	0.0335	336	0.0	———	152	20.46	1.81	305	252	170,780
78	67	12&20– A1	U.D.L	0.0452	321	0.0	———	152	26.02	1.92	305	237	348,700
79	67	15A1	U.D.L	0.0134	336	0.0	———	152	19.22	1.44	381	316	310,350
80	67	17–(A&B)–1	U.D.L	0.0209	371	0.0	———	152	18.39	1.88	305	243	251,047

... CONTINUED TABLE (6.12):

Test no.	Ref. no.	code	Loading Type	ρ	f_y (N/mm^2)	r	f_{yt} (N/mm^2)	b (mm)	f_c' (N/mm^2)	a_v/d	h_t (mm)	d (mm)	Total experim. Failure load (N)
81	67	18A1	U.D.L	0.0268	336	0.0	——	152	20.25	1.45	381	316	484,260
82	67	13A1	U.D.L	0.0080	371	0.0	——	152	20.25	1.43	381	319	237,220
83	67	14A1	U.D.L	0.0105	371	0.0	——	152	22.81	1.88	305	243	179,260
84	67	17A1	U.D.L	0.0177	336	0.0	——	152	21.08	1.91	305	240	211,360
85	67	19A1	U.D.L	0.0353	336	0.0	——	152	21.29	1.91	305	240	321,050
86	67	21A1	U.D.L	0.0493	321	0.0	——	203	21.28	1.92	305	238	451,260
87	67	$3AAU_9$	U.D.L	0.0199	371	0.0	——	152	12.58	1.79	305	256	256,840
88	67	4AAU	U.D.L	0.0263	371	0.0	——	152	12.58	1.80	305	254	223,846
89	67	5AAU	U.D.L	0.0335	394	0.0	——	152	12.30	1.81	305	252	269,329
90	67	6AAU	U.D.L	0.0430	321	0.0	——	152	11.81	1.83	305	250	268,440

... CONTINUED TABLE (6.12):

Test no.	Ref. no.	code	Loading Type	ρ	f_y (N/mm^2)	r	f_{yt} (N/mm^2)	b (mm)	f_c' (N/mm^2)	a_v/d	h_t (mm)	d (mm)	Total experim. Failure load (N)
91	67	3AU	U.D.L	0.0199	371	0.0	———	152	13.76	2.39	305	256	194,416
92	67	4AU	U.D.L	0.0263	394	0.0	———	152	12.72	2.40	305	254	163,203
93	67	5AU	U.D.L	0.0335	336	0.0	———	152	15.00	2.42	305	252	214,036
94	67	6AU	U.D.L	0.0430	321	0.0	———	152	12.44	2.44	305	250	158,744
95	67	$3AAU_8$	U.D.L	0.0199	371	0.0	———	152	34.63	1.79	305	256	306,790
96	67	6–(A&B)1	U.D.L	0.0341	321	0.0046	332	152	30.00	1.94	381	314	517,250
97	67	9A1	U.D.L	0.0341	321	0.0049	332	152	30.89	2.43	381	314	408,450
98	67	9B1	U.D.L	0.0341	321	0.0049	332	152	29.93	1.46	381	314	702,753
99	67	213.5b–2	U.D.L	0.0222	336	0.0008	366	254	33.11	2.01	508	254	935,520
100	67	218b–2	U.D.L	0.0222	336	0.0008	366	254	34.70	2.01	508	254	684,020

6.6.3 Presentation of the results:

The results obtained in this study are summarized in Table (6.13), it should be noted that the values given in this table represent the computed / experimental failure loads.

TABLE (6.13)

Test no.	C_f = 0.60	C_f = 0.80	C_f = 1.00
01	0.92	1.15	1.32
02	1.06	1.20	1.30
03	0.73	0.95	1.07
04	1.05	1.09	1.14
05	0.96	1.00	1.06
06	0.77	1.06	1.23
07	0.96	1.04	1.21
08	1.08	1.08	1.16
09	1.10	0.89	1.04
10	1.03	1.01	1.00
11	0.86	0.84	0.93
12	1.08	1.04	1.17

... CONTINUED TABLE (6.13)

Test no.	C_f = 0.60	C_f = 0.80	C_f = 1.00
13	1.10	1.19	1.28
14	0.91	0.96	1.04
15	0.97	1.04	1.15
16	0.84	1.02	1.11
17	1.01	1.12	1.19
18	1.21	1.24	1.24
19	1.27	1.27	1.24
20	1.02	1.04	1.09
21	1.02	0.94	1.04
22	1.42	1.48	1.57
23	1.64	1.65	1.73
24	1.69	1.72	1.76
25	1.33	1.41	1.46
26	1.44	1.52	1.56
27	1.44	1.44	1.48
28	1.09	1.11	1.17

... CONTINUED TABLE (6.13)

Test no.	C_f = 0.60	C_f = 0.80	C_f = 1.00
29	1.12	1.12	1.12
30	1.32	1.32	1.34
31	1.12	1.15	1.24
32	1.21	1.33	1.44
33	1.28	1.35	1.47
34	1.13	1.23	1.34
35	1.35	1.47	1.57
36	1.26	1.50	1.62
37	1.13	1.16	1.27
38	1.40	1.47	1.57
39	1.03	1.23	1.48
40	1.24	1.53	1.75
41	1.33	1.51	1.84
42	1.11	1.24	1.57
43	1.28	1.53	1.78
44	1.19	1.42	1.65

... CONTINUED TABLE (6.13)

Test no.	C_f = 0.60	C_f = 0.80	C_f = 1.00
45	0.88	0.93	1.04
46	0.97	1.19	1.41
47	1.41	1.66	1.89
48	2.19	2.22	2.32
49	1.22	1.22	1.32
50	1.13	1.15	1.24
51	0.86	1.02	1.19
52	0.59	0.71	0.79
53	0.66	0.79	0.90
54	1.22	1.41	1.51
55	0.73	0.79	0.86
56	1.54	1.68	1.80
57	1.50	1.75	1.87
58	1.80	1.87	1.94
59	1.84	1.89	1.91
60	1.80	1.84	1.87

... CONTINUED TABLE (6.13)

Test no.	C_f = 0.60	C_f = 0.80	C_f = 1.00
61	1.73	1.73	1.76
62	1.67	1.80	1.82
63	1.07	1.24	1.32
64	0.91	0.97	1.02
65	1.10	1.16	1.19
66	1.34	1.36	1.38
67	0.92	1.01	1.05
68	0.81	0.91	1.06
69	1.34	1.40	1.46
70	1.83	1.97	2.11
71	1.44	1.51	1.58
72	0.99	1.16	1.35
73	0.72	0.89	1.01
74	0.55	0.62	0.75
75	0.84	0.94	1.14
76	1.35	1.70	2.03

... CONTINUED TABLE (6.13)

Test no.	C_f = 0.60	C_f = 0.80	C_f = 1.00
77	0.87	0.97	1.11
78	0.96	1.10	1.21
79	0.91	0.93	0.95
80	0.91	0.99	1.08
81	0.71	0.79	1.10
82	0.85	0.85	0.85
83	0.84	0.84	0.84
84	0.95	0.99	1.03
85	0.85	0.99	1.12
86	0.87	1.06	1.23
87	0.76	0.86	0.95
88	0.80	1.03	1.22
89	0.78	0.95	1.19
90	0.74	0.91	1.16
91	1.01	1.19	1.30
92	1.07	1.52	1.79

... CONTINUED TABLE (6.13)

Test no.	C_f = 0.60	C_f = 0.80	C_f = 1.00
93	1.03	1.29	1.50
94	1.17	1.45	1.81
95	0.77	0.79	0.82
96	0.98	1.00	1.06
97	0.86	0.91	0.95
98	0.85	0.86	0.90
99	0.74	0.76	0.91
100	1.19	1.19	1.23

TABLE (6.14)

Comparison of experimental mode of failure with mode of failure for different values of C_f

TEST No.	Experimental mode of failure	$C_f = 0.60$	$C_f = 0.80$	$C_f = 1.00$
1	Diagonal Tension	Shear	Shear	Shear–Flexure
2	Diagonal Tension	Shear	Shear–Flexure	Flexure
3	Diagonal Tension	Shear	Shear	Shear–Flexure
4	Diagonal Tension	Shear–Flexure	Shear–Flexure	Shear–Flexure
5	Diagonal Tension	Shear	Shear–Flexure	Shear–Flexure
6	Diagonal Tension	Shear	Shear	Shear–Flexure
7	Diagonal Tension	Shear	Shear	Flexure
8	Diagonal Tension	Shear–Flexure	Shear–Flexure	Flexure
9	Diagonal Tension	Shear–Flexure	Shear	Shear
10	Diagonal Tension	Shear	Shear–Flexure	Shear–Flexure
11	Diagonal Tension	Shear–Flexure	Shear–Flexure	Shear–Flexure
12	Diagonal Tension	Shear–Flexure	Shear	Shear–Flexure
13	Diagonal Tension	Shear	Shear–Flexure	Shear–Flexure
14	Diagonal Tension	Shear	Shear–Flexure	Shear–Flexure

... Continued TABLE (6.14)

TEST No.	Experimental mode of failure	$C_f = 0.60$	$C_f = 0.80$	$C_f = 1.00$
15	Diagonal Tension	Shear	Shear–Flexure	Flexure
16	Diagonal Tension	Shear	Shear–Flexure	Shear–Flexure
17	Diagonal Tension	Shear	Shear–Flexure	Shear–Flexure
18	Diagonal Tension	Shear–Flexure	Shear–Flexure	Shear–Flexure
19	Diagonal Tension	Shear–Flexure	Shear–Flexure	Shear–Flexure
20	Diagonal Tension	Shear	Shear–Flexure	Shear–Flexure
21	Diagonal Tension	Shear–Flexure	Shear	Shear–Flexure
22*	Instability of the flange	Shear–Flexure	Shear–Flexure	Flexure
23*	Instability of the flange	Shear–Flexure	Shear–Flexure	Flexure
24*	Instability of the flange	Flexure	Flexure	Flexure
25*	Instability of the flange	Shear–Flexure	Flexure	Flexure
26*	Instability of the flange	Shear–Flexure	Flexure	Flexure
27*	Instability of the flange	Flexure	Flexure	Flexure
28*	Instability of the flange	Shear–Flexure	Shear–Flexure	Flexure
29*	Instability of the flange	Flexure	Flexure	Flexure
30*	Instability of the flange	Flexure	Shear–Flexure	Flexure
31	SHEAR	Shear	Shear–Flexure	Shear–Flexure

... Continued TABLE (6.14)

TEST No.	Experimental mode of failure	$C_f = 0.60$	$C_f = 0.80$	$C_f = 1.00$
32	Shear	Shear–Flexure	Shear–Flexure	Flexure
33	Shear	Shear–Flexure	Shear–Flexure	Shear–Flexure
34	Shear	Shear	Shear–Flexure	Flexure
35	Shear	Shear	Shear–Flexure	Shear–Flexure
36	Shear	Shear	Shear–Flexure	Shear–Flexure
37	Shear	Shear	Shear	Shear–Flexure
38	Shear	Shear	Shear	Shear–Flexure
39	Diagonal Tension	Shear	Shear–Flexure	Shear–Flexure
40	Diagonal Tension	Shear	Shear	Shear–Flexure
41	Diagonal Tension	Shear	Shear	Shear–Flexure
42	Diagonal Tension	Shear	Shear	Shear
43	Diagonal Tension	Shear	Shear	Shear
44	Diagonal Tension	Shear	Shear	Shear
45	Diagonal Tension	Shear	Shear	Shear–Flexure
46	Shear	Shear	Shear	Shear
47	Shear	Shear	Shear	Shear–Flexure
48	Shear	Shear–Flexure	Flexure	Flexure

... Continued TABLE (6.14)

TEST No.	Experimental mode of failure	$C_f = 0.60$	$C_f = 0.80$	$C_f = 1.00$
49	Shear	Shear	Shear	Shear–Flexure
50	Shear	Shear	Shear	Shear–Flexure
51	Shear–Flexure	Shear	Shear	Shear
52	Shear	Shear	Shear	Shear
53	Shear	Shear–Flexure	Shear	Shear–Flexure
54	Shear	Shear	Shear–Flexure	Flexure
55	Shear	Shear	Shear–Flexure	Flexure
56	Diagonal Tension	Shear–Flexure	Shear–Flexure	Flexure
57	Diagonal Tension	Shear	Shear–Flexure	Flexure
58	Diagonal Tension	Shear–Flexure	Flexure	Flexure
59	Diagonal Tension	Shear–Flexure	Flexure	Flexure
60	Diagonal Tension	Shear–Flexure	Flexure	Flexure
61	Diagonal Tension	Shear–Flexure	Shear–Flexure	Flexure
62	Diagonal Tension	Shear–Flexure	Flexure	Flexure
63	Diagonal Tension	Shear	Shear–Flexure	Shear–Flexure
64	Diagonal Tension	Shear–Flexure	Shear–Flexure	Shear–Flexure

... Continued TABLE (6.14)

TEST No.	Experimental mode of failure	$C_f = 0.60$	$C_f = 0.80$	$C_f = 1.00$
65	Diagonal Tension	Shear–Flexure	Shear–Flexure	Shear–Flexure
66	Diagonal Tension	Shear–Flexure	Shear–Flexure	Shear–Flexure
67	Shear	Shear	Shear	Shear
68	Shear	Shear	Shear	Shear
69	Shear	Shear–Flexure	Shear–Flexure	Shear–Flexure
70	Shear	Shear–Flexure	Shear–Flexure	Flexure
71	Diagonal Tension	Shear	Shear–Flexure	Shear–Flexure
72	Diagonal Tension	Shear	Shear	Shear
73	Diagonal Tension	Shear	Shear	Shear–Flexure
74	Diagonal Tension	Shear	Shear	Shear
75	Diagonal Tension	Shear	Shear	Shear–Flexure
76	Diagonal Tension	Shear	Shear	Shear
77	Diagonal Tension	Shear	Shear	Flexure
78	Shear–Flexure	Shear	Shear–Flexure	Shear–Flexure
79	Diagonal Tension	Shear–Flexure	Shear–Flexure	Shear–Flexure

... Continued TABLE (6.14)

TEST No.	Experimental mode of failure	$C_f = 0.60$	$C_f = 0.80$	$C_f = 1.00$
80	Diagonal Tension	Shear	Shear–Flexure	Shear–Flexure
81	Diagonal Tension	Shear	Shear	Flexure
82	Flexure	Shear–Flexure	Shear–Flexure	Shear–Flexure
83	Flexure	Shear–Flexure	Shear–Flexure	Shear–Flexure
84	Diagonal Tension	Shear	Shear–Flexure	Shear–Flexure
85	Diagonal Tension	Shear	Shear	Shear–Flexure
86	Shear–Flexure	Shear	Shear	Shear–Flexure
87	Diagonal Tension	Shear	Shear–Flexure	Shear–Flexure
88	Diagonal Tension	Shear	Shear	Shear
89	Flexure	Shear	Shear	Shear
90	Diagonal Tension	Shear	Shear	Shear
91	Diagonal Tension	Shear	Shear–Flexure	Shear–Flexure
92	Diagonal Tension	Shear	Shear–Flexure	Shear–Flexure
93	Flexure	Shear	Shear	Shear–Flexure
94	Diagonal Tension	Shear	Shear	Shear

... Continued TABLE (6.14)

TEST No.	Experimental mode of failure	$C_f = 0.60$	$C_f = 0.80$	$C_f = 1.00$
95	Flexure	Shear	Shear	Shear
96	Flexure	Shear	Shear	Flexure
97	Flexure	Shear	Shear	Shear–Flexure
98	Flexure	Shear	Shear	Shear
99	Flexure	Shear	Shear	Shear
100	Shear	Shear–Flexure	Shear–Flexure	Shear–Flexure

It should be noted that some of the investigators give different names for shear failure such as diagonal tension, shear compression, arch rib, etc...

In the above tables, the following designations have been used :

Shear failure : When at failure tensile reinforcement does not yield.

Shear–Flexure failure: When at failure tensile reinforcement starts yielding.

Flexure failure : When strain in tensile reinforcement exceeds 2% at failure.

From the results shown in Table (6.13), and for each value of the crushing factor C_f, plots of numerical versus experimental failure loads {Fig.(6.34) to Fig.(6.36)} and plots of numerical/experimental failure load ratio versus shear–span to depth ratio {Fig.(6.37) to Fig.(6.39)} were carried out. The least–square approach was used to determine the best approximating line (best fitting curve) for these curves.

The general problem of fitting the best least–square line to these results involves minimizing the following expression :

$$\sum_{i=1}^{n} \left[y_i - (ax_i + b) \right]^2 \quad \text{with respect to the parameters a and b.}$$

For a minimum to occur it is necessary that :

$$\frac{\partial}{\partial a} = \sum_{i=1}^{n} \left[y_i - (ax_i + b) \right]^2 = 2 \sum_{i=1}^{n} (y_i - ax_i - b)(-x_i) = 0 \qquad (6.7)$$

and

$$\frac{\partial}{\partial b} = \sum_{i=1}^{n} \left[y_i - (ax_i + b) \right]^2 = 2 \sum_{i=1}^{n} (y_i - ax_i - b)(-1) = 0 \qquad (6.8)$$

The solution of this system of equations is :

$$a = \frac{n (\Sigma x_i . y_i) - (\Sigma x_i)(\Sigma y_i)}{n(\Sigma x_i^2) - (\Sigma x_i)^2} \qquad (6.9)$$

$$b = \frac{(\Sigma x_i^2)(\Sigma y_i) - (\Sigma x_i . y_i)(\Sigma x_i)}{n(\Sigma x_i^2) - (\Sigma x_i)^2} \qquad (6.10)$$

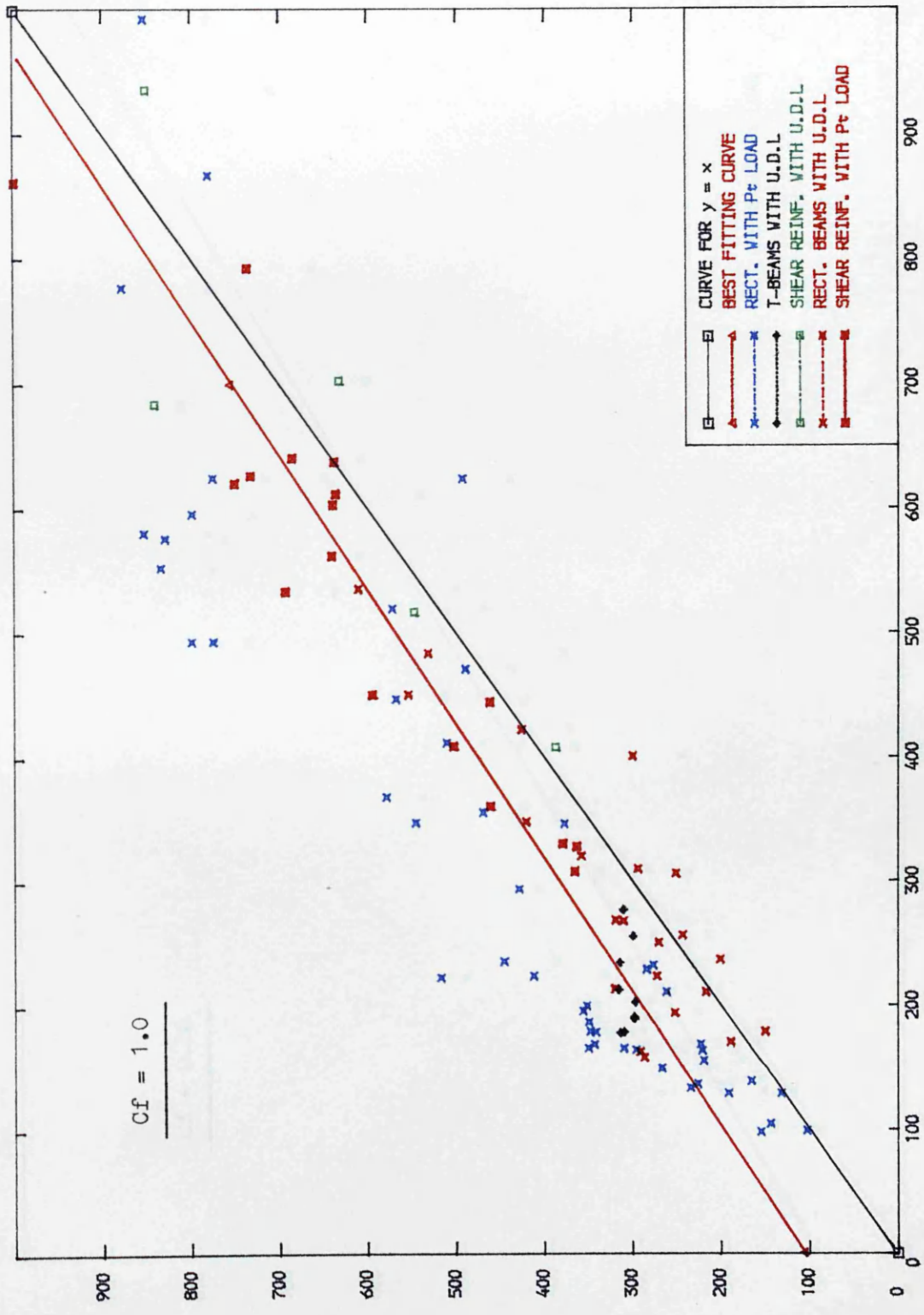

NUMERICAL FAILURE LOAD vs EXPERIMENTAL FAILURE LOAD

FIGURE (6.34) COMPARISON OF NUMERICAL AND EXPERIMENTAL FAILURE LOADS (Cf =1.00)

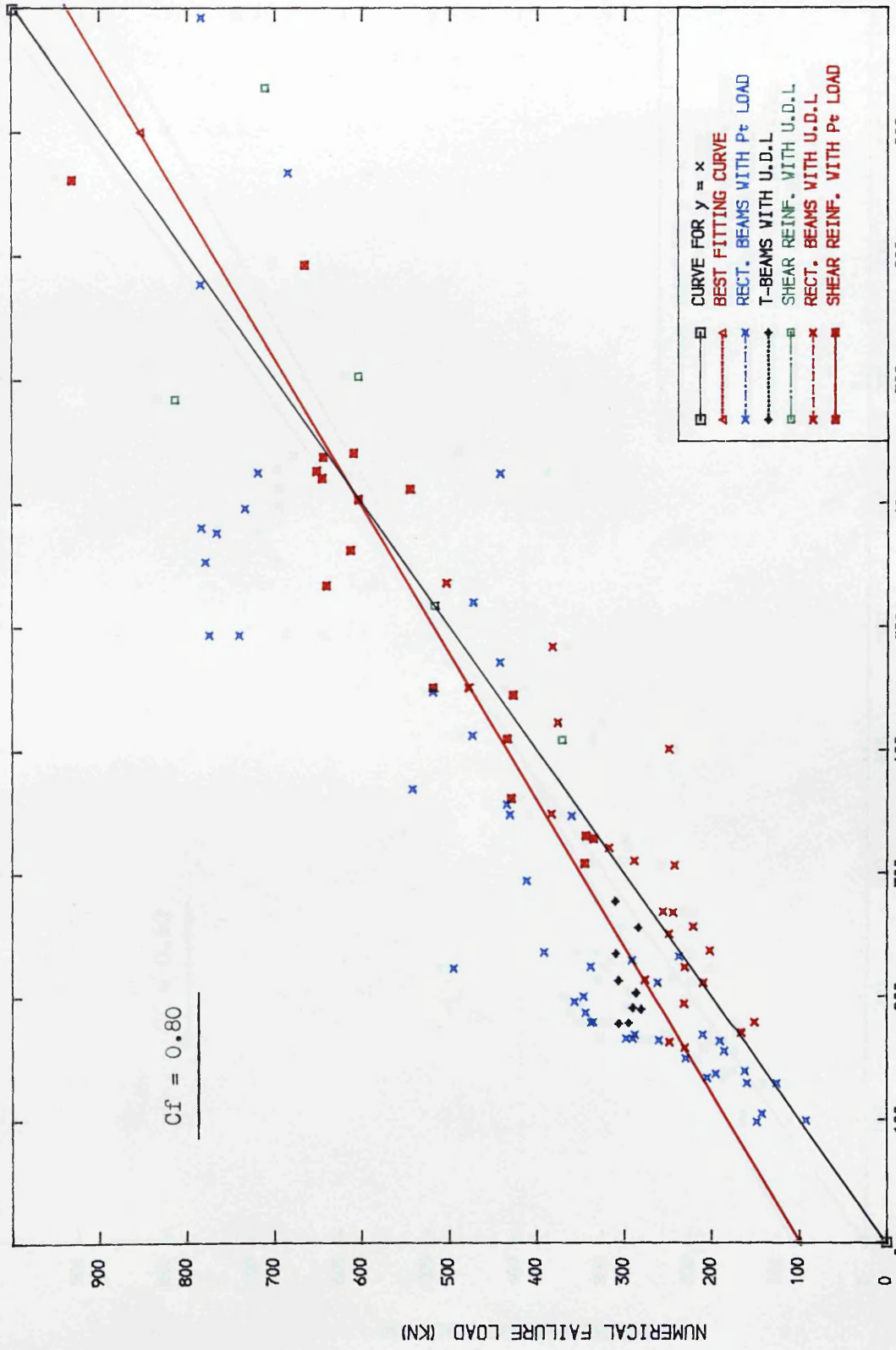

NUMERICAL FAILURE LOAD vs EXPERIMENTAL FAILURE LOAD

FIGURE (6.35) COMPARISON OF NUMERICAL AND EXPERIMENTAL FAILURE LOADS (Cf =0.80)

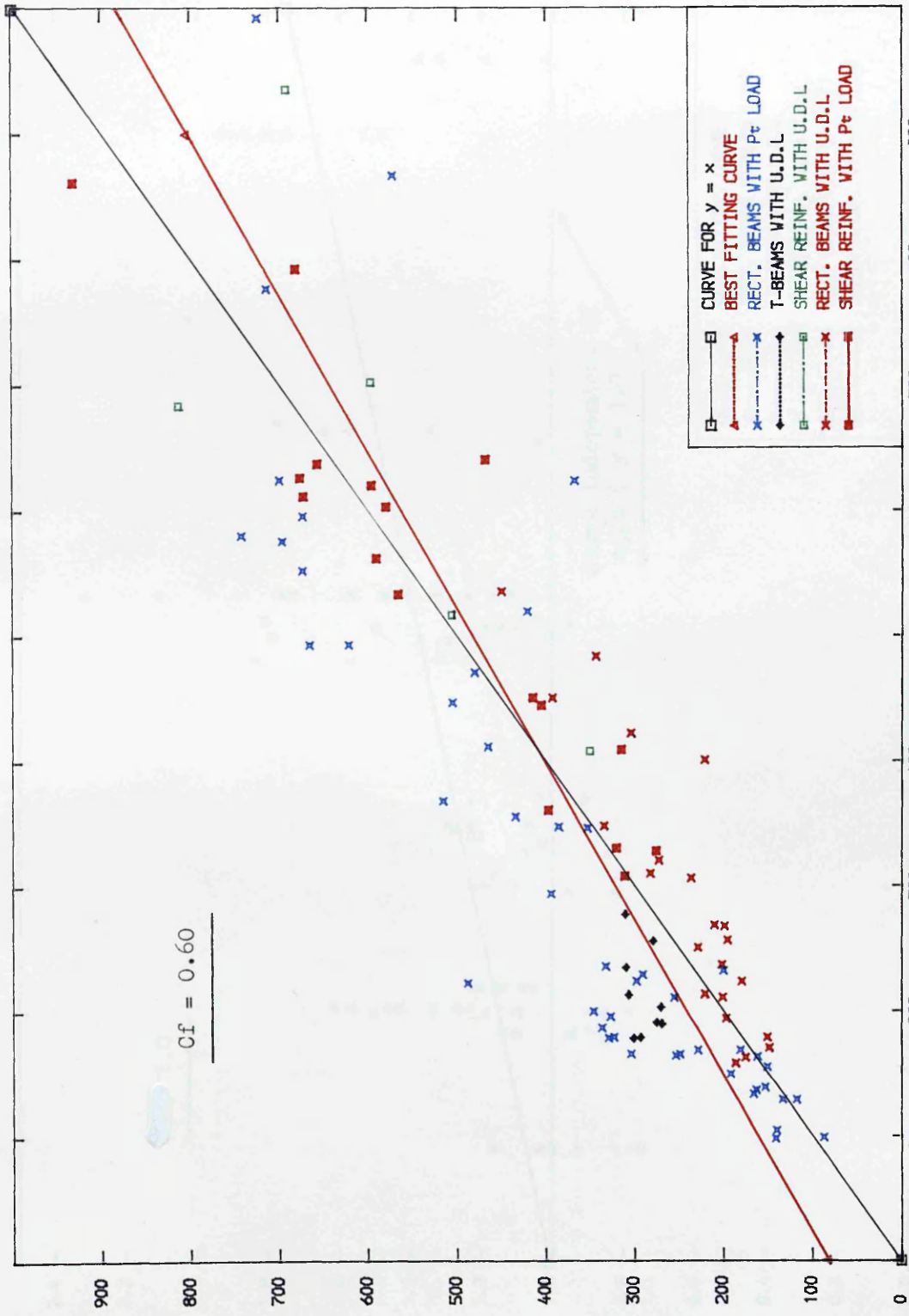

NUMERICAL FAILURE LOAD vs EXPERIMENTAL FAILURE LOAD

FIGURE (6.36) COMPARISON OF NUMERICAL AND EXPERIMENTAL FAILURE LOADS (Cf =0.60)

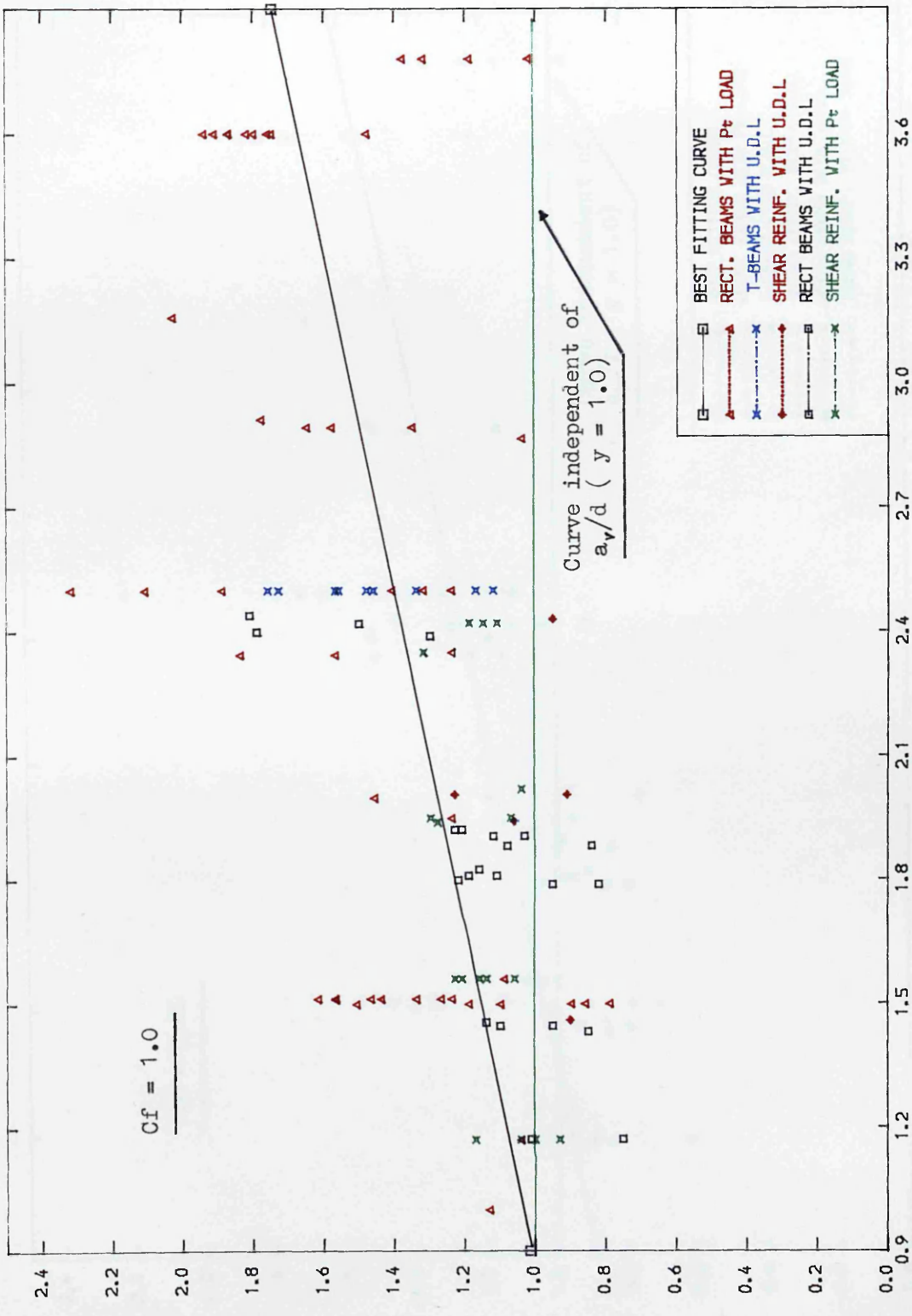

NUMERICAL FAILURE LOAD vs a_v/d RATIO, FOR Cf = 1.00

FIGURE (6.37) EFFECT OF a_v/d RATIO ON THE COMPARISON (Num. Against Exp.)

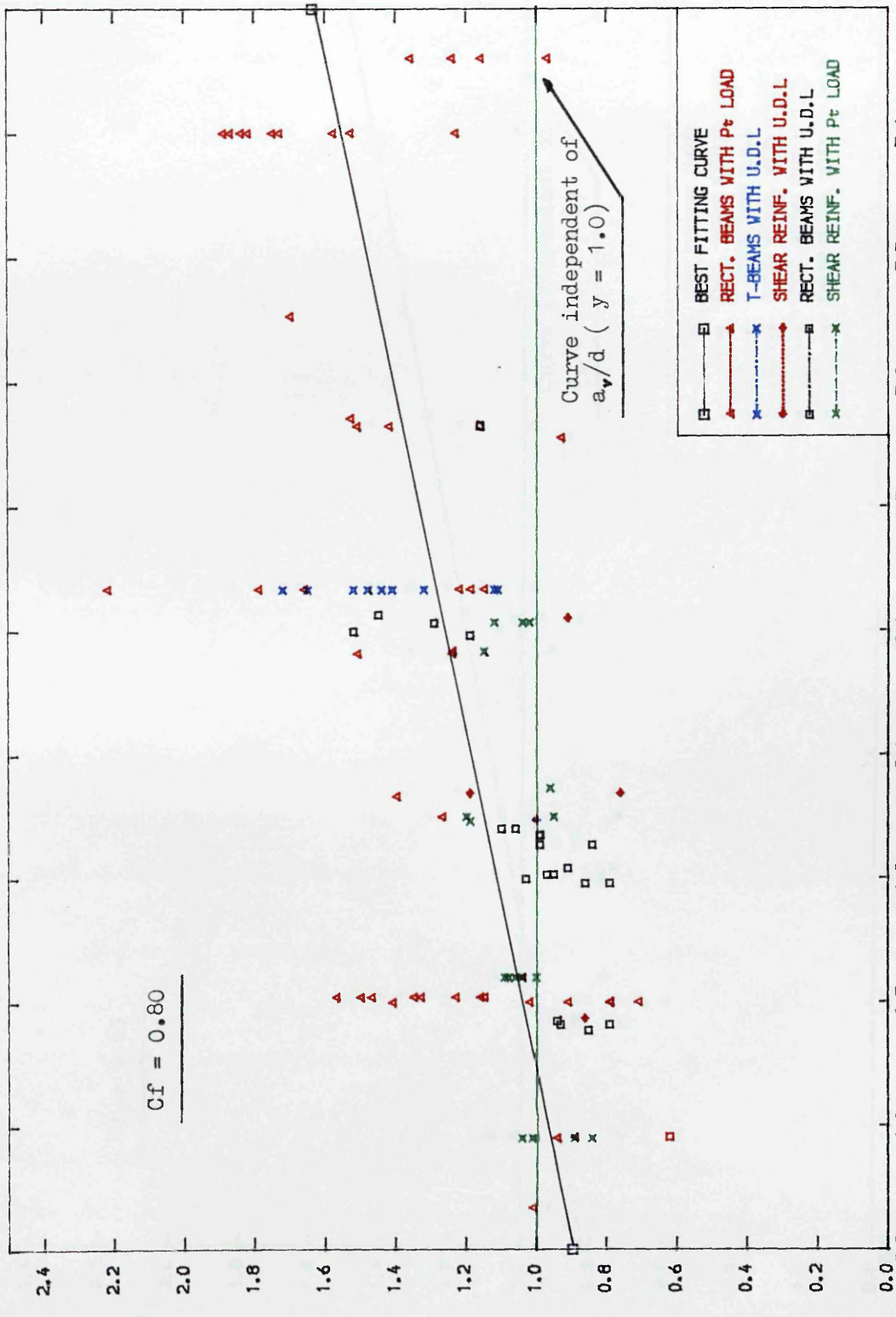

NUMERICAL FAILURE LOAD vs a_v/d RATIO, FOR Cf = 0.80

FIGURE (6.38) EFFECT OF a_v/d RATIO ON THE COMPARISON (Num. Against Exp.)

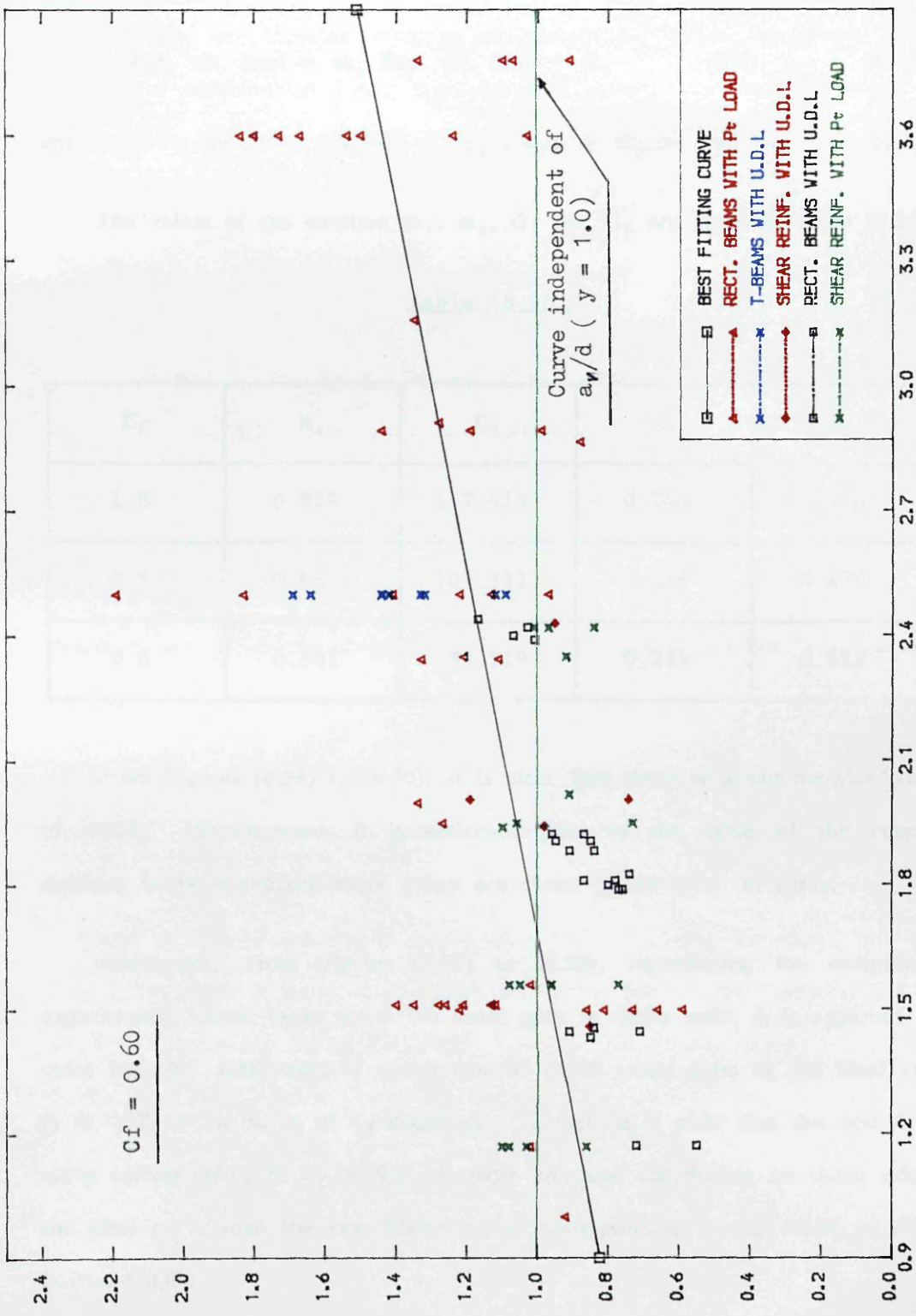

NUMERICAL FAILURE LOAD vs a_v/d RATIO, FOR Cf = 0.60

FIGURE (6.39) EFFECT OF a_v/d RATIO ON THE COMPARISON (Num. Against Exp.)

The best approximating line corresponding for each curve are given in the following form :

$$\text{Num. ult. load} = m_1 \text{ Exp. ult. load} + C_1 \quad \text{(KN)} \qquad (6.11)$$

and $$\text{Num./exp. ult load} = m_2 \cdot a_v/d + C_2 \qquad (6.12)$$

The values of the constant m_1, m_2, C_1 and C_2 are given in Table (6.15) :

Table (6.15)

C_f	m_1	C_1	m_2	C_2
1.0	0.928	107.418	0.244	0.794
0.8	0.835	101.532	0.246	0.675
0.6	0.801	83.919	0.229	0.618

From Figures (6.34) to (6.36), it is clear that there is a considerable scatter of results. Furthermore, it is noticeable that as the value of the concrete crushing factor is reduced more points are closer to the (y = x) curve.

Additionally, from Figures (6.37) to (6.39), representing the computed / experimental failure loads versus the shear span to depth ratio, it is apparent that more balanced distribution of points can be found either sides of the ideal curve (y = 1.0) as the value of C_f decreases. In fact, it is clear that the best fitting curve corresponding to C_f = 0.6 has more balanced distribution on either side of the ideal curve than the best fitting curves corresponding to the values of C_f = (1.0 and 0.8).

Since there is a considerable scatter in the results corresponding to all the studied values of the crushing factor C_f, a statistical study proved to be necessary to assess the most suitable value of this parameter. First, histograms for the computed / experimental failure loads for each value of the crushing factor were produced Fig.(6.40) to (6.42). Then arithmetic means and standard deviation were calculated and are given in Table (6.15).

From these histograms, it appears that the best curve that can be obtained should be close to the normal distribution i.e. the curve that has least skewness.

Since the equation of the normal distribution is expressed in terms of the arithmetic mean and the standard deviation of the distribution, it follows that the actual shape of the curve for any distribution will depend upon those two values, and that the shapes of the curves for different distributions will be different. The most suitable will be the one with the smallest value of the standard deviation, and where the arithmetic mean has the majority of the recorded values clustered about it.

The normal distribution is a curve for an infinity of points, and although the results of this present investigation are discrete values but they can still be likened to normal distribution. For instance it is necessary to have $\simeq$ 68% of the total number of the results contained within $\pm\ \underline{\sigma}$ from the mean, and about 95% lying within 2 standard deviations on either side of the mean, and finally about 99.73% within $\pm 3\ \underline{\sigma}$ Fig.(6.43). In this investigation closer the mean is to the value 1.00 , better the results.

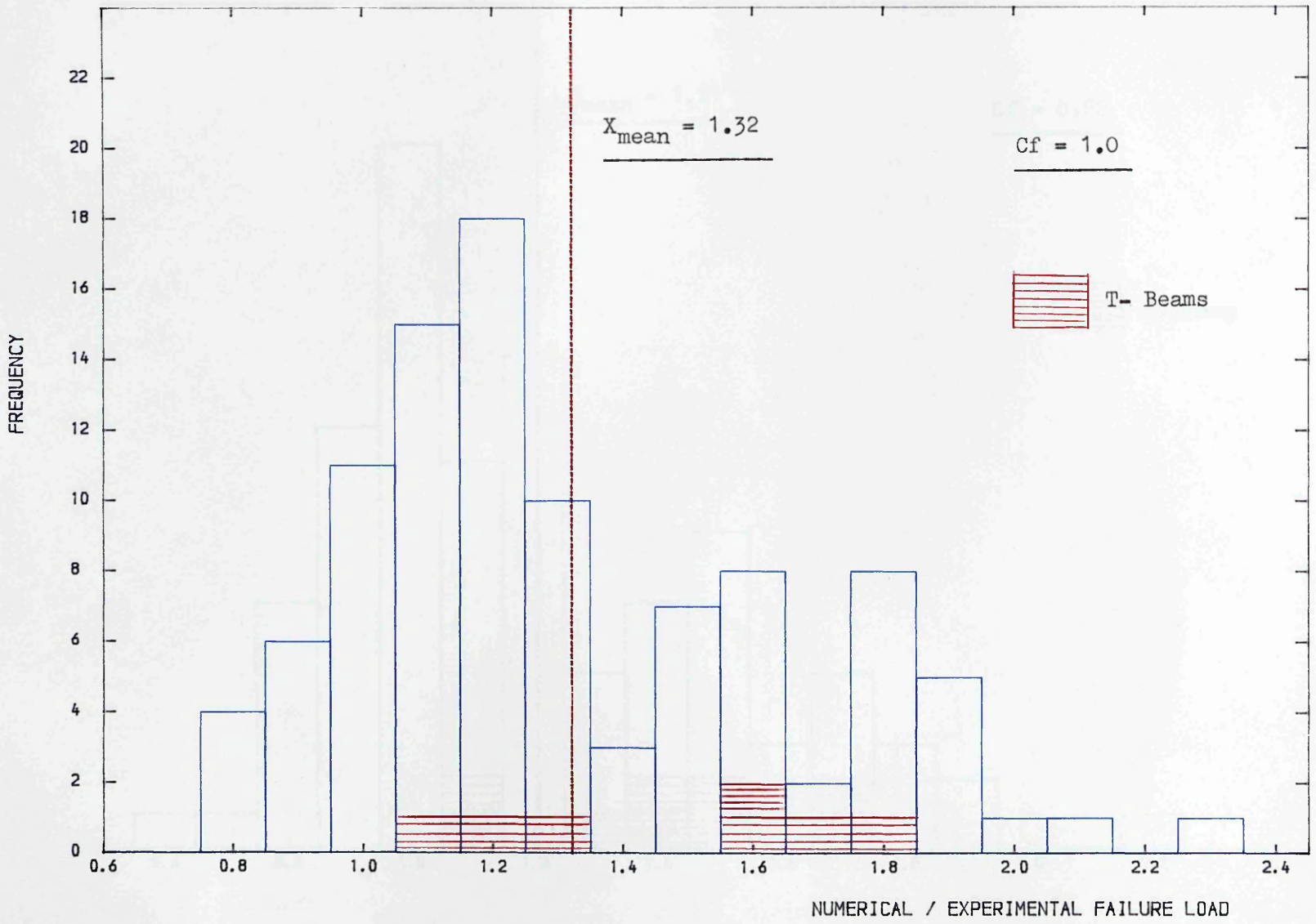

FIGURE (6.40) HISTOGRAM OF RESULTS FOR CRUSHING FACTOR Cf = 1.00

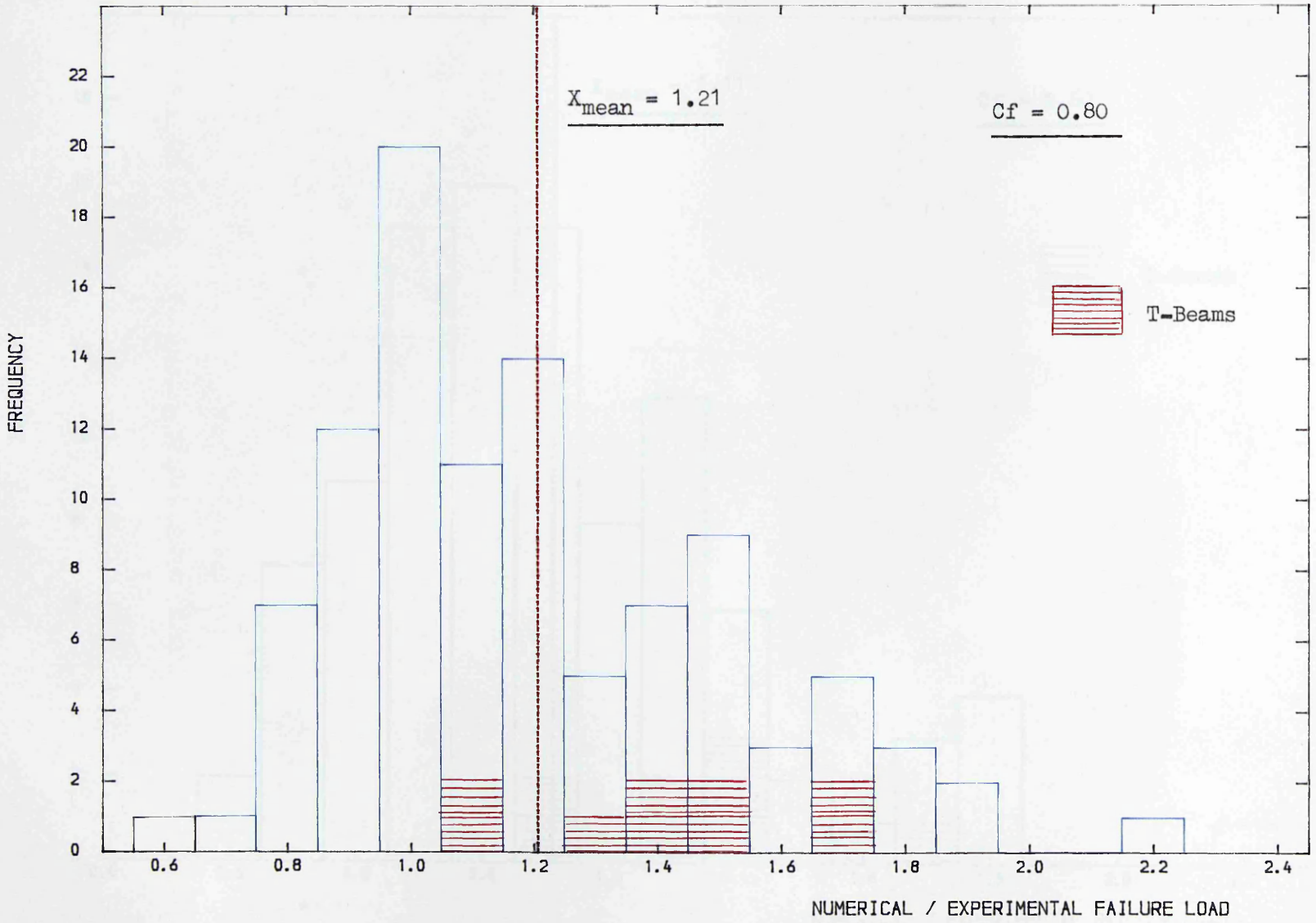

FIGURE (6.41) HISTOGRAM OF RESULTS FOR CRUSHING FACTOR Cf = 0.80

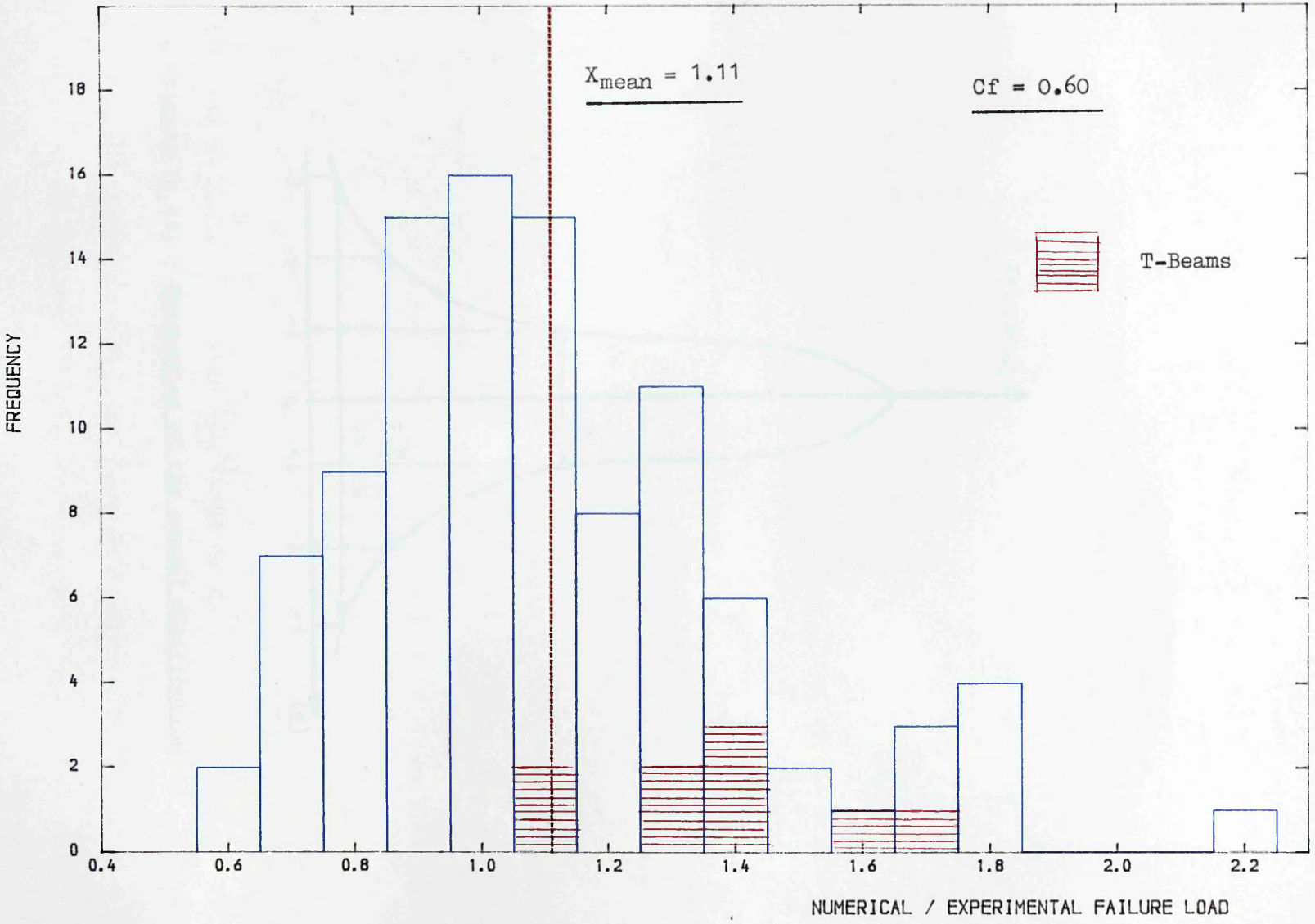

FIGURE (6.42) HISTOGRAM OF RESULTS FOR CRUSHING FACTOR Cf = 0.60

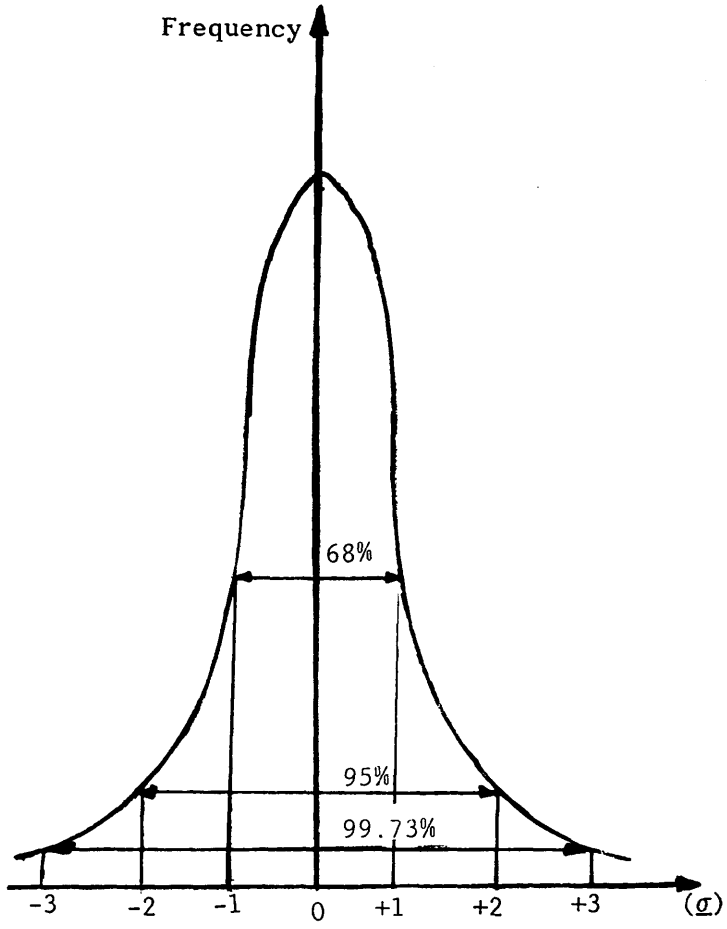

FIGURE (6.43) : Properties of the normal distribution

statistical results:

Table (6.16)

C_f	X_{mean}	σ
1.00	1.3211	0.3314
0.80	1.2061	0.3133
0.60	1.1092	0.3085

a) Case of $C_f = 1.0$:

About 68 results should be in the range ($X_{mean} \pm \sigma$). In fact 69 results are within this range.

Around 95 results have to be in the range ($X_{mean} \pm 2\ \sigma$). Actually, 96 tests are in this range.

Finally, there was only one test outside the range ($X_{mean} \pm 3\ \sigma$).

b) Case of $C_f = 0.8$:

From 100 results 68 are in the range ($X_{mean} \pm \sigma$), 96 are in the range ($X_{mean} \pm 2\ \sigma$) and finally, only one test was found to be outside the range ($X_{mean} \pm 3\ \sigma$).

c) Case of $C_f = 0.6$:

For the necessary 68 results that should be in the range ($X_{mean} \pm \sigma$), there are 71 results in this range.

However, 94 instead of 95 of the results are in the range ($X_{mean} \pm 2\ \sigma$). Finally, only one odd result was found outside the range ($X_{mean} \pm 3\ \sigma$).

6.6.4 Discussion of the results:

From the results shown in {Figure (6.34) to Figure (6.42)} the following observations can be made :

1– It can be seen that there is a considerable scatter of results for all the crushing factor C_f studied values.

2– Generally, smaller the crushing factor C_f, lower the predicted failure load.

3– For beams with shear reinforcement (total of 22 beams) the results were better than for beams without shear reinforcement. The obtained mean values are : (1.11 for C_f = 0.8) and (0.96 for C_f = 0.6). This can be explained by the fact that in this numerical analysis full bond is assumed between concrete and steel, and as the bars are considered to be one–dimensional elements the effect of dowel action is ignored. However, in practice when an inclined crack opens, part of the shear force is sustained by the bars through dowel action, and as this force increases it causes some cracks to occur along the line parallel to the bars. Consequently, a premature collapse of the beam is caused by anchorage failure. On the other hand, in the numerical analysis such thing is ignored and failure cannot happen unless concrete crushes and/or the steel bars yield. For this reason, the numerical analysis gives an overestimation of the failure loads. However, this is not the case when shear reinforcement are present, because by sustaining the main reinforcement they can prevent the beam from anchorage failure as found by Chana[16].

4– For T–beams analysed, it was found that the ultimate load was generally overestimated. The mean values obtained are as follows :

(1.47 for C_f = 1.0), (1.42 for C_f = 0.80) and (1.39 for C_f = 0.6). This is generally due to the fact that the program used ignores the 3–dimensional nature of T–beams.

5– It can be noticed that for high values of concrete strength, C_f has little effect. This is certainly due to the fact that the beams fail before any considerable crushing take place. Therefore decreasing the value of the crushing factor was found to have little effect on lowering the predicted failure load. It was noticed also that in some of the tests on beams with high strength concrete that the computed failure loads were found to have almost twice the values of the experimental failure loads. It is possible that there are errors in the quoted values of experimental failure loads. For example insignificant changes of one of the experimental variables viz concrete compressive strength was found to almost double the failure load, or sometimes doubling this same variable was found to have no effect on the failure load or even have the reverse effect on the failure load. Examples of these are :

(test 52– 54), and (test 48–47) where the concrete compressive was increased to almost the double value while the failure load was found to have decreased.

6– For high strength concrete, it was found that greater the shear– span to depth ratio, higher is the computed value of the shear failure load.

7– For rectangular beams with uniformly distributed loads (total of 28 beams), good agreement was generally found between computed and experimental failure loads. The obtained mean values are : (1.12 for $C_f = 1.0$), (0.99 for $C_f = 0.80$) and (0.88 for $C_f = 0.60$).

8– It was found that, smaller the concrete compressive strength, more effective is the the crushing factor in reducing the value of the computed ultimate load such as : (Test.no : 6, and 86 to 94), where the average decrease of the failure load, corresponding to the decrease of the crushing factor C_f from 1.0 to 0.60, was found to be around 40%. Furthermore, the lowest values of the comparison were found for small values of concrete compressive strength.

9– Finally, It can be noticed from Table (6.14) that by decreasing the value of C_f most of the tests failure mode have changed from a ductile type of failure to a more brittle type which is generally in agreement with the experiment.

6.6.5 Conclusion:

From this analysis, it appears that the most suitable value of the crushing factor C_f is 0.6. Because firstly, it was found that for this value of C_f better agreement was found between numerical and experimental types of failure, and secondly, the mean value of the results corresponding to C_f is found to be the closest to 1.00, and its corresponding standard deviation σ is the smallest.

It has to be kept in mind that the crushing factor C_f is a numerical device which does not reflect the true behaviour of concrete.

CHAPTER 7

CONCLUSIONS AND RECOMMENDATIONS FOR FUTURE WORK

7.1 General conclusions:

From the numerical analysis reported in this thesis the conclusions that can be drawn are as follows :

1– The variation of the value of concrete strength f_t has no effect on the failure load and the mode of failure of reinforced concrete beams.

2– The shear retention factor β has little effect on the ultimate shear strength of reinforced concrete beams.

3– Concrete uniaxial compressive strength f_c' has a great effect on the failure load. Thus, a reduction of 10% of the value of f_c' is associated with the same percentage decrease in the failure load. Additionally, concrete compressive strength f_c' has an important effect on the mode of failure of reinforced concrete beams. Consequently, by decreasing the value of f_c' the mode of failure can change from shear failure where the collapse of the beam is sudden and brittle, to a more ductile type of failure.

4– The crushing factor C_f has a great influence on the failure load load and type of failure. Therefore, if after crushed concrete is allowed to exhibit some strain softening (this is accomplished by having $C_f < 1.0$), this can decrease the failure load provided that failure happens by crushing of concrete.

However, the crushing factor C_f is only a numerical device used here as a parameter.

5– The scatter of the results is mainly due to 'scatter' in the experimental data provided. The most important of all that experimental material data is the compressive strength of concrete f_c'.

6– The most accurate results for comparison are obtained for beams with shear reinforcement.

7– The program used is not suitable for the anlysis of T–beams owing to the fact that it ignores the three dimensional aspect of T– beams.

8– From the statistical study it was found that the value 0.60 for C_f gives a good prediction of the failure load. The prediction of about 65% of the results are to an accuracy of $\pm$ 25%. Therefore, a value of 0.60 is suggested to the crushing factor C_f.

7.2 Suggestions for future work:

i) As some of the results might be influenced by the fact that the program does not take account of dowel action, it is recommended to include it in the analysis. One way of doing it might be to include special beam elements as shown in Figure (7.1). This element has the advantage of including bending effects with only translational degrees of freedom.

ii) A large number of T–beams should be analysed provided that they are properly modelled. One possibility is to use geometric constraints to connect the web and the flange.

iii) The present work has concentrated only on the ultimate load. It would be useful to see the accuracy that can be obtained in terms of predicting limit load at first yield of steel. Additionally any study of the load–deflexion trend can be very important.

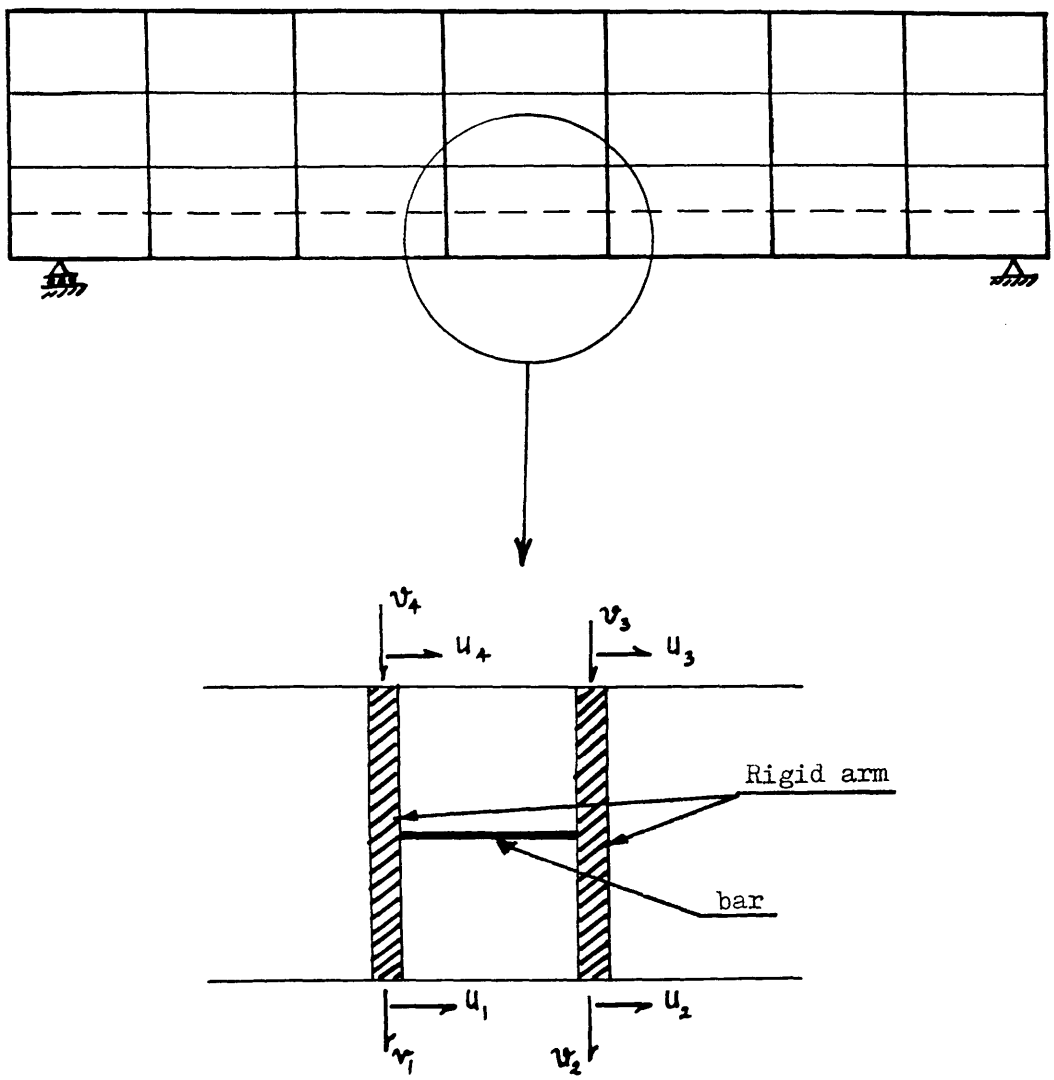

Figure (7.1) : Beam element with only translations as degrees of freedom

REFERENCES

1) BRESLER, B., and MacGREGOR, J. G.
Review of concrete beams failing in shear.
Journal of structural division, ASCE, Vol. 93, (February–1967), pp. 343–372.

2) BRESLER, B., and SCORDELIS, A. C.
Shear strength of reinforced concrete beams.
Journal ACI. Proceedings Vol. 60, (January–1963), pp. 51–74.

3) KOTSOVOS, M. D.
Mechanisms of shear failure.
Magazine of concrete research, Vol.35, (June–1983), pp. 99–106.

4) KANI, M. W., HUGGINS, M. W., and WITTKOP, R. R.
KANI on shear in reinforced concrete.
Department of Civil Engineering, University of Toronto press (1979).

5) The joint ASCE–ACI Task committee 426 on shear and diagonal tension.
The shear strength of reinforced concrete members.
Journal of Structural Division , ASCE, Vol. 99, (June–1973), pp. 1091–1187.

6) FENWICK, R. C., and PAULAY, T.
Mechanisms of shear resistance of concrete beams.
Journal of structural division, ASCE, Vol. 94, (October–1968), pp. 2325–2350.

7) KANI, G. N. J.
A rational theory for the function of web reinforcement.
Journal ACI, Proceedings Vol. 66, (March–1969), pp. 185–197.

8) KANI, G. N. J.
Basic facts concerning shear failure
Journal ACI, Proceedings Vol. 63, (June–1966), pp. 675–692.

9) PLACAS, A., and REGAN, P. E.
Shear failure of reinforced concrete beams.
Proceedings, ACI, Vol. 68, (October–1971), pp. 763–773.

10) RAJAGOPALAN, K. S., and FERGUSON, P. M.
Exploratory shear tests emphazing percentage of longitudinal reinforcement.
Journal ACI, Vol. 68, (August–1968), pp. 634–638.

11) ZSUTTY, T.
Shear strength prediction for separate categories of simple beams tests.
Journal ACI, Vol. 68, (February–1971), pp. 138–143.

12) ACHARYA, D. N., and KEMP, K. O.
Significance of dowel forces on the shear failure of rectangular beams with web reinforcement.
Proceedings, ACI, Vol. 62, (October–1965), pp. 1265–1278.

13) BARON, M. J.
Shear strength of reinforced concrete beams at points of bar cutoff.
Journal ACI, Vol. 63, (January–1966), pp. 127–134.

14) MATHEY, R., and WATSTEIN, D.
Shear strength of beams without web reinforcement containing deformed bars of different yield strengths.
Journal ACI, Vol. 60, (February–1963), pp. 183–208.

15) FERGUSON, P. M., and MATLOOB, F. M.
Effect of bar cutoff on bond and shear strength of reinforced concrete beams.
Journal ACI, Vol. 56, (July–1959), pp. 5–24.

16) CHANA, P. S.
Analytical and experimental studies of shear failures in reinforced concrete beams.
Proc. Instn. Civ. Engrs, Part 2, (December–1988), 85, pp. 609–628.

17) LEONHARDT, F., and WALTER, R.
The Sttutgart Shear Tests, 1961
Translation No. 111, Cement & Concrete Association, 1964.

18) MPHONDE, A. G., and FRANTZ, G. C.
Shear tests of high and low strength concrete beams without stirrups.
Journal ACI, Vol. 81, *(July–August 1984), pp. 350–357.*

19) CHANA, P. S.
Shear failure of reinforced concrete beams.
Ph.D Theses, London University 1986.

20) KANI, G. N. J.
How safe are *our large reinforced concrete beams.*
Journal ACI, Proc. Vol. 64, (March–1967), pp. 128–141.

21) TAYLOR, H. P. J.
The shear strength of large beams.
Proceedings, ASCE, Vol. 98, (November–1972), pp. 2473–2490.

22) DIAZ DE COSSIO, R.
Discussion of reference 53.
Journal ACI, Vol. 59, (September–1962), pp. 1323–1332.

23) FERGUSON, P. M.
Some implications of recent diagonal tension tests.
Journal ACI, Proceedings Vol. 53, (August–1956), pp. 157–172.

24) TAUB, J., and NEVILLE, A. M.
Resistance to shear of reinforced concrete beams.
Part 1–Beams without web reinforcement.
Proceedings, ACI, Vol. 57, (August–1970), pp. 193–220.

25) BRESLER, B., and PISTER, K. S.
Strength of concrete under combined stresses.
Proceedings, ACI, Vol. 55, (September–1958), pp. 321–345.

26) OJHA, S. K.
The shear strength of rectangular reinforced and prestressed concrete beams.
Magazine of concrete research, Vol. 19, (September–1967), pp. 173–184.

27) KANI, G. N J.
The riddle of shear failure and its solution.
Proceedings, ACI, Vol. 61, (April–1964), pp. 441–467.

28) REGAN, P. E.
Shear in reinforced concrete beams.
Magazine of concrete research, Vol. 21, (March–1969), pp. 31–42.

29) MIRZA, S. A., and MacGREGOR, J. G.
Statistical study of shear strength of reinforced concrete slender beams.
Journal ACI, Vol. 76, (November–1979), pp. 1159–1177.

30) ZIENKIEWICZ, O. C.
The finite element method
Mac Graw–Hill Book Company, 3rd Edition, 1977.

31) DESAI, C. S., and ABEL, J. F.
Introduction to the finite element method.
Van Nostrand Reinhold Company, 1972.

32) PHILLIPS, D. V.
Nonlinear Analysis of Structural Concrete by Finite Element Methods.
Ph.D. Thesis, University of Wales, 1973.

33) CHEN, W. F.
Plasticity in reinforced concrete.
Mac Graw–Hill Book Company, Inc., New York, 1981.

34) SHAH, S. P., and WINTER, G.
Inelastic behaviour and fracture of concrete.
Journal ACI, Vol. 63, (September–1966), pp. 925–930.

35) DESAI, P., and KRISHNAN, S.
Equation for the stress–strain curve of concrete.
Journal ACI, Vol. 61, (March–1964), pp. 345–350.

36) HOGNESTED, E., HANSEN, N. W., and McHENRY, D.
Concrete stress distribution in ultimate strength design.
Journal ACI, Vol. 52, (December–1955), pp. 455–480.

37) HUGHES, B. P., and CHAPMAN, G. P.
The complete stress–strain curve for concrete in direct tension.
Bulletin RILEM, No. 30, 1966, pp. 95–97. (quoted by 46).

38) MADU, R. M.
Characteriszation of the stress–strain curves for reinforced concrete under uniaxial tension.
Magazine of Concrete Research, Vol. 27, (December–1975), pp. 210–218.

39) LEINBERG, A. C.
A stress–strain function of concrete subjected to short term loading.
Magazine of Concrete Research, Vol. 61, (March–1964), pp. 345–350.

40) AHMED, S. H., and SHAH, S. P.
Complete triaxial stress–strain curves for concrete.
Journal of Structural Division, ASCE, Vol. 108, (April–1982), pp. 728–742.

41) CHEN, W. F., and SALEEB, A. F.
Constitutive equations for engineering materials.
Volume 1: Elasticity and Modeling.
A Wiley–Interscience Publication, 1982.

42) MYLREA, T. D.
Bond and anchorage.
Journal ACI, Vol. 44, (March–1948), pp. 521–552.

43) SCORDELIS, A. C.
General Report–Basic Problem.
IASS Symposium on the nonlinear behaviour of reinforced concrete spatial structures, Vol. 3, (July–1978), pp. 35–70.

44) KUPFER, H., and HILSDORF, H. K.
Behaviour of concrete under combined compressive stresses.
Journal ACI, Vol. 66, (August–1969), pp. 656–666.

45) RICHART, F. E., BRANDTZAEG, A., and BROWN, R. L.
A study of the failure of concrete under combined compressive stresses.
Bulletin No. 185, University of Illinois, Engng. Expt. Station, Urbana, Illinois, (November–1928), pp. 1–102. (quoted by 32).

46) LIU, T. C. Y., NILSON, A. H., and SLATE, F. O.
Stress–strain response and fracture of concrete in uniaxial and biaxial compression.
Journal ACI, Vol. 69, (May–1972), pp. 291–295.

47) KOTSOVOS, M. D., and NEWMAN, J. B.
Generalized stress–strain relation for concrete.
Journal of the engineering mechanics division, ASCE , Vol. 104, (August–1978), pp. 845–856.

48) COWAN, H. J.
The strength of plain, reinforced and prestressed concrete under the action of combined stresses.
Magazine of concrete research, Vol. 5, (December–1953), pp. 75–86.

49) HIGASHIOMA, R., and SCHNOBRICH, W. C.
Lumped parameter analysis for shear failure in the end slabs of cylindrical prestressed concrete pressure vessels.
Civ. Eng. studies, Structural Research Report No. 363, University of Illinois, Urbana, Illinois, 1970.

50) HAND, F. R., PECKHOLD, D. A., and SCHNOBRICH, W. C.
Nonlinear layered analysis of reinforced concrete plates and shells.
Journal of the structural division, ASCE, Vol. 99, (July–1973), pp. 1491–1505. (Quoted by 54)

51) AL– MAHAIDI, R. S. H.
Analysis of reinforced concrete deep members.
Report No. 79–1, Dept. of Structural Engineering, Cornell University, (January–1979). (Quoted by 54)

52) PHILLIPS, D. V., and AL–MANASEER, A. A.
Numerical study of some post–cracking material parameters affecting nonlinear solutions in reinforced concrete deep beams.
Canadian Jounal of civil.engineering, Vol. 14, (November–1987)

53) ACI Committee 326
Shear and diagonal tension.
Proceedings, ACI , Vol. 59, (Jan–Feb–Mar, 1962), pp. 1–30, 277–334, and 353–396.

54) ABDELHAFEZ, L. M.
Direct design of reinforced concrete skew slabs.
Ph.D Thesis, Glasgow University, 1986.

55) BATHE, K. J.
Finite element procedures in engineering analysis.
Prentice–Hall, Inc., Englewood Cliffs, New Jersey, USA, 1982.

56) HINTON, E., and OWEN, D. R. G.
Computational Modeling of Reinforced Concrete Structures.
Pineridge Press Ltd; 1986.

57) BURDEN, R. L., and FAIRES, J. D.
Numerical Analysis.
Prindle, Weber & Schmidt, Boston, Third Edition, 1984.

58) KENNEDY, J. B., and NEVILLE, A. M.
Basic statistical methods for engineers and scientists.
Harper & Row, Publishers, Inc; 2nd Edition, 1976.

59) AL–MANASEER, A. A.
A nonlinear Finite element study of reinforced concrete beams.
Ph.D thesis, Glasgow University, 1983.

60) REICHMANN, W. J.
Use and abuse of statistics.
Published by Penguin Books, 1968.

61) MPHONDE, A. G.
Aggregate interlock interlock in high strength reinforced concrete beams.
Proceedings of the institution of civil engineers, Part 2, Vol. 85, (September–1988), pp. 397–413.

62) RAMAKRISHNAN, V.
Behaviour and ultimate strength of reinforced concrete in shear.
PSG College of Technology, Coimbatore, India, (January–1969).

63) SHEAR STUDY GROUP.
The shear strength of reinforced concrete beams.
Institution of Structural Engineers, (January–1969).

64) Task committee on Finite Element Analysis of reinforced concrete structures of the structural division committee on concrete and Masonry structures.
Finite element analysis of reinforced concrete.
ASCE, USA, 1982.

65) OWEN, D. R. J., and HINTON, E.
Finite elements in Plasticity : Theory and Practice.
Pineridge Press Ltd, Swansea, U.K, 1980.

66) CEDOLIN, L., and NILSON, A. H.
A convergence study of iterative methods applied to finite element analysis of reinforced concrete.
International Journal for numerical methods in engineering, Vol.12,1978.

67) KREFELD, W. J., and THURSTON, C. W.
Studies of the shear and diagonal tension strength of simply supported reinforced concrete beams.
Journal ACI, Vol. 63, (April–1966), pp. 451–475.

68) CLARK, A. P.
Diagonal tension in reinforced concrete beams.
Journal ACI, Vol. 48, (October–1951), pp. 145–156.

69) PHILLIPS, D. V., and ZIENKIEWICZ, O. C.
Finite element Nonlinear analysis of concrete structures.
Proc. Instn. Civ. Engrs, Part 2, Vol. 61, (March–1976), pp. 59–88.

70) SWAMY, R. N., ANDRIOPOULOS, A., and ADEPEGBA, D.
Arch action and Bond in concrete shear failures.
Journal of the structural division, ASCE, Vol. 96, (June–1970), pp. 1069–1091.

71) BROMS, B. B.
Shear strength of reinforced concrete beams.
Journal of the structural division, ASCE, Vol. 95, (June–1969), pp. 1339–1358.

72) MORETTO, O.
An investigation of the strength of welded stirrups in reinforced concrete beams.
Journal ACI, Vol. 17, (November–1945), pp. 141–164.

73) TAYLOR, R.
Some shear tests on reinforced concrete T–beams with stirrups.
Magazine of concrete research, Vol. 12, (November–1960), pp. 145–154.

74) KOTSOVOS, M. D., BOBROWSKI, J., and EIBL, J.
Behaviour of reinforced concrete T–beams in shear.
The structural Engineer, Vol.65b, No. 1, (March–1987), pp. 1–10.

75) NILSON, A. H.
Nonlinear analysis of reinforced concrete by the finite element.
Journal ACI, Vol. 65, (September–1968), pp. 757–766.

76) MOODY, K. G., VIEST, I. M., ELSTNER, R. C. and HOGNESTAD,E.
Shear strength of reinforced concrete beams. Part 1–Tests of simple beams.
Journal ACI, Vol. 26, (December–1954), pp. 317–332.

77) KREFELD, W. J., and THURSTON, C. W.
Contribution of longitudinal steel to shear resistance of reinforced concrete beams.
Journal ACI, Vol. 63, (March–1966), pp. 325–344.

78) DIAZ DE COSSIO, R., and SIESS, C. P.
Behaviour and strength in shear of beams and frames without web reinforcement.
Journal ACI, Vol. 56, (February–1962), pp. 695–735.

79) FOK, W. F.
The shear strength of reinforced concrete T–beams with unreinforced and shear–reinforced webs.
Ph.D theses, Glasgow university, 1972.

80) KOTSOVOS, M. D.,
Behaviour of reinforced concrete beams with a shear span to depth ratio between 1.0 and 2.5.
Journal ACI, Vol. 81, (May–June 1984), pp. 279– 286.

81) ZSUTTY, T.
Beam shear strength prediction by analysis of existing data.
Journal ACI, Vol. 65, (November–1968), pp. 943–951.

82) CHONG; O. Y.
Ultimate shear strength of uniformly loaded reinforced concrete T–beams.
M.Sc Theses, Glasgow university, 1980.

83) CEDOLIN, L., and DEI POLI, S.
Finite element studies of shear–critical of reinforced concrete beams.
Journal of the engineering mechanics division, Proc. ASCE, Vol. 103, (June–1977), pp. 395–410.

84) SUIDAN, M., and SCHNOBRICH, W. C.
Finite element analysis of reinforced concrete.
Journal of the structural division, ASCE, Vol. 99, (October–1973), pp.2109–2122.

85) NGO, D., and SCORDELIS, A. C.
Finite element analysis of reinforced concrete beams.
Journal ACI, Vol. 64, (March–1967), pp. 152–163.

APPENDIX

The crushing factor C_f used as parameter in this study is a numerical device introduced into the program to take account of the strain softening phenomenon occuring in concrete after crushing. Consequently, this factor has an effect only on the post crushing behaviour of concrete. Thus, the uniaxial compressive stress for concrete is reduced to a value equal to the concrete uniaxial compressive strength by the crushing factor C_f i.e :

$$\sigma = f_c' \cdot C_f \qquad (N/mm^2) \qquad (A1)$$

Where σ : Concrete uniaxial compressive stress after crushing.

This is illustrated in Figure (A), where the experimental uniaxial behaviour of concrete is compared to the numerical model used (for different values of the crushing factor C_f).

From this Figure it can be seen that greater the decrease in the value of C_f the sharper is the decrease of the post crushing value of the concrete uniaxial compressive stress. Thus, when one of the principal stresses of concrete exceeds the uniaxial compressive strength concrete at this point, it crushes and the stress is reduced following equation (A1).

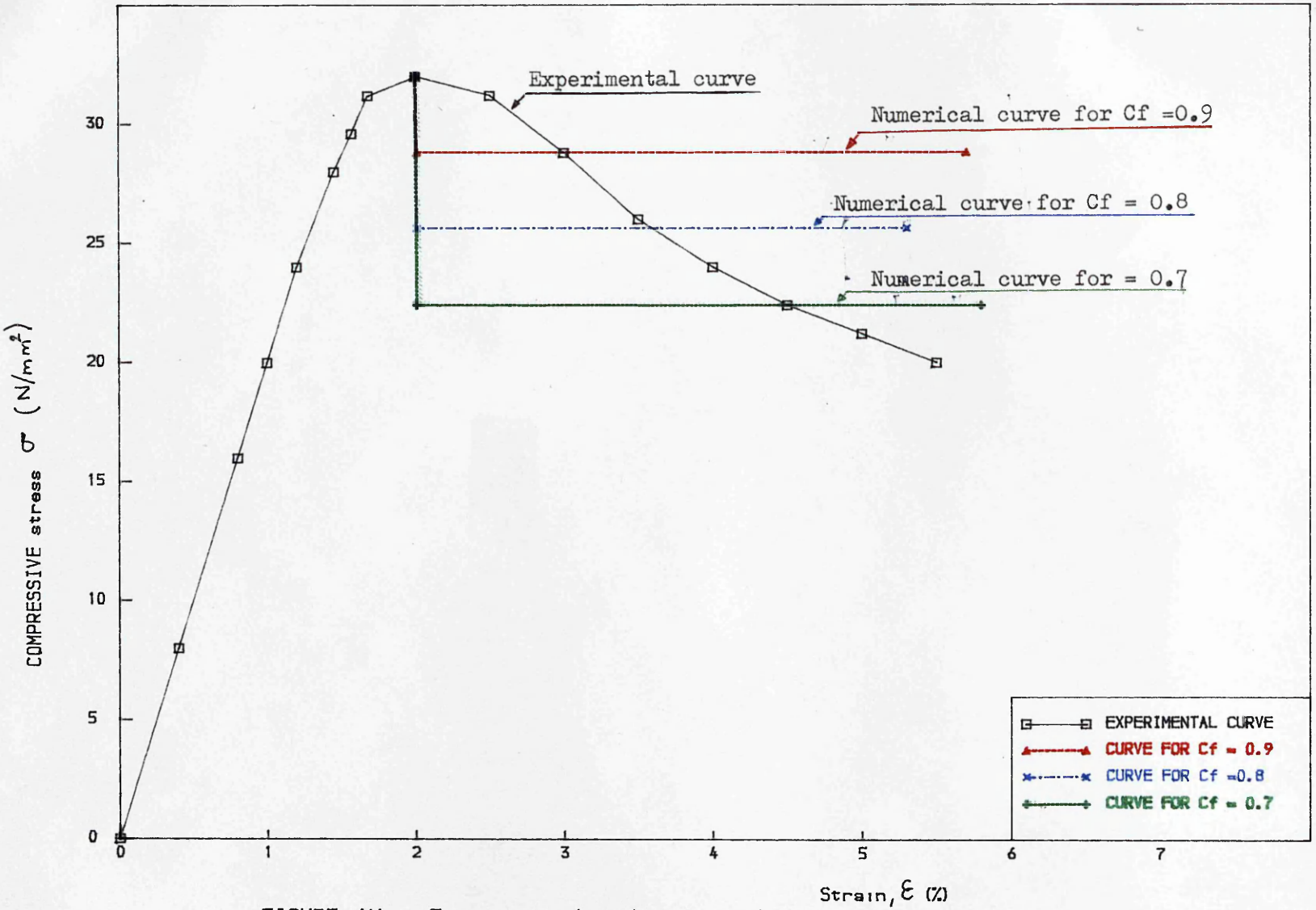

FIGURE (A) : Experimental and numerical uniaxial compressive stress-strain curves for concrete